TECHNICAL NOTE R-229

HALL AND PHOTORESPONSE MEASUREMENTS ASSOCIATED WITH ULTRAVIOLET AND NEAR ULTRAVIOLET DEGRADATION OF THIN ZINC OXIDE FILMS

May 1967

Prepared For

SPACE THERMODYNAMICS BRANCH
RESEARCH PROJECTS LABORATORY
GEORGE C. MARSHALL SPACE FLIGHT CENTER

Prepared By

RESEARCH LABORATORIES
ADVANCED SYSTEMS AND TECHNOLOGIES GROUP
BROWN ENGINEERING COMPANY, INC.
HUNTSVILLE, ALABAMA

Contract No. NAS8-20166

By

M. L. McDaniel
R. R. Mitchell
Dr. H. J. Watson

ABSTRACT

The optical and electrical parameters of zinc oxide change (degrade) as a result of material exposure to certain spectral radiation; the causal spectral range is in the visible and ultraviolet. Charge carrier density and majority carrier mobility have been measured in thin, polycrystalline, zinc oxide film; these measurements were made for several levels of degradation.

Photoresponse, as a manifestation of degradation, is compared for ambient pressures of one atmosphere and approximately 10^{-10} atmospheres. This response study is made for two spectral levels, 3650 Å and 4350 Å radiation.

Approved:

H. J. Watson

H. J. Watson, Manager
Experimental Physics
Department

Approved:

R. C. Watson

R. C. Watson, Jr.
Vice President

TABLE OF CONTENTS

	Page
INTRODUCTION	1
EXPERIMENTAL TECHNIQUE	3
EXPERIMENTAL RESULTS	13
Electrical Conductivity	13
Hall Measurements	15
Photoconduction	24
CONCLUSIONS	61
REFERENCES	63
APPENDIX - RESISTANCE AND TIME RATE CHANGE OF RESISTANCE VERSUS DURATION OF IRRADIATION AND RECOVERY TIME	65

LIST OF FIGURES

Figure	Title	Page
1	Vacuum System in Evaporation Mode	4
2	Substrate, Connector Lands, and Zinc Oxide Film Configuration.	5
3	Substrate Holder Employed During Irradiation	7
4	Vacuum System in Measurement Mode	9
5	Measurement Schematic	10
6	Relative Transmission of Unfiltered Ultraviolet as a Function of Zinc Oxide Film Conductivity	14
7	Majority Carrier Density as a Function of Duration of Unfiltered Ultraviolet Irradiation.	19
8	Majority Carrier Mobility as a Function of Time for Steady, Unfiltered, Ultraviolet Irradiation.	20
9	Effective Mobility as a Function of the Depression of the Energy Bands at the Surface (reproduced from Ref. 1)	23
10	Particulate Zinc Oxide Degradation Model.	25
11	Fast Photoconductivity of Zinc Oxide Film Under 5600 Å Irradiation.	27
12	Recovery of Degraded Film Upon Admission to Atmosphere.	28
13	Photoresponse and Recovery for Three Energy Levels of Irradiation as a Function of Time	30
14	Expected Model at Steady State Conditions for Various Temperatures	33
15	Photocurrent Response - 3650 Å Irradiation	35
16	Photocurrent Response - 3650 Å Irradiation	36
17	Photocurrent Recovery from 3650 Å Irradiation	38

LIST OF FIGURES (Continued)

Figure	Title	Page
18	Photocurrent Recovery from 3650 Å Irradiation	40
19	Photocurrent Recovery from 3650 Å Irradiation	41
20	Photocurrent Recovery from 3650 Å Irradiation	42
21	Photocurrent Response - 4350 Å Irradiation	43
22	Photocurrent Response - 4350 Å Irradiation	44
23	Photocurrent Response - 4350 Å Irradiation	46
24	Photocurrent Response - 4350 Å Irradiation	47
25	Photocurrent Recovery from 4350 Å Irradiation	48
26	Photocurrent Recovery from 4350 Å Irradiation	49
27	Photocurrent Recovery from 4350 Å Irradiation	50
28	Photocurrent Recovery from 4350 Å Irradiation	51
29	Steady State Degradation Level as Determined by Prior Irradiation and Temperature.	53
30	Photocurrent as a Function of Temperature and Irradiation.	54
31	Filter Transmission and Relative Line Intensity of U-V Lamp.	55
32	Modification of Donor Level Structure	58

INTRODUCTION

One of the many important facets of the complex problem of space flight is that of environmental control of the space vehicle. Of these environmental factors, the thermal control necessary must be considered fundamental. Paramount in thermal control considerations in space with the attendant unfiltered solar radiation is vehicle surface coating as characterized by the solar absorptance coefficient (α_s) and emittance (ϵ). In thermal environmental design these parameters must be considered since they indicate the expected gain and loss of energy from solar radiation and emission, respectively.

To date, zinc oxide has exhibited the most acceptable ratio of solar absorptance to emittance of materials examined and has subsequently been incorporated as pigmentation in thermal control coatings. Experience has been, however, that zinc oxide does not exhibit solar absorptance as a constant when subject to solar radiation. This is manifested by the increase of the α_s to ϵ ratio. Complication and a reduction of thermal design reliability are quite naturally inherent to this situation of a variable coefficient of solar absorptance and hence correction of this condition is sought.

To better understand this observed degradation (increase of absorptance coefficient) of zinc oxide in terms of basic physical principles, experimental investigations have been initiated. The point of view was taken that a thorough understanding of the degradation mechanism would either make possible the conditioning of zinc oxide so as to effect the desensitization of α_s in zinc oxide or would aid in the development of a more suitable material for this use.

The majority of work on zinc oxide has been carried out either on single crystals or sintered polycrystalline samples. In either case, the subject samples under study have been, for the most part, bulk materials having low surface-to-volume ratio. Eminent investigators[1,2]

attribute the conduction phenomenon in zinc oxide to surface condition. Since the absorption coefficient is functionally dependent on conductivity, it is felt that thin film studies of photoconduction in zinc oxide should reveal pertinent information regarding radiation-absorption relation because the surface-to-volume ratio in an evaporated film can be made extremely large compared to the same ratio in bulk samples.

The principal parameter is taken as conductivity of the polycrystalline films. Each sample is physically continuous and due to the fact that the material is the oxide, oxide interface effects need not be considered. The material conductivity is examined in the light of Hall measurements, pressure, film temperature, film thickness, degree of crystallinity, energy of damaging radiation and intensity of damaging irradiation. An attempt is made to explain these data within the framework of existing models for photoconduction in zinc oxide.

EXPERIMENTAL TECHNIQUE

The physical vacuum apparatus (Figure 1) in which the films were evaporated and subsequently examined consists of a stainless steel, nickel-plated lower section, mated to a heavy duty pyrex glass tower which defines the work volume. This system, pumped by an NRC Model 206 Orb-ion pump and roughed by an Ultek cryosorption pump, is capable of 10^{-8} torr without special preparation and is oil free.

Under ultrahigh vacuum (10^{-7} torr range), a wound-wire molybdenum source containing 99.999 percent pure zinc pellets is heated electrically to cause evaporation of the zinc onto a specially prepared quartz substrate (Figure 2) 15 centimeters distant. Initial evaporations tended to coat the substrate preferentially, coating some areas of the unmasked substrate and failing to coat adjacent areas altogether. This condition was attributed to the presence of oil films on the substrate. The standard treatment of hot water and detergent washes followed by several distilled water rinses and subsequent storage in a dessicator improved this condition, but not to the point where an acceptable evaporation could be relied upon. A final step of baking the substrate in excess of 500°C either in the vacuum chamber or in atmosphere was added to the above mentioned procedure and resulted in very acceptable film adherence to the substrate. Extreme care, however, was mandatory in the handling of the substrate following the heat treatment. An acid and water cleaned stainless steel forceps would contaminate the substrate with body oil if the forceps were held by the bare hand. Surgical gloves were necessarily employed for handling the cleaned substrate with forceps.

Substrate lands, comprising the control current and Hall voltage connecting areas, were produced by a silk-screen process using silver-palladium as the screened material. This material did not produce rectification (non ohmic) contacts. Silver-palladium adheres well to quartz, has high conductivity, and solders readily.

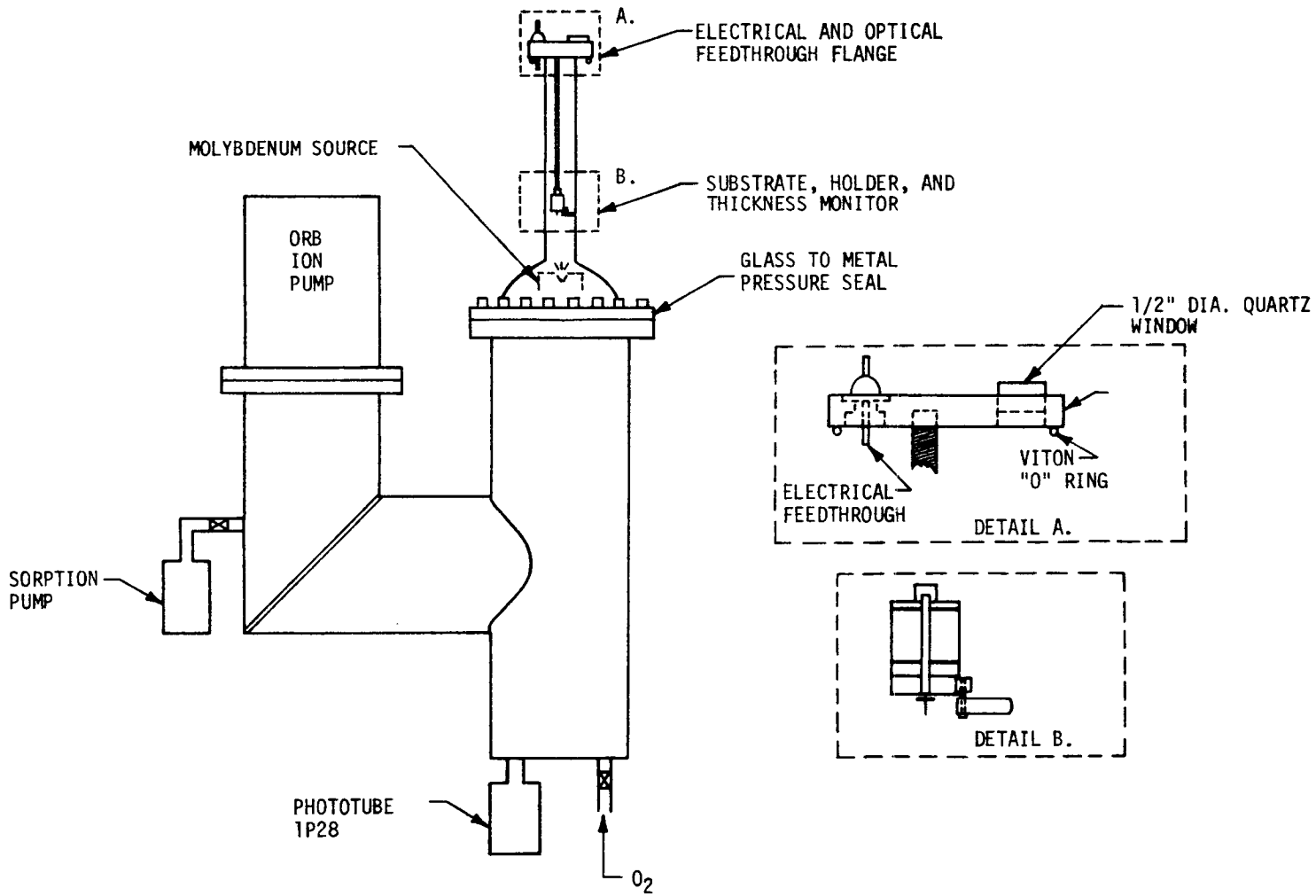

Figure 1. Vacuum System in Evaporation Mode

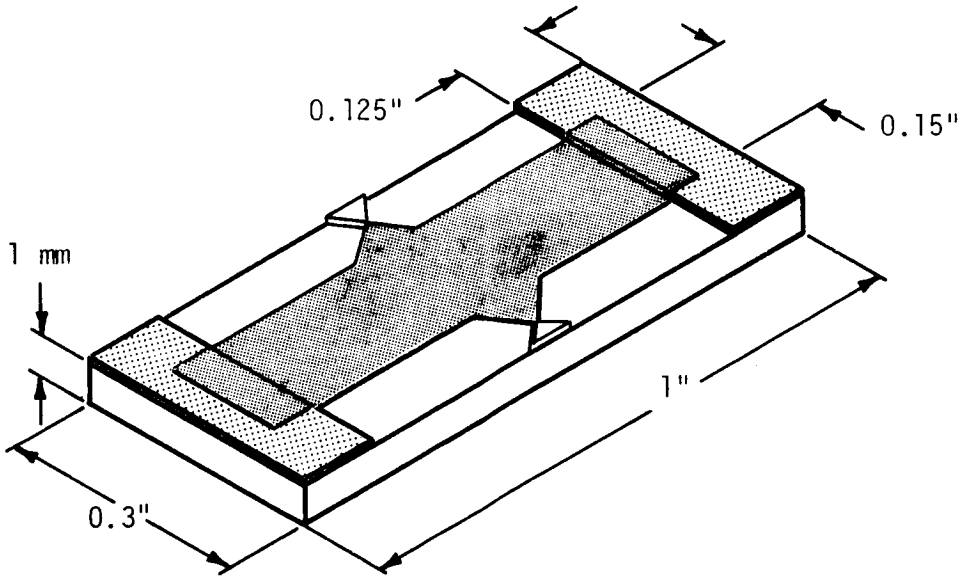

Figure 2. Substrate, Connector Lands, and Zinc Oxide Film Configuration

In thin film work of almost any nature, film thickness is a most important parameter, the present case not being an exception. Film thickness is measured by the piezoelectric quartz crystal monitoring head of the Sloan DTM3 film thickness monitor unit. Accuracy claimed for this device is ± 2 percent. The absolute accuracy should probably not be better than ± 75 Å of zinc oxide. The crystal and head, as shown in detail B of Figure 1, is positioned so as to provide support of the boron nitride substrate holder.

Following completion of evaporation, the film is removed from the vacuum system, measured for resistance and then oxidized in atmosphere. The oxidation process is carried out in a link belt feed, multizone, doping furnace. Specifically, the oxidizing treatment consists of the following:

(a) Nine minutes at 450°C

(b) Nine minutes at 750°C

(c) Nine minutes at 850°C

(d) Six minutes at 500°C

Quenching is initiated at 500°C in air.

Following oxidation, electrical leads are attached to the silver-palladium lands. The leads are either #36 gauge copper wire, soft soldered to the lands or 0.001-inch diamter gold wire with thermocompression bonded to the lands. The latter procedure is followed for films which were due for high temperature cycling. The film-substrate-lead ensemble is then positioned in a boron-nitride holder (Figure 3), the entire unit then being remounted in the vacuum system.

Film temperature can be controlled from room temperature up to 250°C by means of nichrome heater wire wound about the threaded boron-nitride holder. This material, boron-nitride, is a machinable, hydroscopic,

insulative compound which exhibits excellent thermal conduction characteristics. This is evidenced by the almost immediate response of the low mass chromel-alumel thermocouple positioned next to the quartz substrate. This ensemble normally takes less than five minutes to reach thermal equilibrium for a given power setting.

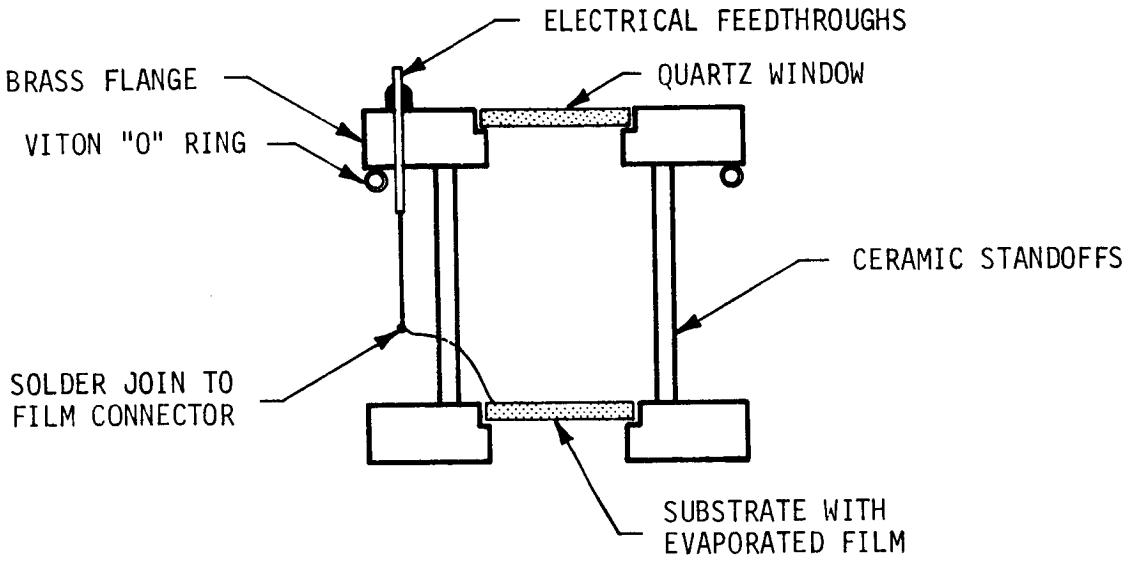

Figure 3. Substrate Holder Employed During Irradiation

The ultraviolet source is a Hanovia-type 616A high pressure mercury arc lamp. Radiated spectral energy values are given in Table 1.

The magnetic field necessary for the Hall measurements is supplied by the axial field of a Magion UFS-3 solenoidal electromagnet, capable of 4,000 Gauss at the film under test conditions.

The transmitted portion of the damaging radiation is monitored by a 1P28 phototube (3400 Å ± 50 Å maximum response wavelength). Partial pressure of oxygen or any chosen gas can be obtained through the use of the Whitey leak valve in juxtaposition with the phototube. Rates of leakage small enough to effect changes as low as $\pm 1 \times 10^{-7}$ torr in pressure are achieved regularly. The system in the measurement mode, without the electrical wiring, is shown in Figure 4.

TABLE 1

SPECTRAL ENERGY DISTRIBUTION OF RADIATED MERCURY LINES IN HANOVIA HIGH-PRESSURE QUARTZ MERCURY-VAPOR LAMP

Mercury Lines (angstroms)	
13673 (infrared)	0.95
11287	0.85
10140	1.30
5780 (yellow)	1.50
5461 (green)	1.50
4358 (blue)	0.84
4045 (violet)	0.51
3660 (U-V.)	1.82
3341	0.18
3130	1.30
3025	0.57
2967	0.30
2894	0.19
2804	0.19
2753	0.08
2700	0.09
2652	0.47
2571	0.19
2537 (reversed)*	0.37
2482	0.19
2400	0.12
2380	0.09
2360	0.06
2320	0.02
2224	0.02
Total watts	13.70

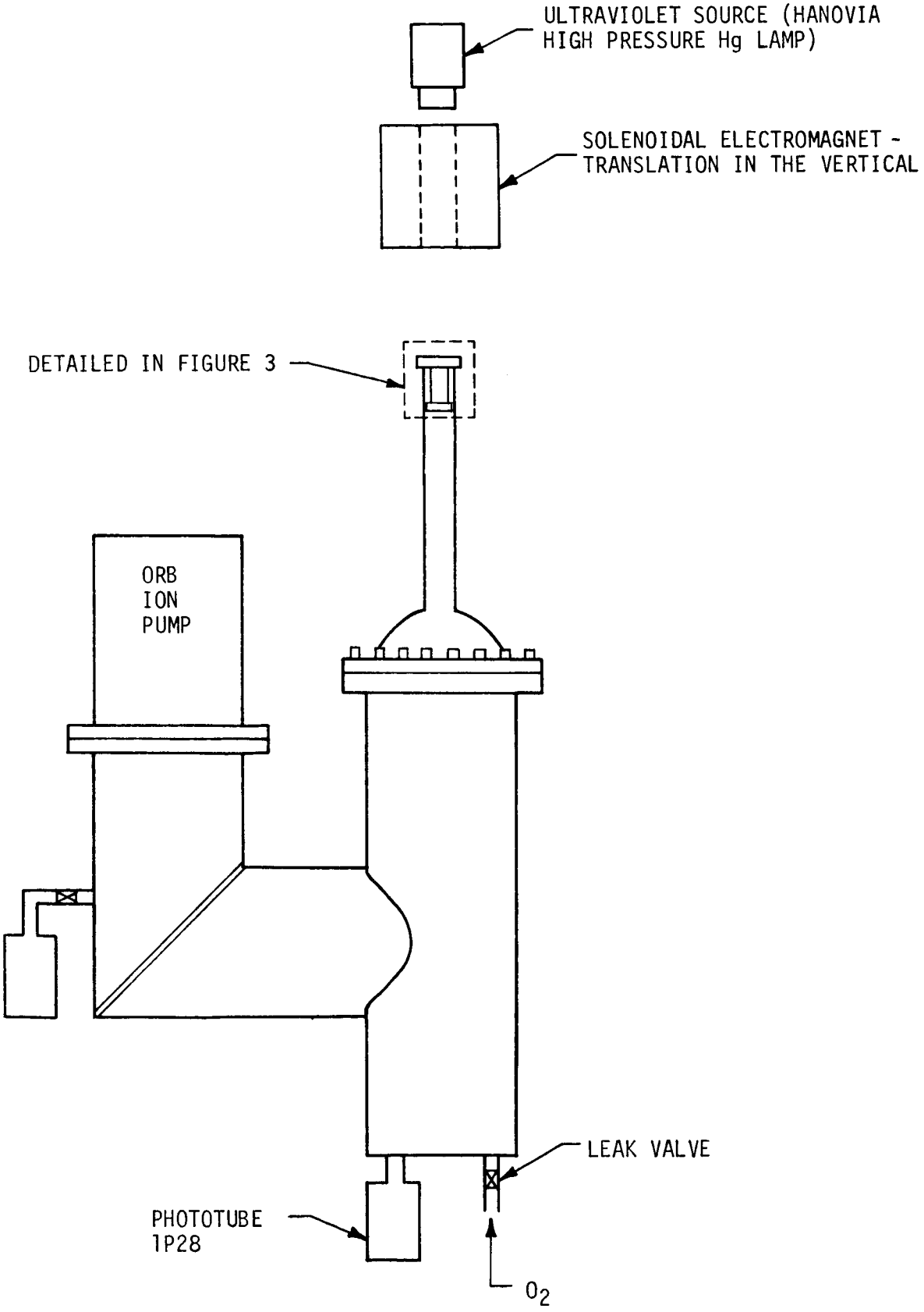

Figure 4. Vacuum System in Measurement Mode

The method of determining film resistance is shown in Figure 5. A constant voltage is impressed across the film and a control resistor in series with the film. The control resistor value is chosen so that its value will not exceed one-hundredth of the film resistance throughout the measurement. Voltage thus obtained across the control resistor is converted to current through the film. Any change in this current is attributed to a change in film resistance.

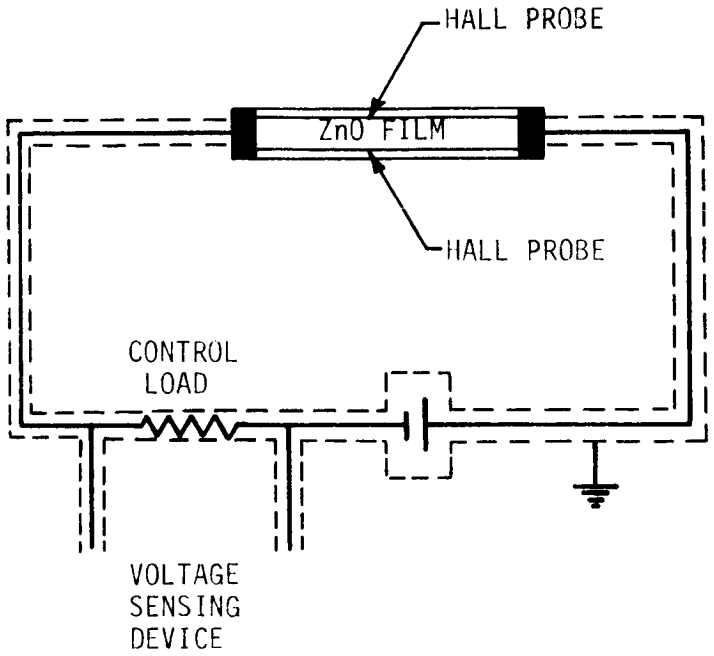

Figure 5. Measurement Schematic

Voltage is read either from a General Radio 1230 electrometer or a Textronic oscilloscope with a type "L" plug in unit and recorded continuously either by a Honeywell Electronic 17 Strip Recorder or a Honeywell 906C Visicorder Oscillograph. Maximum response measurements made on these devices showed that the photoresponse was not limited by the measurement or recording devices.

Measurement of Hall voltage was accomplished using a Keithley 621 electrometer. Current across a 10^{11} ohm load resistor is expressed as Hall voltage. As the impedance between the Hall contact is 10^6 - 10^7 ohms, this arrangement was satisfactory. This is not a null type measurement, but it does not deplete the Hall generator as a source.

EXPERIMENTAL RESULTS

ELECTRICAL CONDUCTIVITY

Although the bulk of the experimental data to date is concerned with the photoresponse of conductivity as a manifestation of absorptance change, two problems are approached experimentally prior to serious investigation of photoresponse. These are the problems concerning the usefulness of electrical parametric measurements in polycrystalline samples and the question of the relative roles played by charge carrier density and carrier mobility in the increase of sample conductance.

Increase of sample conductivity will be considered, for the purpose of subsequent investigation, as manifestation of optical degradation of the zinc oxide (increase of solar absorptance). Since there exist some reservations concerning the usefulness of electrical parametric measurements of particulate samples, a first experiment was conducted to indicate the reliability of the conductivity-absorption association.

A 1500 Å film was irradiated and the transmitted intensity was detected by the 1P28 phototube. The output of the 1P28 is in volts. Simultaneously, sample conductivity was being measured. A plot of $\log (v/v_0)^{\frac{1}{2}}$ versus conductivity (Figure 6) shows, within experimental error, a linear relation. This is the result expected from treating the transmitted radiation as a traveling, electromagnetic, plane wave, in an absorbing medium. This treatment, from ordinary electromagnetic theory, gives

$$\log (v/v_0)^{\frac{1}{2}} = \text{constant } \sigma t \qquad (1)$$

where

v/v_0 - normalized voltage output of the 1P28 phototube,

σ - conductivity,

t - film thickness.

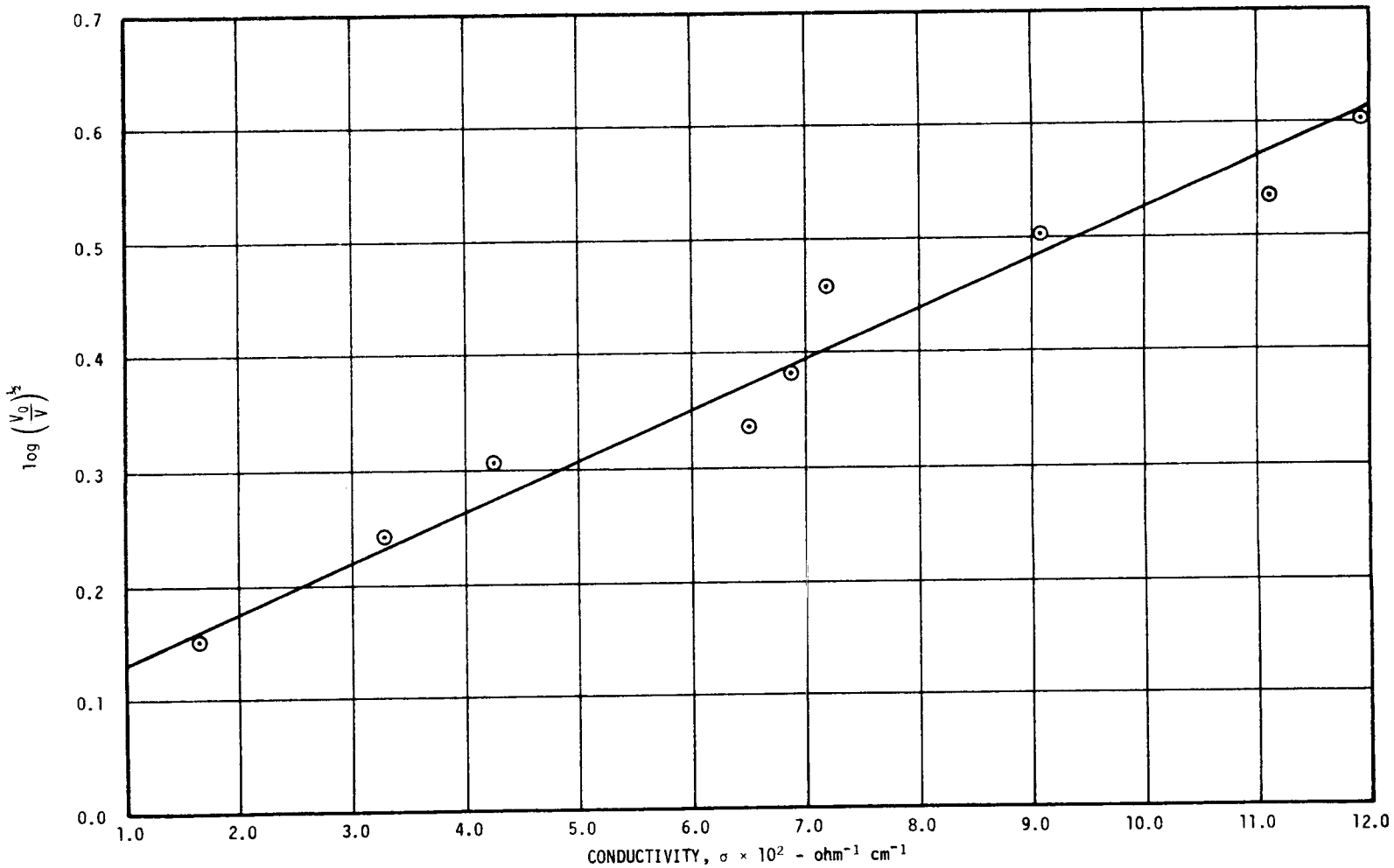

Figure 6. Relative Transmission of Unfiltered Ultraviolet as a Function of Zinc Oxide Film Conductivity

It can be concluded, then, that for polycrystalline zinc oxide films a direct correspondence between measured conductivity and absorptance can be meaningfully established.

HALL MEASUREMENTS

Hall measurements on thin, polycrystalline, zinc oxide films in vacuum were made next. A number of motivations can be cited for this departure. Obviously Hall measurements should provide at least another opinion on the relative importance of mobility and carrier density in the variable absorptance coefficient phenomena. Additionally, if a model for the degradation mechanism is proposed on the basis of subsequent investigation, mobility and charge carrier density data would be of use in establishing the validity of the model. Finally, such information would have comparative value since the earlier quoted mobilities of polycrystalline zinc oxide referred to surface mobilities primarily, as defined by field effect measurements.[2]

The subject film for Hall test was evaporated at a rate of 18 Å/sec to a thickness of 1070 Å.* This is a moderate evaporation rate, producing relatively large crystallites for a given substrate temperature. This particular film was evaporated at a residual pressure of 1×10^{-6} torr, exhibiting a resistance of 1.75 ohms at the conclusion of evaporation. At the conclusion of oxidation, the film's resistance was 2.25×10^{12} ohms. These values correspond to $\rho = 3.5 \times 10^{-6}$ ohms-centimeters for the metal as evaporated and 6.75×10^{6} ohms-centimeters for the oxide. Although the former value agrees well with the accepted value of $6\text{-}8 \times 10^{-6}$ ohms-centimeters for zinc metal, the latter value of the oxide cannot be properly compared inasmuch as there is a large range of reported values for polycrystalline zinc oxide. Suffice it to say that the value falls many decades

*Upon oxidation, film thickness grows to 1500 Å.

short of the value expected of a pure single crystal of zinc oxide. This is attributed, for the most part, to the faults, vacancies, dislocations, frequent terminations of lattice potential and the myriad of similar defects found in polycrystalline structure which gives rise to a continuum of donor levels just below the conduction band, many of which are thermally excited even at room temperature.

After being subjected to vacuum for several hours, prior to first measurements and irradiation, the film resistance under dark conditions had decreased to 4×10^9 ohms. This change was entirely due to placement in the vacuum as is substantiated later. This occurrence was the first indication of the extreme sensitivity to be observed in the thin zinc oxide conduction mechanism.

With the system arranged in the measurement mode as depicted in Figure 4 (with the exception of the electromagnet, which is lowered over the pyrex column so as to center the film on the magnet axis), a control current was passed along the axis of the film. For Hall measurements the source was usually a dry cell on the order of 1 to 3 volts. Typical energy dissipation in the film was limited to one microwatt in order to prevent joule heating. Simultaneously, the ultraviolet source is energized, the transmitted portion of which is received by the 1P28 phototube.

Prior to the energizing of the ultraviolet source, Hall measurements were attempted without success. Even after the ultraviolet source was energized, no Hall voltage could be read until the sample had degenerated from 4×10^9 ohms to the 10^7 ohms range. However, once this threshold had been reached, the Hall voltages were definite and reproducible. The measurement circuit was completely electrically shielded during these measurements in order to keep the noise to a minimum.

Hall measurements were continued at appropriate intervals as degradation of the film continued under unfiltered irradiation from the Hanovia source.

The Hall data resulting from this experimentation is shown in Table 2. Charge carrier density, calculated from the Hall coefficient, is shown in Figure 7 as a function of duration of irradiation (hence degree of degradation). The range of the calculated carrier density appears to be reasonable over the three thousand minute period of irradiation.

It is interesting to note that Karpovich and Zvonkov[3] observed approximately the same range of charge carrier density ($10^{14} \rightarrow 10^{17}$ carrier/cm^3) in thin polycrystalline film of the II-VI compounds of CdS and CdSe. In this experiment however, thermal dependencies were under investigation. Also, in the same work these investigators found similar mobility phenomena which will be discussed shortly. In addition, Heiland[2] found upon investigation of ZnO film prepared in the same manner as those of this investigation and of the same thickness, that the maximum charge carrier density attainable by reducing the film with atomic hydrogen was 10^{18} carriers/cm^3, thereby establishing an upper limit to carrier density expected from photodesorption of oxygen and consistent with our apparent maximum of 10^{17} - 10^{18} carriers/cm^3 by extrapolation.

While it cannot be denied in view of data yet to be presented in this work that oxygen desorption is the controlling mechanism of photodegradation of zinc oxide, it is equally obvious that the mechanism is somewhat more complicated than would be indicated by considering the Elovich desorption rate. It is obvious that the carrier creation rate does not correspond to the Elovich desorption rate.

Figure 8 shows the behavior of carrier mobility as photodegradation develops. The extreme dependency of mobility on degradation level is striking. Such an unexpected behavior, particularly in the first seconds after the threshold measurement, causes justified suspicion. However, in the work of Karpovich and Zvonkov,[3] as mentioned above, a decreasing mobility was observed when charge carrier density increased in similar polycrystalline materials. It appears that this cannot be simply

TABLE 2

EXPERIMENTAL DATA

Control Current (amps)	Calculated Resistance (ohms)	Hall Current (amps)	Hall Voltage (volts)	Hall Constant, R_H (cm^3/coul)	Majority Carrier Density (n/cm^3)	Conductivity, σ (Ω^{-1} cm^{-1})	Mobility, μ (cm^2/V-sec)	Transmission Signal (Vac)	$(V/V_0)^{1/3}$	$(V_0/V)^{1/3}$	log $(V_0/V)^{1/3}$	Lapse Time (min)
0.5×10^{-6}	24.00×10^{6}	40.0×10^{-13}	45.0×10^{-3}	28,700	2.18×10^{14}	1.64×10^{-2}	4.70×10^{2}	52	0.862	1.16	0.1475	10.
1.0×10^{-6}	12.00×10^{6}	9.0×10^{-13}	9.9×10^{-3}	3,140	1.99×10^{15}	3.27×10^{-2}	1.03×10^{2}	40	0.755	1.33	0.2860	50
1.3×10^{-6}	9.25×10^{6}	7.8×10^{-13}	7.8×10^{-3}	1,900	3.30×10^{15}	4.24×10^{-2}	8.05×10^{1}	38	0.737	1.36	0.3080	140
2.0×10^{-6}	6.00×10^{6}	5.0×10^{-13}	5.0×10^{-3}	800	7.85×10^{15}	6.53×10^{-2}	5.20×10^{1}	36	0.717	1.40	0.3360	290
2.1×10^{-6}	5.71×10^{6}	5.0×10^{-13}	5.0×10^{-3}	760	8.24×10^{15}	6.85×10^{-2}	5.20×10^{1}	34	0.697	1.44	0.3850	650
2.2×10^{-6}	5.45×10^{6}	3.5×10^{-13}	3.5×10^{-3}	510	1.24×10^{16}	7.20×10^{-2}	3.63×10^{1}	28	0.632	1.58	0.4590	1130
6.2×10^{-6}	3.87×10^{6}	3.0×10^{-13}	3.0×10^{-3}	150	4.05×10^{16}	10.10×10^{-2}	1.56×10^{1}	26	0.609	1.65	0.5020	1655
6.8×10^{-6}	3.53×10^{6}	2.0×10^{-13}	2.0×10^{-3}	94	6.70×10^{16}	11.10×10^{-2}	1.04×10^{1}	24	0.586	1.71	0.536	2885
7.4×10^{-6}	3.25×10^{6}	1.9×10^{-13}	1.9×10^{-3}	82	7.65×10^{16}	12.05×10^{-2}	9.85×10^{0}	21	0.548	1.83	0.6050	3410

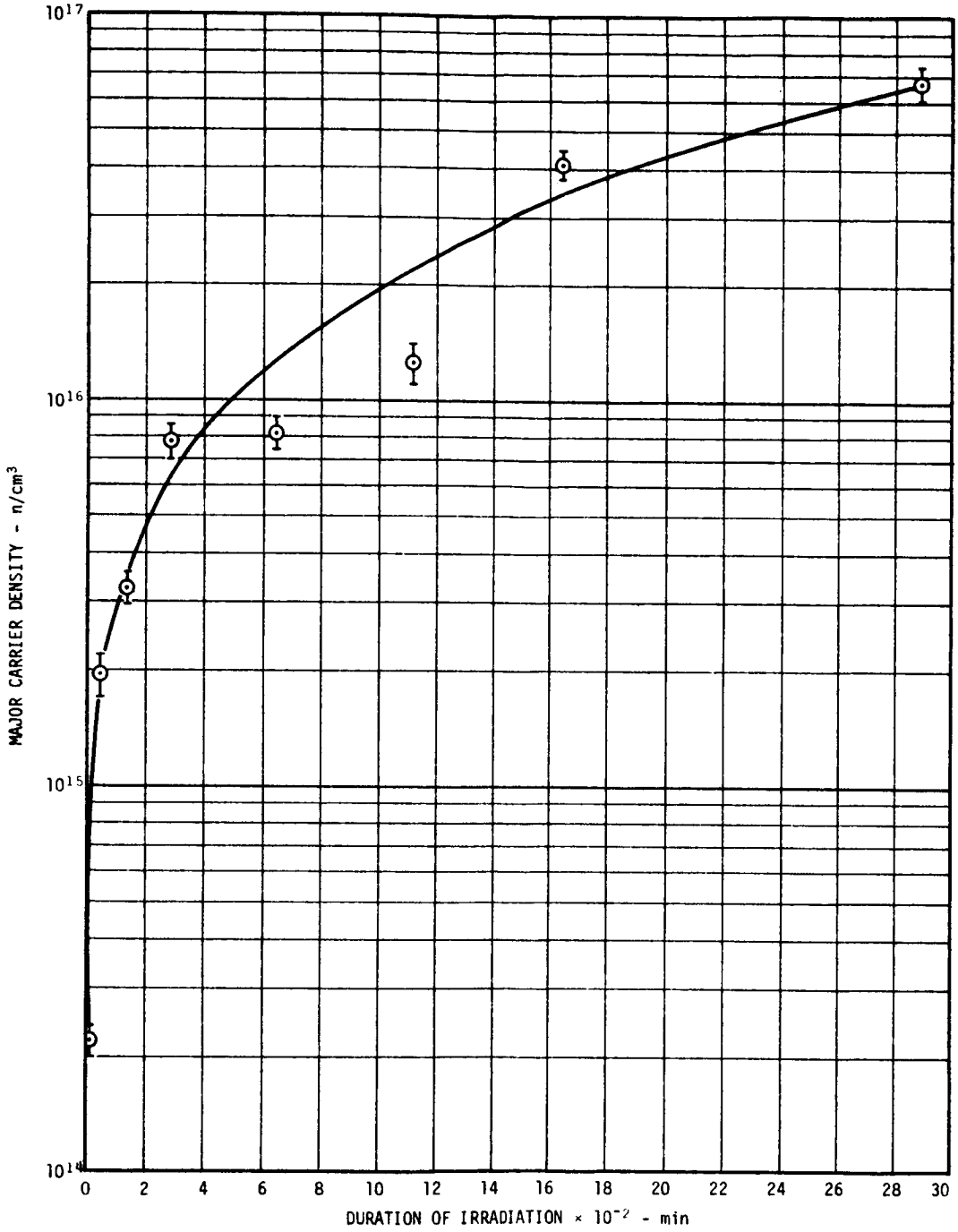

Figure 7. Majority Carrier Density as a Function of Duration of Unfiltered Ultraviolet Irradiation

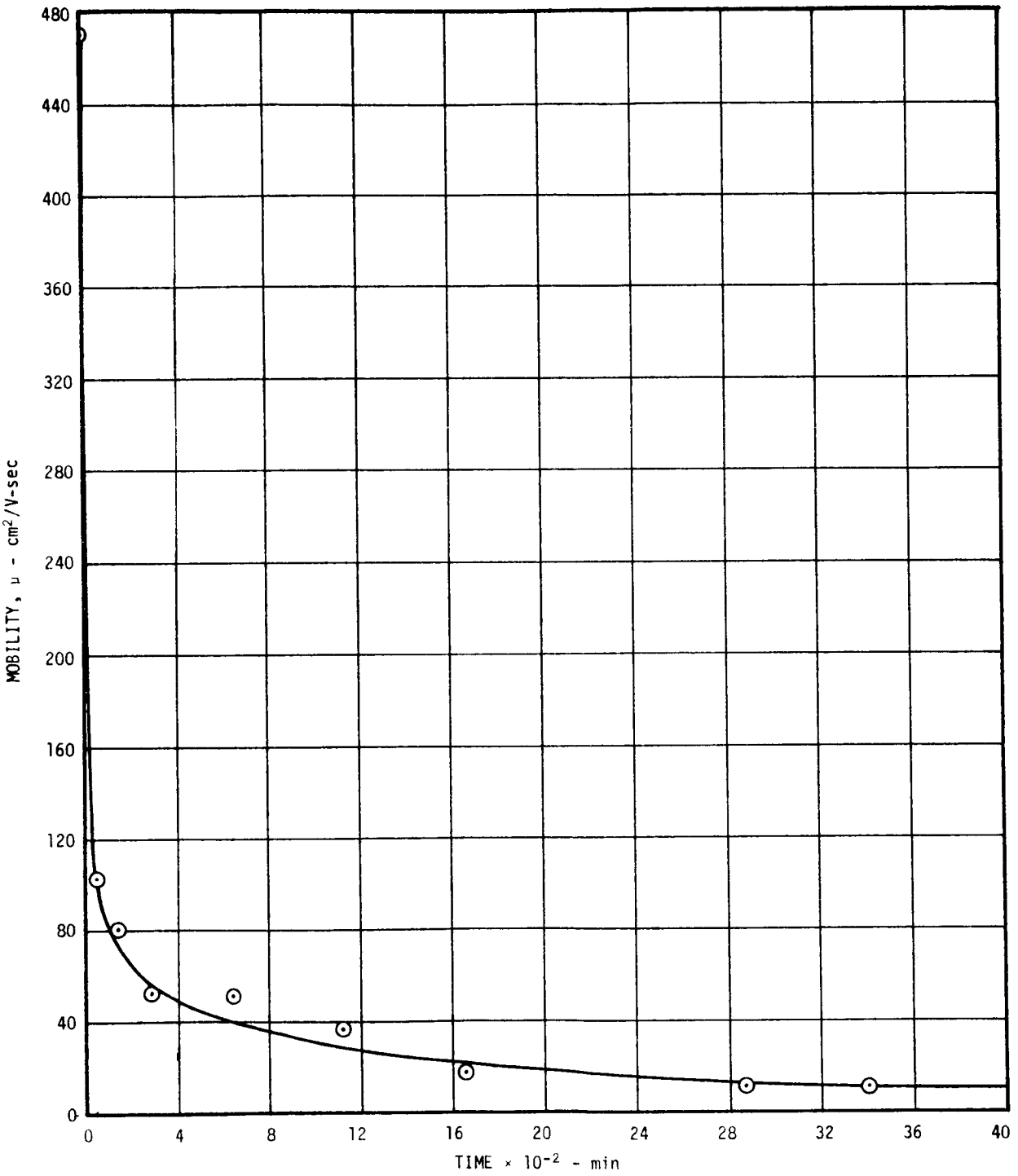

Figure 8. Majority Carrier Mobility as a Function of Time for Steady, Ulfiltered, Ultraviolet Irradiation

explained as a decrease in mean free path length due to the increase of scattering cross section of atomic sites thermally excited. The conduction in this case and their[3] case is widely held as a surface phenomenon and not classical crystal bulk conduction. The fact that as charge carriers are supplied to the conduction band, a similar number of scattering centers in the form of zinc ions are created, might indeed explain part of this behavior.

Conductivity and Hall coefficient are the two measurables. Mobility is not only an expression of a physical condition (mean free path length), but also serves as a constant of equality in the relation given by

$$\sigma = ne\mu \tag{2}$$

where

- n - charge carrier density in carriers/cm^3,
- e - electron charge in coulombs,
- μ - carrier mobility in cm^2/V-sec.

Also from Equation 3,

$$n = -\frac{1}{Re} \tag{3}$$

where R is the Hall constant in cm^3/coulomb, it can be appreciated that the results may be interpreted in more than one way:

(1) The measurement of conductivity and charge carrier density, by independent measurements are correct and hence carrier mobility does indeed behave as shown in Figure 8. Explanation of this behavior is left to some logical phenomena such as an accompanying generation of scattering centers.

(2) The mobility behavior is anomalous and it results from erroneously large measurement of Hall coefficient or an erroneously large measurement of film conductivity. The fact that these measurements progress in a smooth, continuous manner throughout the degradation process does not, however, lend support to this contention.

(3) The conductivity and Hall coefficients are individually and independently accurate, and the anomaly generated in the mobility as a result of demanding the equality of Equation 2, does not represent crystallite mobility, but an effective mobility. The effective mobility expresses the influence of the complex nature of grain to grain conduction.

Depletion of Hall contacts as a source initially cannot be argued, since not only is the required measurement drain current five to six orders lower in magnitude than the control current, but such an effect would be to decrease the Hall coefficient, not increase it as would be necessary to produce the observed effect.

The solution presented in (3) above appears the most promising. Schrieffer,[1] following the methods of Fuchs[4] and Sondheimer[5] concerning the conductivity-mobility relationship in thin metallic films, adopted the treatment of metallic films to consider semiconductive films. The principal point is that Schrieffer considered the space charge field resulting from the surface charge, a condition not existing in the metal films. The results of his work which principally concern this work are shown in Figure 9 as taken from J. R. Schrieffer's paper.[1] Essentially the ratio of effective mobility to bulk mobility is plotted versus the band depression in electron volts.

It must be recalled that Schrieffer's work considers a p type semiconductor, so the energy bands bend downward at the surface. Therefore, to interpret Figure 9 in terms of the n-type zinc oxide, consider that as the abscissa value decreases, it is corresponding to an upward band bending for the n-type model.

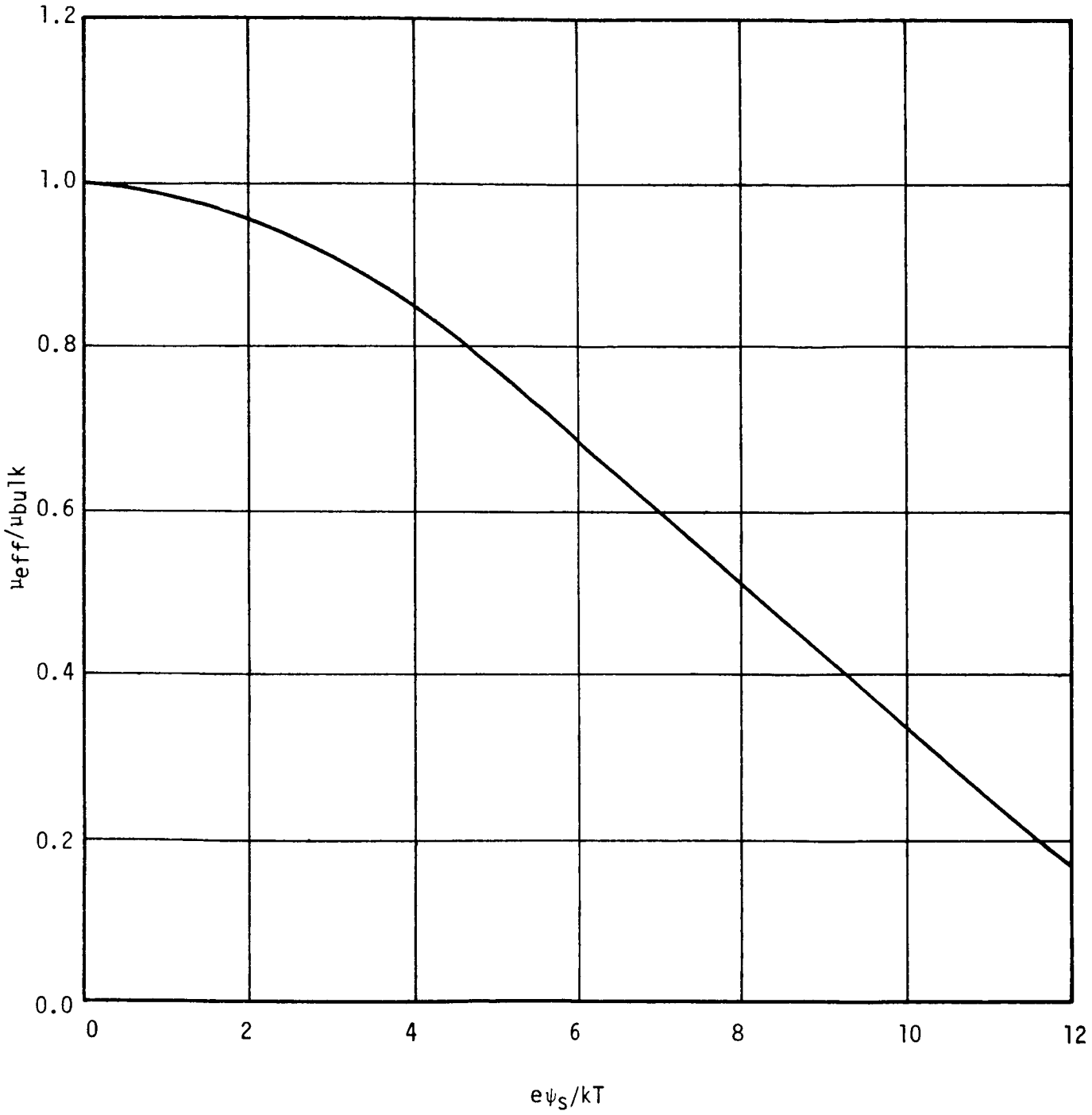

Figure 9. Effective Mobility as a Function of the Depression of the Energy Bands at the Surface (reproduced from Reference 1)

Principally the qualitative support sought from this figure can now be seen. The figure shows that as energy bands are depressed, the effective mobility decreases. This is the very same phenomena observed experimentally and shown in Figure 8. As the zinc oxide is degraded, the upward bending of the energy bands is decreased, the accompanying reduction in measured (effective) mobility being very much in evidence in Figure 8. On the basis of this argument it would also be expected that the mobility would be time dependent as shown, for time rate change of space charge field should follow the general degradation curve, exhibiting an initial quasi-fast response. Therefore, the mobility should have this time form also, which it does.

PHOTOCONDUCTION

Photoconductivity has been studied in continuous zinc oxide films of 425 Å, 730 Å, 1000 Å, and 1500 Å. Principally a short term study is made of photoresponse and recovery since the mechanisms controlling the response are most apparent immediately after initiation of irradiation and immediately after cessation of irradiation. The parameters influencing the photoconduction which are studied are ambient pressure, temperature, energy of spectral radiation, and sample (film) thickness.

Without developing a specific model, we shall view the results in light of a "best guess" modified Wilson semi-conductor model as shown in Figure 10 as a point of departure. This model simply shows the zinc oxide characteristic band gap of approximately 3.2 eV and a quasi-continuum of donor states extending from immediately under the conduction band downward to some arbitrary lower limit. At present the means by which one might make a reasonable estimate of the donor level range is not available. The Fermi level for the moment is arbitrarily placed in this donor level spectrum, insuring some filled donor levels. There is good basis for the placing of the Fermi level in such a manner, for polycrystalline zinc

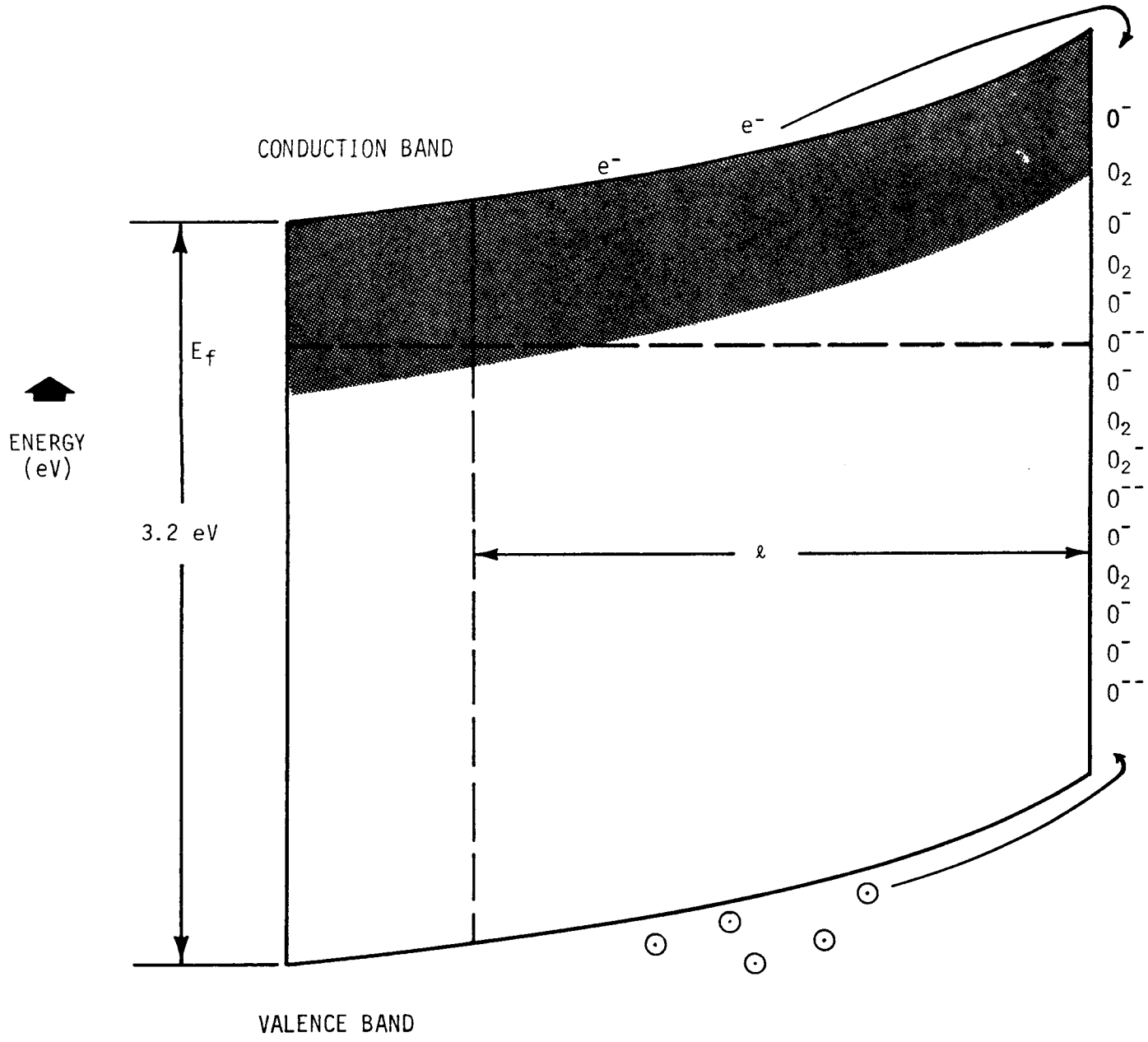

Figure 10. Particulate Zinc Oxide Degradation Model

oxide, in the dark, at room temperature indicates resistivities of 10^8 to 10^9 ohms-centimeters at least. This appears to indicate that a majority of these carriers are coming predominantly from donor levels on the order of 0.025 electron volt below the conduction band and that these levels appear to be degenerate. Krusemeyer[6] found effective mobilities in zinc oxide crystals of the same value of mobilities recorded in this work only when the Fermi level coincided with the conduction band edge.

In Figure 10, the Schottky barrier depth is shown to be influencing nearly the entire bulk of the particulate sample, making both bulk and surface conductivity sensitive to surface charge. The figure shows, as possible absorbed gas, singly and doubly ionized monatomic oxygen and physically absorbed diatomic oxygen.

In examining photoresponse and subsequently attempting to link this phenomena to optical damage of the zinc oxide, there are inherent difficulties. Primarily, material conductivity is considered as the manifestation of optical damage; however, it has been shown that there is not a simple one-to-one correspondence.[7] Upon irradiation, the initial increase of conductivity does not affect the absorption spectra as hoped, with the exception of perhaps a small change in the relatively insignificant (thermodynamically) free carrier absorption. Hence, in examining the photoresponse data, the initial, quasi-fast response must be assumed to be an electronic response, coupled with the initial fast desorption of surface oxygen.

To support the statement that desorption-absorption of oxygen can occur rapidly enough to play a role in the quasi-fast response observed, examine in Figure 11 the response as recorded by a polaroid time exposure of an oscilloscope display of this phenomenon. It is obvious that the quasi-fast response is most readily observed under 3650 Å irradiation. The principal fast rise time appears to start at about three seconds (this measurement was carried out under 10^{-7} torr vacuum). Now compare in Figure 12 the voluntary response of the same film (1500 Å) and a thinner film

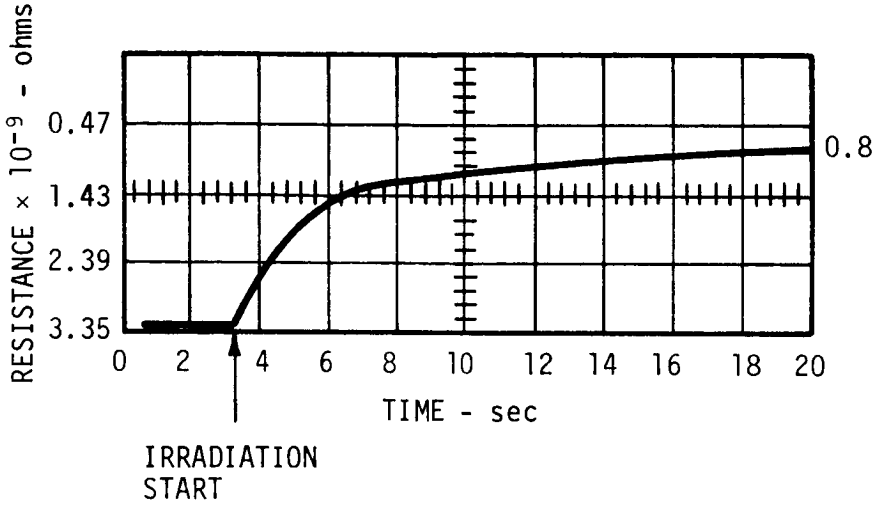

Fast Photoconductivity of Zinc Oxide
Film Under 3650Å Irradiation

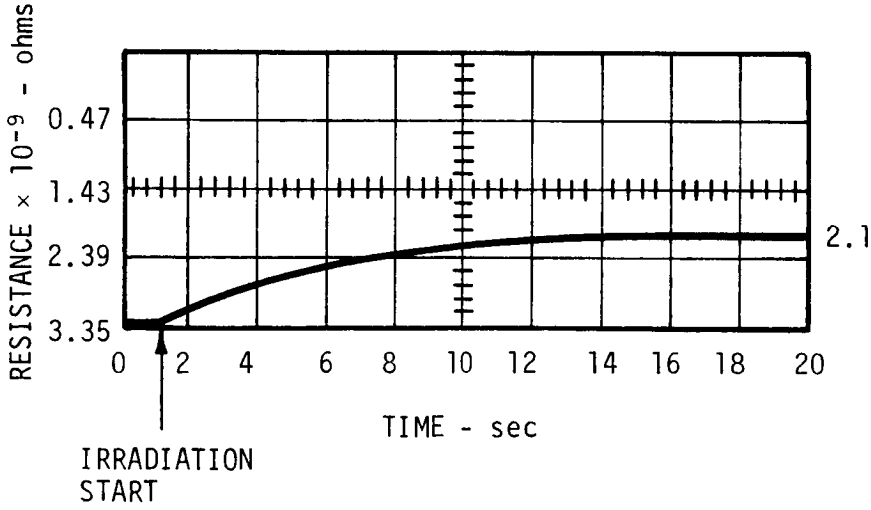

Figure 11. Fast Photoconductivity of Zinc Oxide
Film Under 5600Å Irradiation

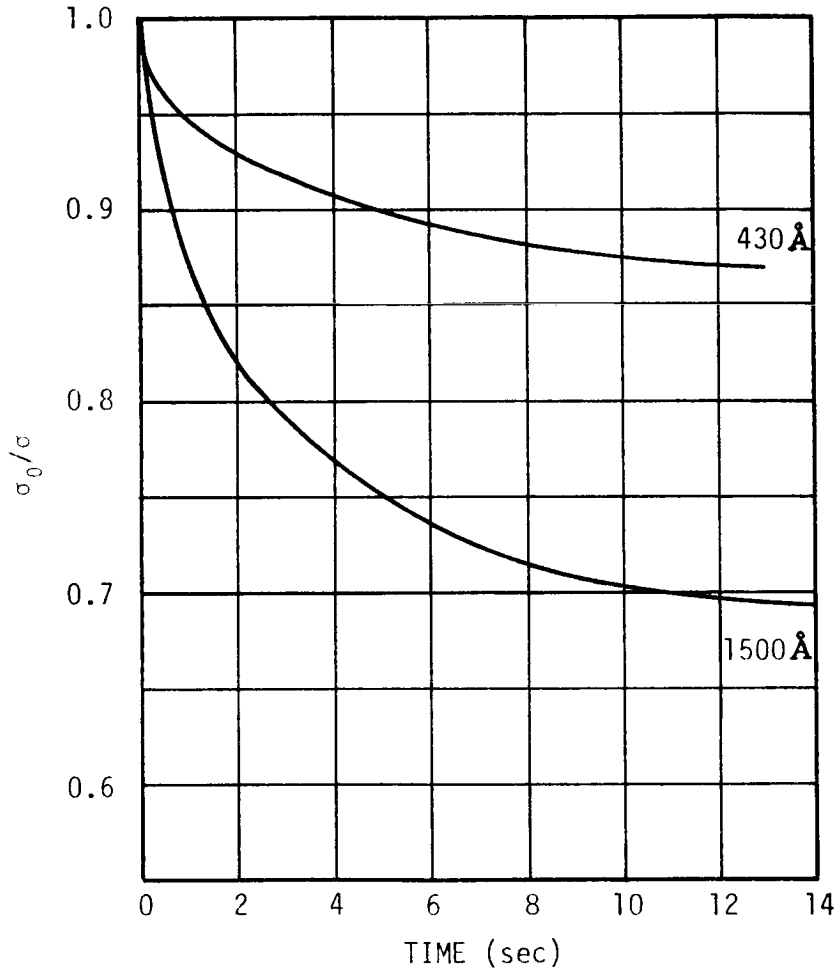

Figure 12. Recovery of Degraded Film Upon Admission to Atmosphere

(425 Å). The films have been degraded and then left under dark vacuum conditions for several hours. The films are then suddenly exposed to the atmosphere and their respective responses recorded. It is apparent that a considerable part of the recovery does occur within the 3-second, quasi-fast response. Although a similar degradation measurement could not be made due to the lack of instant vacuum, it is felt in view of the ready decrease of film resistance as the system is pumped that a similar degradation action can be expected.

To assume that this physical process is aided over this long time lapse by electronic response might be somewhat surprising; however, due to the probable strong trapping to be encountered, an electronic response time on the order of tenths of seconds and seconds is not inconsistent. It will then be assumed, for all intents and purposes, that the slow photoconductivity is associated almost entirely with desorption of oxygen and is indicative of optical damage. Radiation levels have been maintained at low levels in order to better evaluate the response.

Some resistance data is presented in Figure 13. Resistance data is to be considered raw data, not in a form to be used as comparative data unless compared against data for the same film as is the case in Figure 13. A 1500 Å film was irradiated in vacuum with three different spectral energy levels, 5600 Å, 4350 Å, and 3650 Å. The intensity of the 4350 Å and 3650 Å were the same, the 5600 Å being about 25 percent of either of the former. It is quite obvious then that degree of response is not in one-to-one correspondence with intensity. The points to notice at this stage are that

(1) Apparently degree of photoresponse is sensitive to spectral energy level,

(2) The slow degradation slope appears to be nearly constant for the three different conditions, while the quasi-fast response is not,

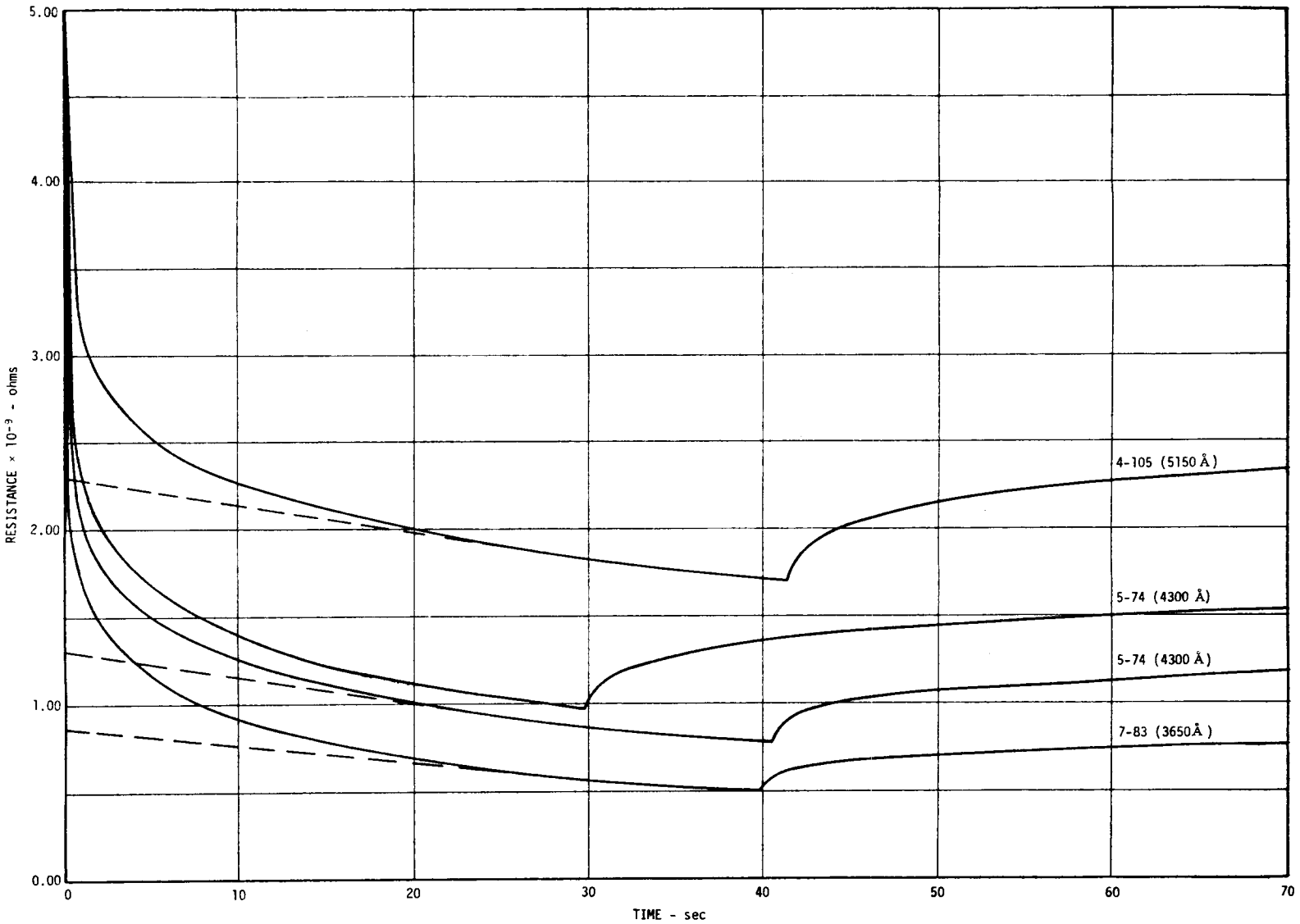

Figure 13. Photoresponse and Recovery for Three Energy Levels of Irradiation as a Function of Time

(3) Apparently both the quasi-fast and slow recovery response are dependent on radiant spectral energy and length of exposure.

It is quite natural to expect (1), for increased spectral energy allows the pumping of lower lying donor states and valence levels. These states lying closer to the Fermi level have a higher occupancy density, resulting in the greater response. It is quite probable that most of the donor states are degenerate (lying below the Fermi level) and are pumped even by the least energetic radiation (5600 Å).

Consideration of (2) will be the basis of more detailed investigation later. From (2) it will be inferred that if the slow process is relatively independent of the fast process, these two major segments of photoresponse can be examined as to extent and rate dependence upon the variable parameters already mentioned above.

Apparently history comparison, along with rate of change data as effected by variation of the above parameters, would be beneficial in examining recovery data, ultimately attempting to integrate the results in a compatible fashion into the final report model.

With these thoughts in mind the following photoresponse measurements and analysis were undertaken. Films ranging from 425 Å to 1500 Å were examined as indicated in the experimental procedures section for photoresponse, varying temperature and pressure. Using the measurement and recording techniques already indicated, the data so obtained was fitted by a least squares routine to a curve of the form

$$R(t) = \exp(a + bt + ct^2) \qquad (4)$$

or

$$R(t) = K \exp(bt + ct^2) \tag{5}$$

where t is time lapse from the event of radiation initiation or cessation, determining the constants by the least squares computational routine. In addition $\dot{R}(t)$ was computed at each data point. Both the R(t) and $\dot{R}(t)$ curves were then plotted versus a time abscissa by the computer. Due to the bulk of this data, these curves and computation outputs are included as Appendix I. When trying to curve-fit the complete degradation section or recovery section, it was found that even the polynomial raised to the exponential could not follow the initial response well. Only by breaking the curves up into shorter segments were reasonable fits obtained. In general, no point error of more than 5 percent was tolerated.

Prior to discussing data, where temperature was a variable, consider the simplified model of Figure 14. Depicted here is the manner in which the model is expected to appear for the various temperature levels prior to irradiation. These are relative models to one another only and are not to be considered as the ultimate quantitative conception. The form of the Fermi level at the surface is a matter of conjecture, particularly for the 25°C case. For this presentation it will be assumed that the Fermi level at the surface is that of the bulk.

Having observed a significant amount of absorbed oxygen being voluntarily released in vacuum at room temperature, it is expected that this voluntary release shall increase in amount as ambient temperature is increased.

The shaded area in Figure 14 near the conduction band represents the donor-trap energy level range, distribution of which is necessarily unspecified. The band bending is again shown to effect the greatest part of the crystallite making conduction throughout the bulk of the material sensitive to surface charge.

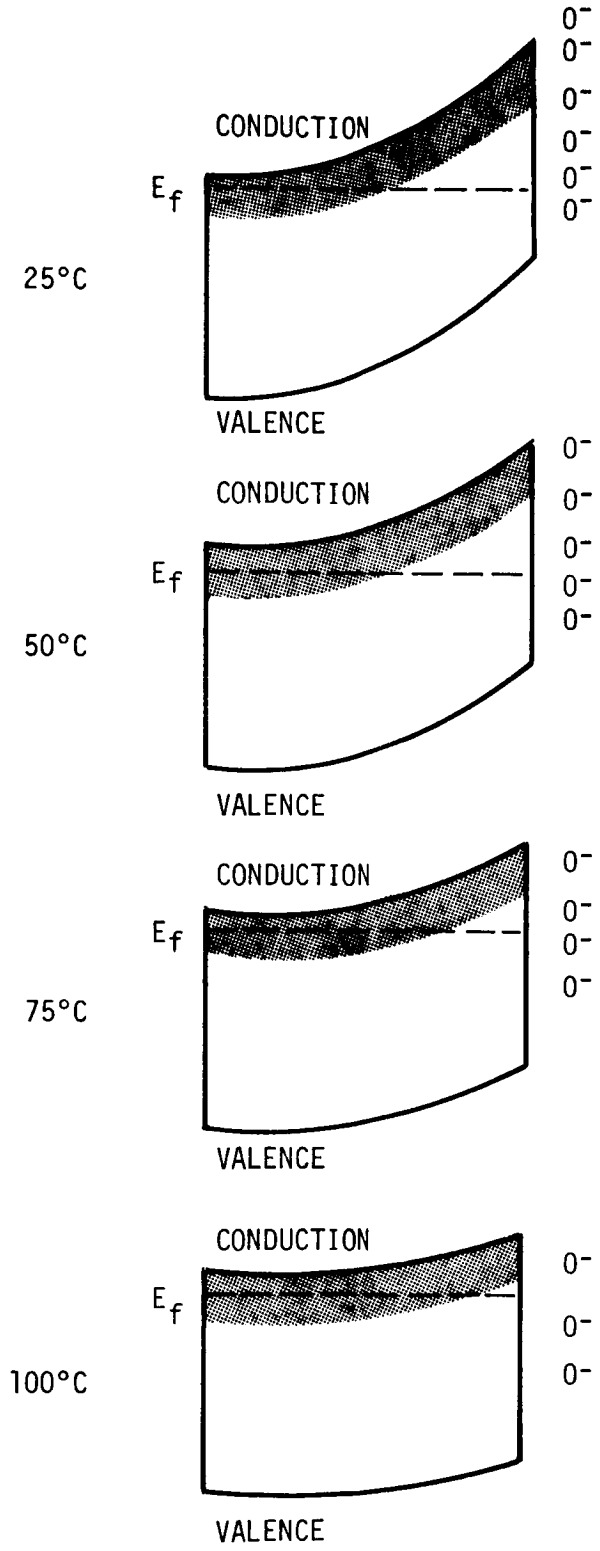

Figure 14. Expected Model at Steady State Conditions for Various Temperatures

Consider now Figures 15 and 16. In Figure 15 is shown the correspondence between photocurrent behavior and duration of 3650 Å irradiation for a 730 Å film in vacuum (10^{-7} torr) and at atmospheric pressure for ambient temperatures of 25°C and 50°C. Figure 16 shows the same data as Figure 15 for 75°C and 100°C ambient. At 25°C, considering experimental error, the data points are the same indicating little, if any, change in the degradation behavior between atmospheric pressure and 10^{-7} torr. At 50°C, however, it is seen that the photocurrent generated in a vacuum is greater than that in atmosphere by an almost constant amount for all points on the curve. This difference is about 1×10^{-10} amperes, apparently indicating that a temperature equilibration of oxygen desorption accounted for, prior to irradiation, enough oxygen desorbed to decrease the film's resistance by about 25 percent. The same phenomenon is apparent for the 75°C level. The photocurrent in vacuum is approximately 6×10^{-10} amperes larger than in atmosphere. The deviation for all points along the curve holds to this differential with impressive regularity. The corresponding reduction in resistance this time is about 35 percent. At this point on the temperature scale the regularity ends. At 100°C, the measurements at atmospheric pressure suffer a reversal of trend while the vacuum measurements do not.[8] On the strength of this evidence some tentative conclusions are warranted. The lightly bound, physically absorbed oxygen (activation energy of this oxygen is about 0.05 eV)[9] is voluntarily partially desorbed in vacuum. The extent of this absorption is dependent not only on the quality of the vacuum (actually it is shown later that the change in voluntary desorption-absorption is barely measurable for vacuum in the molecular flow region, i.e., pressure $< 10^{-3}$ torr), but also upon ambient temperature. The constant differentials between atmosphere and vacuum photocurrent data are interpreted as the result of this voluntary absorption, the process having equilibrated for a given set of state variables. Regressing for a moment it should be said that a license is exercised in labeling the ordinate of these figures concerning photocurrent

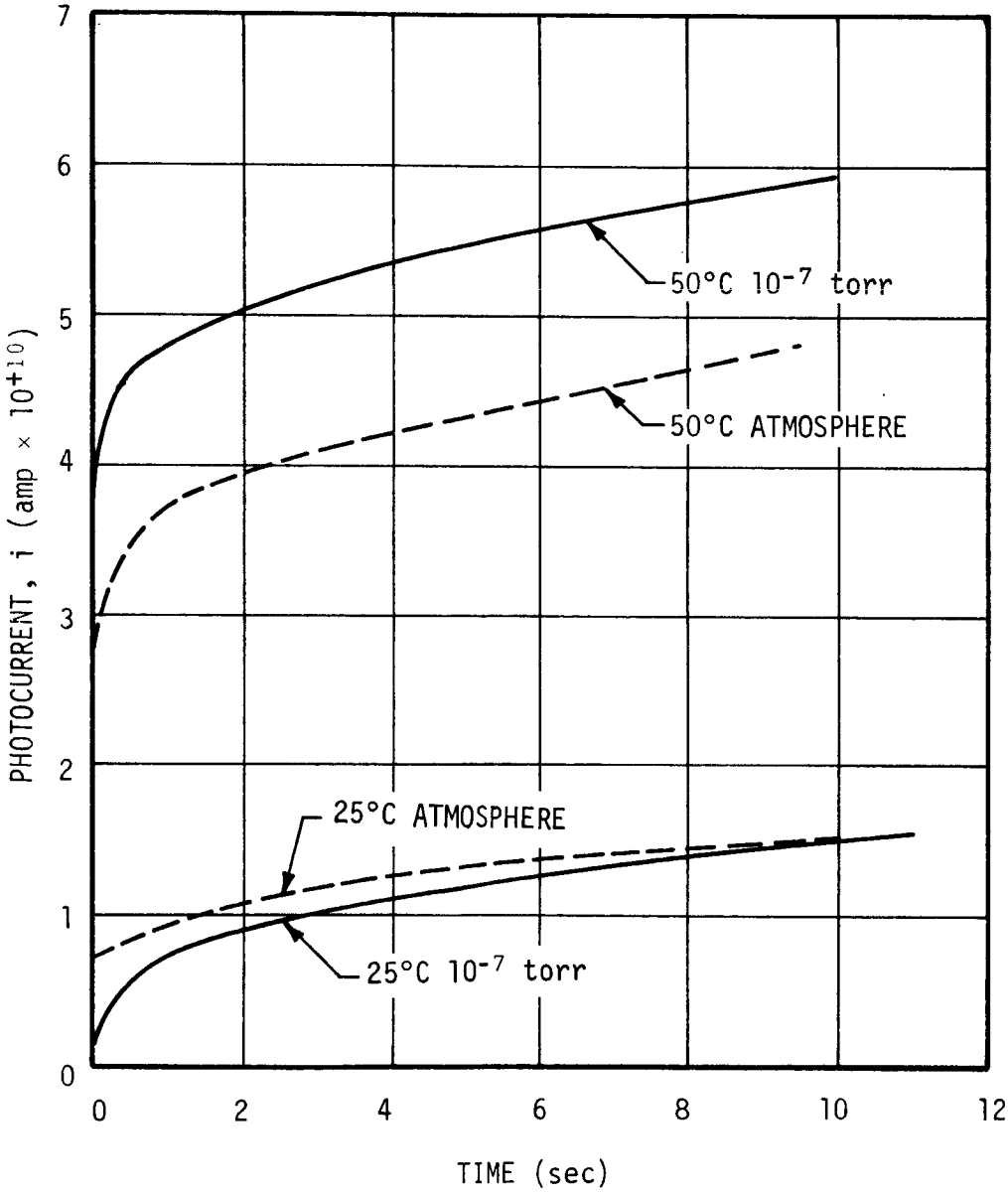

Figure 15. Photocurrent Response - 3650 Å Irradiation

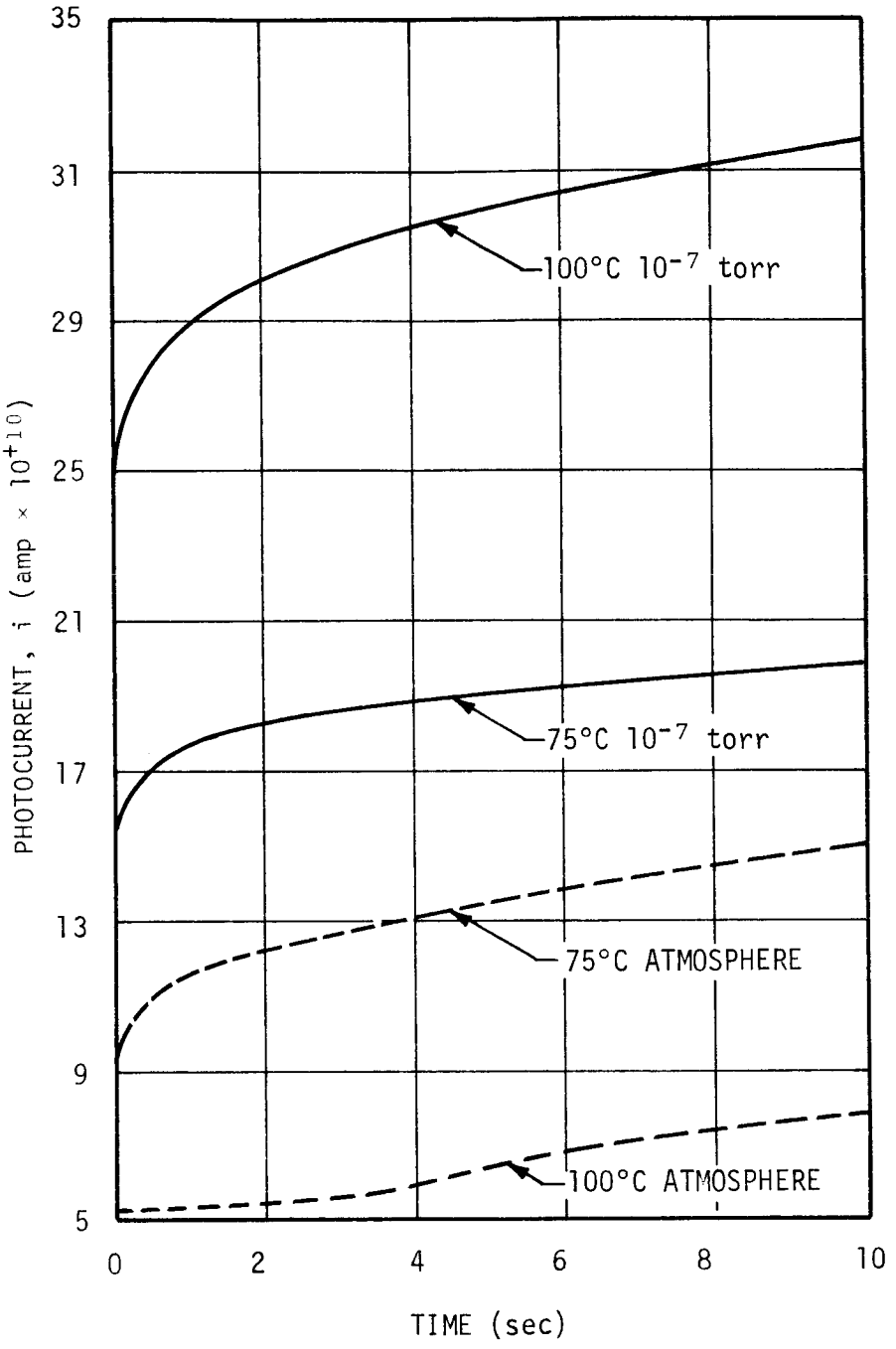

Figure 16. Photocurrent Response - 3650 Å Irradiation

inasmuch as the constant differential is also displayed on the ordinate; however, the significance is easily grasped.

The fact that the film in vacuum loses a good deal more oxygen than the same film in atmosphere can hardly be doubted. The dynamic equilibrium, establishing surface oxygen concentration for a given state of the film, is most definitely dependent upon oxygen partial pressure. If these contentions concerning the physically absorbed oxygen are accurate (recalling that earlier it was speculated that the quasi-fast photoresponse was the result of heavily trapped electronic response and desorption of physical oxygen), then Figures 15 and 16 should indicate a desensitization of the quasi-fast response, at least for the vacuum data, as the physically held oxygen is released. This trend is not apparent in either the vacuum or atmospheric data. This apparent disagreement of data with the proposed model is mitigated, however, when it is considered that as temperature is increased, the trapping effect is decreased.[10] In this light the vacuum data is qualitatively consistent with the proposed process. Unfortunately, at this time no worthwhile remark can be made concerning the quasi-fast response in atmosphere. The worth of Figures 15 and 16 will lie in the information contained in the slow responses. The kinetics of this response appear to be unaffected by ambient pressure until the temperature range of 75°C to 100°C is reached. It is then reasonable to assume that this process deals almost exclusively with the desorbed chemisorbed oxygen because it is seen that something other than oxygen partial pressure controls the kinetics of this process. Under these conditions, degradation of the film by neutralization of chemisorbed oxygen through hole diffusion, which is enhanced by elevation of temperature, is possible providing that subsequent desorption of the neutralized oxygen is not made a condition.

As seen in Figure 17, which is the recovery process at 25°C, the film recovers at a higher rate in atmosphere than in vacuum. At 50°C

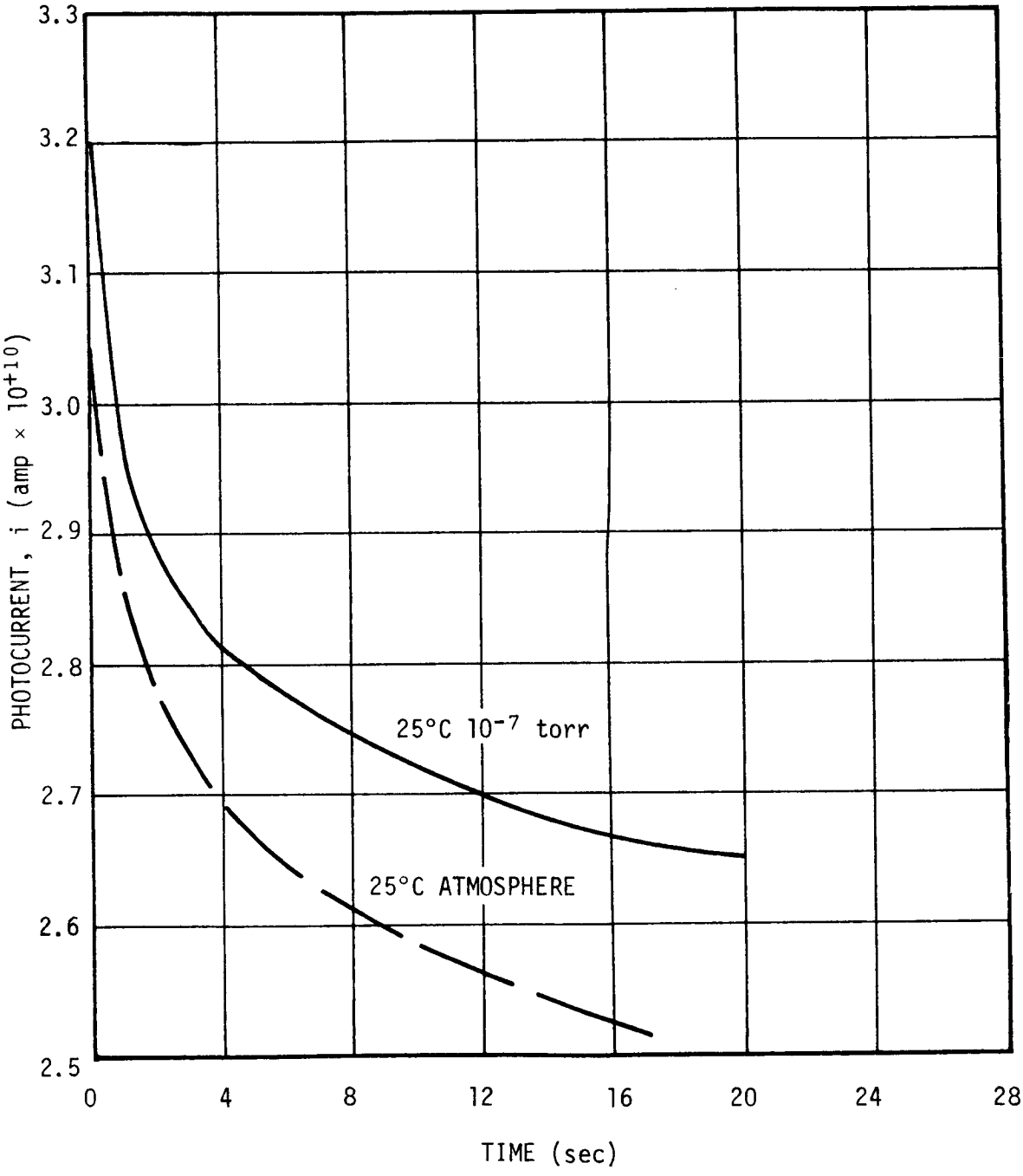

Figure 17. Photocurrent Recovery from 3650 Å Irradiation

(Figure 18) the film again recovers faster in atmosphere than in vacuum. However, relatively speaking, the difference in recovery rates at 50°C is not as great as at 25°C. At 75°C, as shown in Figure 19, there is very little difference between the slow recovery in vacuum and that in atmosphere. At 100°C (Figure 20), which is the temperature at which a reverse of trend was seen in the degradation process, the recovery in both vacuum and atmosphere appear similar, except that the vacuum recovery displays no quasi-fast recovery as does the corresponding curve for atmosphere.

Considering the dimensions of the ordinate there is evidence of strong trapping for both vacuum and atmosphere recovery processes. Additionally, it is interesting to note that while intuitively a faster recovery for both the quasi-fast and slow mechanisms is expected at temperatures greater than 25°C, the difference is almost negligible in the slow mechanism. The conclusion can then be drawn that degradation rate is almost insensitive to partial pressure of oxygen.

Now consider a new set of data taken by an identical experimental procedure on the same films as discussed above, with the only exception being that the damaging radiation is 4350 Å. Generally, the photoresponse and subsequent recovery under a given set of conditions is considerably smaller using 4350 Å irradiation than the same response using 3650 Å irradiation. Not only is the magnitude of the photoresponse smaller for this case (4350 Å), but the structure is somewhat different also. As is seen in Figure 21, at 25°C the slow processes have similar slopes in both vacuum and in atmosphere, as was the case for 3650 Å irradiation. Note that the response in vacuum exhibits no discernible quasi-fast response as do the atmosphere curves and as did the former data.

At 50°C (Figure 22), the vacuum response is seen to follow the trend of increasing initial current as temperature increases. Also the vacuum response still shows no indication of a quasi-fast response. The slow response in vacuum has increased to such a level that there is practically no correlation to the atmosphere response.

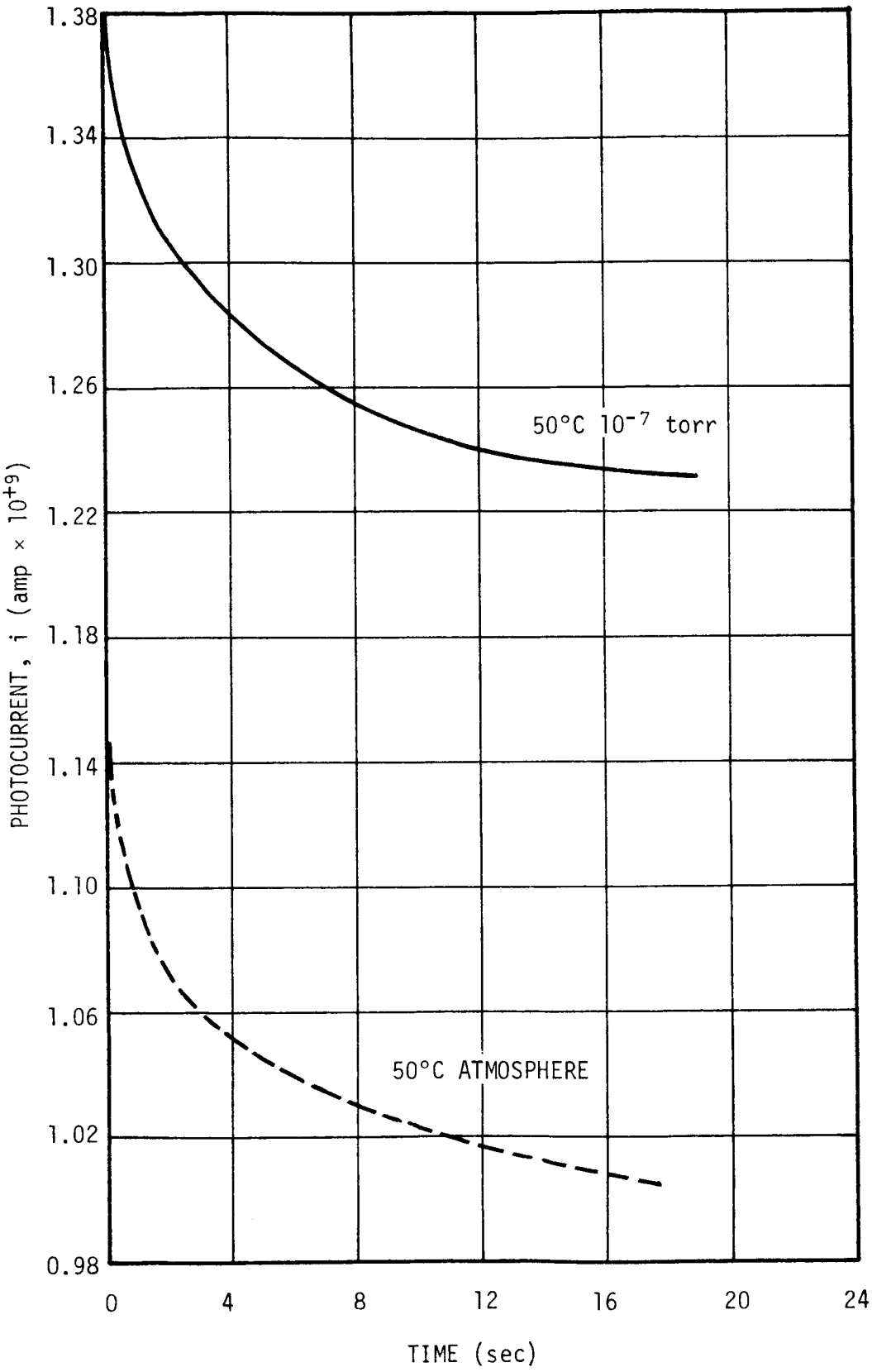

Figure 18. Photocurrent Recovery from 3650 Å Irradiation

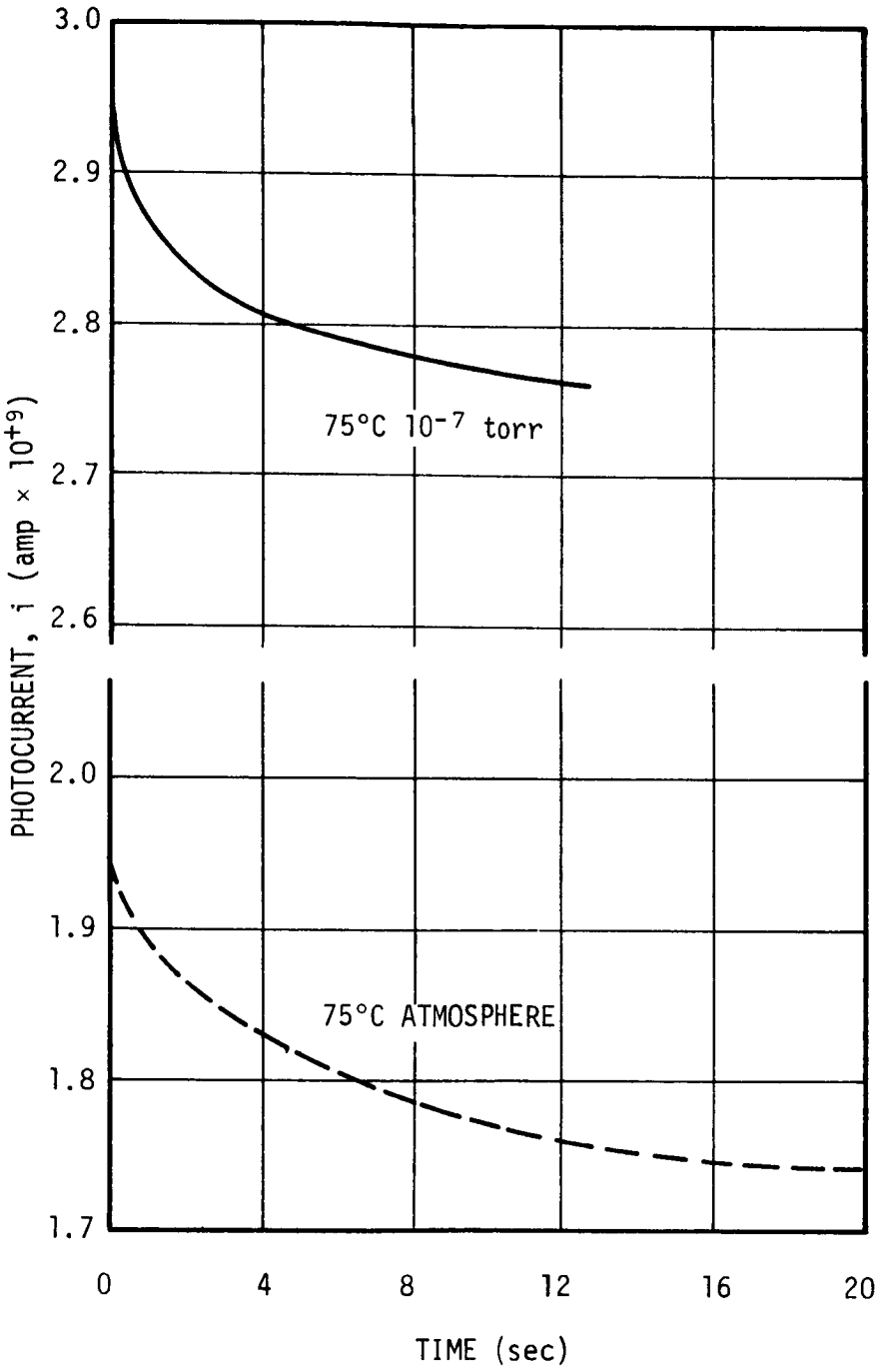

Figure 19. Photocurrent Recovery from 3650 Å Irradiation

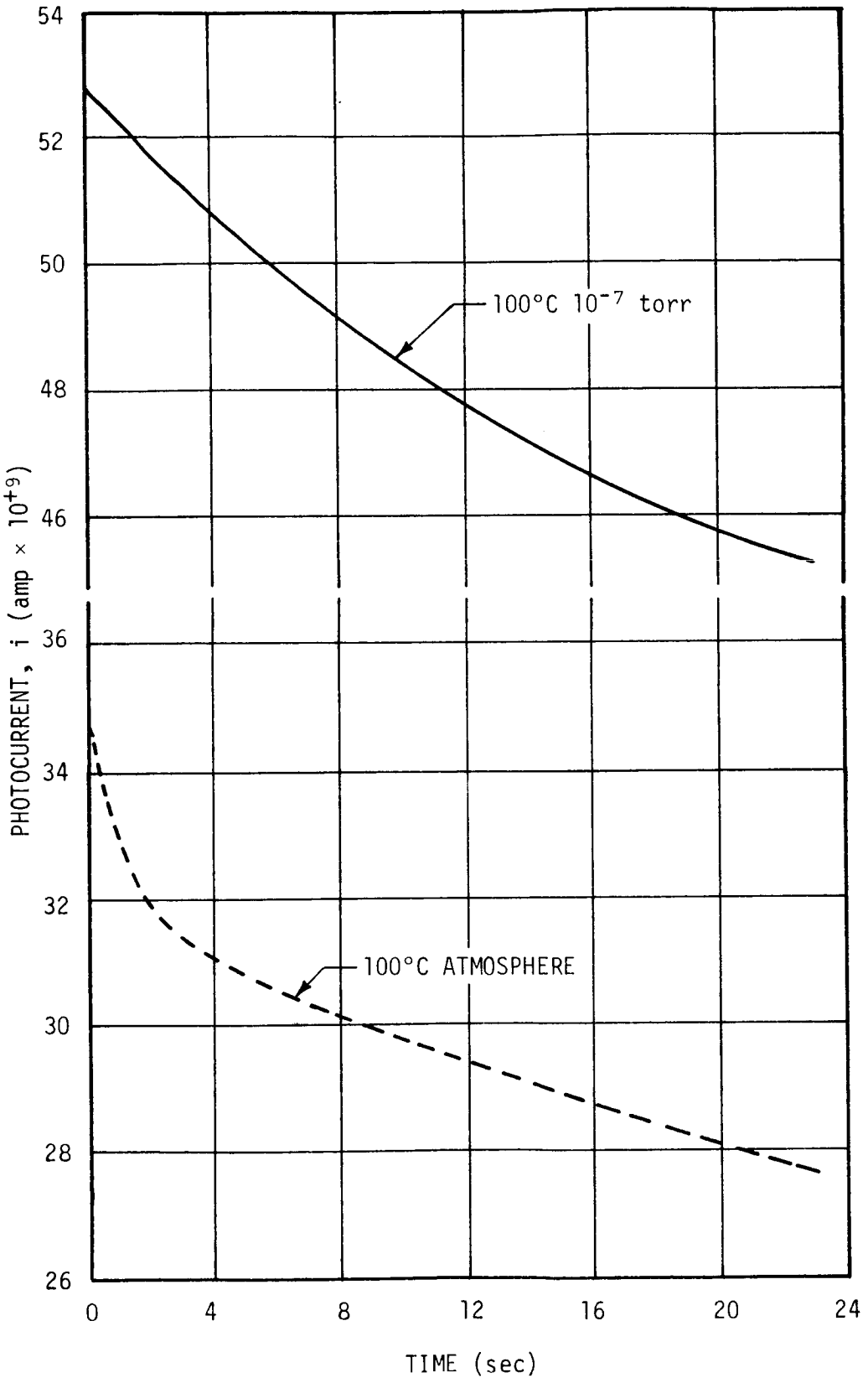

Figure 20. Photocurrent Recovery from 3650 Å Irradiation

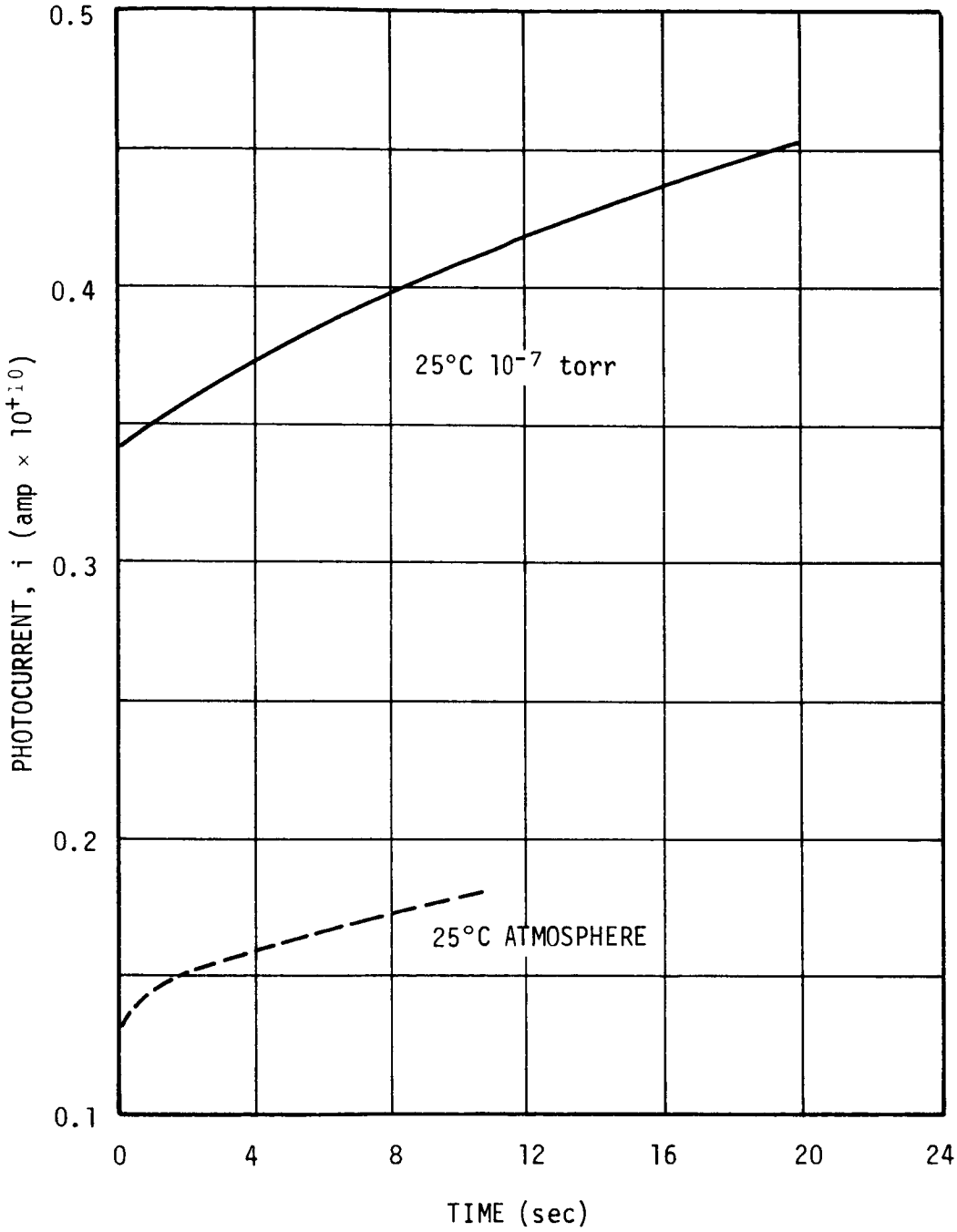

Figure 21. Photocurrent Response - 4350 Å Irradiation

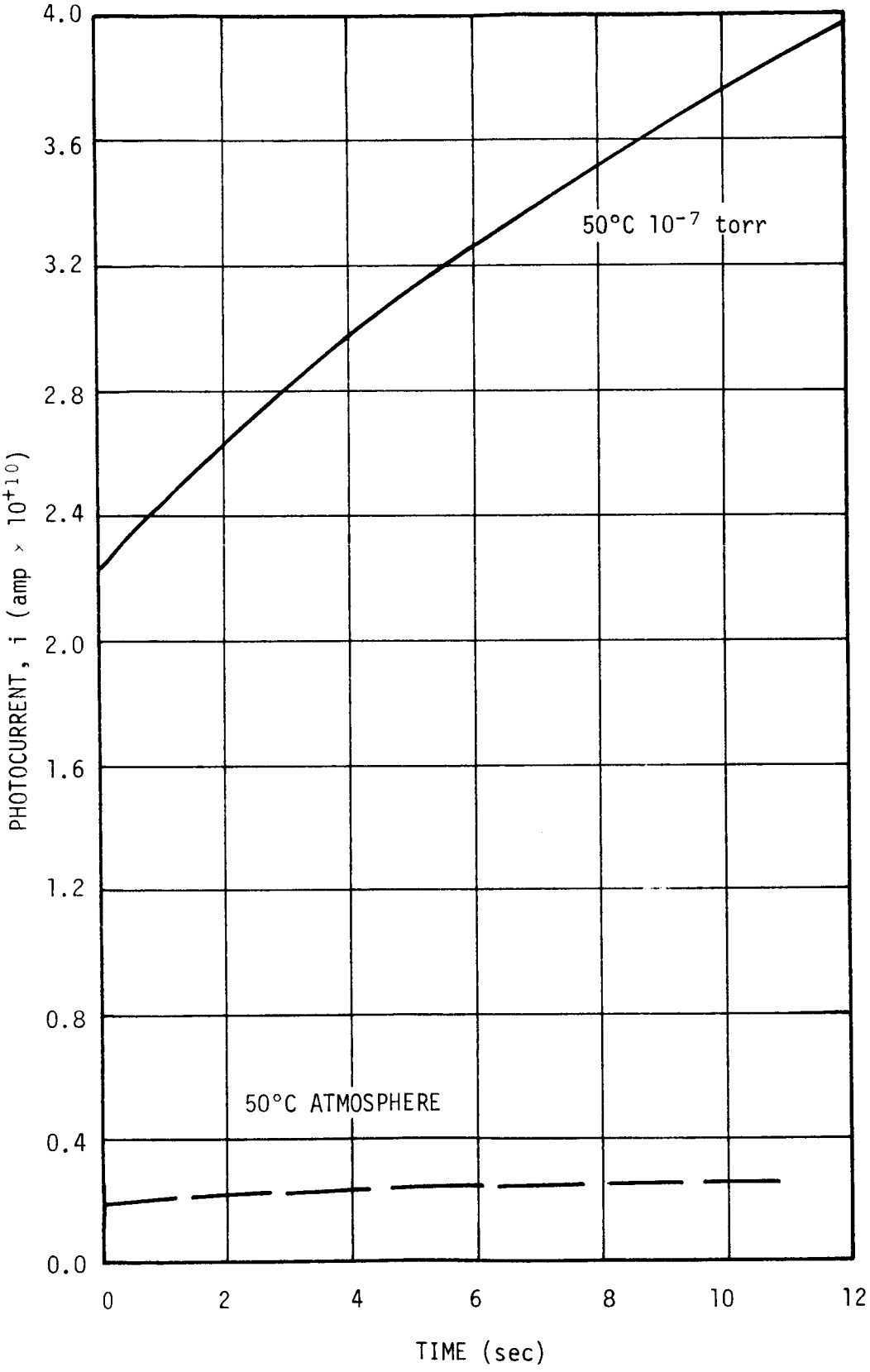

Figure 22. Photocurrent Response - 4350 Å Irradiation

Comparing the atmospheric photoresponse at 75°C with the vacuum response in Figure 23, the atmospheric photoresponse has decreased to a point below the starting level (scale has been adjusted to show structure). The vacuum response has followed the trend of increasing in initial current level, but still fails to display a quasi-fast response.

In Figure 24 (100°C), there is no notable deviation in the vacuum response trend while the atmospheric response has again begun to increase.

The fact that the quasi-fast response in vacuum and in atmosphere due to 4350 Å irradiation is practically nonexistent or very small when compared to 3650 Å irradiation response is disconcerting. The quasi-fast process was tentatively attributed to a strongly trapped electronic response combined with desorption of physically bound oxygen. Since there has been no reason to assume that the donor levels involved in this response could not be excited by the 4350 Å spectral level and since it is known that the physically bound oxygen is very lightly held (activation energy 0.05 eV), for identical incident intensities (which is the case) the response for these two spectral levels should be very nearly the same. This observation then raises serious doubts about the earlier explanation of the quasi-fast response.

The question of the small slow response in atmosphere and the compared rates of the slow response resulting from the two spectral levels of irradiation will be deferred until the recovery from 4350 Å data is discussed.

Figures 25, 26, 27, and 28 show recovery from 4350 Å irradiation for the four temperature levels in vacuum and in atmosphere. Conclusions similar to those found in examining the degradation are reached upon examining the recovery data. In general, the action in atmosphere is too small to be successfully compared to the form of the vacuum data. There is no significant quasi-fast response and trend reversal, with respect to initial currents, is found at 75°C for both vacuum and atmospheric data.

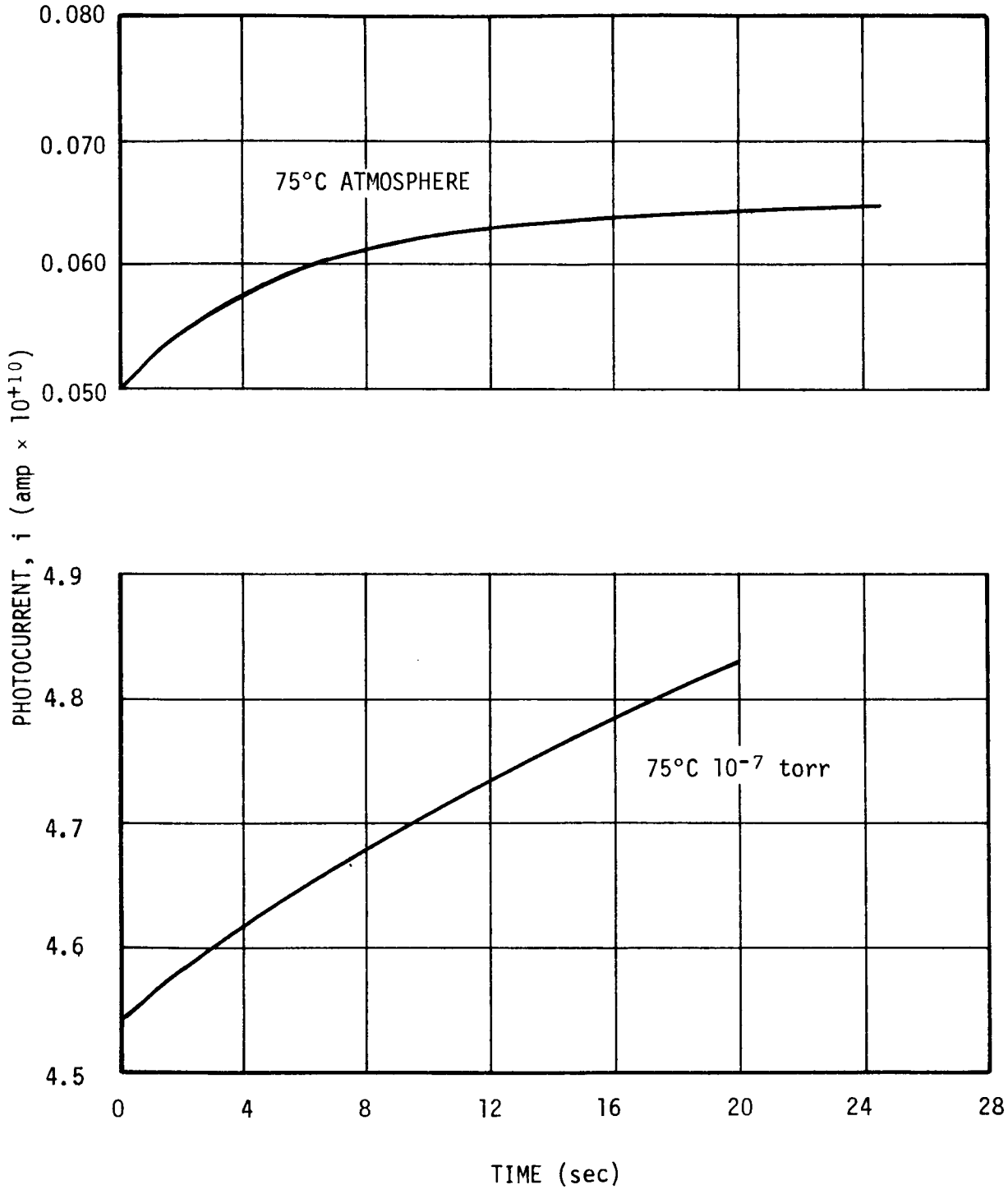

Figure 23. Photocurrent Response 4350 Å Irradiation

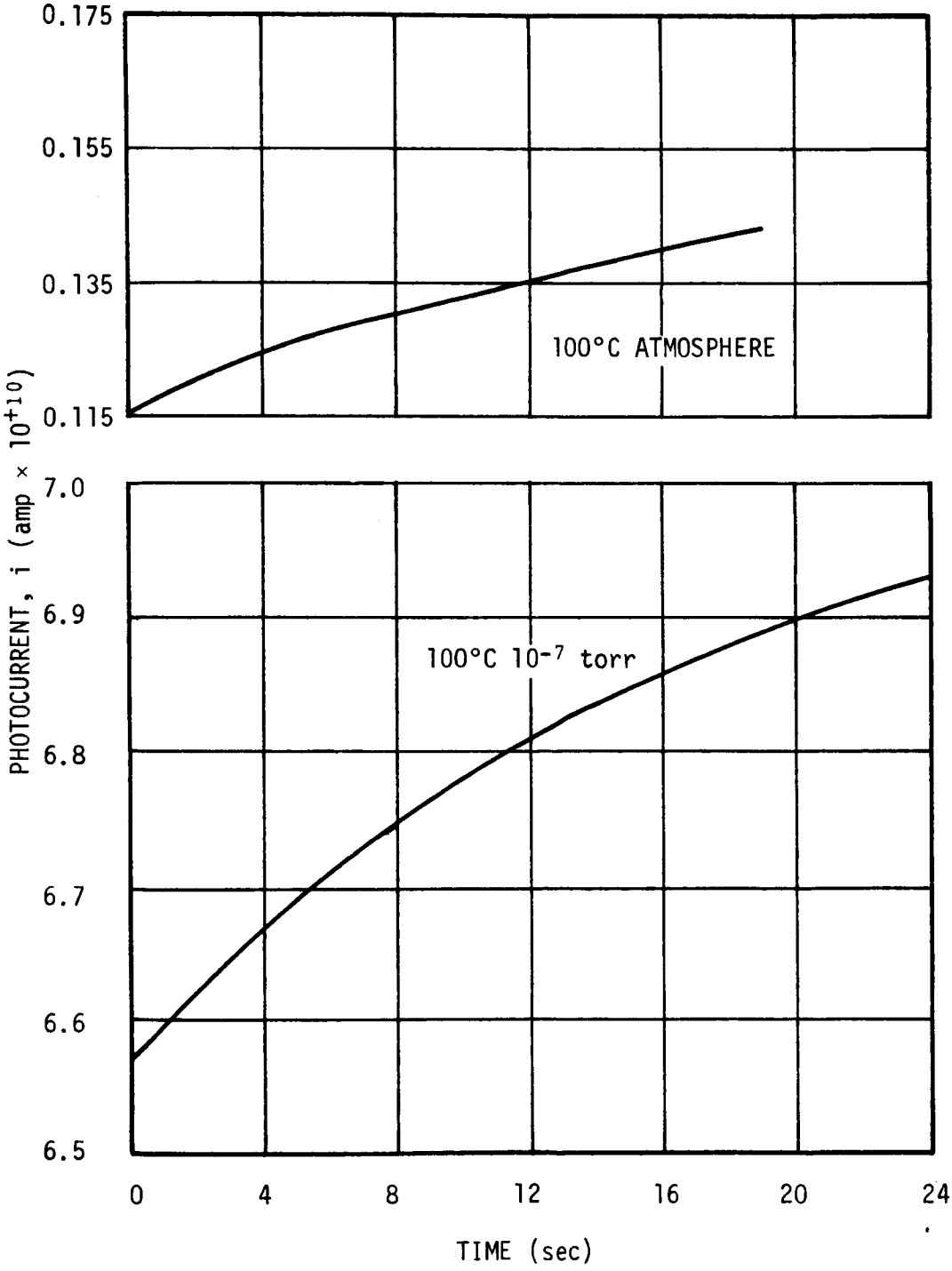

Figure 24. Photocurrent Response - 4350 Å Irradiation

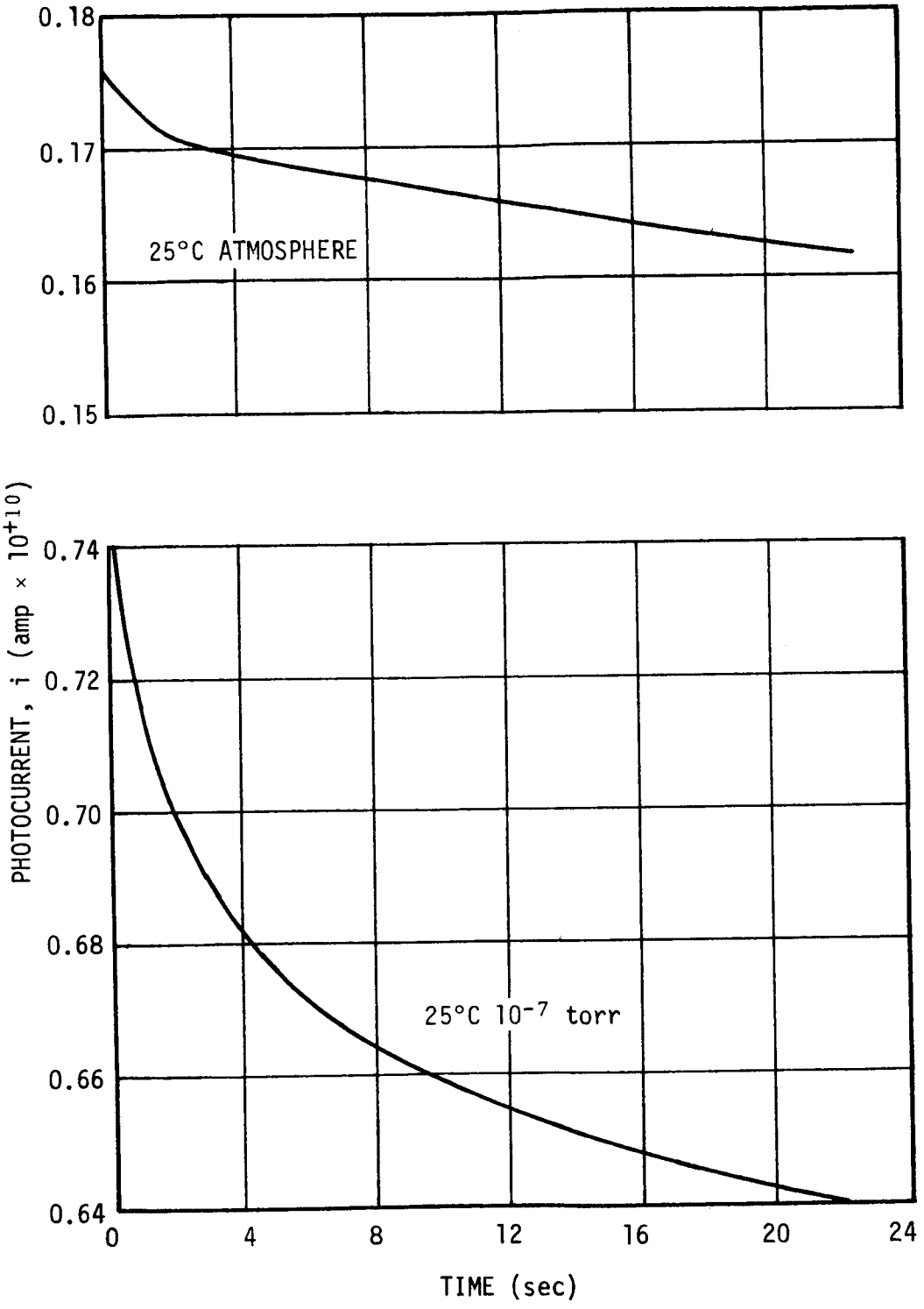

Figure 25. Photocurrent Recovery from 4350 Å Irradiation

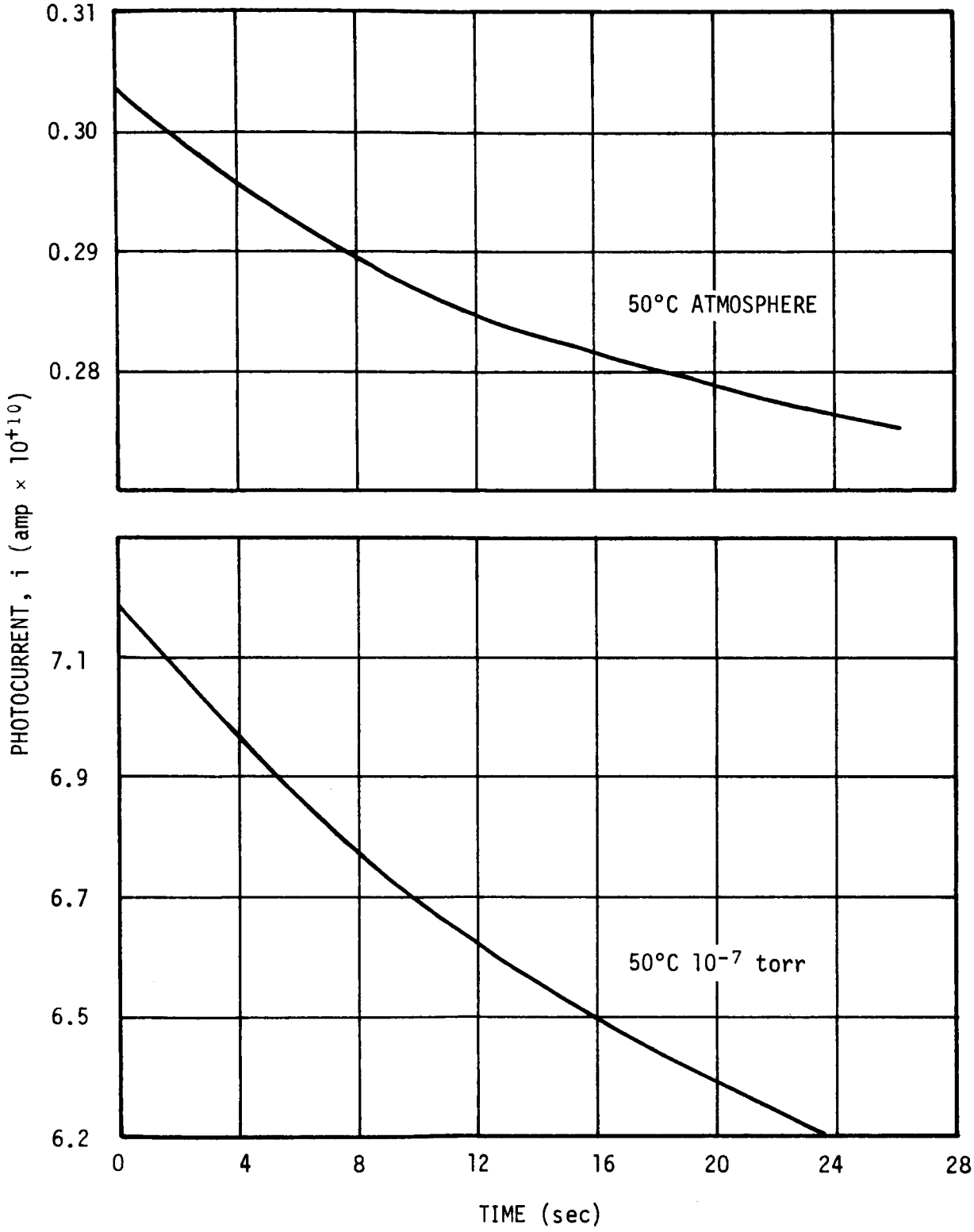

Figure 26. Photocurrent Recovery from 4350 Å Irradiation

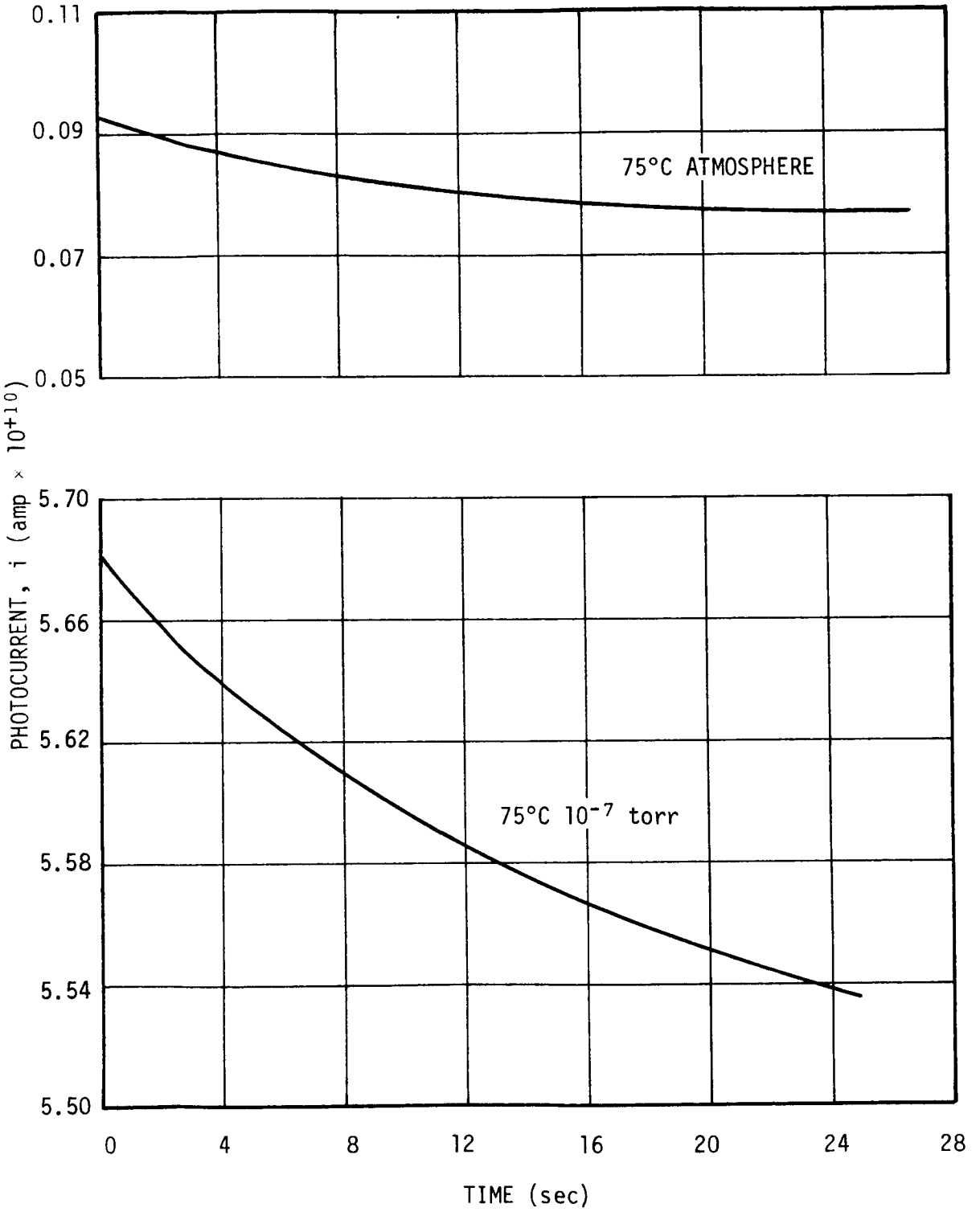

Figure 27. Photocurrent Recovery from 4350 Å Irradiation

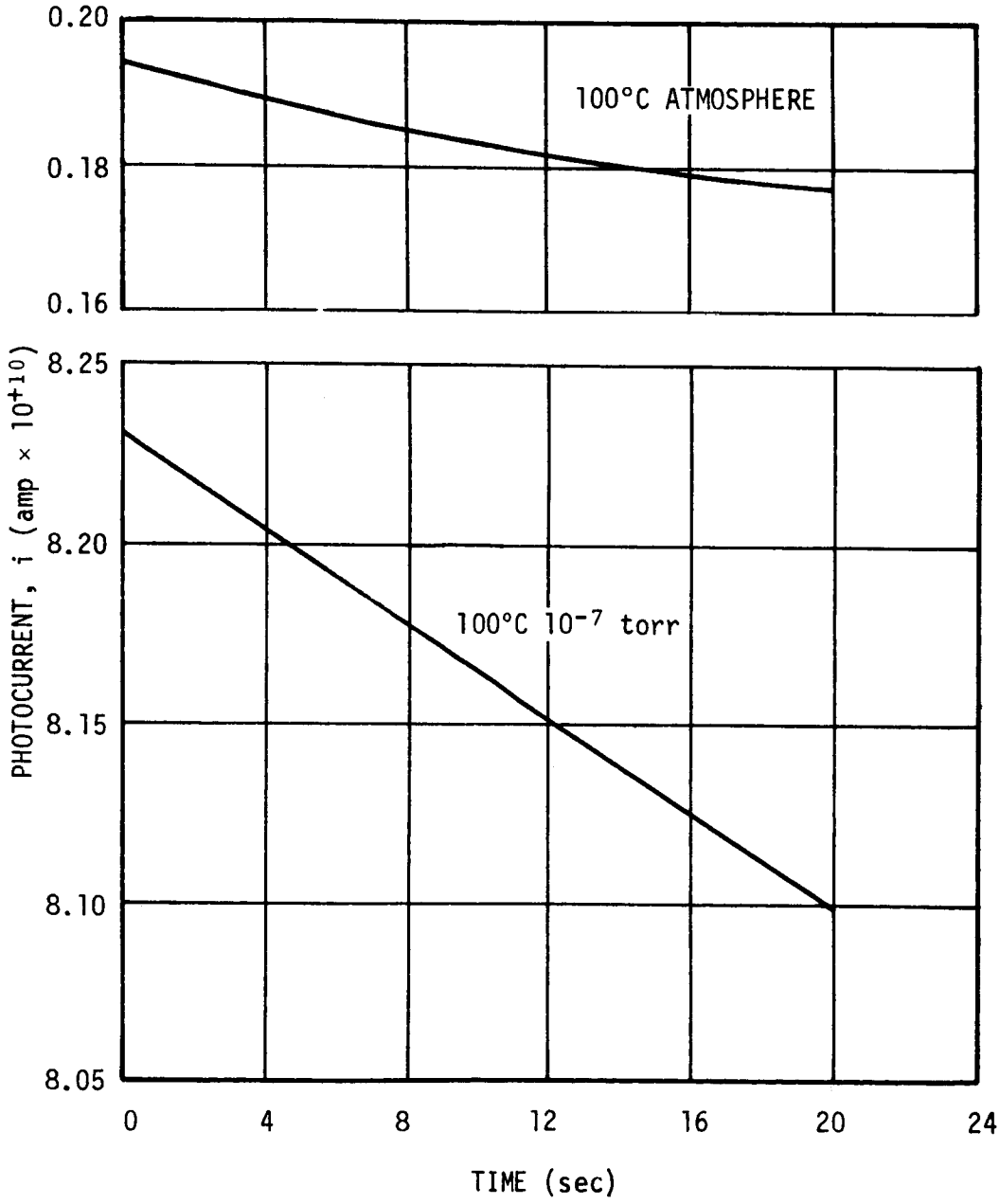

Figure 28. Photocurrent Recovery from 4350Å Irradiation

Although trend reversal, process rates, and initial current have been used as comparative references throughout the examination of photodegradation and recovery, very few quantitative statements have been made. To the end of rectifying this situation and summarizing additional implications of the data discussed above, Figures 29a, 29b, 30a, and 30b are presented. Figure 29a indicates the "initial current level" or the level of degradation assumed by the film in vacuum and in atmosphere where the previous history has included 3650 Å irradiation for all points excepting the 25°C point. We see initial points for the 4350 Å treatment agreeing to within reasonable error (Figure 29b) with the initial points of Figure 29a.

The slopes of the vacuum data in Figures 29a and 29b are, respectively, 2×10^{-11} amp/deg and 0.6×10^{-11} amp/deg. This indicates, that for a given temperature, after having taken into consideration the voluntary release of oxygen in vacuum, the film, subject to 3650 Å will recover after degradation, to a point only one-third that of the same film subject to 4350 Å irradiation (degradation periods for both levels of irradiation are approximately the same). This phenomena cannot be attributed to different intensity levels, since Figure 31 shows the spectral intensity of these two lines to be approximately equal. It cannot be argued that due to different frequencies of irradiation, a larger percent of the more energetic radiation will be absorbed. Even considering the zinc oxide as a good conductor, which the degraded zinc oxide is not ($n < 10^{19}$), the absorption difference between the two spectral levels is easily shown not to exceed 10 percent.

The level to which recovery occurs appears to result from two factors: temperature and spectral level of irradiation. The difference in these recovery levels, as noted in Figures 29a and 29b, must be attributed to differences in spectral irradiation levels only. It is conceivable that hole generation in the bulk, resulting in electron transition to empty donor levels very near the conduction band or to the conduction band itself,

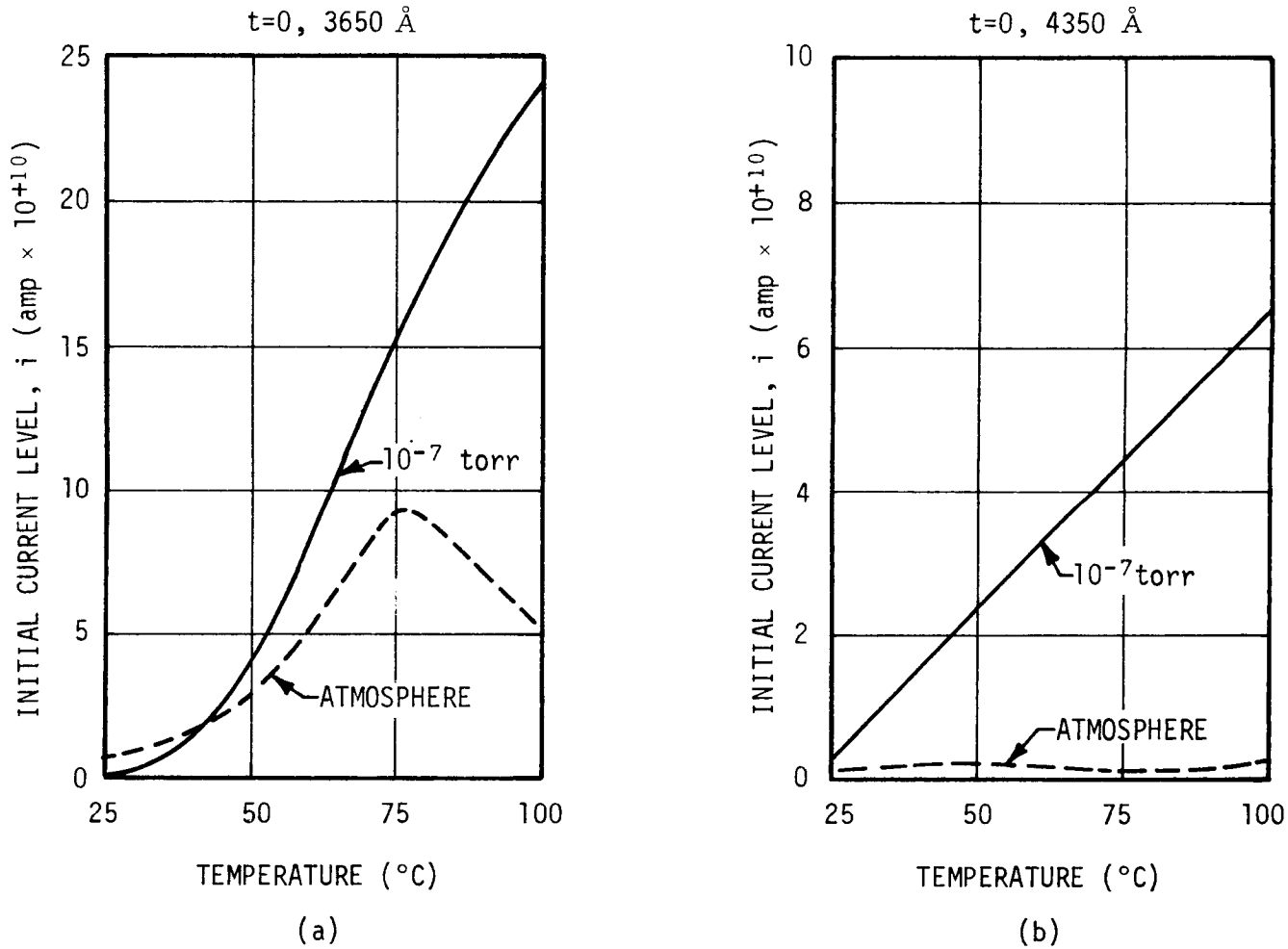

Figure 29. Steady State Degradation Level as Determined by Prior Irradiation and Temperature

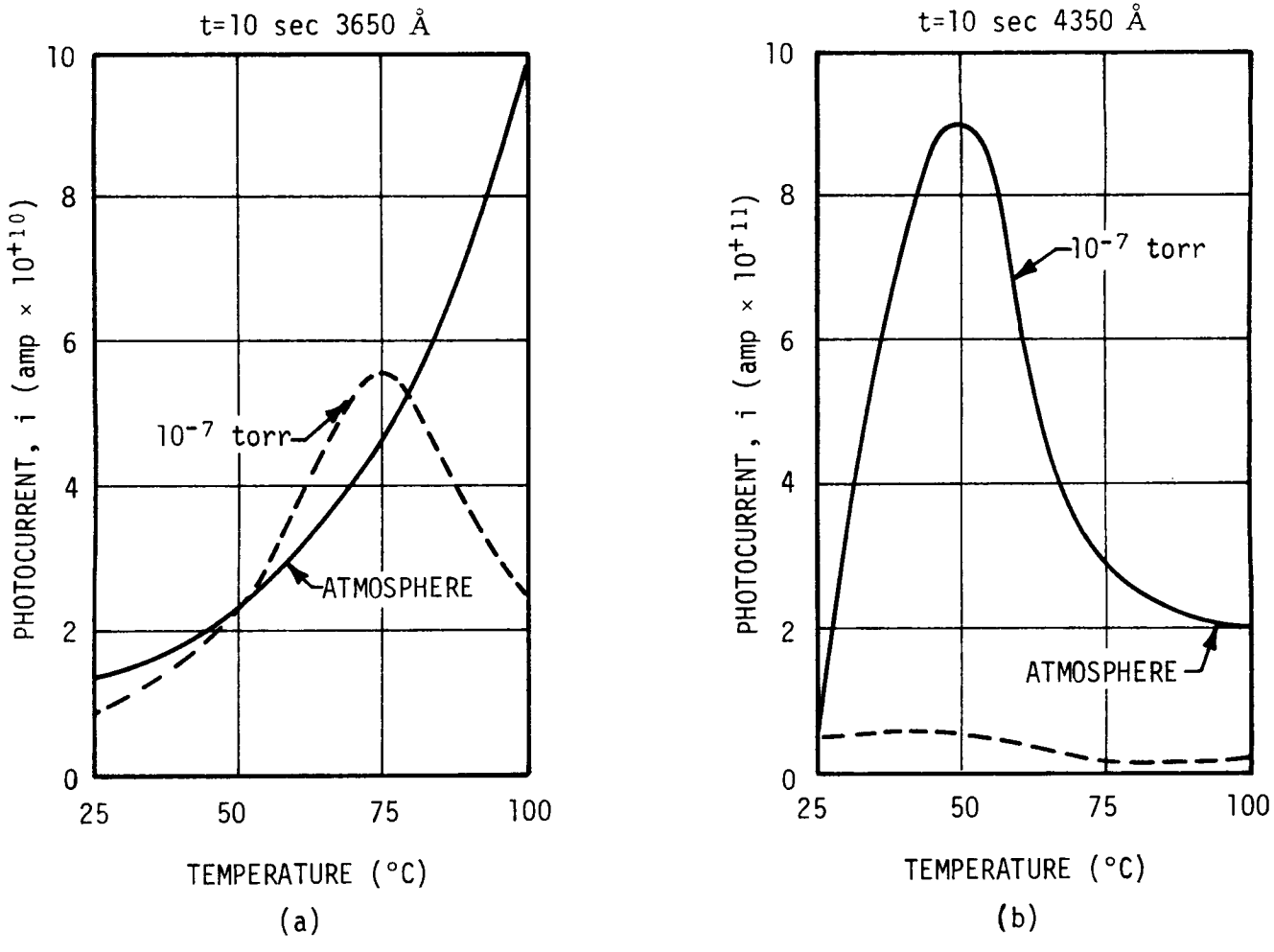

Figure 30. Photocurrent as a Function of Temperature and Irradiation

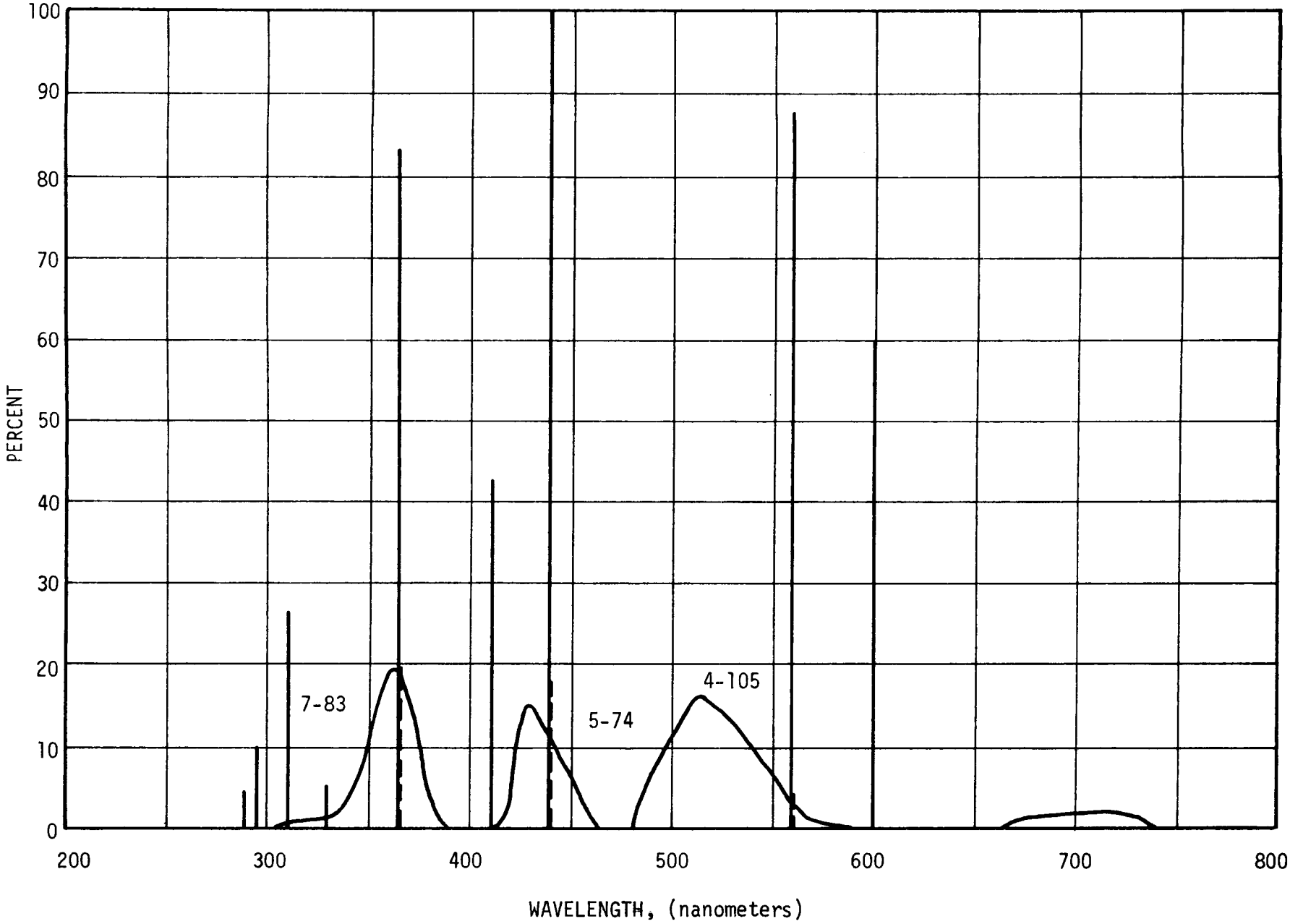

Figure 31. Filter Transmission and Relative Line Intensity of U-V Lamp

would be more efficient for 3650 Å irradiation than for 4350 Å irradiation. It is assumed that as the temperature rises the diffusion coefficient rises, resulting in shorter equilibration times for the hole diffusion, oxygen neutralization process.

In either case the effect is quite obviously not a temperature effect alone. Disregarding the fact that the magnitude of reaction is dependent upon spectral level, authors[8, 11] postulate that conductivity, hence the photocurrent, behaves in the following fashion:

$$\sigma = A \exp(-\beta/kT) \quad . \tag{6}$$

The β is related to donor level with respect to the conduction band (in eV). T is temperature in degrees Kelvin, k is the Boltzmann constant, and A is an arbitrary constant. It is apparent that neither the 3650 Å nor the 4350 Å case is dominated completely by an exponential of this type alone.

The initial current level for the film in atmosphere is given as a function of temperature in Figures 29a and 29b by the broken line. Most significant is the result in Figure 29b, in which there is practically no significant temperature structure. Apparently, comparing to the vacuum data of Figure 29b, there is a dependency of recovery level and partial pressure of oxygen. It seems necessary that, in order for the degradation to proceed, the neutralized oxygen must be removed from the material surface.

The behavior of the atmosphere curve in Figure 29a agrees well with thermal excitation equation (Equation 6). It has a maximum value at 75°C, which is the point that doubly ionized oxygen formation begins to be appreciable. No thermal structure for 29b is observed on this scale since the 25°C initial current is very small. A significant amount of doubly ionized oxygen is assumed to occur between 50°C and 75°C.

On the scale presented in Figure 29b, the form of the atmospheric data is not clear, but examination of the original data shows a reversal of the trend towards increased initial conductivities between 50°C and 75°C. This same effect is seen between 75°C and 100°C in Figure 29a. At this point this phenomenon is considered to be the result of doubly ionized surface oxygen becoming predominant.

Comparison of the atmospheric initial current-temperature data for the two levels of spectral irradiation is disconcerting. Even in atmosphere, Figure 29a shows that the film degrades and then recovers to some semi-permanent level, above which no recovery is seen in any reasonable period of time. It has been established earlier that there is quite probably desorption of oxygen in atmosphere as a result of irradiation, but it is not immediately apparent why the film will not reabsorb and recover to its original conductivity value. From Figure 29a it would be logical to conclude that the atmosphere initial current-temperature curve is indeed the form of the conductivity-temperature relation, except for the information available from Figure 29b. For this case there is very little temperature structure, indicative that the form of the initial current curve in atmosphere in Figure 29a is not due to thermal generation of carriers.

There is, however, an alternate explanation consistent with the basic model (Figure 10) and the experimental results which will simultaneously preserve the integrity of the conductivity-temperature relation (Equation 6). Consider Figure 32.

In the first 0.05 eV of the donor structure below the conduction band, there is a quasi-continuum of donor levels. The minimum levels, from which thermal excitation can occur for a given temperature, are indicated. It will be assumed that the Fermi level lies very close to the conduction band, as is indicated by mobility data, but does not lie in the donor spectrum which can be excited thermally.

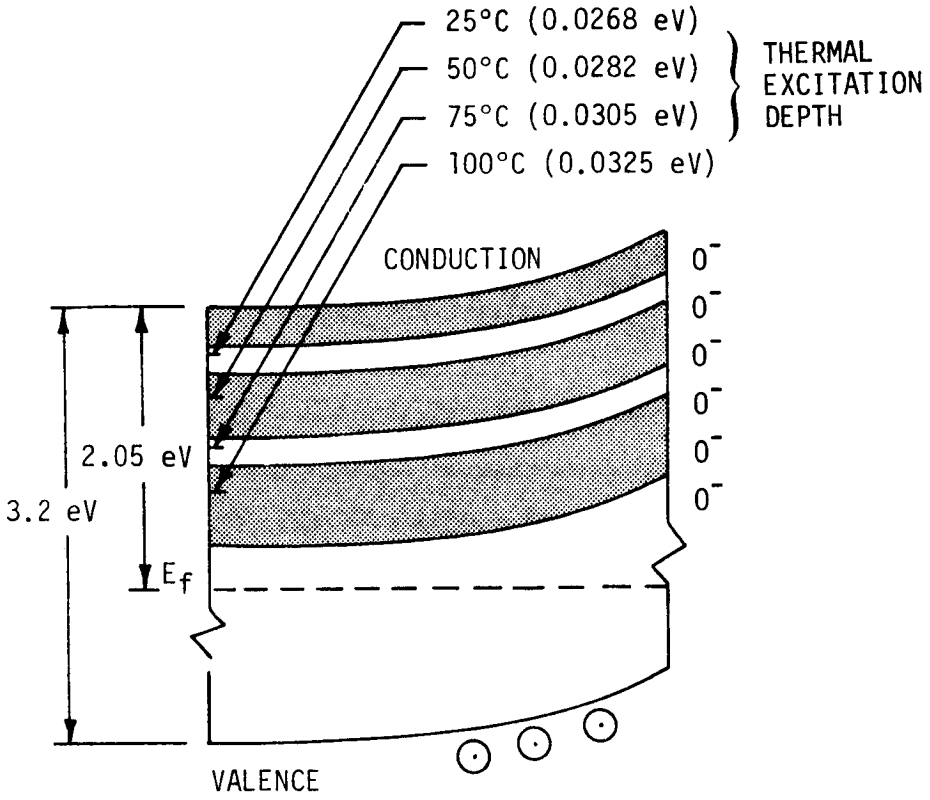

Figure 32. Modification of Donor Level Structure

Figures 30a and 30b represent photocurrent generated ten seconds after initiation of irradiation. In these data the initial current has been subtracted out in order to display some of the kinetics of the response at the various temperature levels. Figure 30a indicates that as temperature is increased, the rate of oxygen neutralization is increased, since hole diffusion is enhanced by higher temperature. Also, it is recognized that as hole-electron pairs are created, the occupation density of the donor level is increased as was suggested in discussing Figure 32. This leads to an apparent increase by thermal excitation of the photoresponse. Much the same argument applies to the atmospheric data in Figure 30a, except for the breakover at 75°C, already attributed to possible doubly ionized oxygen formation.

In general, the photocurrent data of Figure 30b resulting from 4350 Å irradiation shows a small respone in comparison to Figure 30a. The lack of photoresponse and temperature structure in atmosphere is reasonable in view of the mechanism described in Figure 32.

The vacuum response of Figure 29b is rather unusual. More precise information is needed concerning donor level distribution before a speculation about its behavior can be made. It was noted in the original data that the photoresponse in vacuum for 4350 Å radiation was sensitive at the 50°C level only. This will be discussed in detail in a later report.

The argument to show why the film irradiated with 3650 Å radiation exhibits a recognizable temperature dependency when the same film subject to 4350 Å radiation does not is based on probable occupation density of the donor levels by charge carriers. It is felt that when the zinc oxide is formed, the only manner in which the low resistivities can be explained is by consideration of charge carriers thermally generated from the donor levels very near the conduction band (< 0.05 eV). It is expected that the Fermi level does not lie within 0.05 eV of the conduction band so these levels are depleted as surface absorption of oxygen occurs.

Repopulation of these thermally excitable levels is needed if a thermal effect of conductivity is to take place. Here then is the difference between the two irradiation levels. The 3650 Å (3.4 eV) radiation upon forming a hole-electron pair can supply the electron with enough energy for transition to the thermally excitable levels or to the conduction band directly. The 4350 Å (2.85 eV) radiation does not provide sufficient energy for this transition, leaving the thermal levels still somewhat depleted of charge carrier.

This proposed mechanism does not preclude the vacuum thermal response seen in Figure 29b, for in vacuum the surface oxygen is desorbed to some extent, allowing repopulation of the near lying donor levels.

CONCLUSIONS

Majority carrier mobility is found experimentally to decrease significantly when the surface charge on zinc oxide is partially removed. It is felt that this behavior is due to an increase in bulk scattering centers and the approach to the surface by the charge carriers resulting in considerable surface scattering.

It has been shown that up to a critical temperature, the degree to which the physically bound surface oxygen has been removed does not affect the slow response of zinc oxide. Further, it has been indicated that the slow response is not sensitive to ambient gas pressure. It is this slow response which is associated with the desorption of chemically bound oxygen. Evidence of strong trapping has been observed in the degradation process involving 3650 Å irradiation.

It has been shown that for comparable intensities, 3650 Å (3.4 eV) radiation will damage zinc oxide at a faster rate and to a greater extent than 4350 Å (2.85 eV) radiation. A tentative explanation for this phenomenon has been given in terms of a band structure model.

Only Hall measurements and photocurrent response measurements have been discussed in this report. The incremental pressure voluntary response measurements, the time rate change of conductivity measurements, and the film thickness correlation results are to be discussed in a separate report which will immediately follow this report.

REFERENCES

1. Schrieffer, J. R., Phys. Rev., 97, 641 (1955)

2. Heiland, G., J. Phys. Chem. Solids, 22, 227 (1961)

3. Karpovich, I. A. and B. N. Zvonkov, Soviet Phys. - Solid Stage, 6, 11 (May 1965)

4. Fuchs, K., Proc. Cambridge Phil. Soc., 34, 199 (1938)

5. Sondheimer, E. H., Phys. Rev., 80, 401 (1950)

6. Krusemeyer, H. J., Phys. Rev., 114, 655 (1959)

7. Private Communication, S. Greenberg, Lockheed Research Laboratory, Palo Alto, California

8. Hahn, E. E., J. Appl. Phys., 22, 855 (1951)

9. McKellar, L. A., et al, "Solar-Radiation-Induced Damage to Optical Properties of ZnO-Type Pigments", Lockheed Missiles and Space Company, Contract No. NAS8-11266, September 1965

10. Mark, P., "RCA Review", pp. 461, (December 1965)

11. Harrison, S. E., Phys. Rev., 93, 52 (1953)

APPENDIX

RESISTANCE AND TIME RATE CHANGE OF RESISTANCE VERSUS DURATION OF IRRADIATION AND RECOVERY TIME

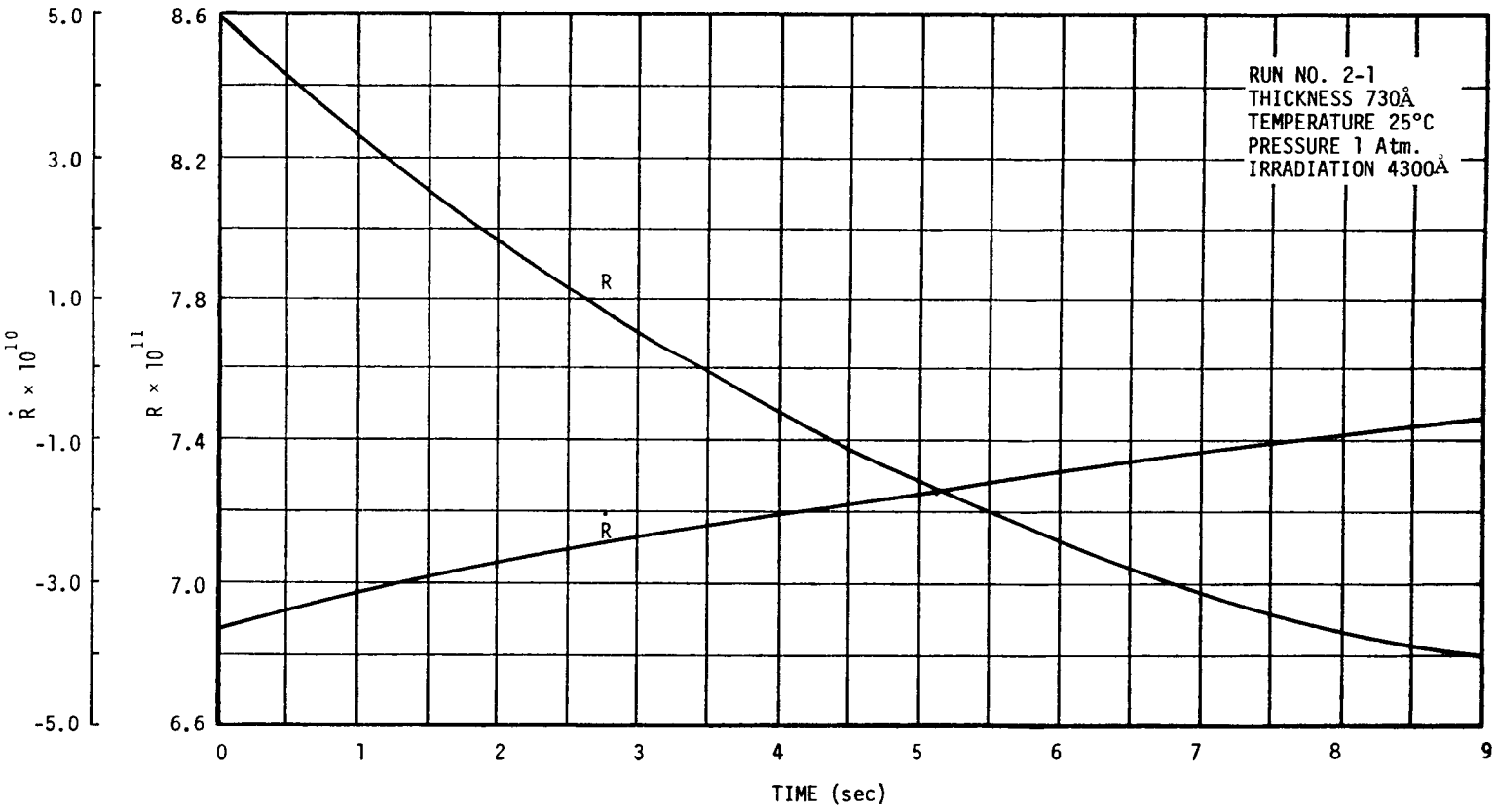
RUN NO. 2-1
THICKNESS 730Å
TEMPERATURE 25°C
PRESSURE 1 Atm.
IRRADIATION 4300Å
R
Ṙ
Ṙ × 10^10
R × 10^11
5.0
3.0
1.0
-1.0
-3.0
-5.0
8.6
8.2
7.8
7.4
7.0
6.6
0
1
2
3
4
5
6
7
8
9
TIME (sec)

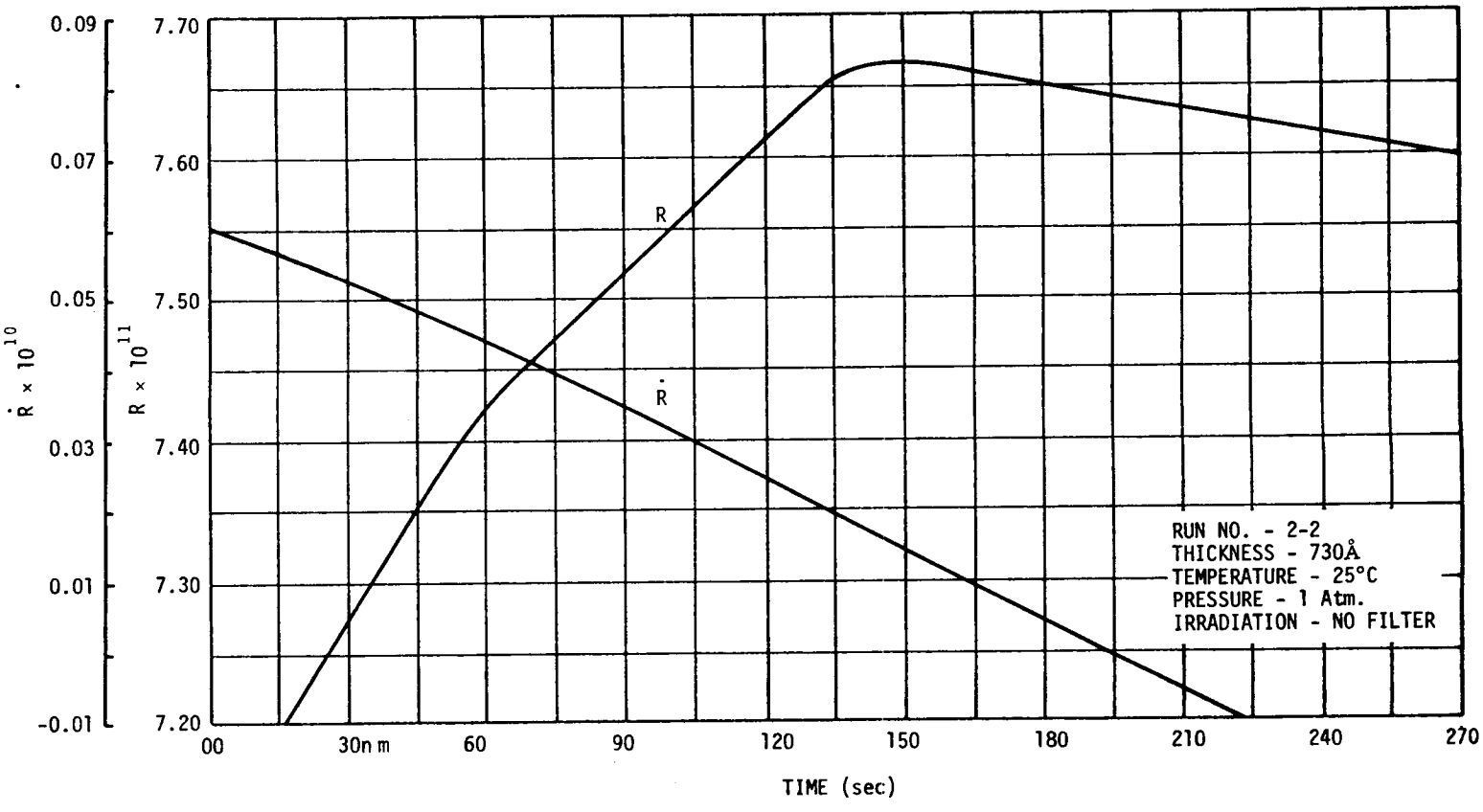
0.09
0.07
0.05
0.03
0.01
-0.01
$\dot{R} \times 10^{10}$
7.70
7.60
7.50
7.40
7.30
7.20
$R \times 10^{11}$
R
$\dot{R}$
RUN NO. - 2-2
THICKNESS - 730Å
TEMPERATURE - 25°C
PRESSURE - 1 Atm.
IRRADIATION - NO FILTER
00
30n m
60
90
120
150
180
210
240
270
TIME (sec)

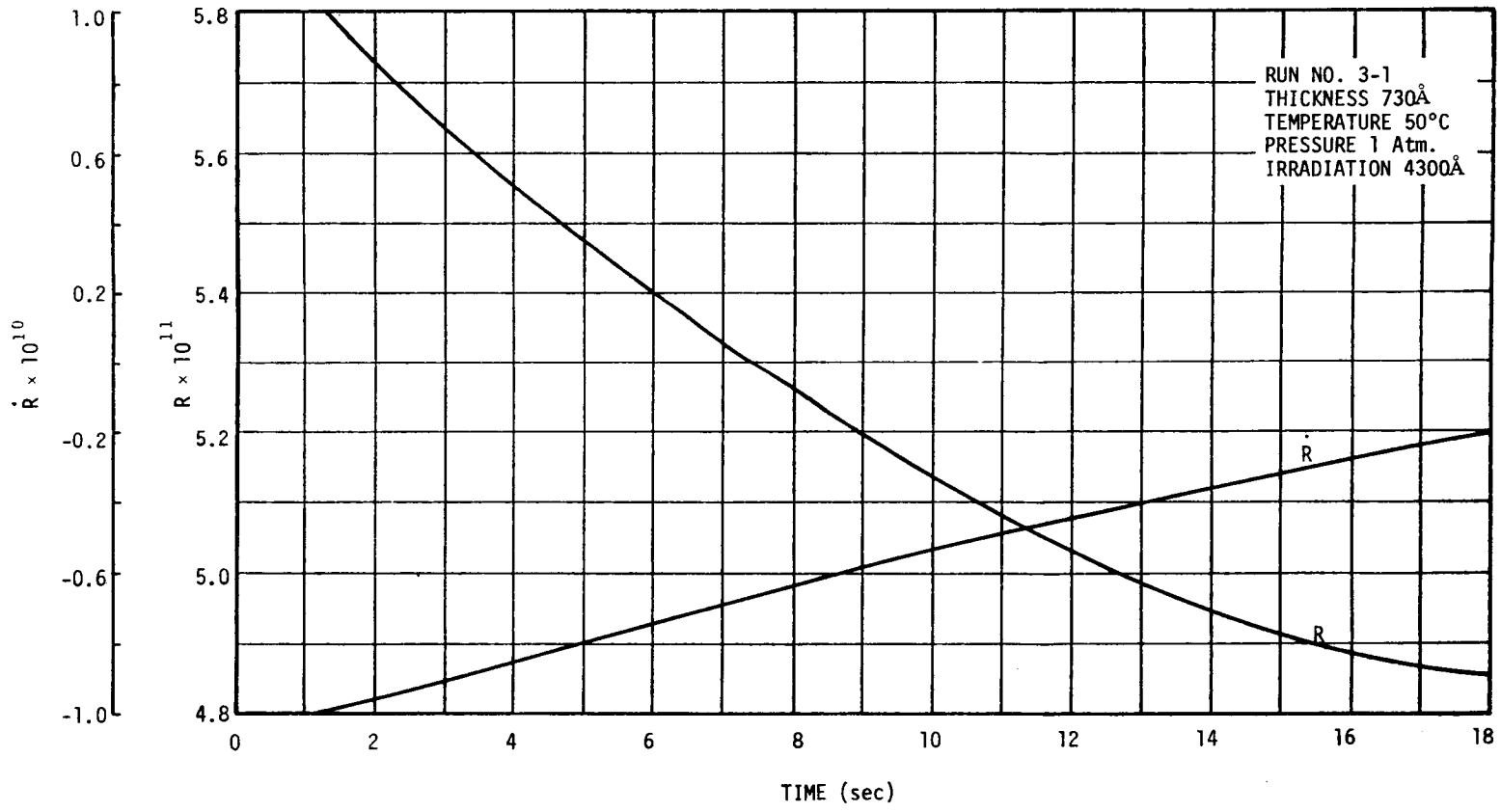
RUN NO. 3-1
THICKNESS 730Å
TEMPERATURE 50°C
PRESSURE 1 Atm.
IRRADIATION 4300Å
$\dot{R} \times 10^{10}$
$R \times 10^{11}$
1.0
0.6
0.2
-0.2
-0.6
-1.0
5.8
5.6
5.4
5.2
5.0
4.8
0
2
4
6
8
10
12
14
16
18
TIME (sec)
$\dot{R}$
R

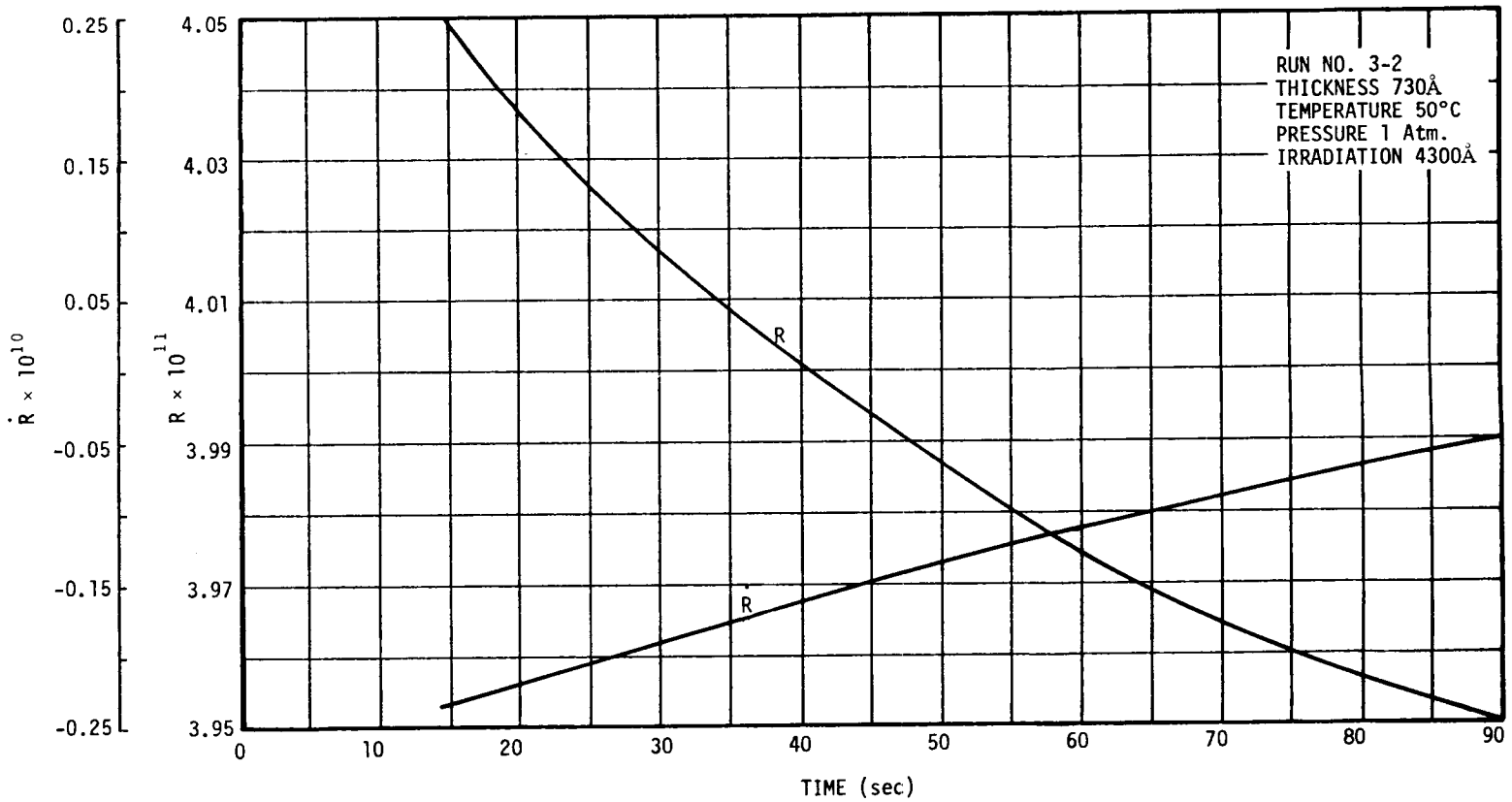
RUN NO. 3-2
THICKNESS 730Å
TEMPERATURE 50°C
PRESSURE 1 Atm.
IRRADIATION 4300Å
R
Ṙ
Ṙ × 10^10
R × 10^11
0.25
0.15
0.05
-0.05
-0.15
-0.25
4.05
4.03
4.01
3.99
3.97
3.95
0
10
20
30
40
50
60
70
80
90
TIME (sec)

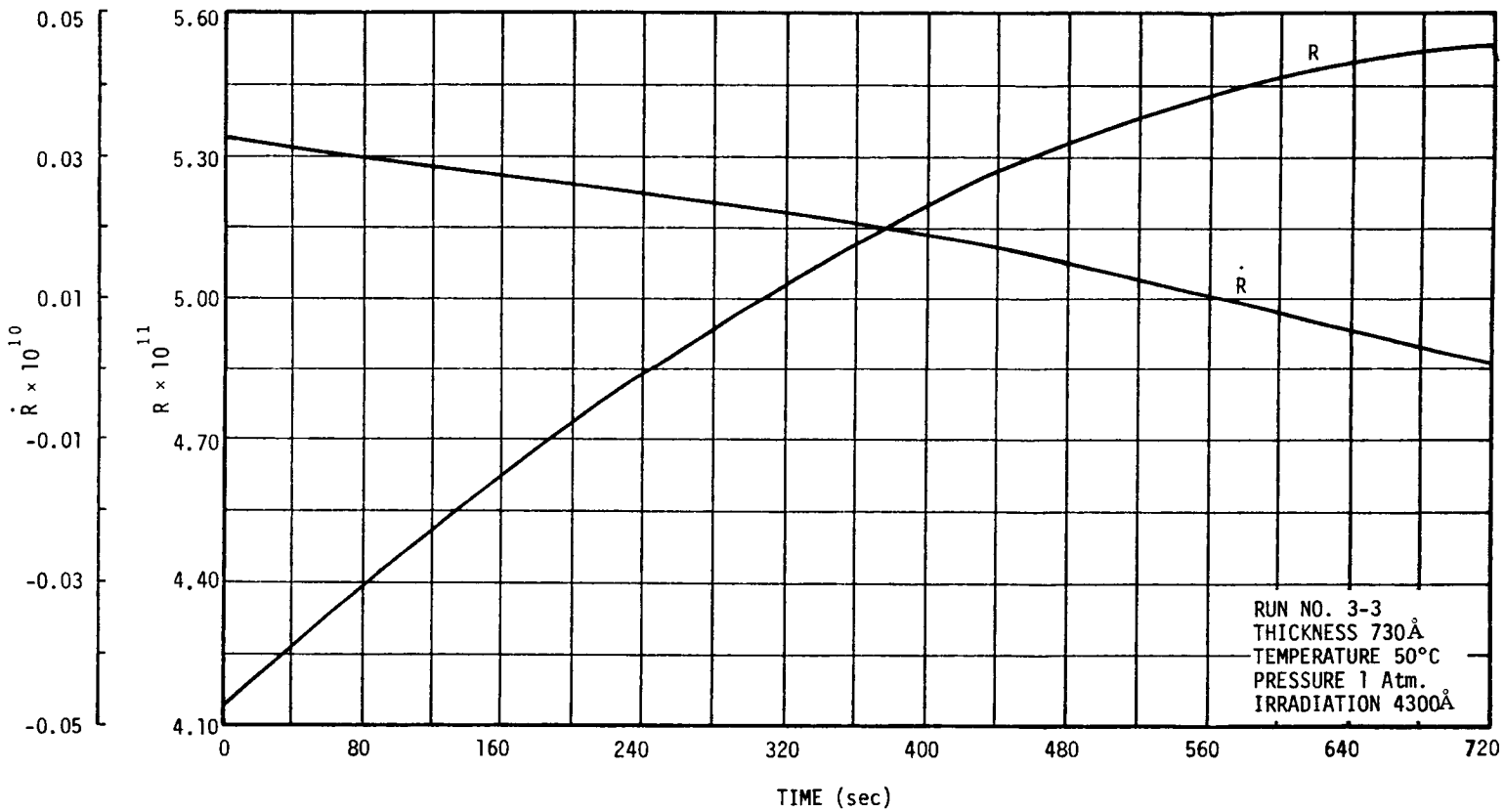
0.05
0.03
0.01
-0.01
-0.03
-0.05
$\dot{R} \times 10^{10}$
5.60
5.30
5.00
4.70
4.40
4.10
$R \times 10^{11}$
0
80
160
240
320
400
480
560
640
720
TIME (sec)
R
$\dot{R}$
RUN NO. 3-3
THICKNESS 730Å
TEMPERATURE 50°C
PRESSURE 1 Atm.
IRRADIATION 4300Å

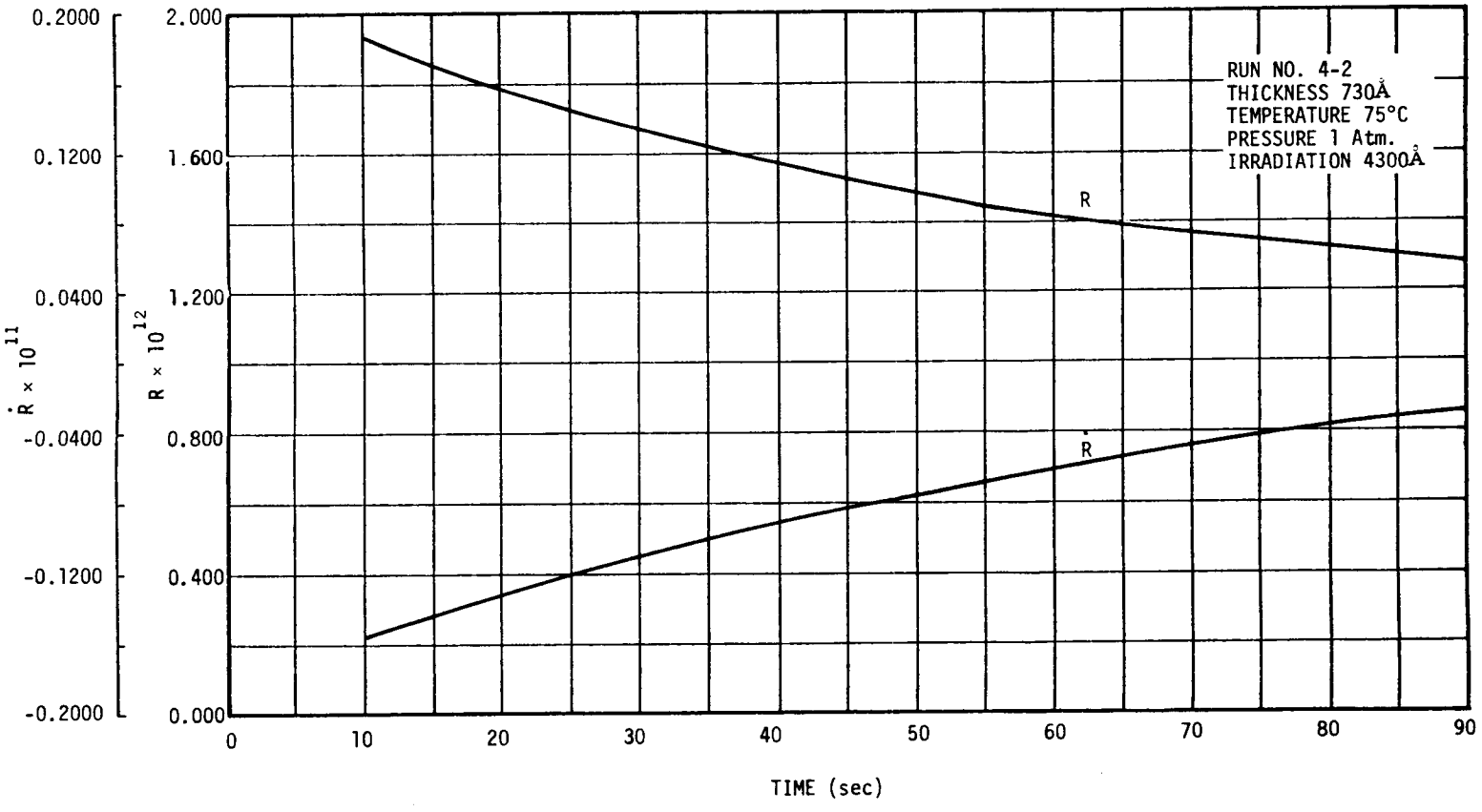
RUN NO. 4-2
THICKNESS 730Å
TEMPERATURE 75°C
PRESSURE 1 Atm.
IRRADIATION 4300Å
R
Ṙ
Ṙ × 10^11
R × 10^12
0.2000
0.1200
0.0400
-0.0400
-0.1200
-0.2000
2.000
1.600
1.200
0.800
0.400
0.000
0
10
20
30
40
50
60
70
80
90
TIME (sec)

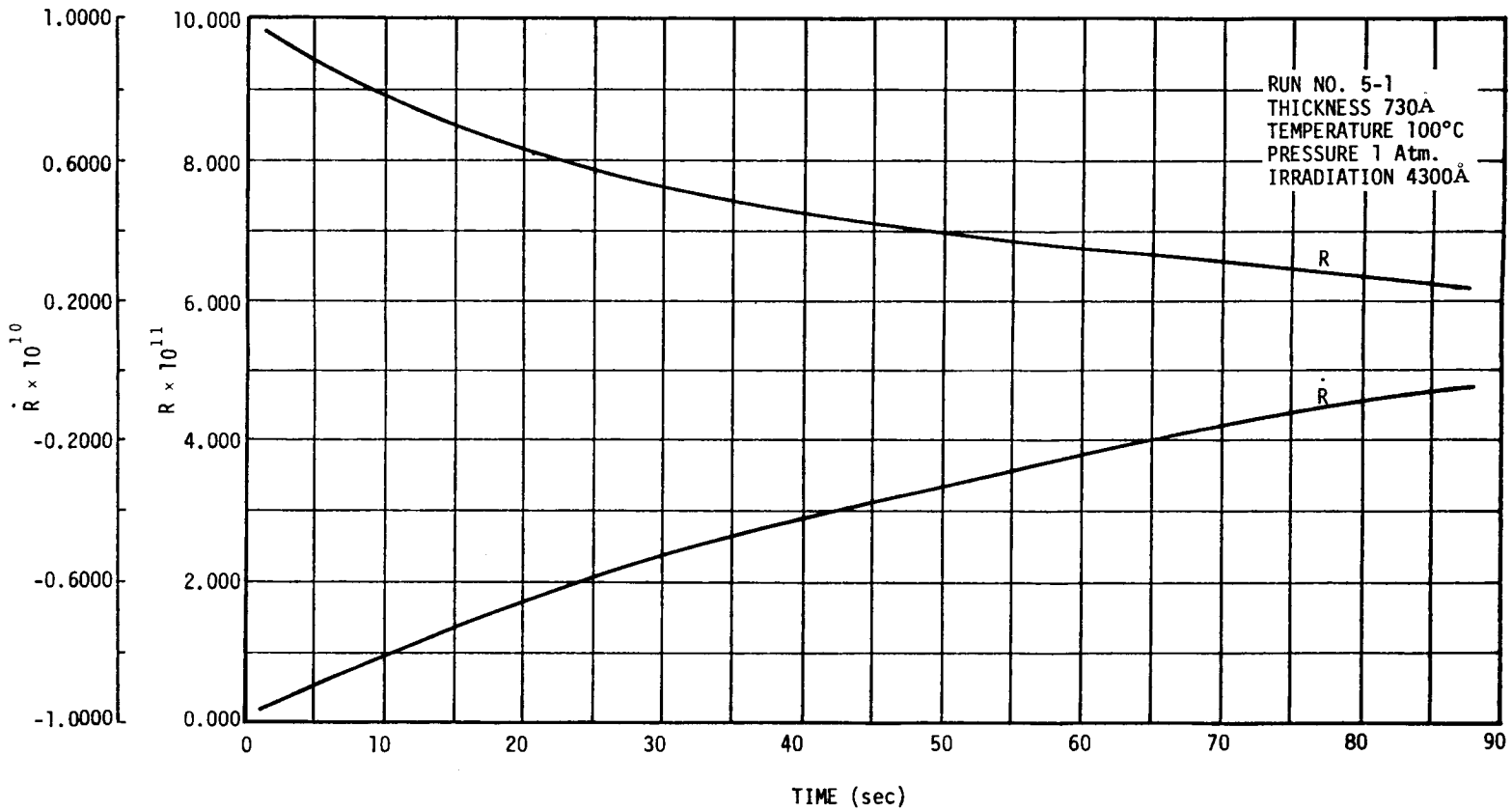
RUN NO. 5-1
THICKNESS 730Å
TEMPERATURE 100°C
PRESSURE 1 Atm.
IRRADIATION 4300Å
R
Ṙ
Ṙ × 10^10
R × 10^11
1.0000
0.6000
0.2000
-0.2000
-0.6000
-1.0000
10.000
8.000
6.000
4.000
2.000
0.000
0
10
20
30
40
50
60
70
80
90
TIME (sec)

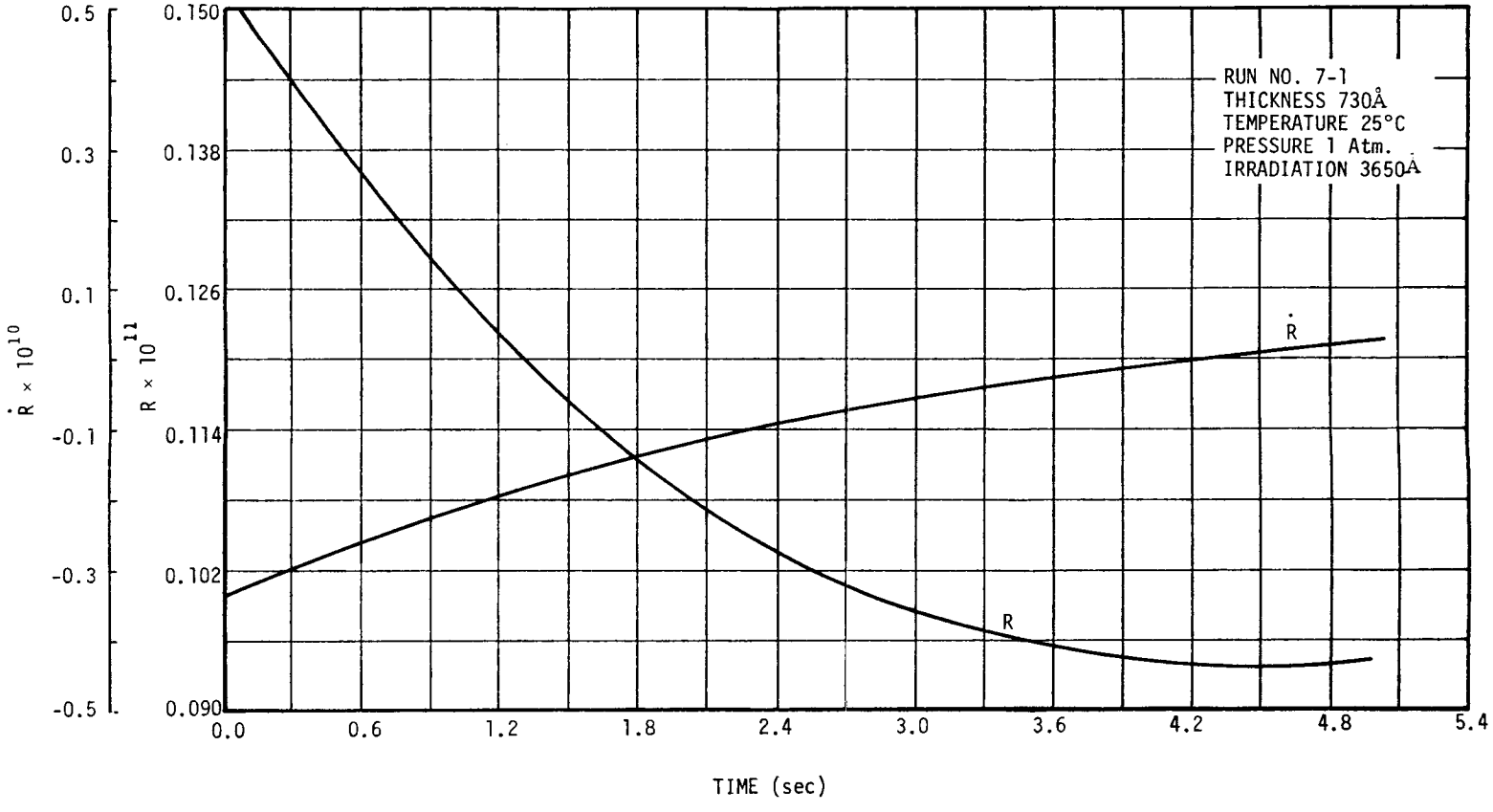
RUN NO. 7-1
THICKNESS 730Å
TEMPERATURE 25°C
PRESSURE 1 Atm.
IRRADIATION 3650Å
$\dot{R} \times 10^{10}$
$R \times 10^{11}$
0.5
0.3
0.1
-0.1
-0.3
-0.5
0.150
0.138
0.126
0.114
0.102
0.090
0.0
0.6
1.2
1.8
2.4
3.0
3.6
4.2
4.8
5.4
TIME (sec)
$\dot{R}$
R

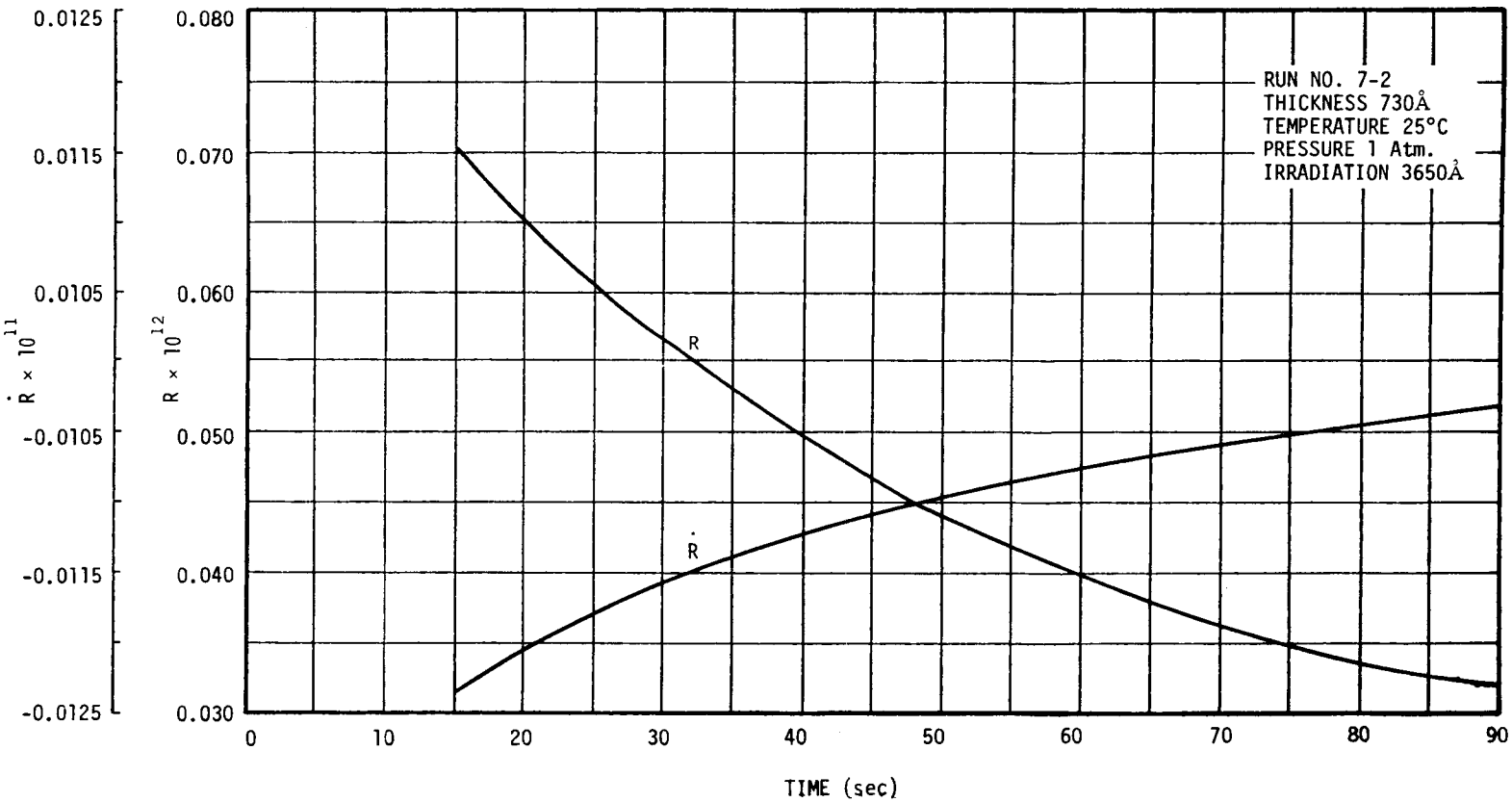
0.0125
0.0115
0.0105
-0.0105
-0.0115
-0.0125
$\dot{R} \times 10^{11}$
0.080
0.070
0.060
0.050
0.040
0.030
$R \times 10^{12}$
0
10
20
30
40
50
60
70
80
90
TIME (sec)
R
$\dot{R}$
RUN NO. 7-2
THICKNESS 730Å
TEMPERATURE 25°C
PRESSURE 1 Atm.
IRRADIATION 3650Å

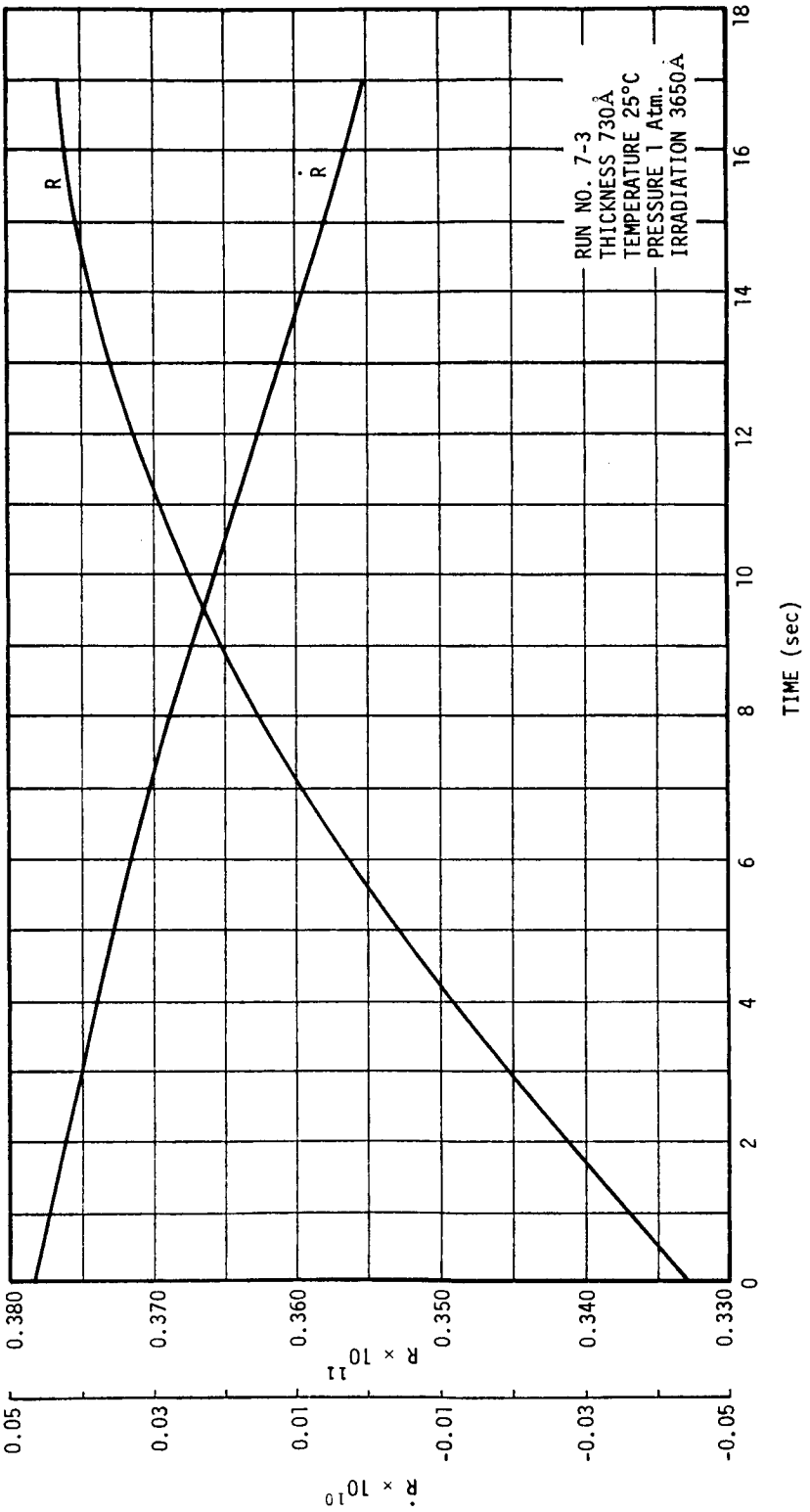
RUN NO. 7-3
THICKNESS 730Å
TEMPERATURE 25°C
PRESSURE 1 Atm.
IRRADIATION 3650Å
R
Ṙ
TIME (sec)
0
2
4
6
8
10
12
14
16
18
R × 10^11
0.380
0.370
0.360
0.350
0.340
0.330
Ṙ × 10^10
0.05
0.03
0.01
-0.01
-0.03
-0.05

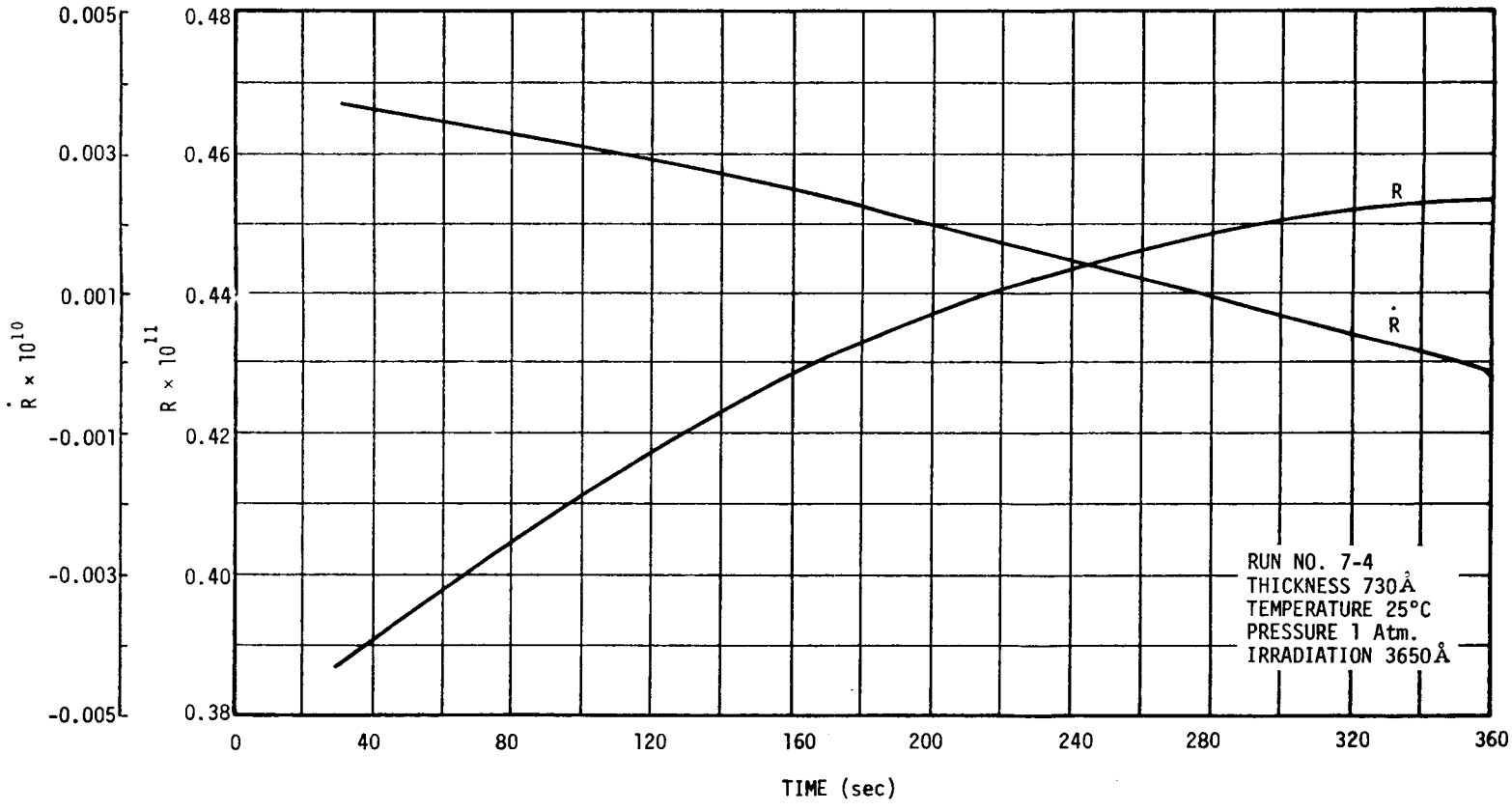
0.005
0.003
0.001
-0.001
-0.003
-0.005
$\dot{R} \times 10^{10}$
0.48
0.46
0.44
0.42
0.40
0.38
$R \times 10^{11}$
0
40
80
120
160
200
240
280
320
360
TIME (sec)
R
$\dot{R}$
RUN NO. 7-4
THICKNESS 730Å
TEMPERATURE 25°C
PRESSURE 1 Atm.
IRRADIATION 3650Å

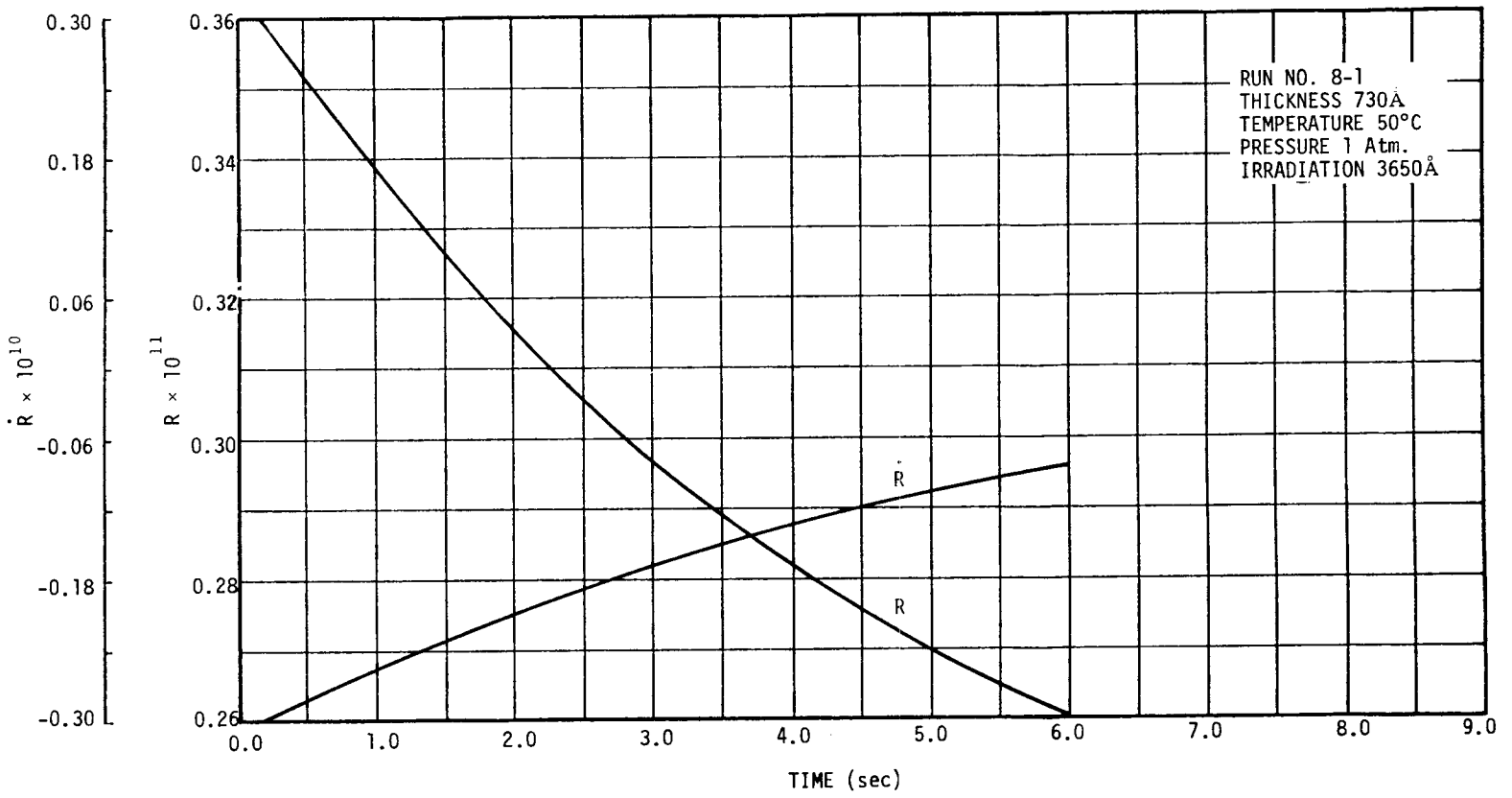
RUN NO. 8-1
THICKNESS 730Å
TEMPERATURE 50°C
PRESSURE 1 Atm.
IRRADIATION 3650Å
$\dot{R} \times 10^{10}$
$R \times 10^{11}$
0.30
0.18
0.06
-0.06
-0.18
-0.30
0.36
0.34
0.32
0.30
0.28
0.26
0.0
1.0
2.0
3.0
4.0
5.0
6.0
7.0
8.0
9.0
TIME (sec)
$\dot{R}$
R

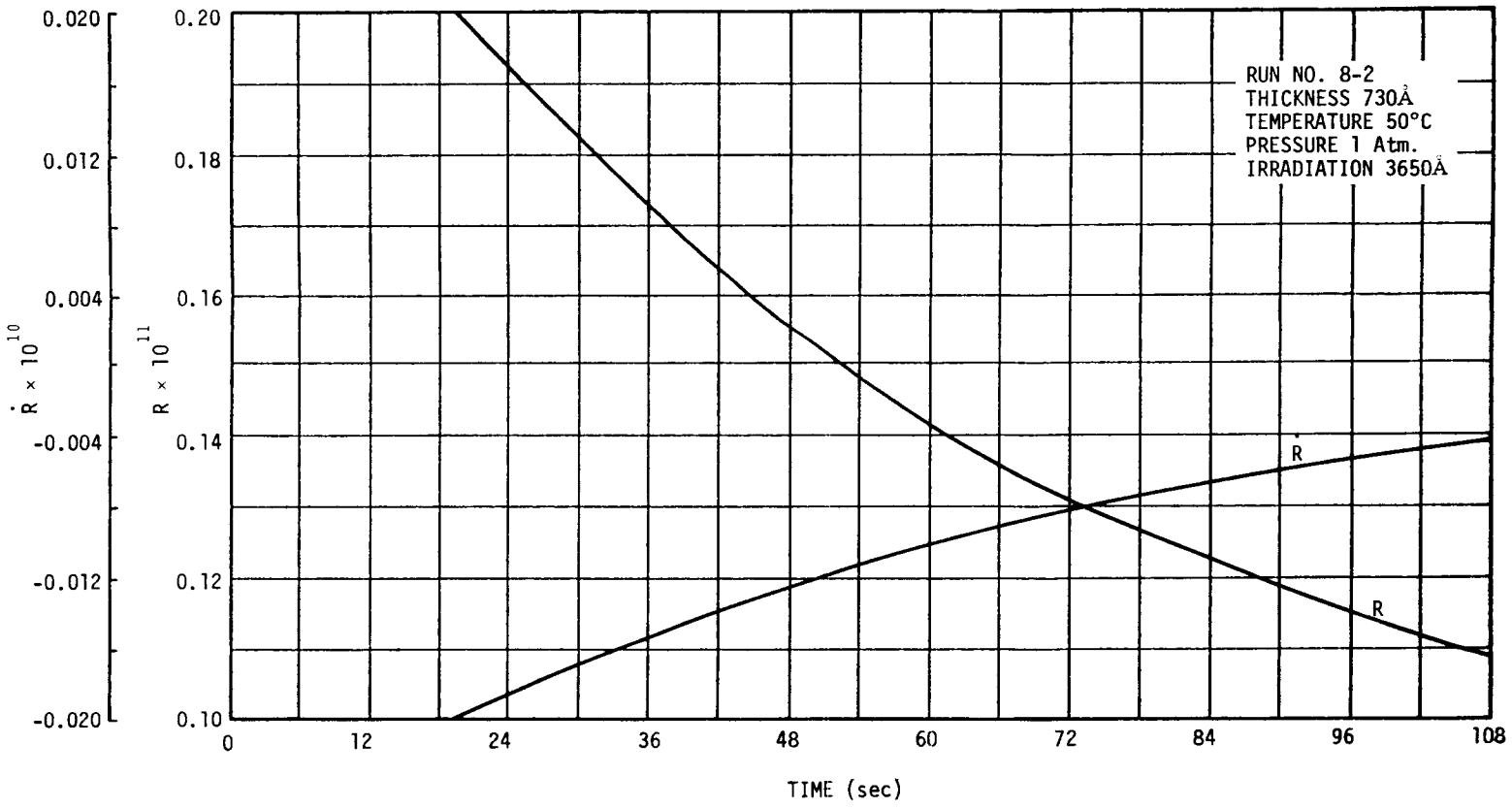
RUN NO. 8-2
THICKNESS 730Å
TEMPERATURE 50°C
PRESSURE 1 Atm.
IRRADIATION 3650Å
$\dot{R} \times 10^{10}$
$R \times 10^{11}$
0.020
0.012
0.004
-0.004
-0.012
-0.020
0.20
0.18
0.16
0.14
0.12
0.10
0
12
24
36
48
60
72
84
96
108
TIME (sec)
$\dot{R}$
R

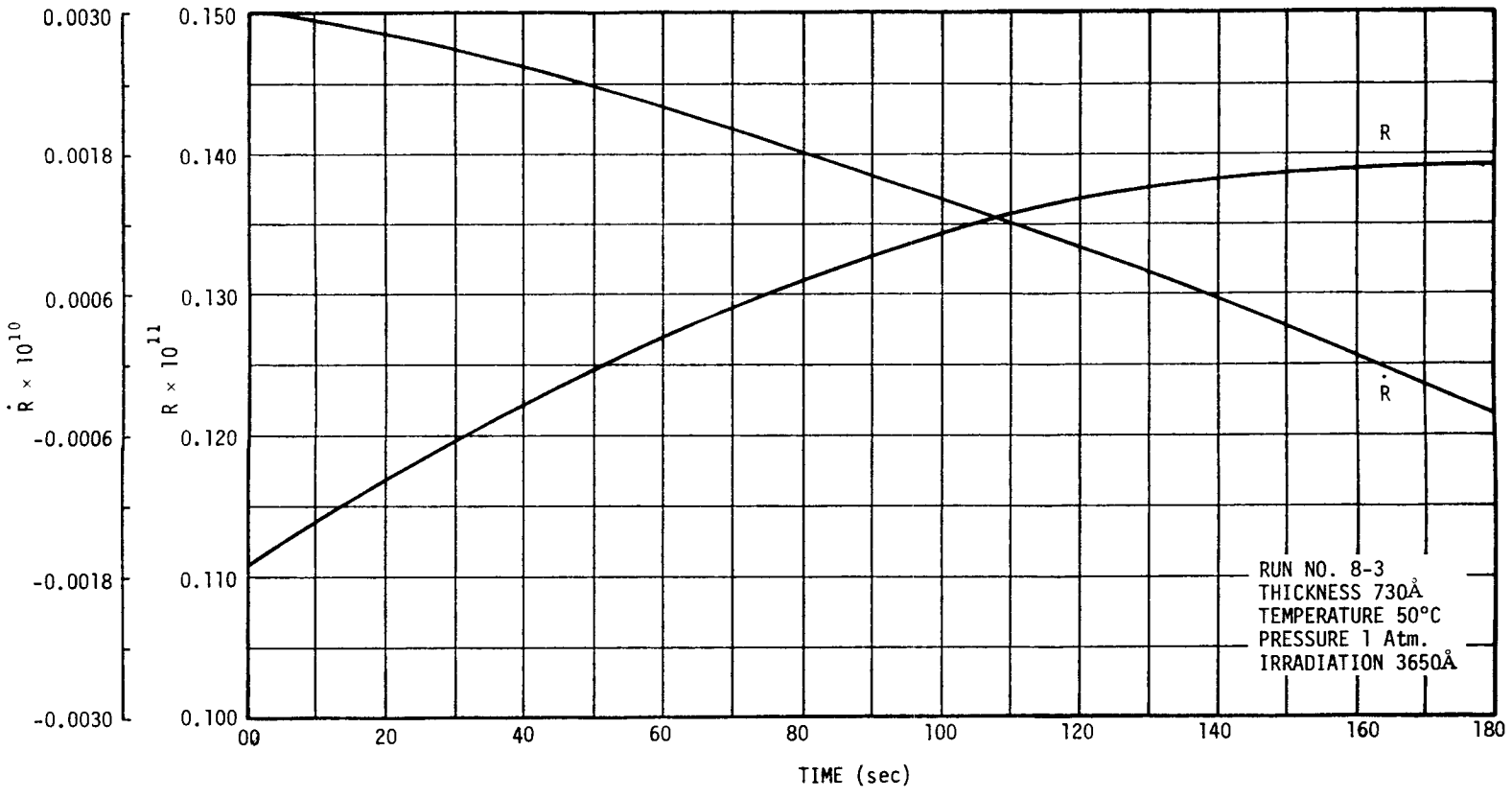
0.0030
0.0018
0.0006
-0.0006
-0.0018
-0.0030
$\dot{R} \times 10^{10}$
0.150
0.140
0.130
0.120
0.110
0.100
$R \times 10^{11}$
00
20
40
60
80
100
120
140
160
180
TIME (sec)
R
$\dot{R}$
RUN NO. 8-3
THICKNESS 730Å
TEMPERATURE 50°C
PRESSURE 1 Atm.
IRRADIATION 3650Å

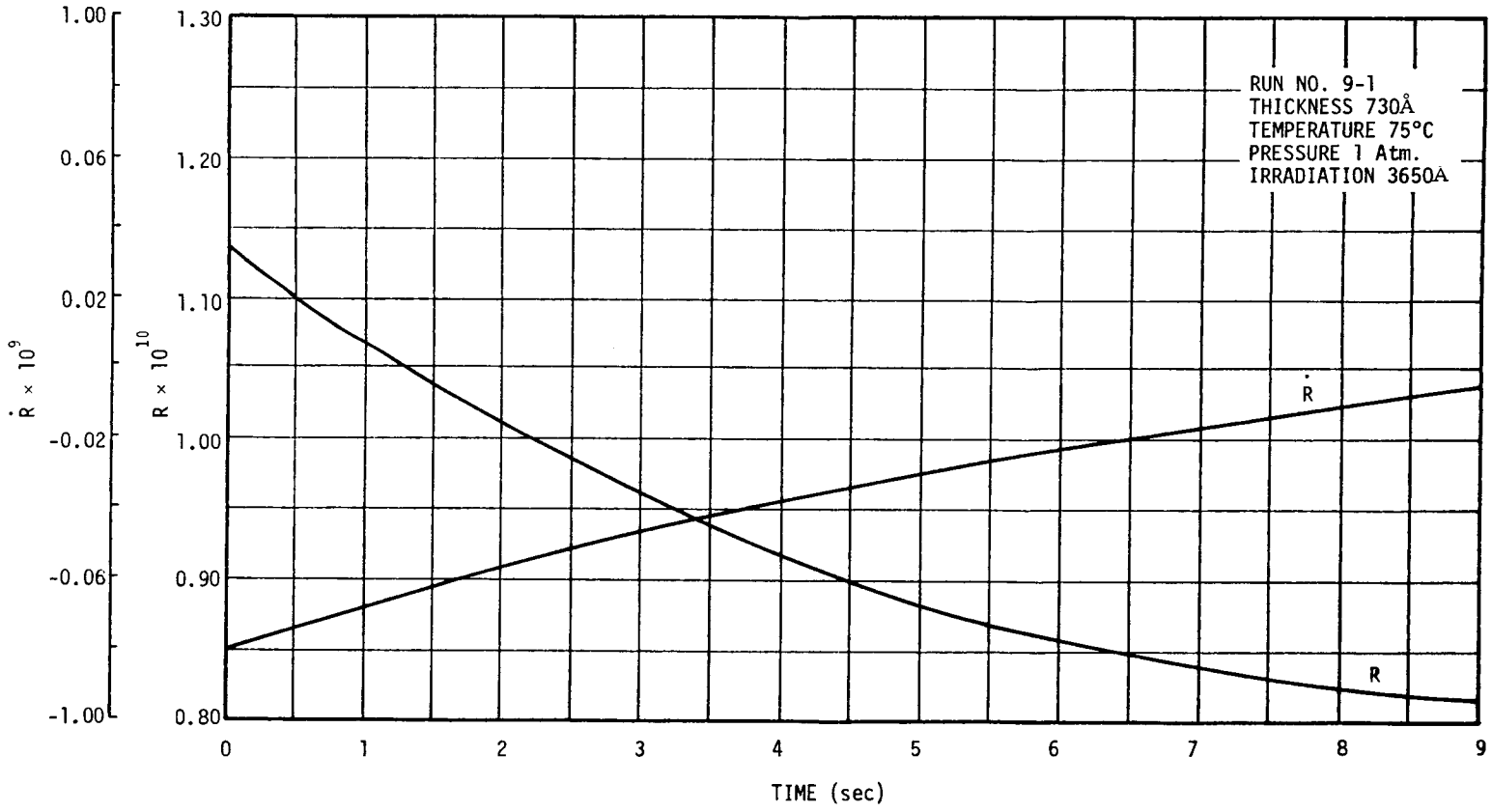
RUN NO. 9-1
THICKNESS 730Å
TEMPERATURE 75°C
PRESSURE 1 Atm.
IRRADIATION 3650Å
$\dot{R} \times 10^9$
$R \times 10^{10}$
1.00
0.06
0.02
-0.02
-0.06
-1.00
1.30
1.20
1.10
1.00
0.90
0.80
0
1
2
3
4
5
6
7
8
9
TIME (sec)
$\dot{R}$
R

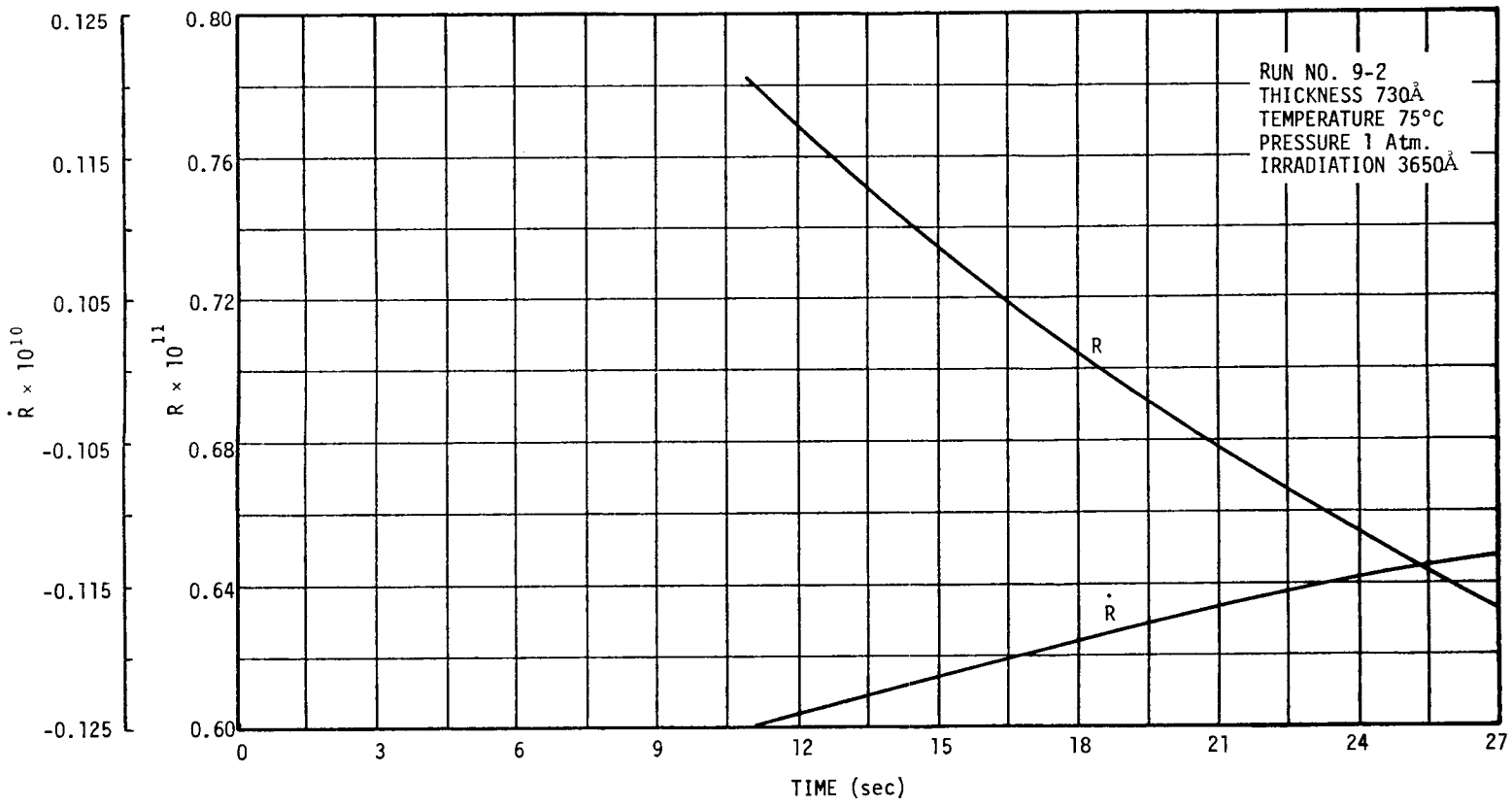
RUN NO. 9-2
THICKNESS 730Å
TEMPERATURE 75°C
PRESSURE 1 Atm.
IRRADIATION 3650Å
R
Ṙ
Ṙ × 10^10
R × 10^11
0.125
0.115
0.105
-0.105
-0.115
-0.125
0.80
0.76
0.72
0.68
0.64
0.60
0
3
6
9
12
15
18
21
24
27
TIME (sec)

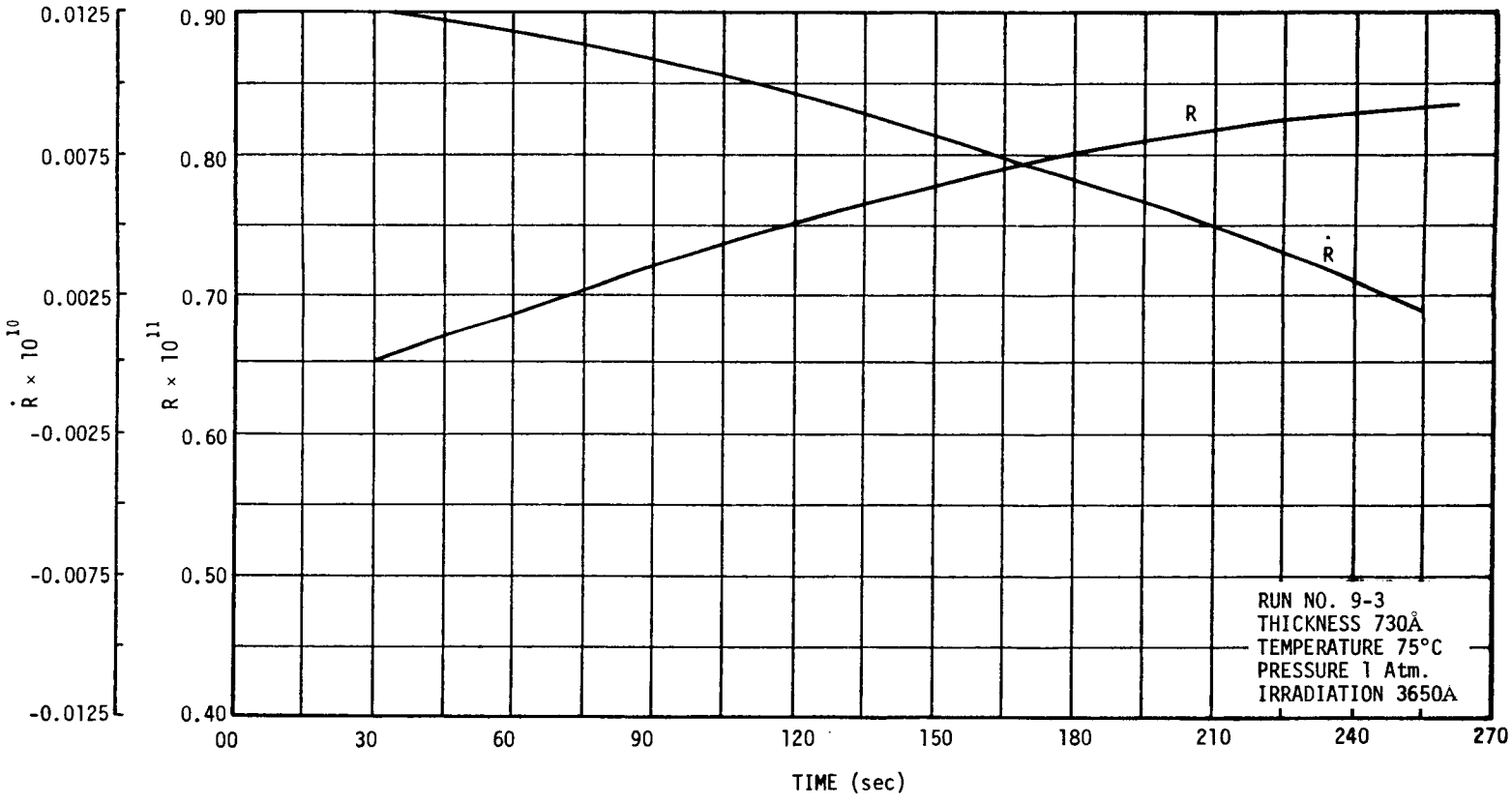
0.0125
0.0075
0.0025
-0.0025
-0.0075
-0.0125
$\dot{R} \times 10^{10}$
0.90
0.80
0.70
0.60
0.50
0.40
$R \times 10^{11}$
00
30
60
90
120
150
180
210
240
270
TIME (sec)
R
$\dot{R}$
RUN NO. 9-3
THICKNESS 730Å
TEMPERATURE 75°C
PRESSURE 1 Atm.
IRRADIATION 3650A

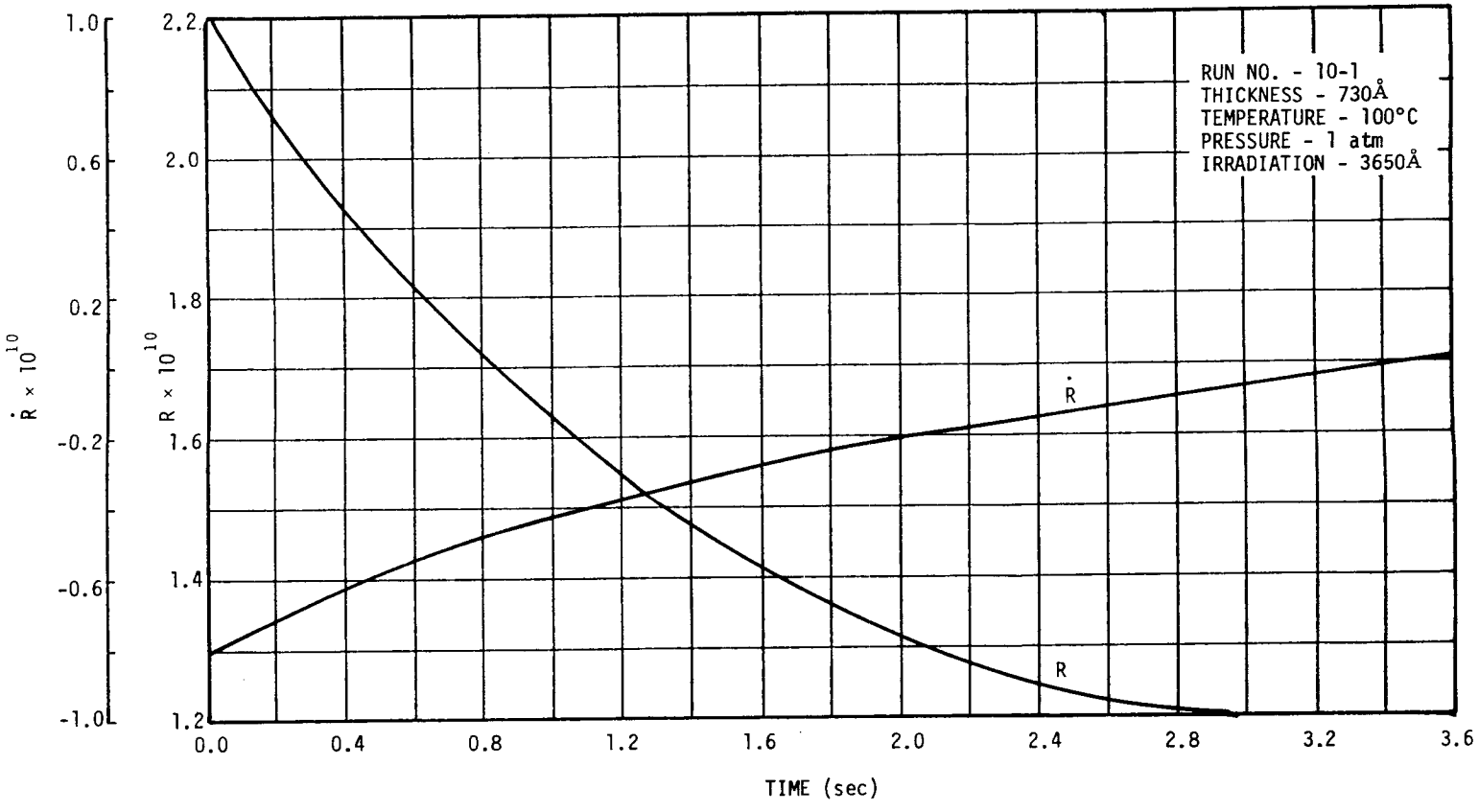
RUN NO. - 10-1
THICKNESS - 730Å
TEMPERATURE - 100°C
PRESSURE - 1 atm
IRRADIATION - 3650Å
$\dot{R} \times 10^{10}$
$R \times 10^{10}$
1.0
0.6
0.2
-0.2
-0.6
-1.0
2.2
2.0
1.8
1.6
1.4
1.2
0.0
0.4
0.8
1.2
1.6
2.0
2.4
2.8
3.2
3.6
TIME (sec)
$\dot{R}$
R

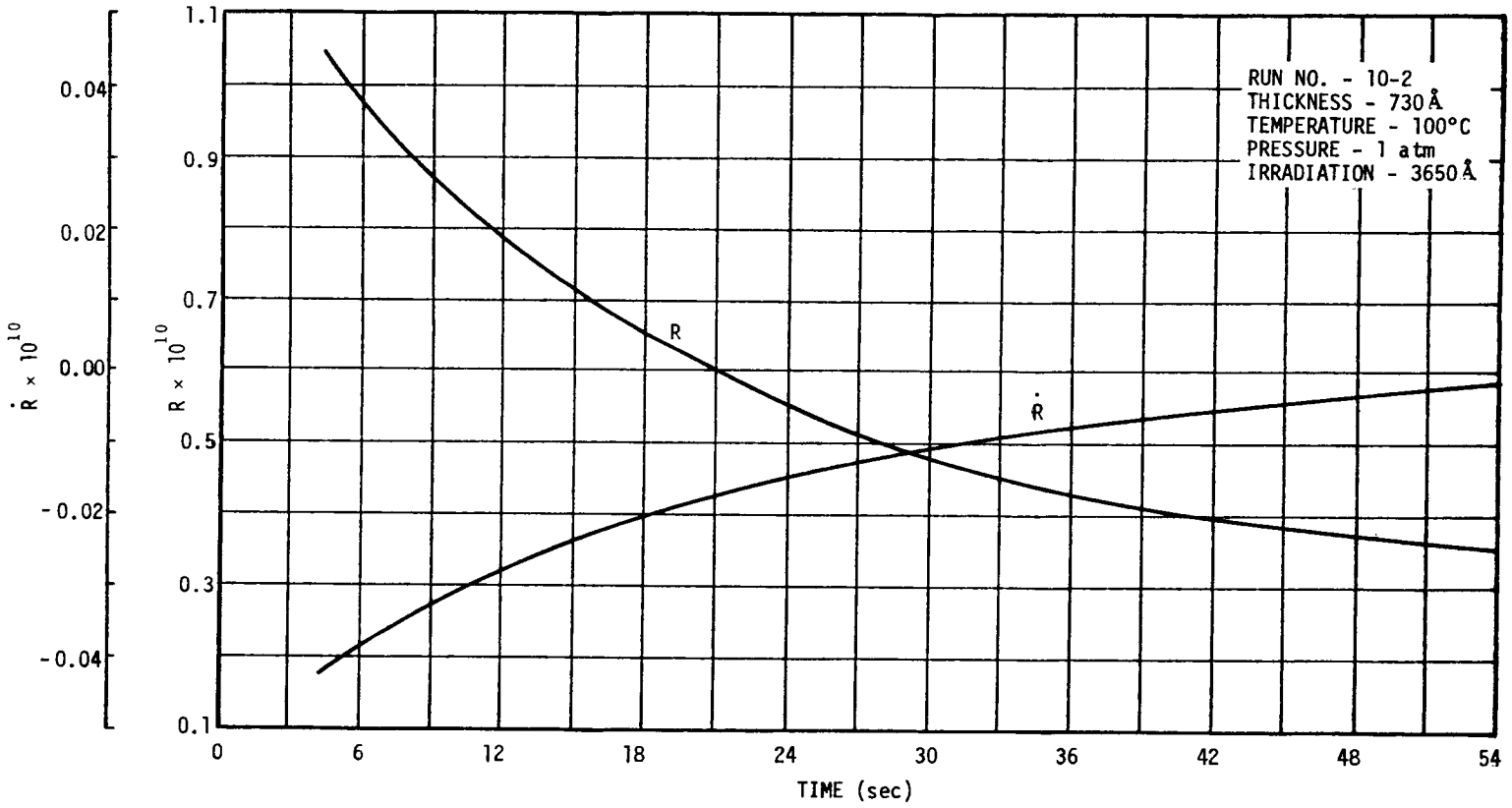
RUN NO. - 10-2
THICKNESS - 730 Å
TEMPERATURE - 100°C
PRESSURE - 1 atm
IRRADIATION - 3650 Å
R
Ṙ
Ṙ × 10^10
R × 10^10
0.04
0.02
0.00
-0.02
-0.04
1.1
0.9
0.7
0.5
0.3
0.1
0
6
12
18
24
30
36
42
48
54
TIME (sec)

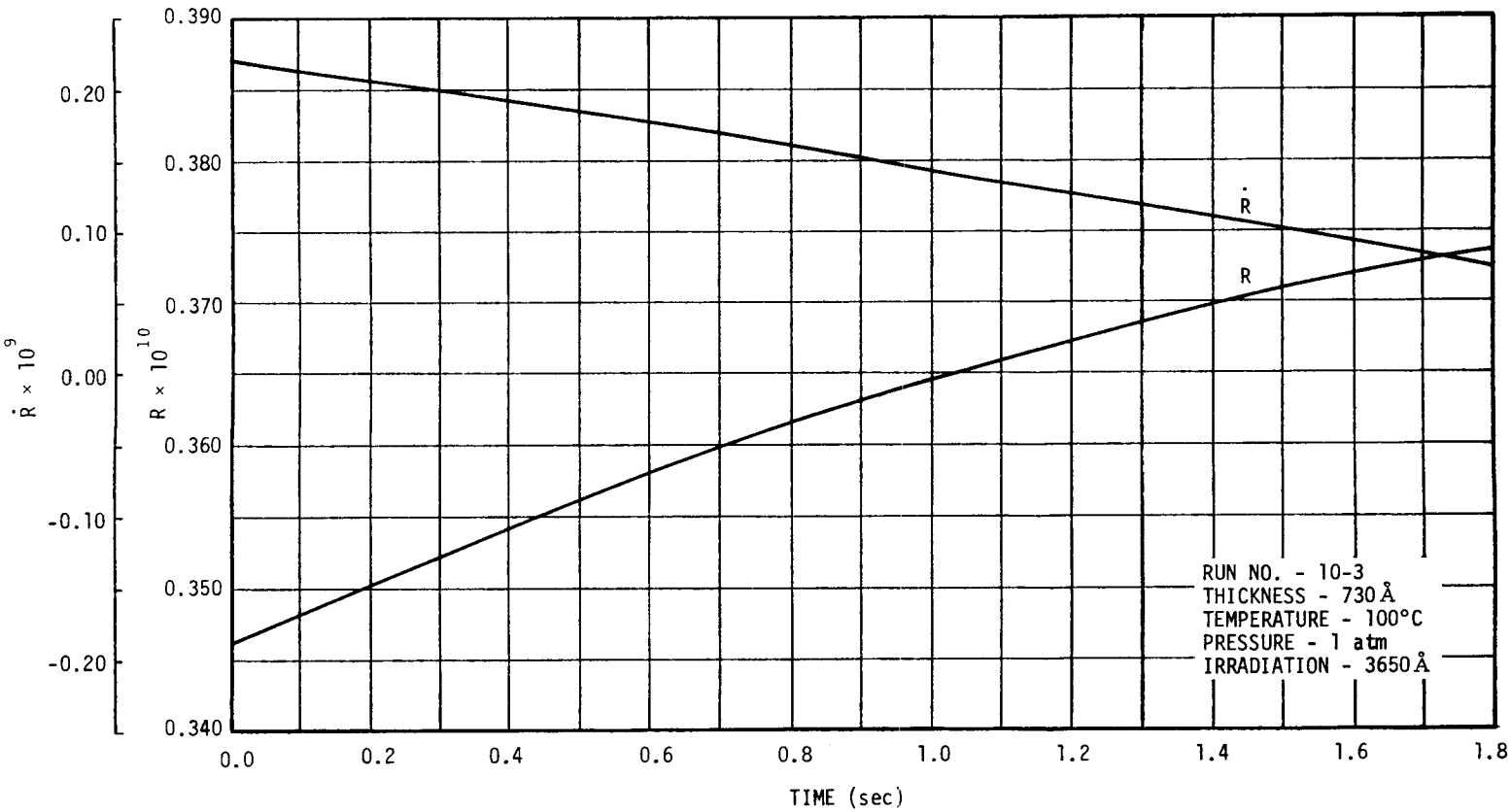
0.390
0.380
0.370
0.360
0.350
0.340
0.20
0.10
0.00
-0.10
-0.20
$\dot{R} \times 10^9$
$R \times 10^{10}$
0.0
0.2
0.4
0.6
0.8
1.0
1.2
1.4
1.6
1.8
TIME (sec)
$\dot{R}$
R
RUN NO. - 10-3
THICKNESS - 730 Å
TEMPERATURE - 100°C
PRESSURE - 1 atm
IRRADIATION - 3650 Å

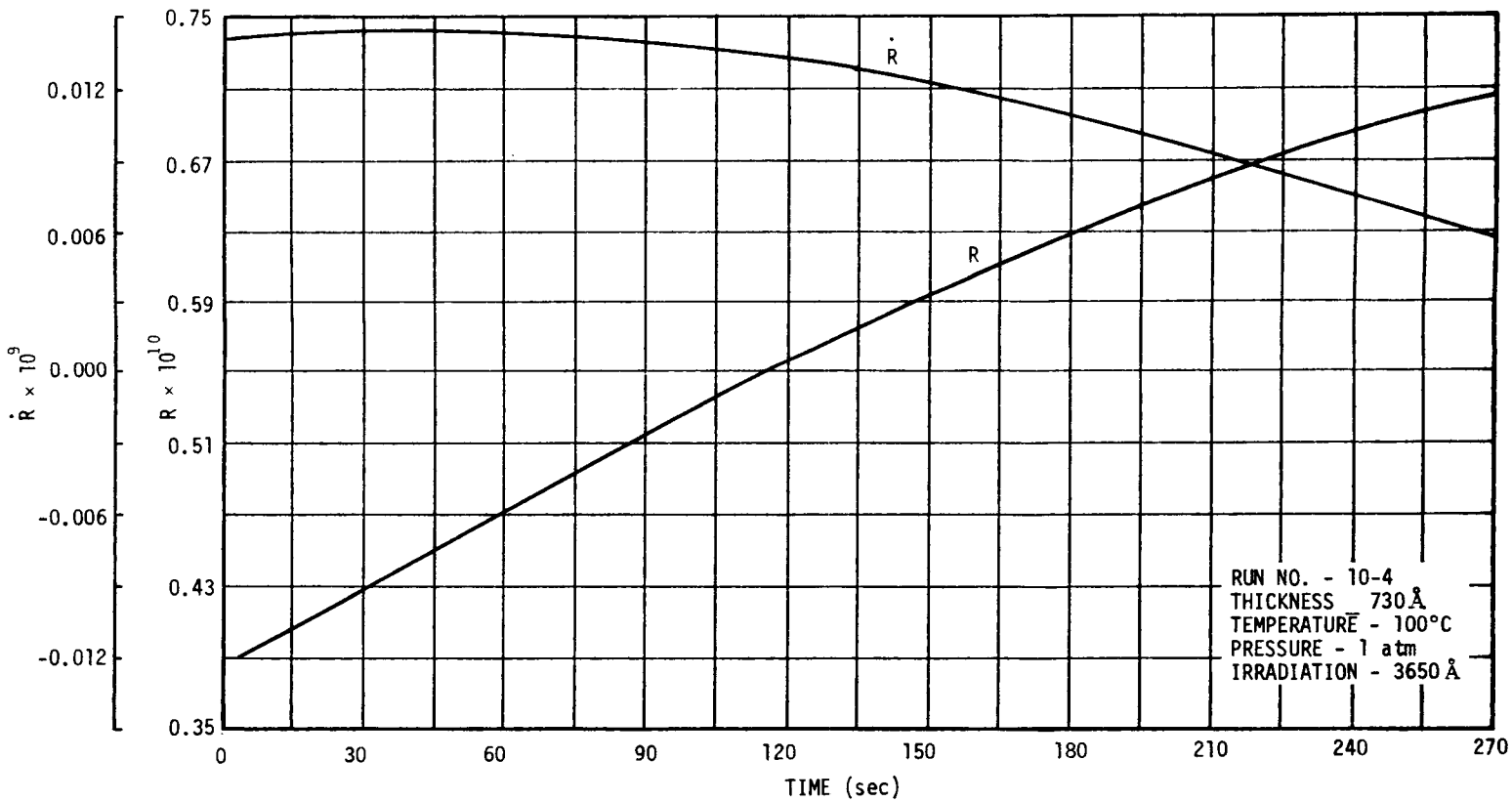
0.75
0.67
0.59
0.51
0.43
0.35
0.012
0.006
0.000
-0.006
-0.012
$\dot{R} \times 10^9$
$R \times 10^{10}$
$\dot{R}$
R
0
30
60
90
120
150
180
210
240
270
TIME (sec)
RUN NO. - 10-4
THICKNESS 730 Å
TEMPERATURE - 100°C
PRESSURE - 1 atm
IRRADIATION - 3650 Å

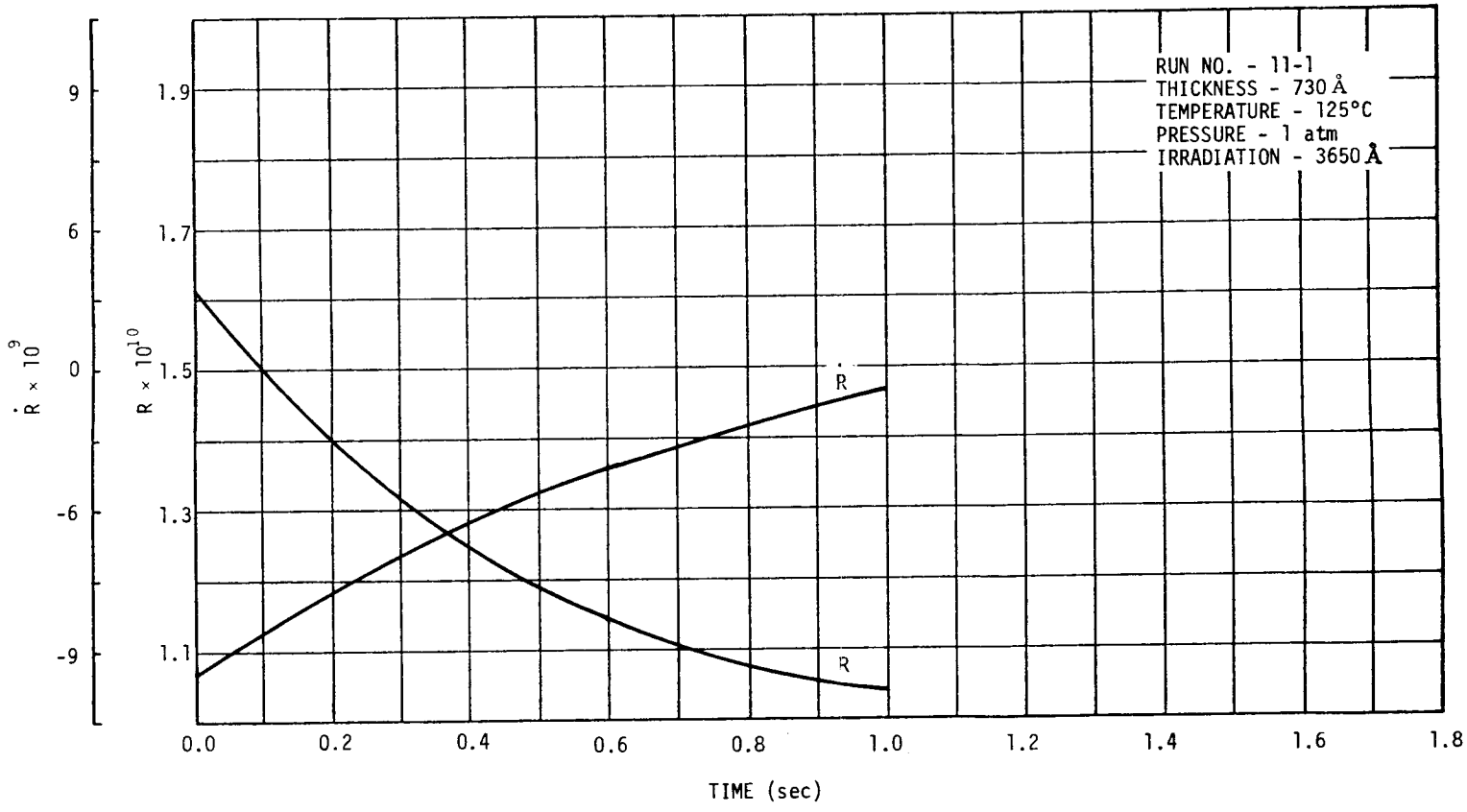
RUN NO. - 11-1
THICKNESS - 730 Å
TEMPERATURE - 125°C
PRESSURE - 1 atm
IRRADIATION - 3650 Å
$\dot{R} \times 10^9$
$R \times 10^{10}$
9
6
0
-6
-9
1.9
1.7
1.5
1.3
1.1
$\dot{R}$
R
0.0
0.2
0.4
0.6
0.8
1.0
1.2
1.4
1.6
1.8
TIME (sec)

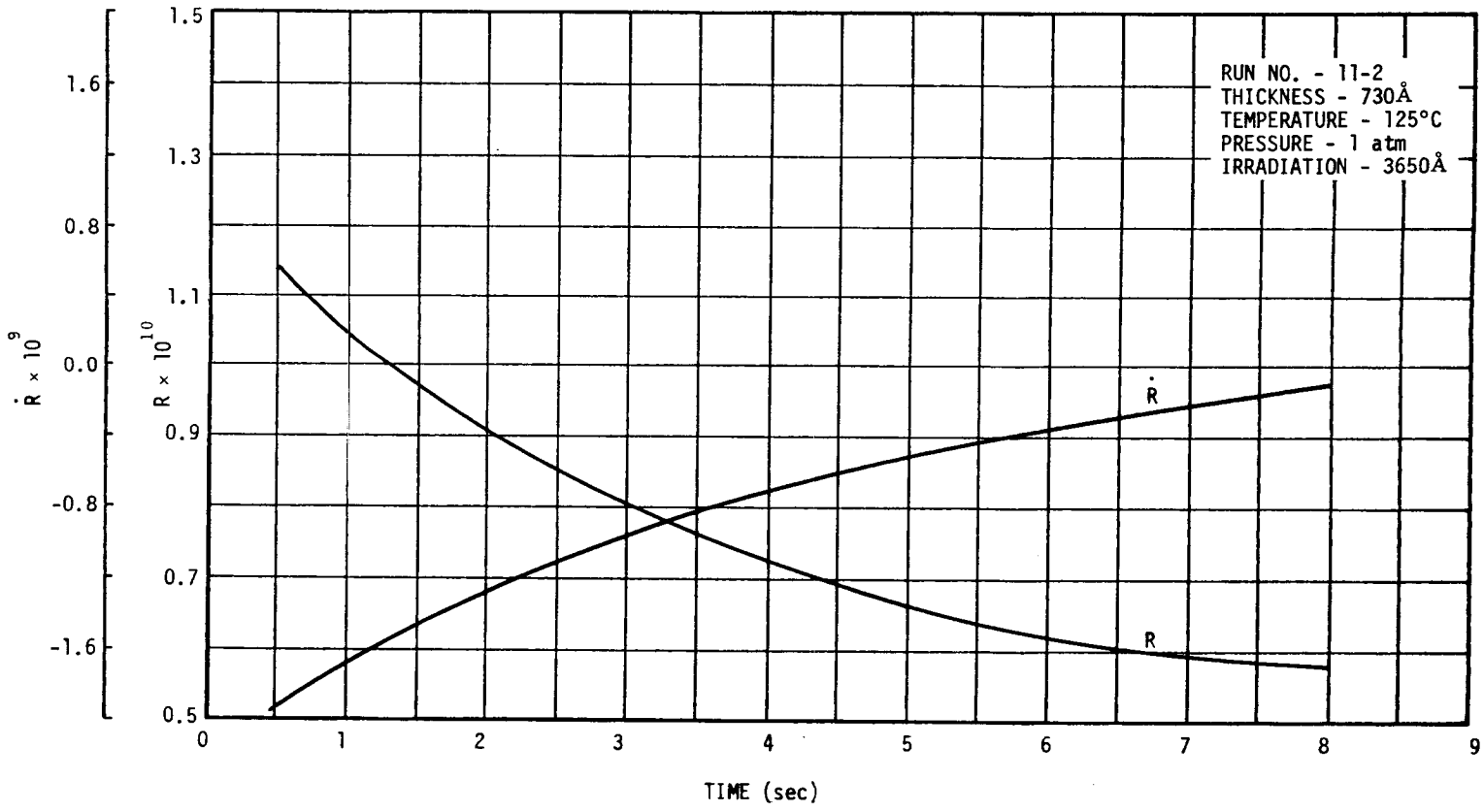
RUN NO. - 11-2
THICKNESS - 730Å
TEMPERATURE - 125°C
PRESSURE - 1 atm
IRRADIATION - 3650Å
$\dot{R} \times 10^9$
$R \times 10^{10}$
1.6
0.8
0.0
-0.8
-1.6
1.5
1.3
1.1
0.9
0.7
0.5
$\dot{R}$
R
0
1
2
3
4
5
6
7
8
9
TIME (sec)

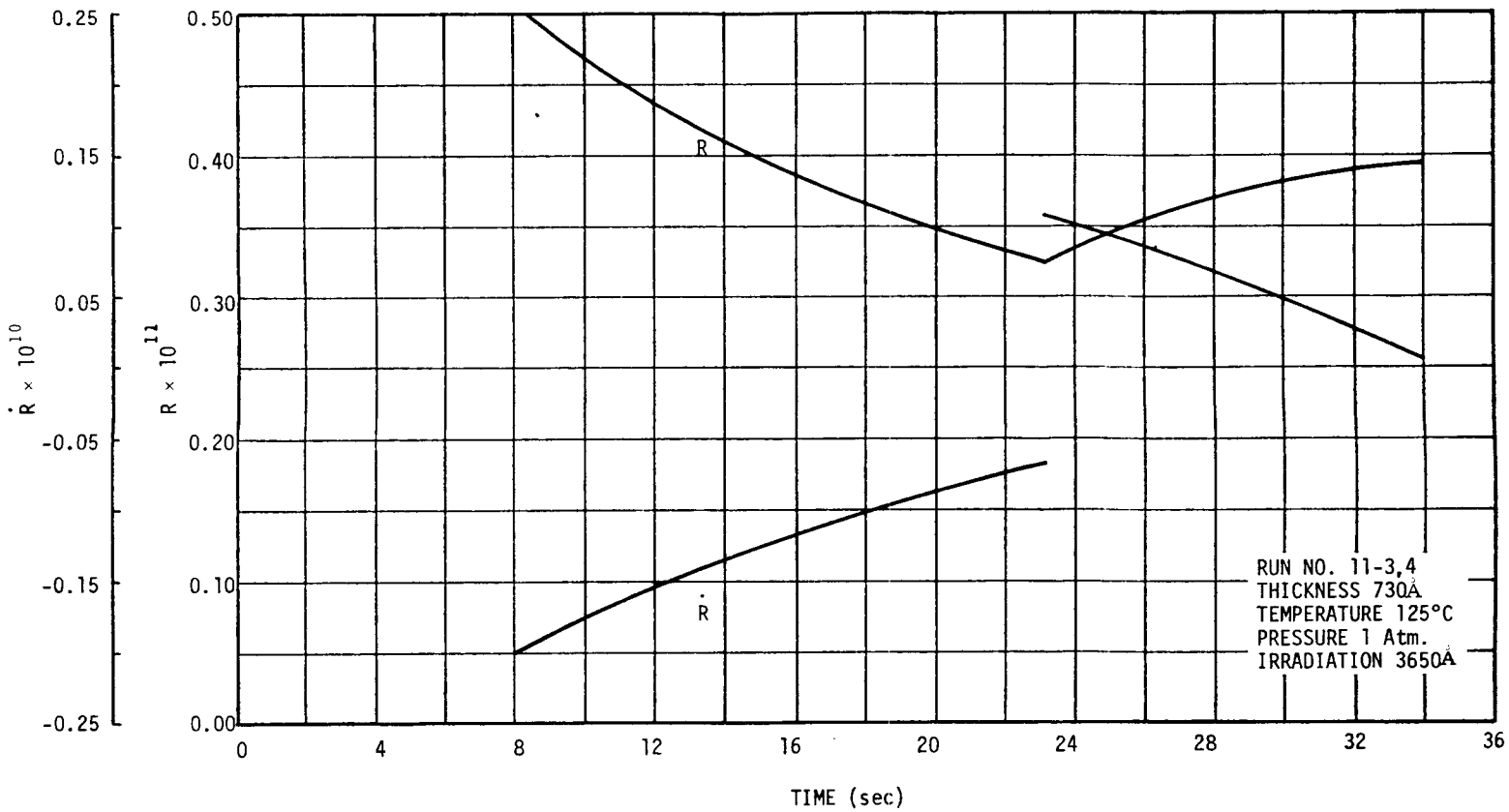
0.25
0.15
0.05
-0.05
-0.15
-0.25
$\dot{R} \times 10^{10}$
0.50
0.40
0.30
0.20
0.10
0.00
$R \times 10^{11}$
R
$\dot{R}$
0
4
8
12
16
20
24
28
32
36
TIME (sec)
RUN NO. 11-3,4
THICKNESS 730Å
TEMPERATURE 125°C
PRESSURE 1 Atm.
IRRADIATION 3650Å

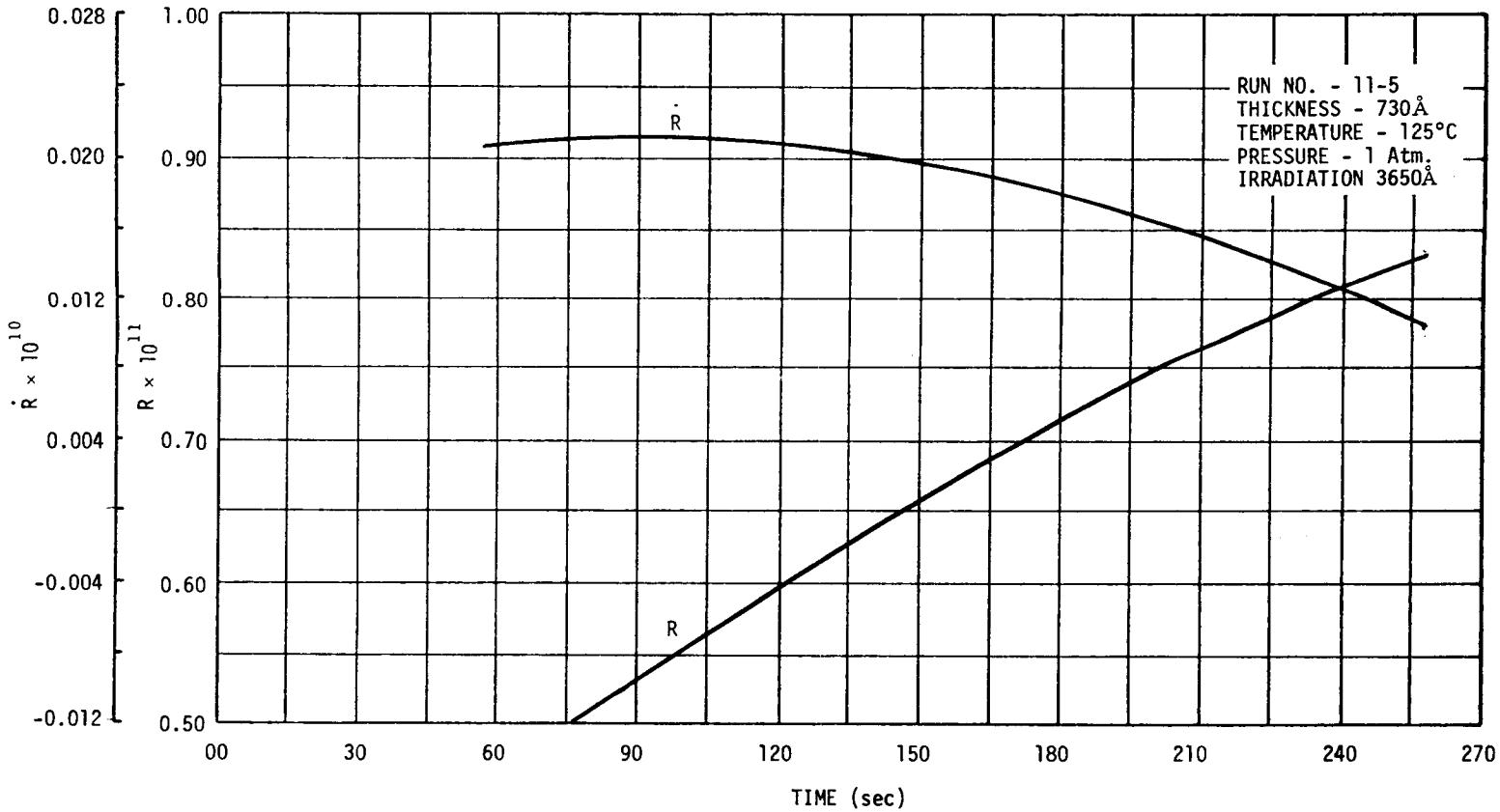
RUN NO. - 11-5
THICKNESS - 730Å
TEMPERATURE - 125°C
PRESSURE - 1 Atm.
IRRADIATION 3650Å
Ṙ
R
Ṙ × 10^10
R × 10^11
0.028
0.020
0.012
0.004
-0.004
-0.012
1.00
0.90
0.80
0.70
0.60
0.50
00
30
60
90
120
150
180
210
240
270
TIME (sec)

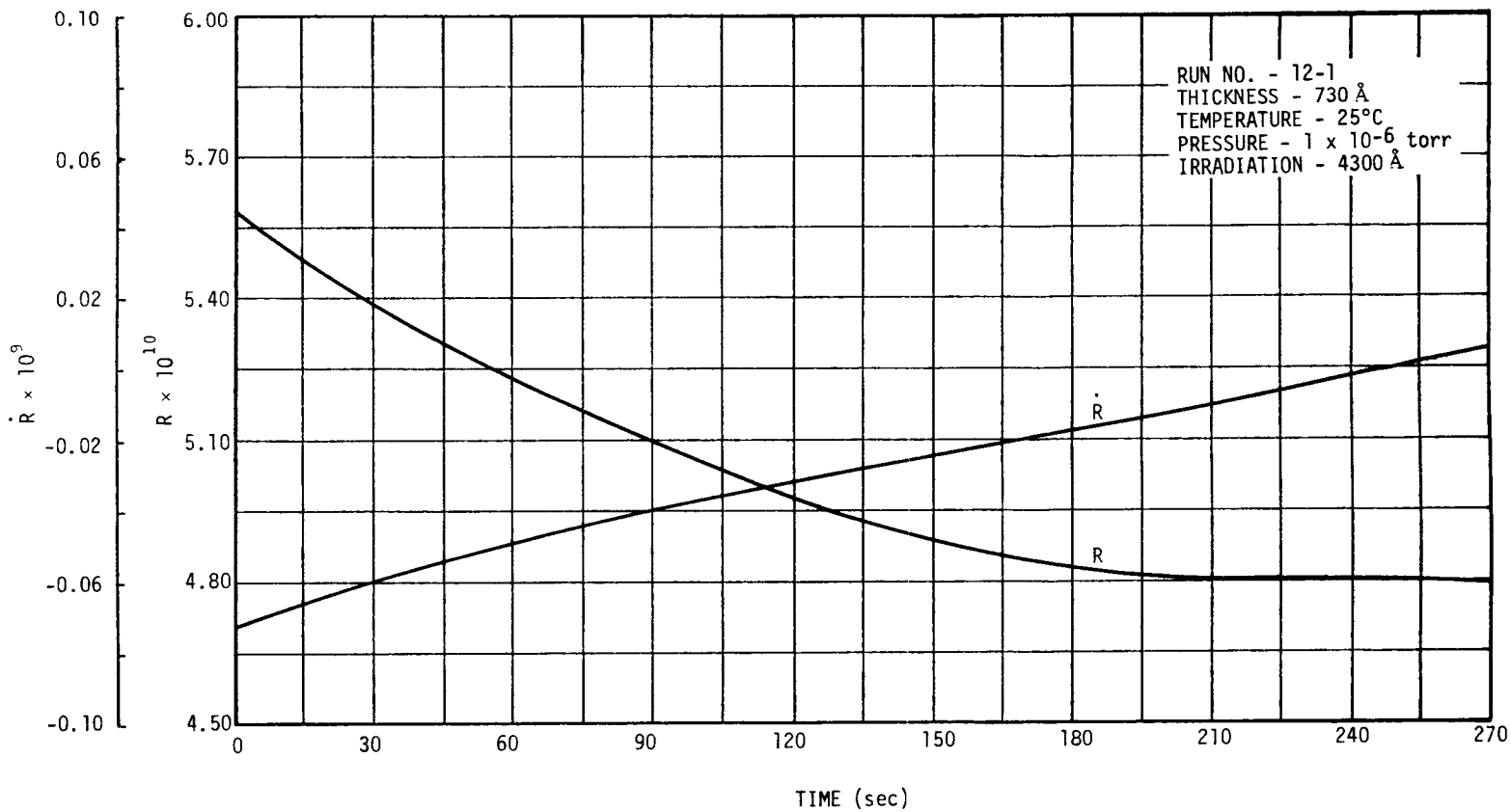
RUN NO. - 12-1
THICKNESS - 730 Å
TEMPERATURE - 25°C
PRESSURE - 1 x 10-6 torr
IRRADIATION - 4300 Å
Ṙ
R
Ṙ × 10^9
R × 10^10
0.10
0.06
0.02
-0.02
-0.06
-0.10
6.00
5.70
5.40
5.10
4.80
4.50
0
30
60
90
120
150
180
210
240
270
TIME (sec)

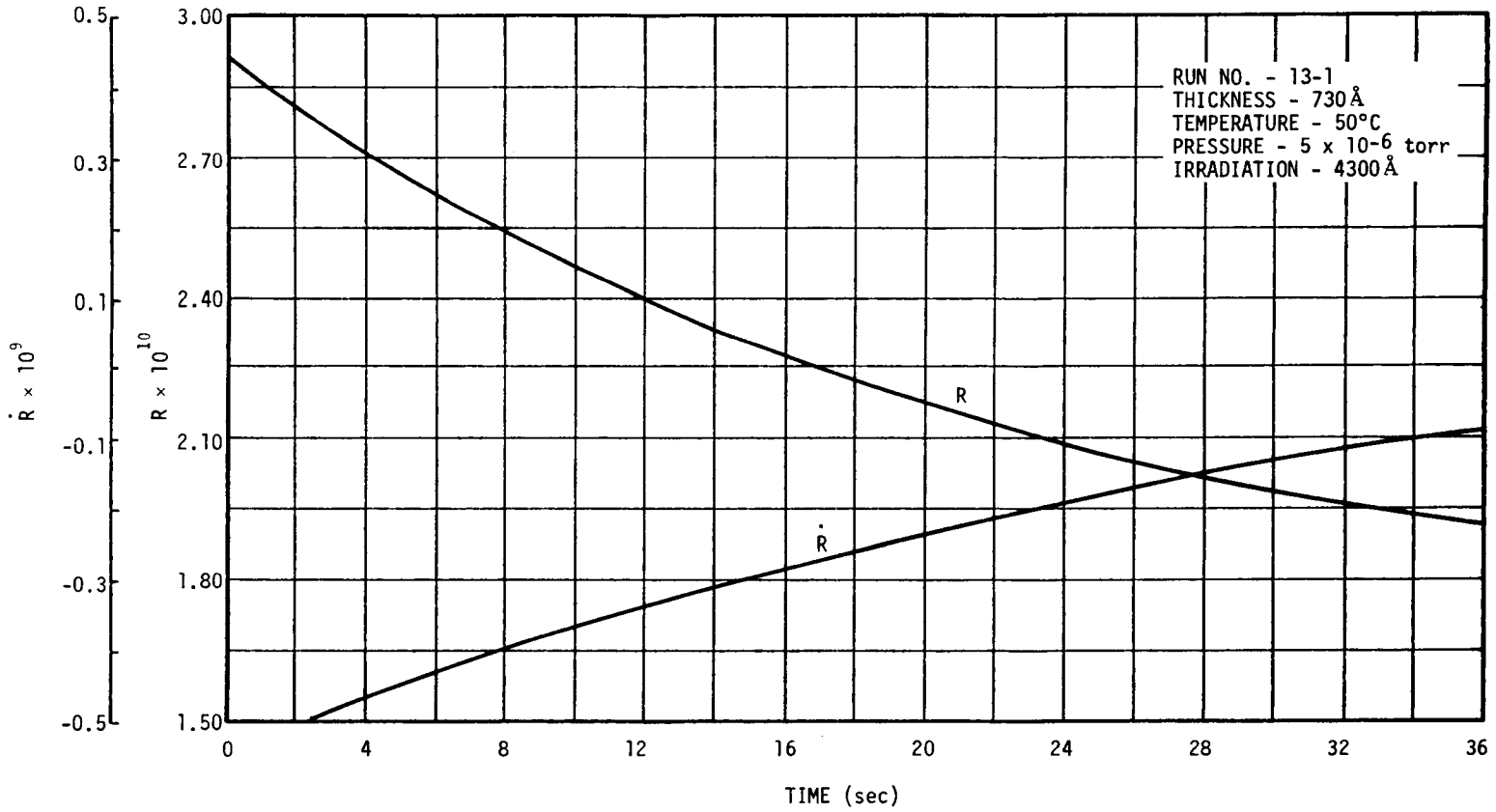
RUN NO. - 13-1
THICKNESS - 730Å
TEMPERATURE - 50°C
PRESSURE - 5 x 10-6 torr
IRRADIATION - 4300Å
R
Ṙ
Ṙ × 10^9
R × 10^10
0.5
0.3
0.1
-0.1
-0.3
-0.5
3.00
2.70
2.40
2.10
1.80
1.50
0
4
8
12
16
20
24
28
32
36
TIME (sec)

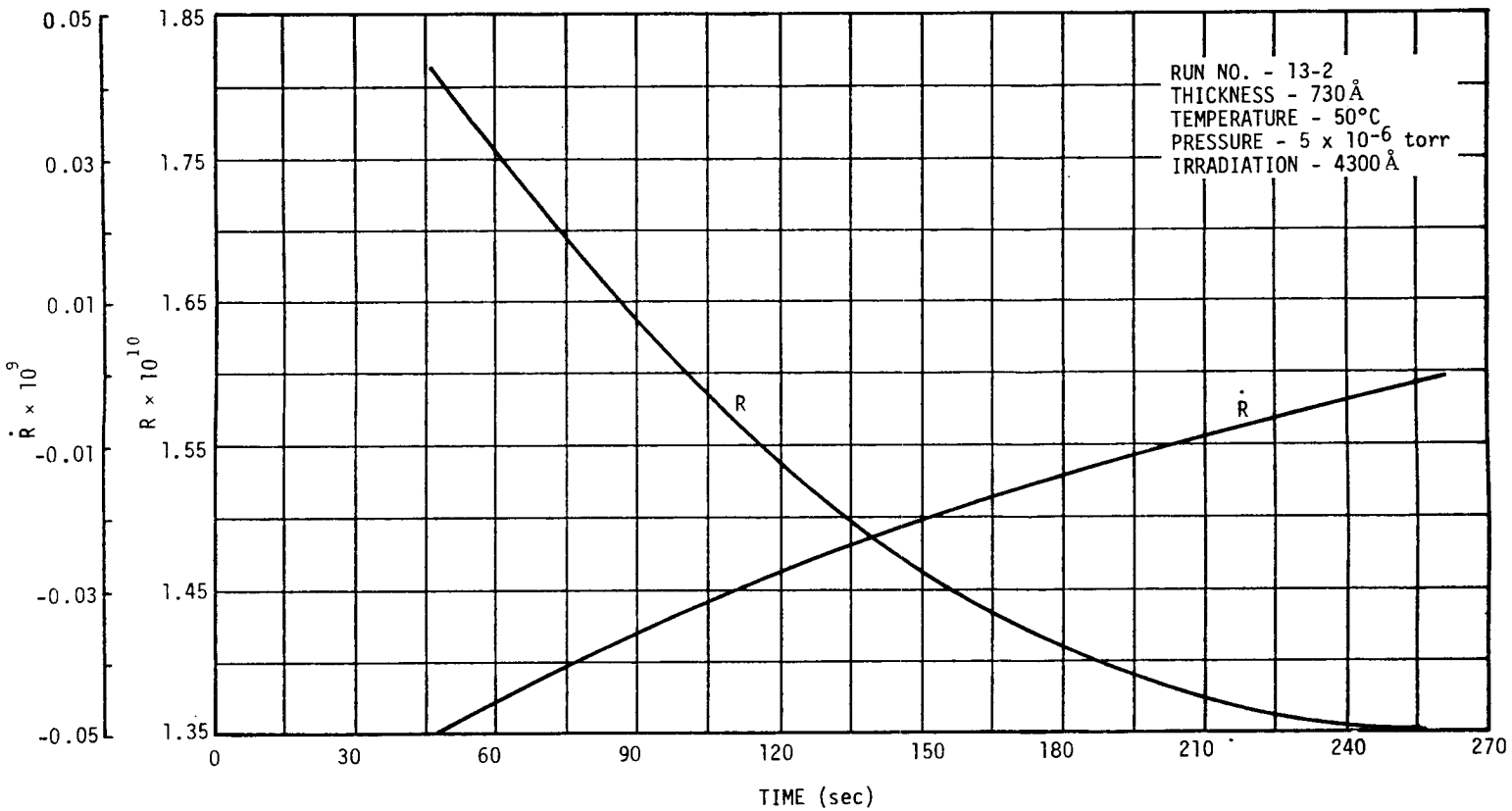
RUN NO. - 13-2
THICKNESS - 730 Å
TEMPERATURE - 50°C
PRESSURE - 5 x 10^-6 torr
IRRADIATION - 4300 Å
R
Ṙ
Ṙ × 10^9
R × 10^10
0.05
0.03
0.01
-0.01
-0.03
-0.05
1.85
1.75
1.65
1.55
1.45
1.35
0
30
60
90
120
150
180
210
240
270
TIME (sec)

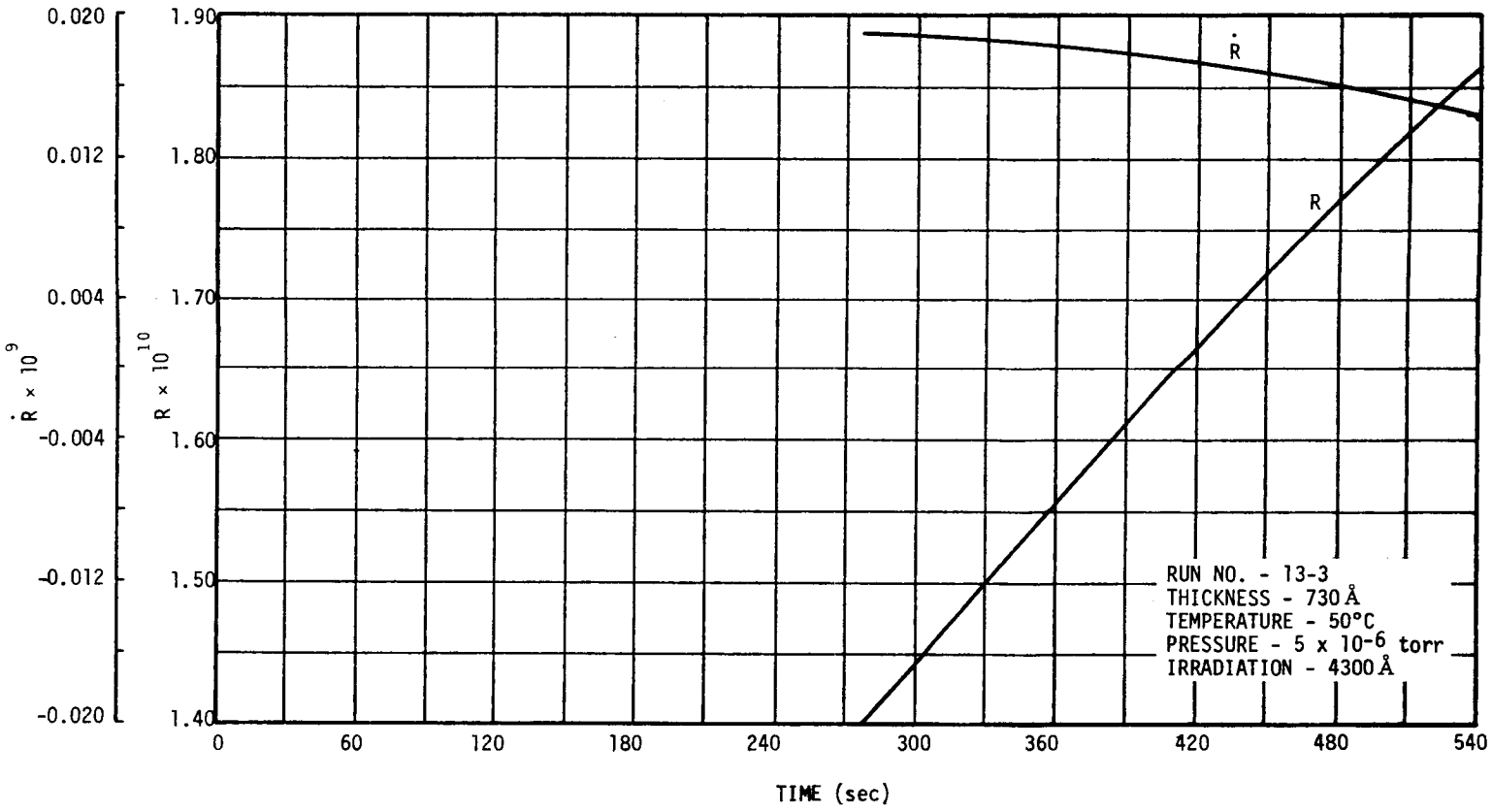
0.020
0.012
0.004
-0.004
-0.012
-0.020
$\dot{R} \times 10^9$
1.90
1.80
1.70
1.60
1.50
1.40
$R \times 10^{10}$
0
60
120
180
240
300
360
420
480
540
TIME (sec)
$\dot{R}$
R
RUN NO. - 13-3
THICKNESS - 730 Å
TEMPERATURE - 50°C
PRESSURE - 5 x 10-6 torr
IRRADIATION - 4300 Å

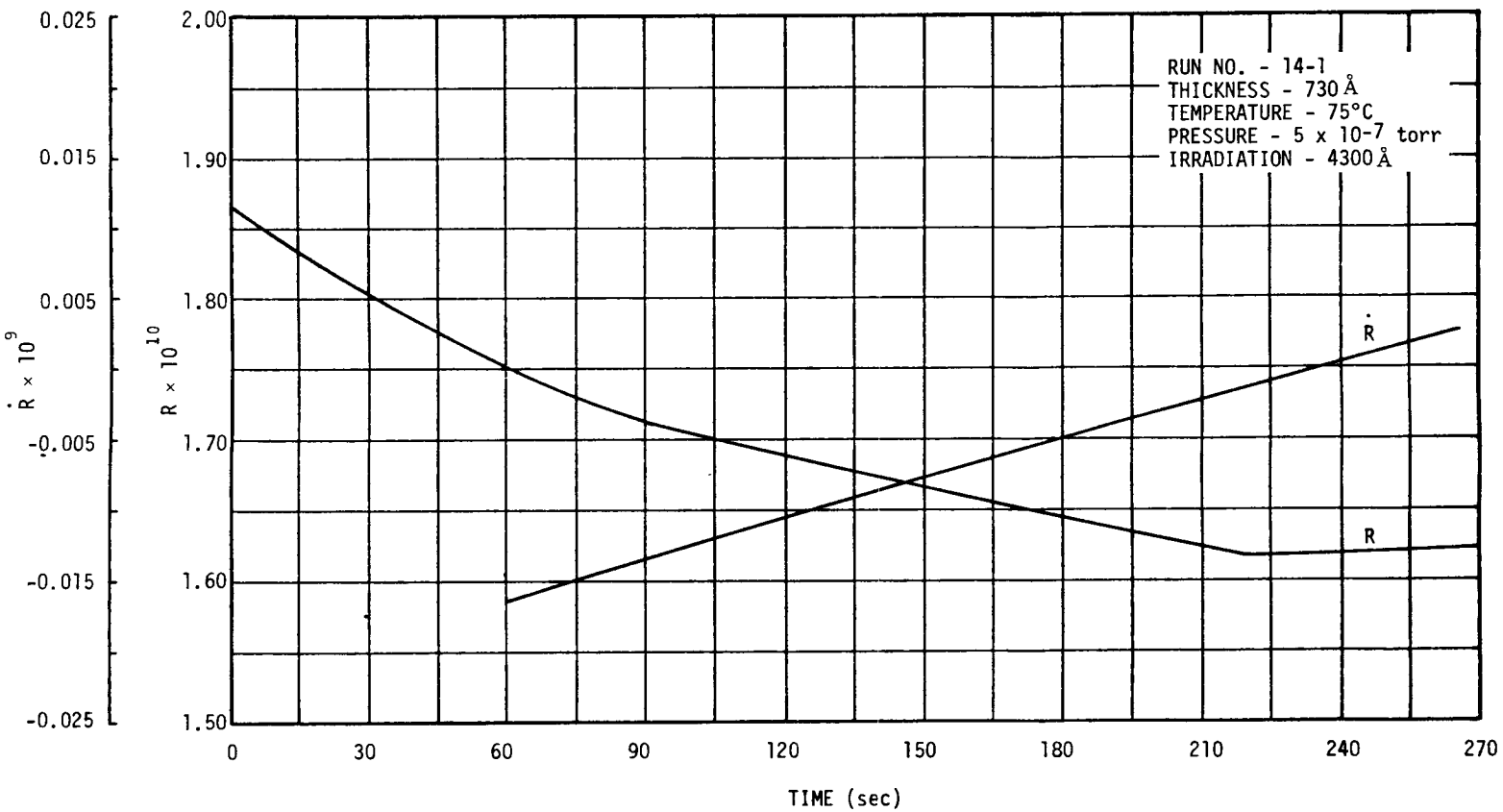
RUN NO. - 14-1
THICKNESS - 730 Å
TEMPERATURE - 75°C
PRESSURE - 5 x 10-7 torr
IRRADIATION - 4300 Å
Ṙ
R
Ṙ × 10^9
R × 10^10
0.025
0.015
0.005
-0.005
-0.015
-0.025
2.00
1.90
1.80
1.70
1.60
1.50
0
30
60
90
120
150
180
210
240
270
TIME (sec)

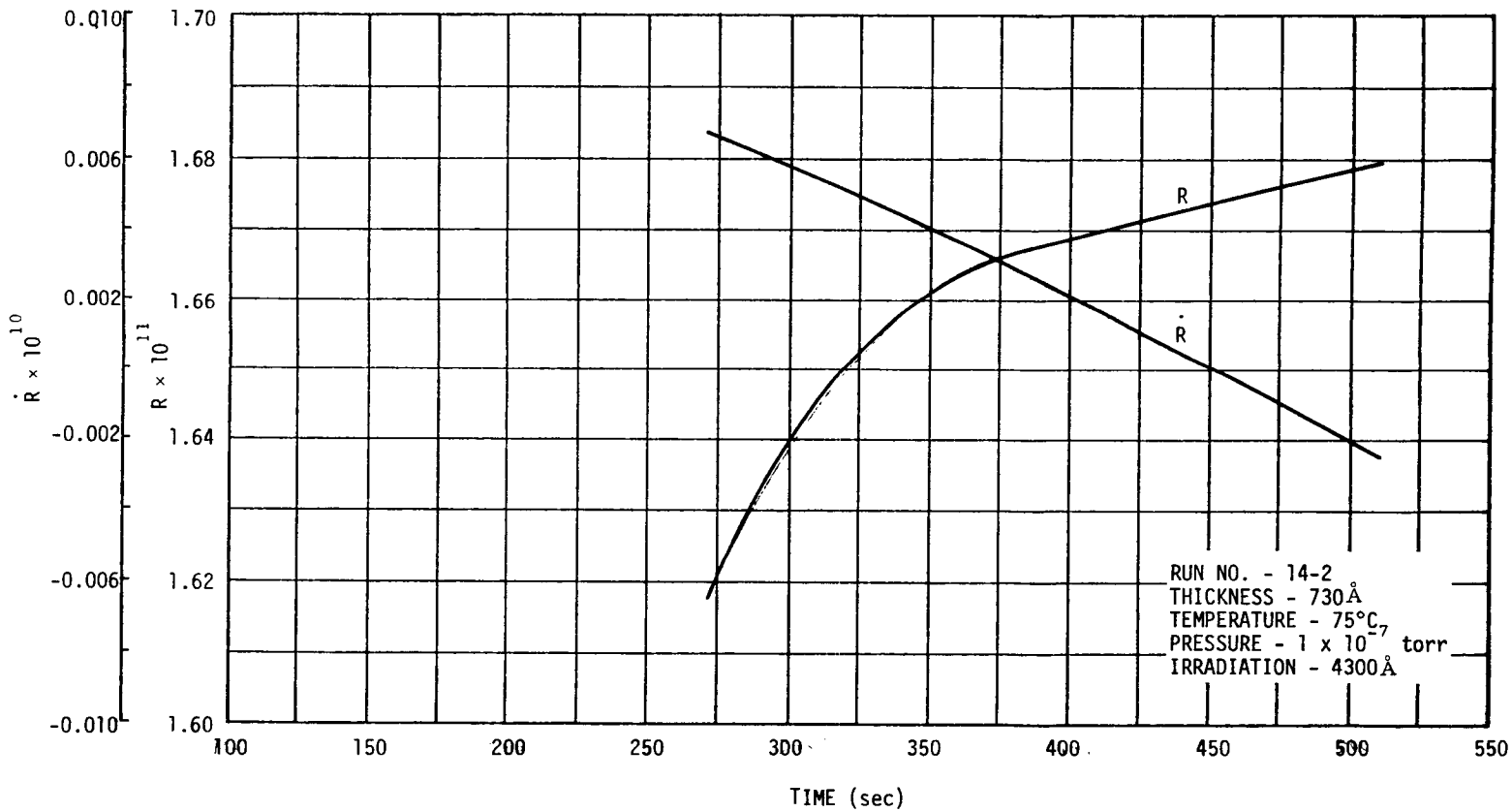
0.010
0.006
0.002
-0.002
-0.006
-0.010
$\dot{R} \times 10^{10}$
1.70
1.68
1.66
1.64
1.62
1.60
$R \times 10^{11}$
100
150
200
250
300
350
400
450
500
550
TIME (sec)
R
$\dot{R}$
RUN NO. - 14-2
THICKNESS - 730Å
TEMPERATURE - 75°C
PRESSURE - 1 x 10^{-7} torr
IRRADIATION - 4300Å

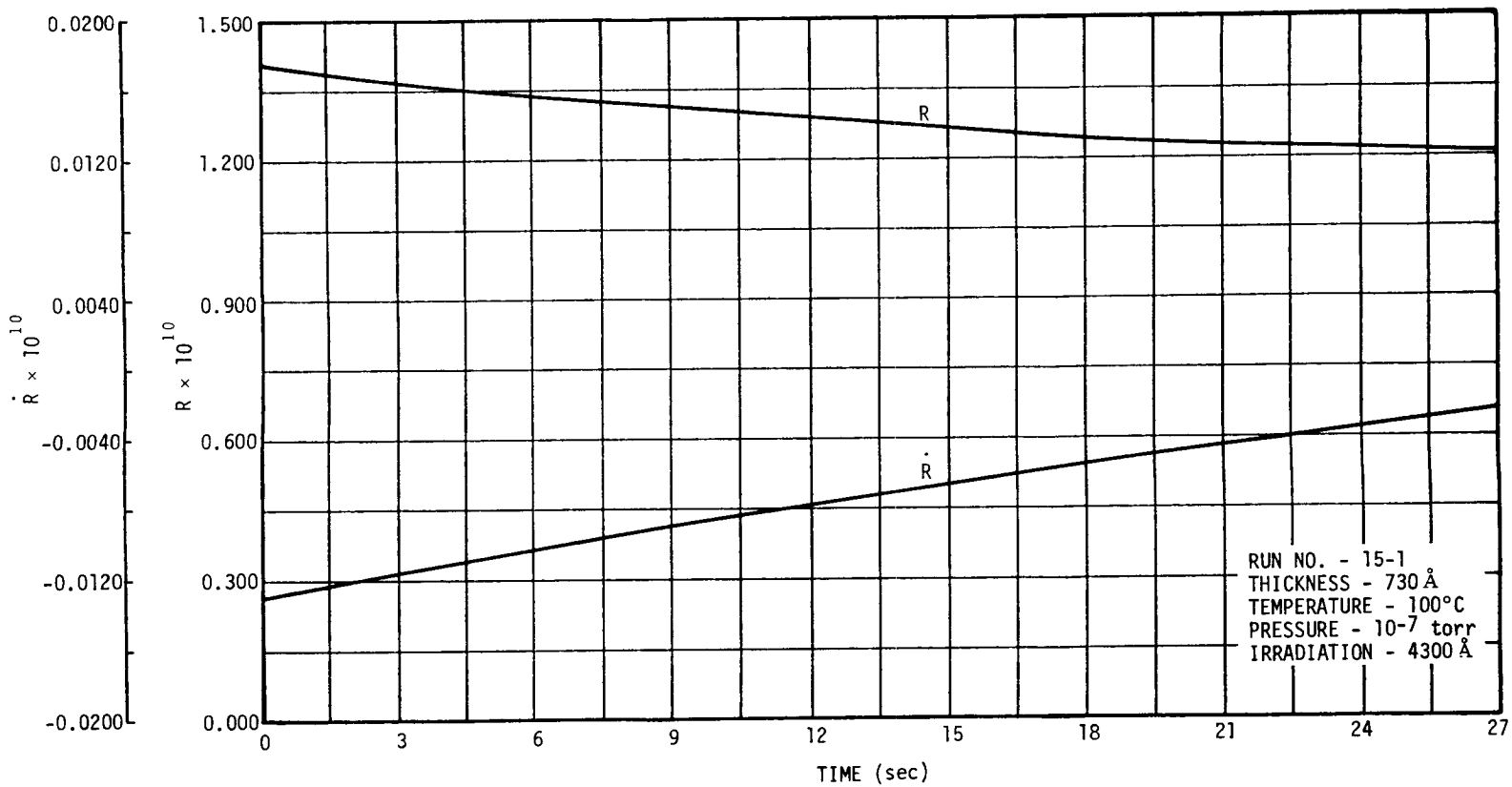
0.0200
0.0120
0.0040
-0.0040
-0.0120
-0.0200
$\dot{R} \times 10^{10}$
1.500
1.200
0.900
0.600
0.300
0.000
$R \times 10^{10}$
R
$\dot{R}$
0
3
6
9
12
15
18
21
24
27
TIME (sec)
RUN NO. - 15-1
THICKNESS - 730 Å
TEMPERATURE - 100°C
PRESSURE - 10^{-7} torr
IRRADIATION - 4300 Å

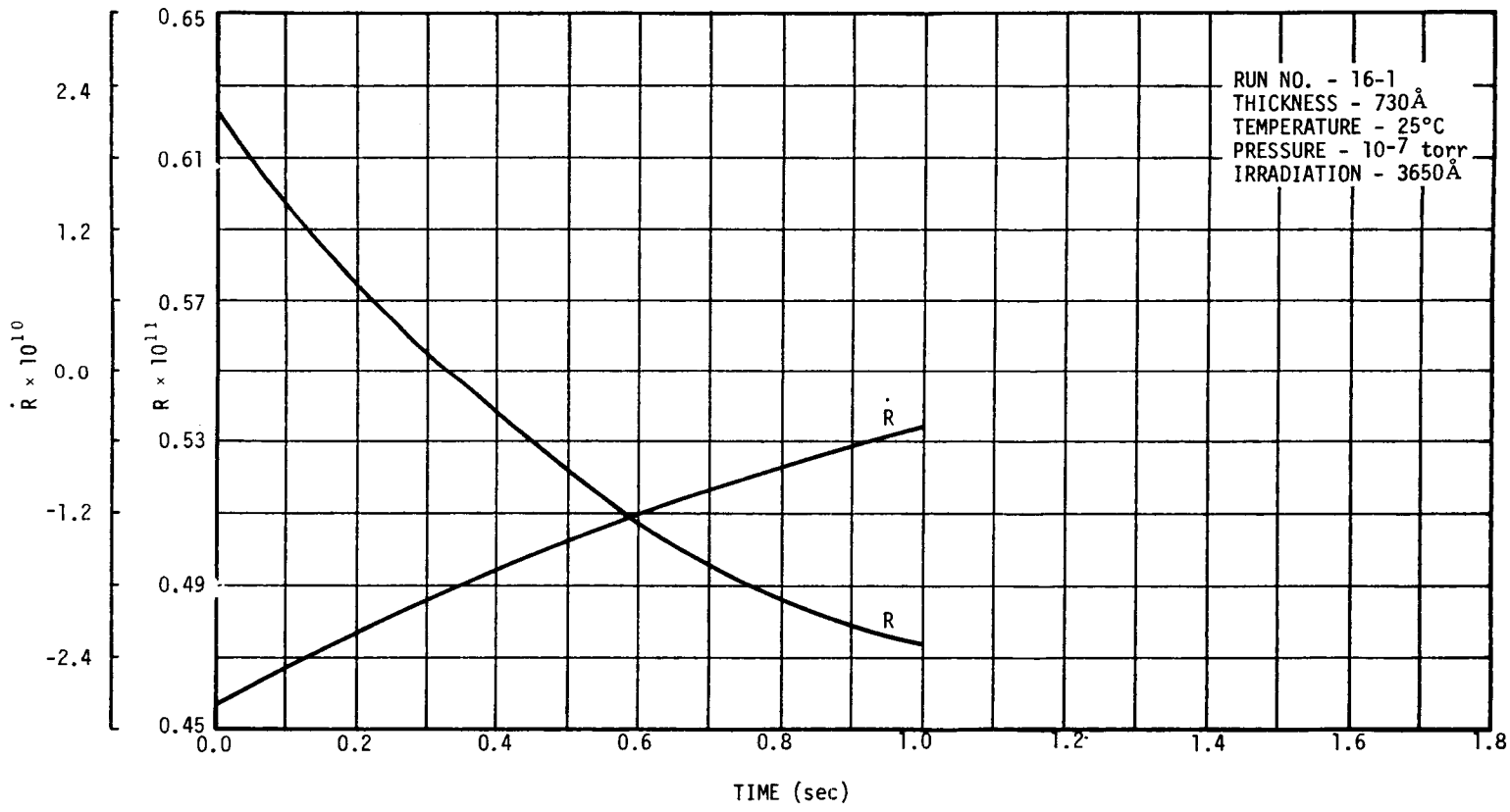
RUN NO. - 16-1
THICKNESS - 730Å
TEMPERATURE - 25°C
PRESSURE - 10^{-7} torr
IRRADIATION - 3650Å
$\dot{R} \times 10^{10}$
$R \times 10^{11}$
2.4
1.2
0.0
-1.2
-2.4
0.65
0.61
0.57
0.53
0.49
0.45
$\dot{R}$
R
0.0
0.2
0.4
0.6
0.8
1.0
1.2
1.4
1.6
1.8
TIME (sec)

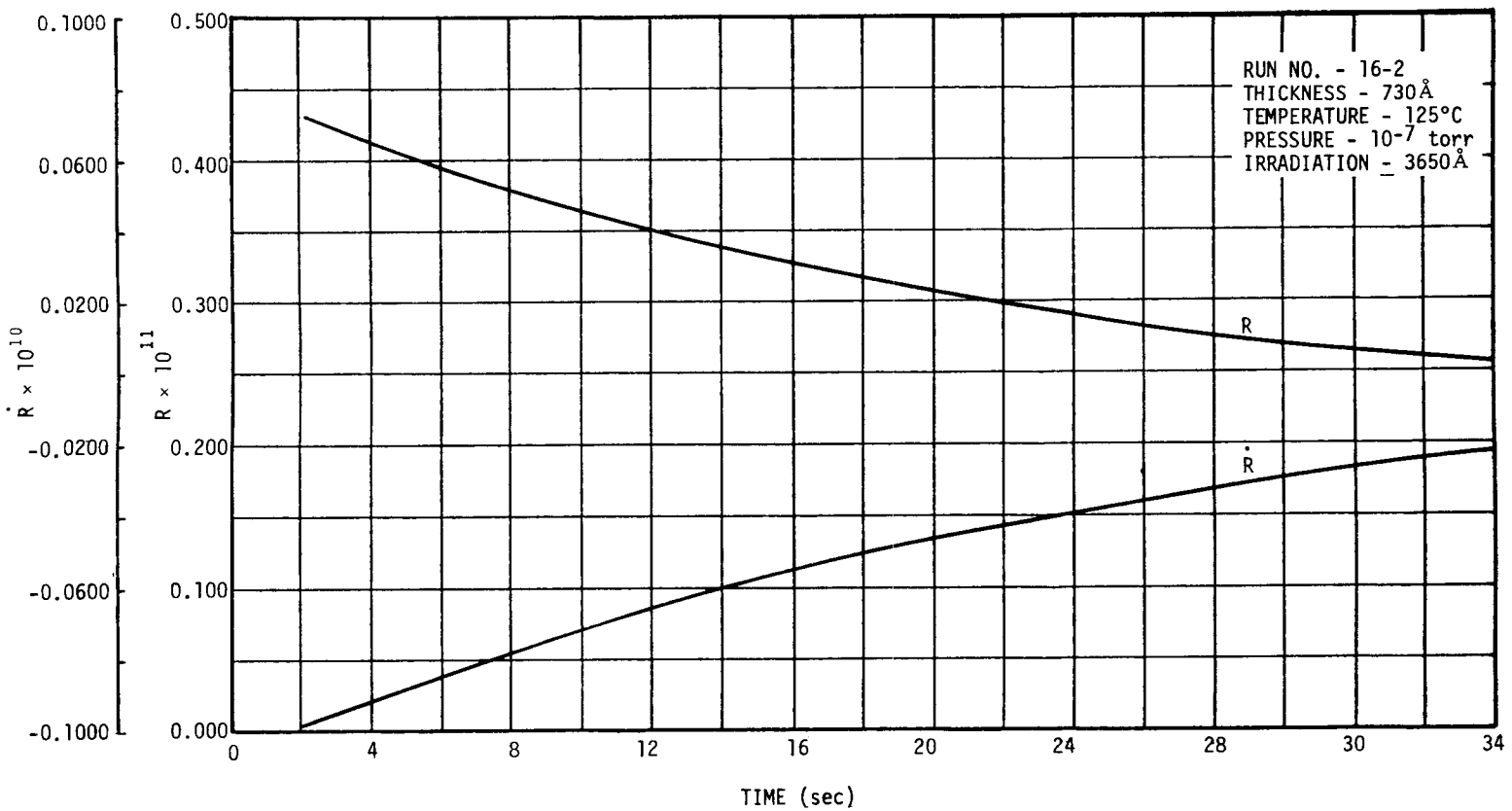
RUN NO. - 16-2
THICKNESS - 730Å
TEMPERATURE - 125°C
PRESSURE - 10^{-7} torr
IRRADIATION - 3650Å
R
Ṙ
$\dot{R} \times 10^{10}$
$R \times 10^{11}$
0.1000
0.0600
0.0200
-0.0200
-0.0600
-0.1000
0.500
0.400
0.300
0.200
0.100
0.000
0
4
8
12
16
20
24
28
30
34
TIME (sec)

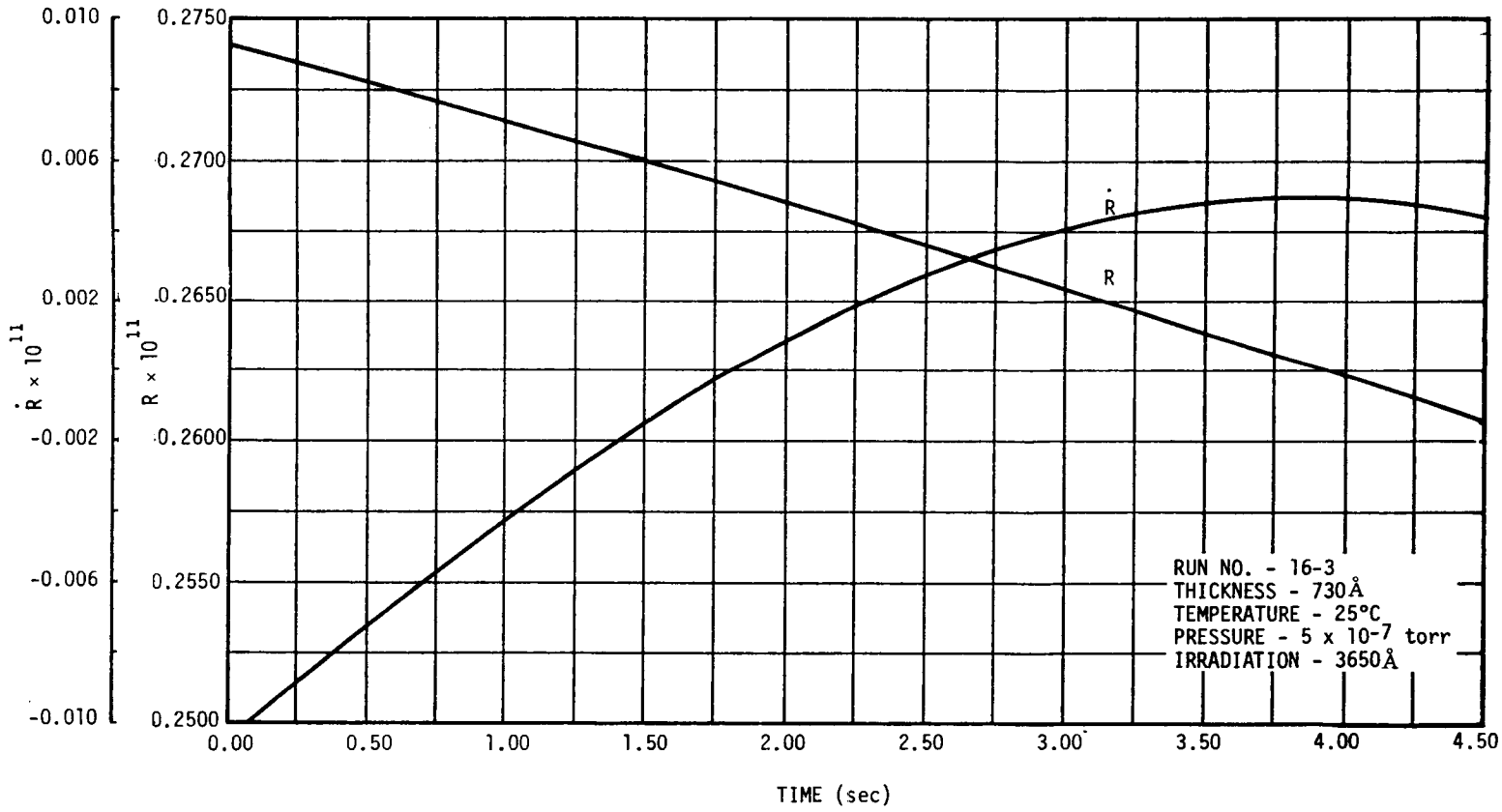
0.010
0.006
0.002
-0.002
-0.006
-0.010
$\dot{R} \times 10^{11}$
0.2750
0.2700
0.2650
0.2600
0.2550
0.2500
$R \times 10^{11}$
0.00
0.50
1.00
1.50
2.00
2.50
3.00
3.50
4.00
4.50
TIME (sec)
$\dot{R}$
R
RUN NO. - 16-3
THICKNESS - 730Å
TEMPERATURE - 25°C
PRESSURE - 5 x 10^{-7} torr
IRRADIATION - 3650Å

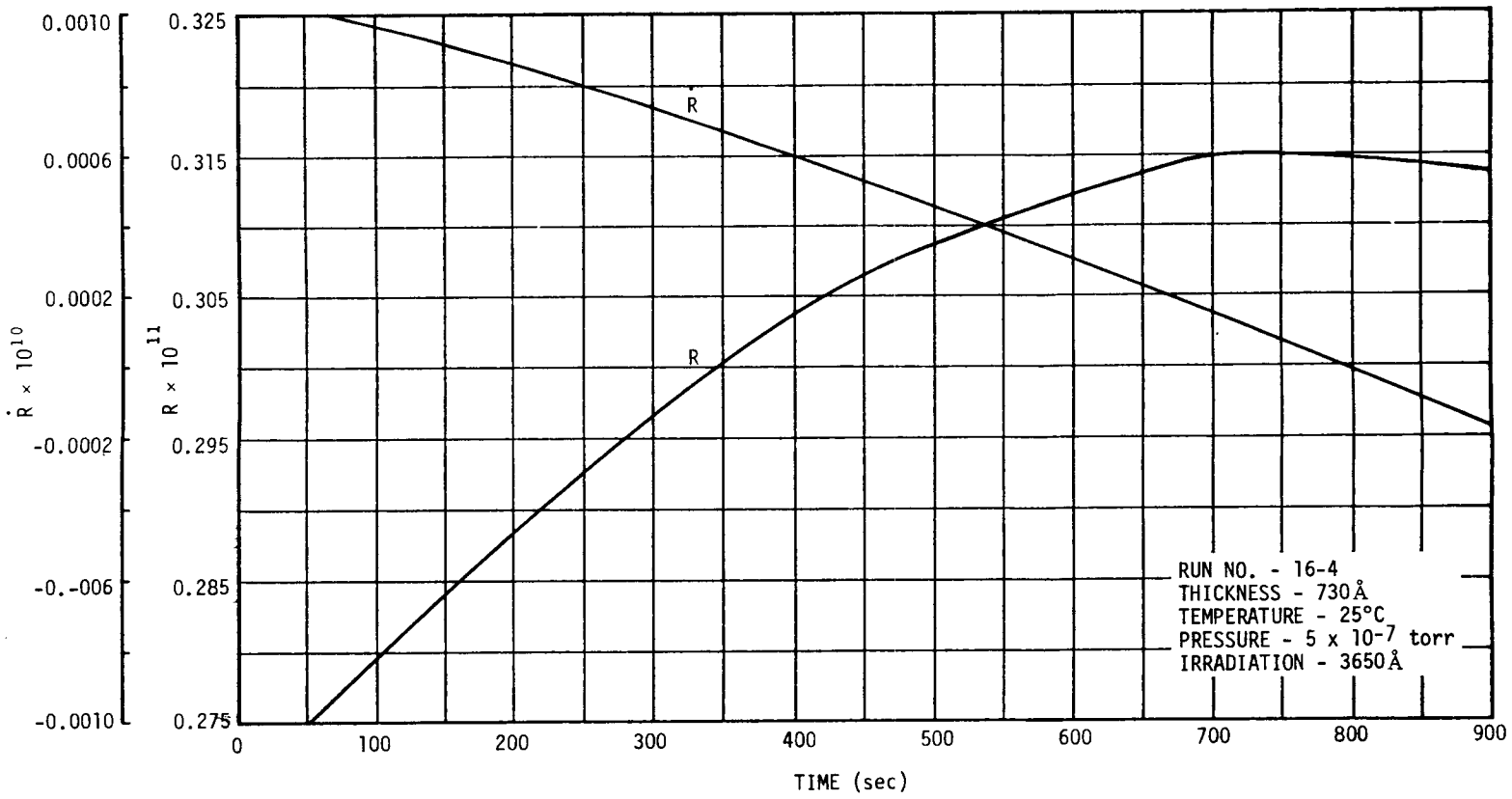
0.0010
0.0006
0.0002
-0.0002
-0.-006
-0.0010
$\dot{R} \times 10^{10}$
0.325
0.315
0.305
0.295
0.285
0.275
$R \times 10^{11}$
$\dot{R}$
R
0
100
200
300
400
500
600
700
800
900
TIME (sec)
RUN NO. - 16-4
THICKNESS - 730Å
TEMPERATURE - 25°C
PRESSURE - 5 x 10^{-7} torr
IRRADIATION - 3650Å

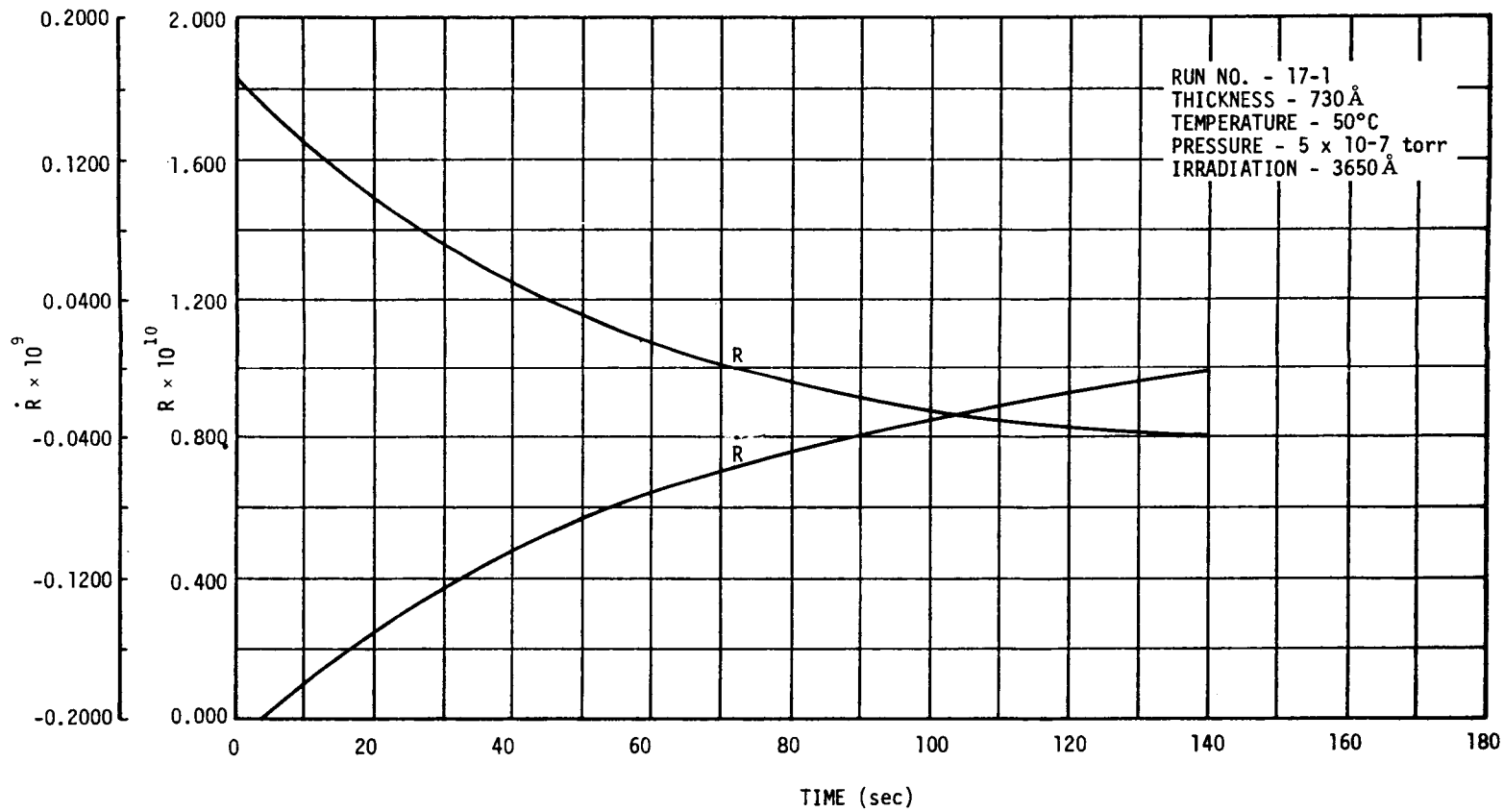
RUN NO. - 17-1
THICKNESS - 730Å
TEMPERATURE - 50°C
PRESSURE - 5 x 10-7 torr
IRRADIATION - 3650Å
R
Ṙ
Ṙ × 10^9
R × 10^10
0.2000
0.1200
0.0400
-0.0400
-0.1200
-0.2000
2.000
1.600
1.200
0.800
0.400
0.000
0
20
40
60
80
100
120
140
160
180
TIME (sec)

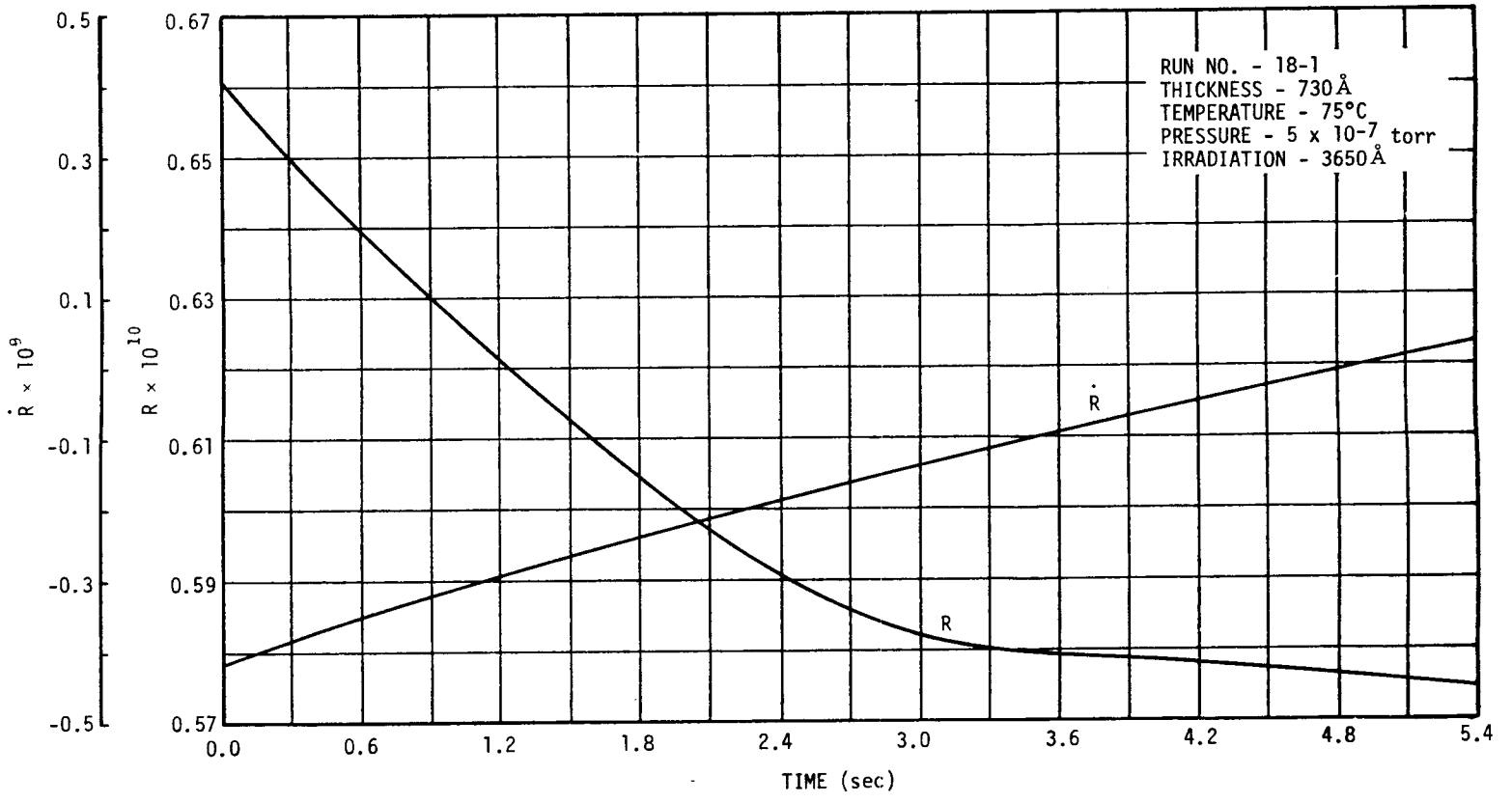
RUN NO. - 18-1
THICKNESS - 730Å
TEMPERATURE - 75°C
PRESSURE - 5 x 10-7 torr
IRRADIATION - 3650Å
Ṙ × 10^9
R × 10^10
0.5
0.3
0.1
-0.1
-0.3
-0.5
0.67
0.65
0.63
0.61
0.59
0.57
0.0
0.6
1.2
1.8
2.4
3.0
3.6
4.2
4.8
5.4
TIME (sec)
Ṙ
R

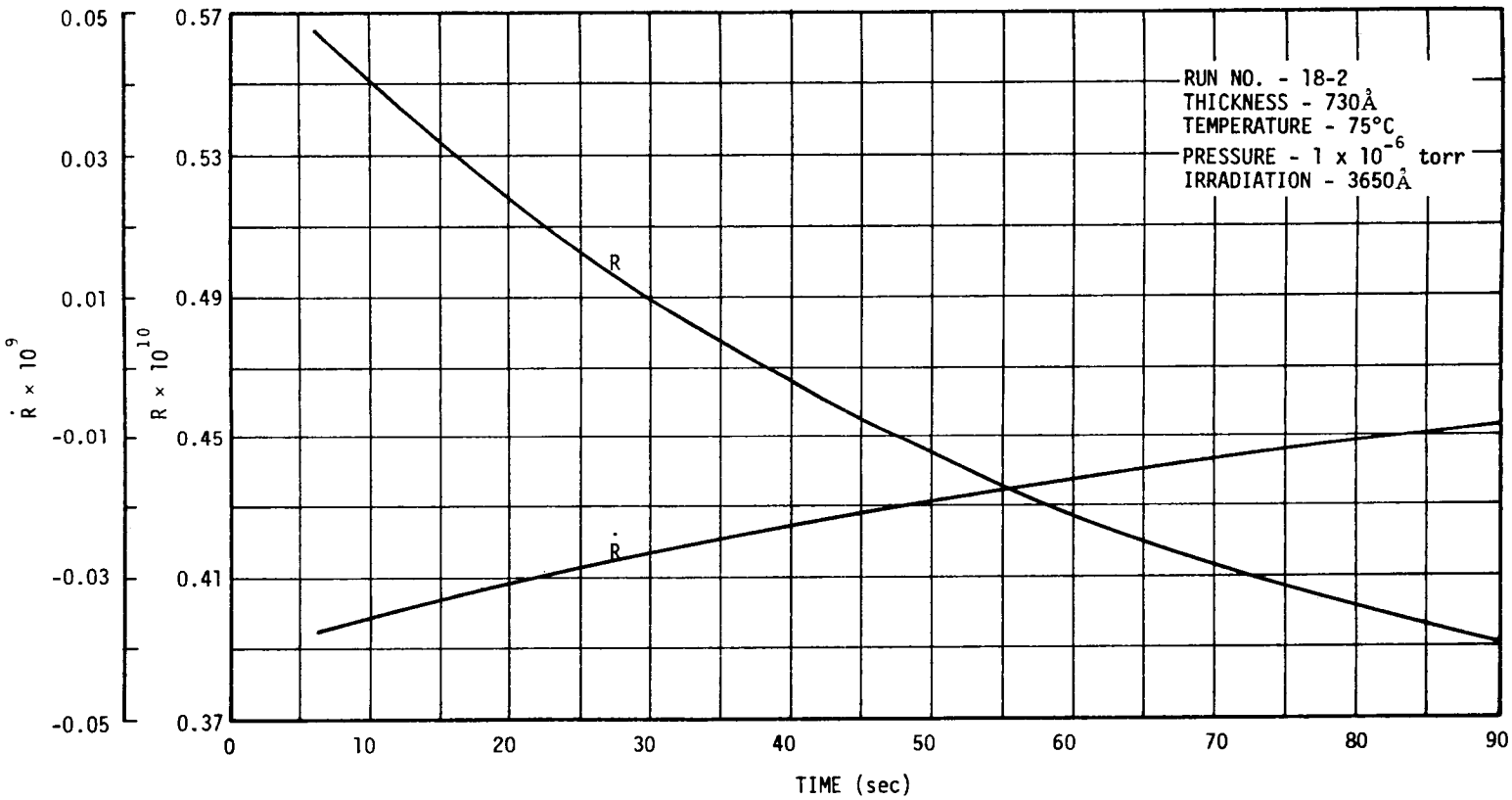
RUN NO. - 18-2
THICKNESS - 730Å
TEMPERATURE - 75°C
PRESSURE - 1 x 10^-6 torr
IRRADIATION - 3650Å
R
Ṙ
Ṙ × 10^9
R × 10^10
0.05
0.03
0.01
-0.01
-0.03
-0.05
0.57
0.53
0.49
0.45
0.41
0.37
0
10
20
30
40
50
60
70
80
90
TIME (sec)

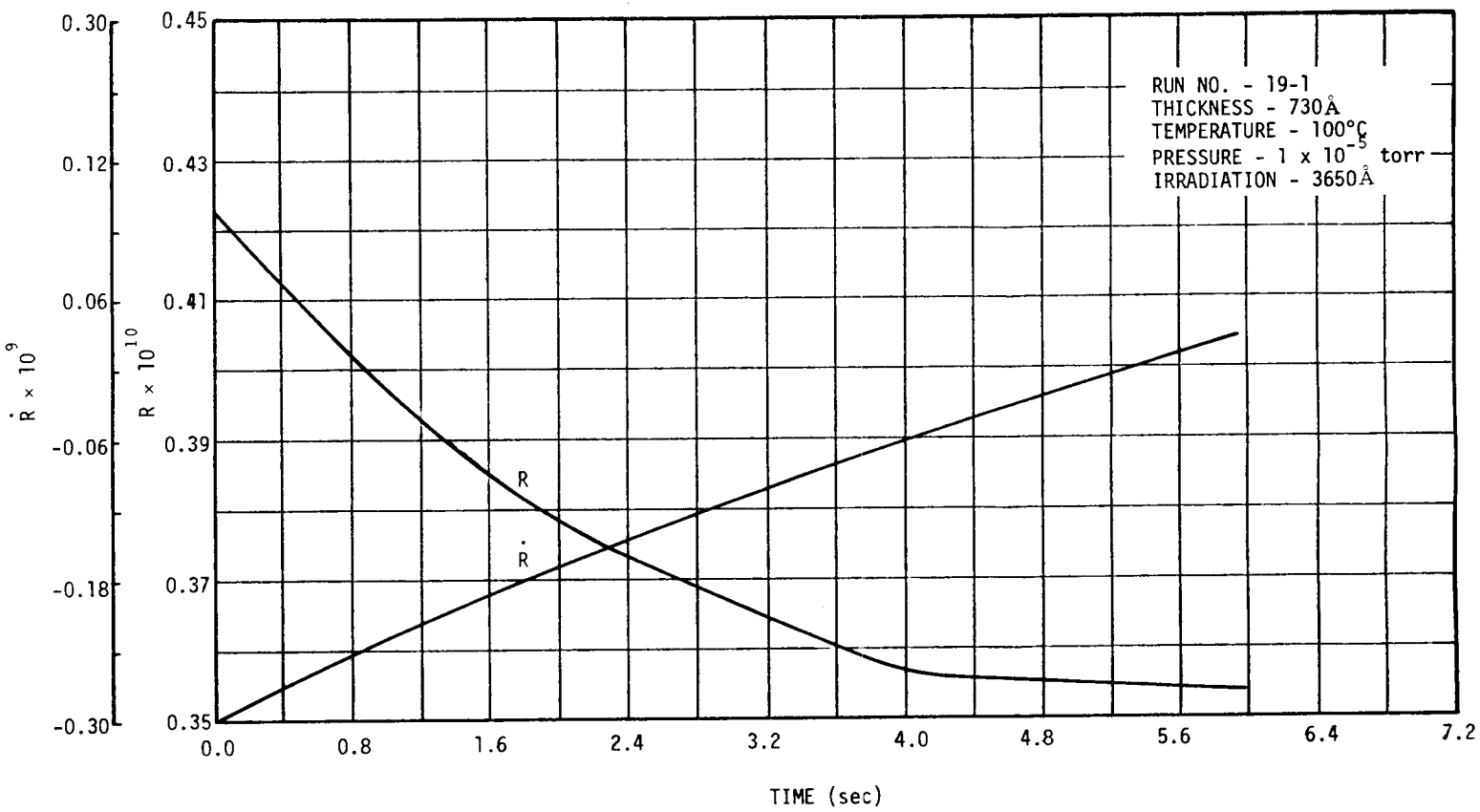
RUN NO. - 19-1
THICKNESS - 730Å
TEMPERATURE - 100°C
PRESSURE - 1 x 10^-5 torr
IRRADIATION - 3650Å
R
Ṙ
Ṙ × 10^9
R × 10^10
0.30
0.12
0.06
-0.06
-0.18
-0.30
0.45
0.43
0.41
0.39
0.37
0.35
0.0
0.8
1.6
2.4
3.2
4.0
4.8
5.6
6.4
7.2
TIME (sec)

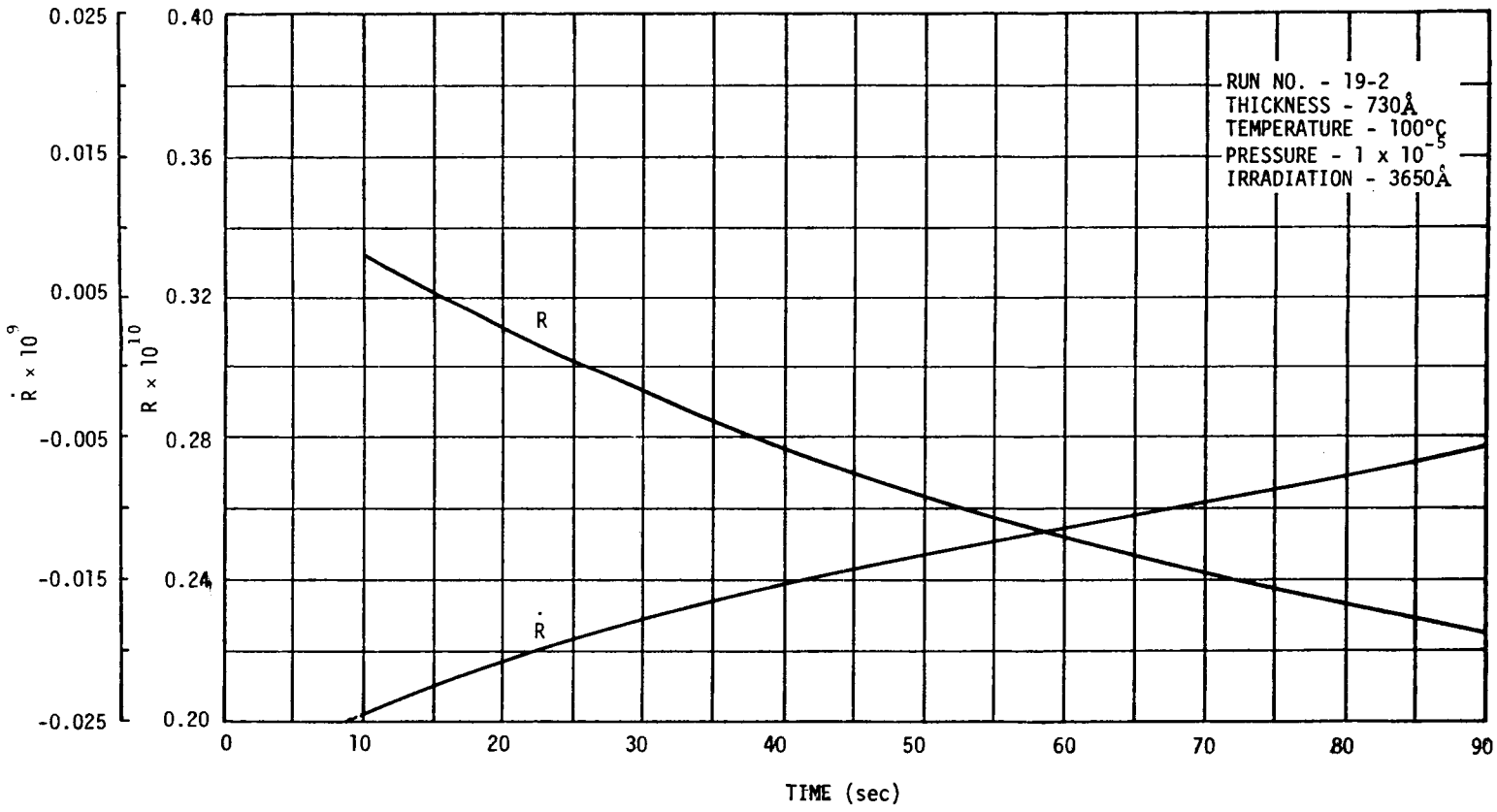
RUN NO. - 19-2
THICKNESS - 730Å
TEMPERATURE - 100°C
PRESSURE - 1 x 10^-5
IRRADIATION - 3650Å
R
Ṙ
Ṙ × 10^9
R × 10^10
0.025
0.015
0.005
-0.005
-0.015
-0.025
0.40
0.36
0.32
0.28
0.24
0.20
0
10
20
30
40
50
60
70
80
90
TIME (sec)

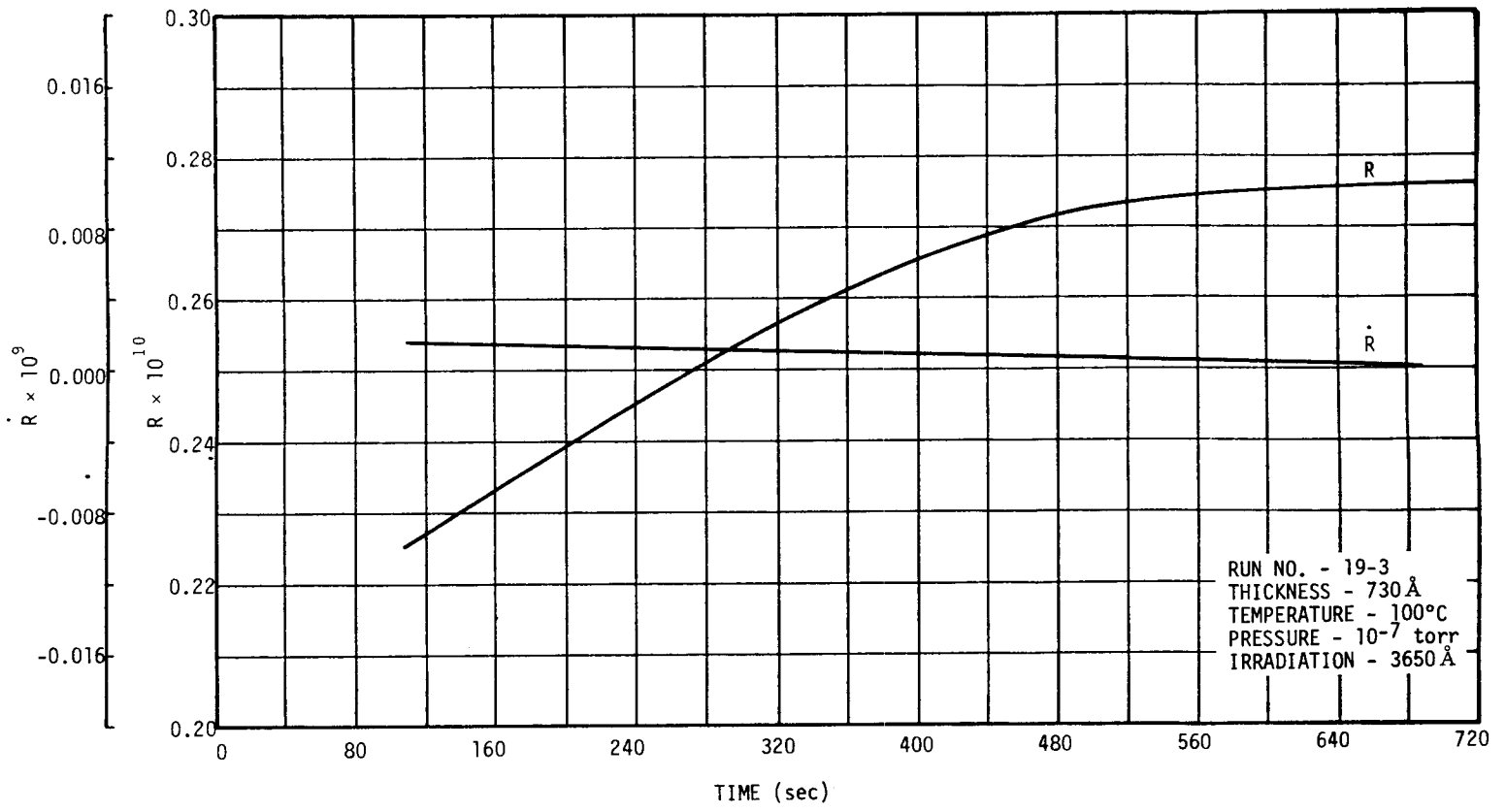
0.30
0.28
0.26
0.24
0.22
0.20
0.016
0.008
0.000
-0.008
-0.016
$\dot{R} \times 10^9$
$R \times 10^{10}$
R
$\dot{R}$
RUN NO. - 19-3
THICKNESS - 730 Å
TEMPERATURE - 100°C
PRESSURE - 10^{-7} torr
IRRADIATION - 3650 Å
0
80
160
240
320
400
480
560
640
720
TIME (sec)

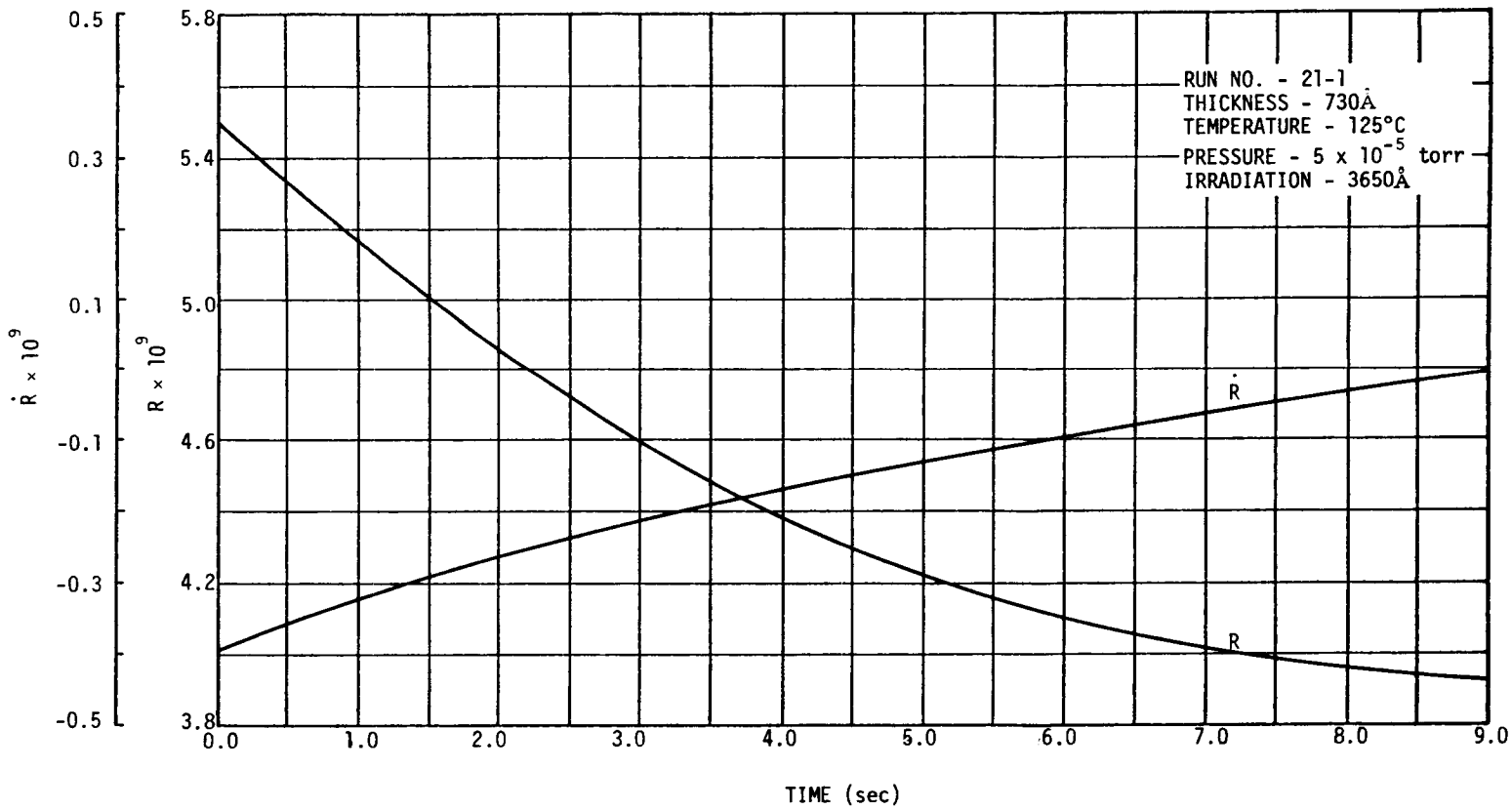
RUN NO. - 21-1
THICKNESS - 730Å
TEMPERATURE - 125°C
PRESSURE - 5 x 10^-5 torr
IRRADIATION - 3650Å
Ṙ
R
Ṙ × 10^9
R × 10^9
0.5
0.3
0.1
-0.1
-0.3
-0.5
5.8
5.4
5.0
4.6
4.2
3.8
0.0
1.0
2.0
3.0
4.0
5.0
6.0
7.0
8.0
9.0
TIME (sec)

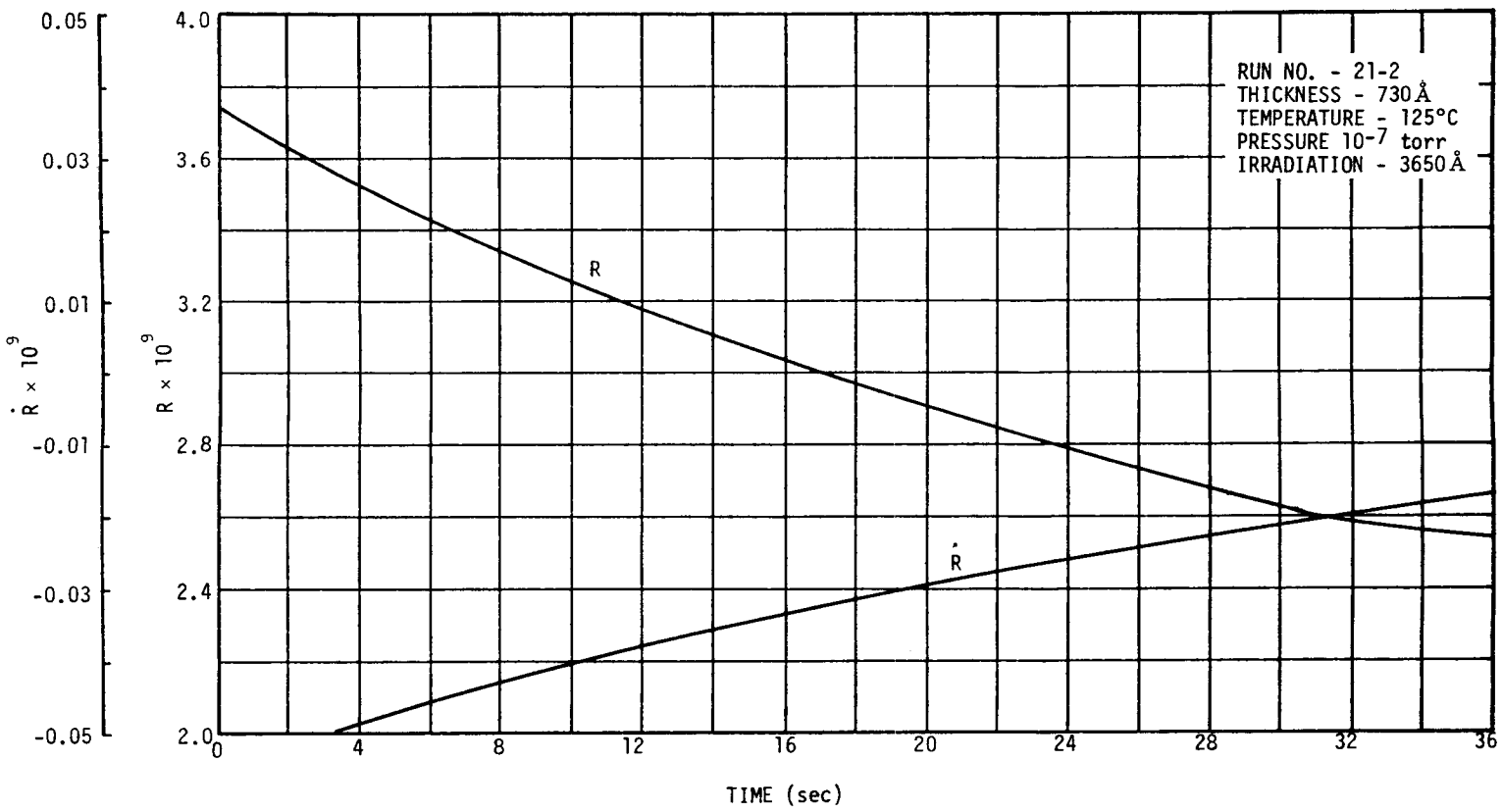
RUN NO. - 21-2
THICKNESS - 730Å
TEMPERATURE - 125°C
PRESSURE 10^{-7} torr
IRRADIATION - 3650Å
R
$\dot{R}$
$\dot{R} \times 10^9$
$R \times 10^9$
0.05
0.03
0.01
-0.01
-0.03
-0.05
4.0
3.6
3.2
2.8
2.4
2.0
0
4
8
12
16
20
24
28
32
36
TIME (sec)

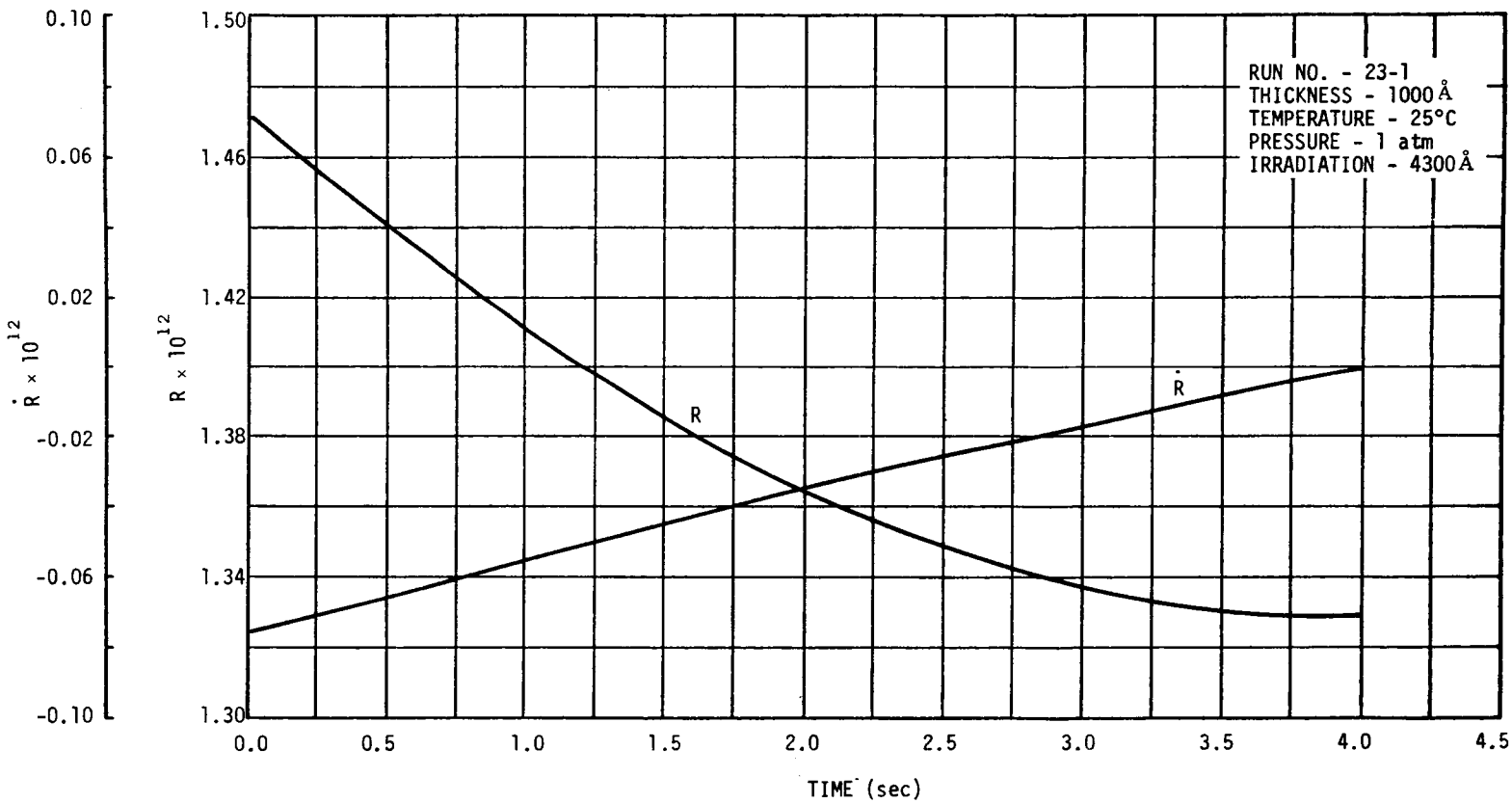
RUN NO. - 23-1
THICKNESS - 1000 Å
TEMPERATURE - 25°C
PRESSURE - 1 atm
IRRADIATION - 4300 Å
R
Ṙ
Ṙ × 10^12
R × 10^12
0.10
0.06
0.02
-0.02
-0.06
-0.10
1.50
1.46
1.42
1.38
1.34
1.30
0.0
0.5
1.0
1.5
2.0
2.5
3.0
3.5
4.0
4.5
TIME (sec)

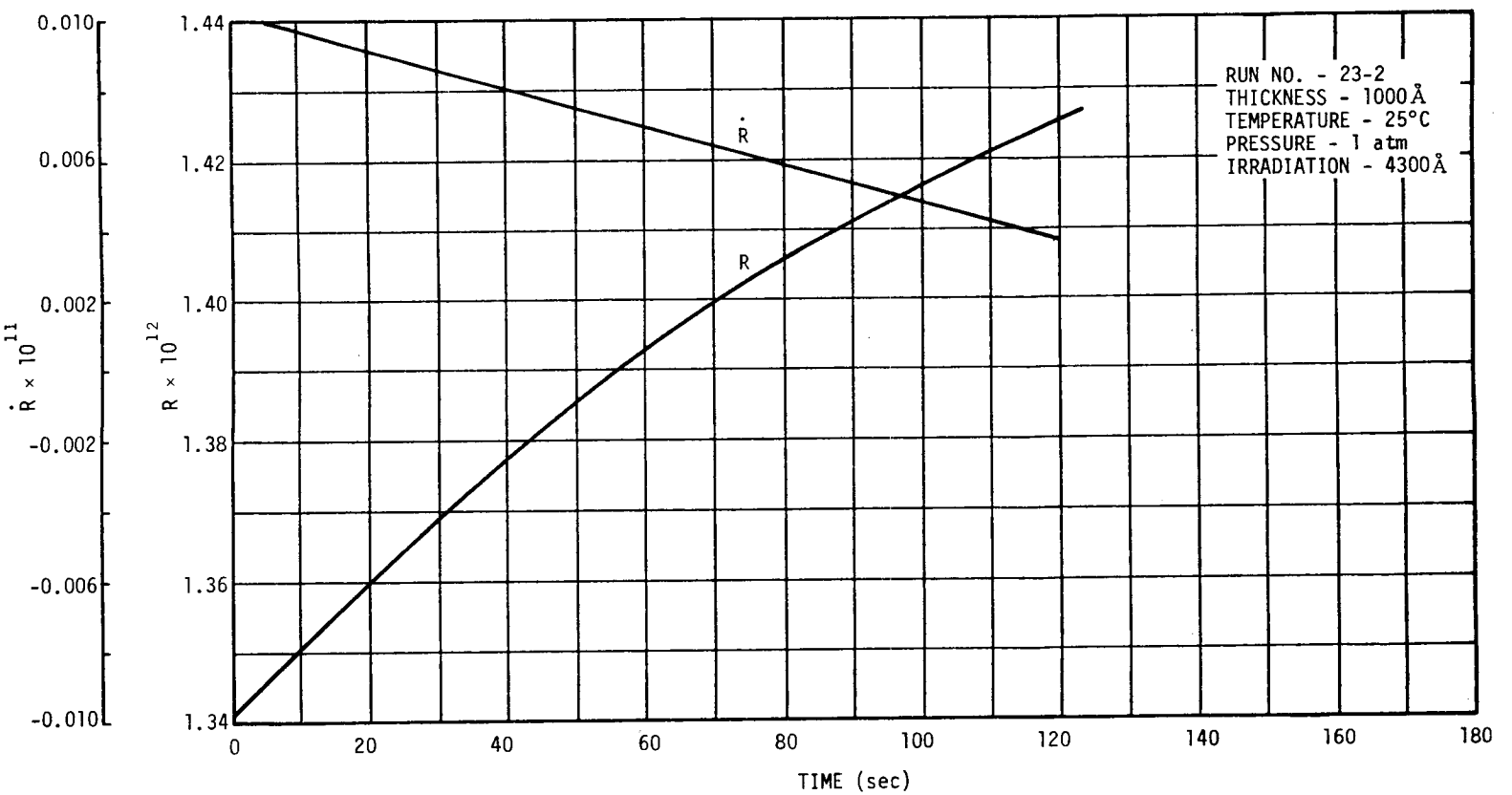
RUN NO. - 23-2
THICKNESS - 1000Å
TEMPERATURE - 25°C
PRESSURE - 1 atm
IRRADIATION - 4300Å
Ṙ
R
Ṙ × 10^11
R × 10^12
0.010
0.006
0.002
-0.002
-0.006
-0.010
1.44
1.42
1.40
1.38
1.36
1.34
0
20
40
60
80
100
120
140
160
180
TIME (sec)

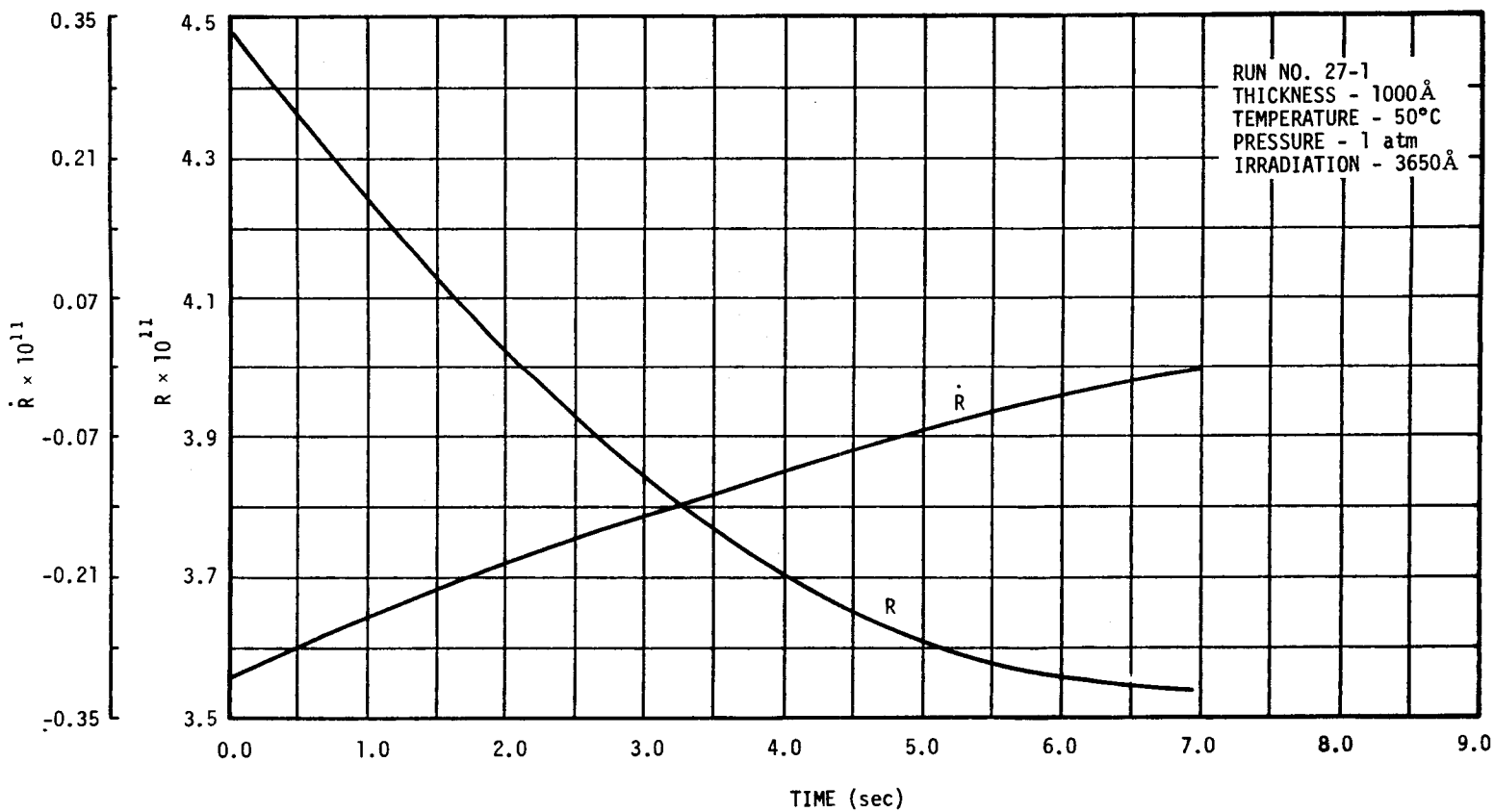
RUN NO. 27-1
THICKNESS - 1000Å
TEMPERATURE - 50°C
PRESSURE - 1 atm
IRRADIATION - 3650Å
$\dot{R} \times 10^{11}$
$R \times 10^{11}$
0.35
0.21
0.07
-0.07
-0.21
-0.35
4.5
4.3
4.1
3.9
3.7
3.5
$\dot{R}$
R
0.0
1.0
2.0
3.0
4.0
5.0
6.0
7.0
8.0
9.0
TIME (sec)

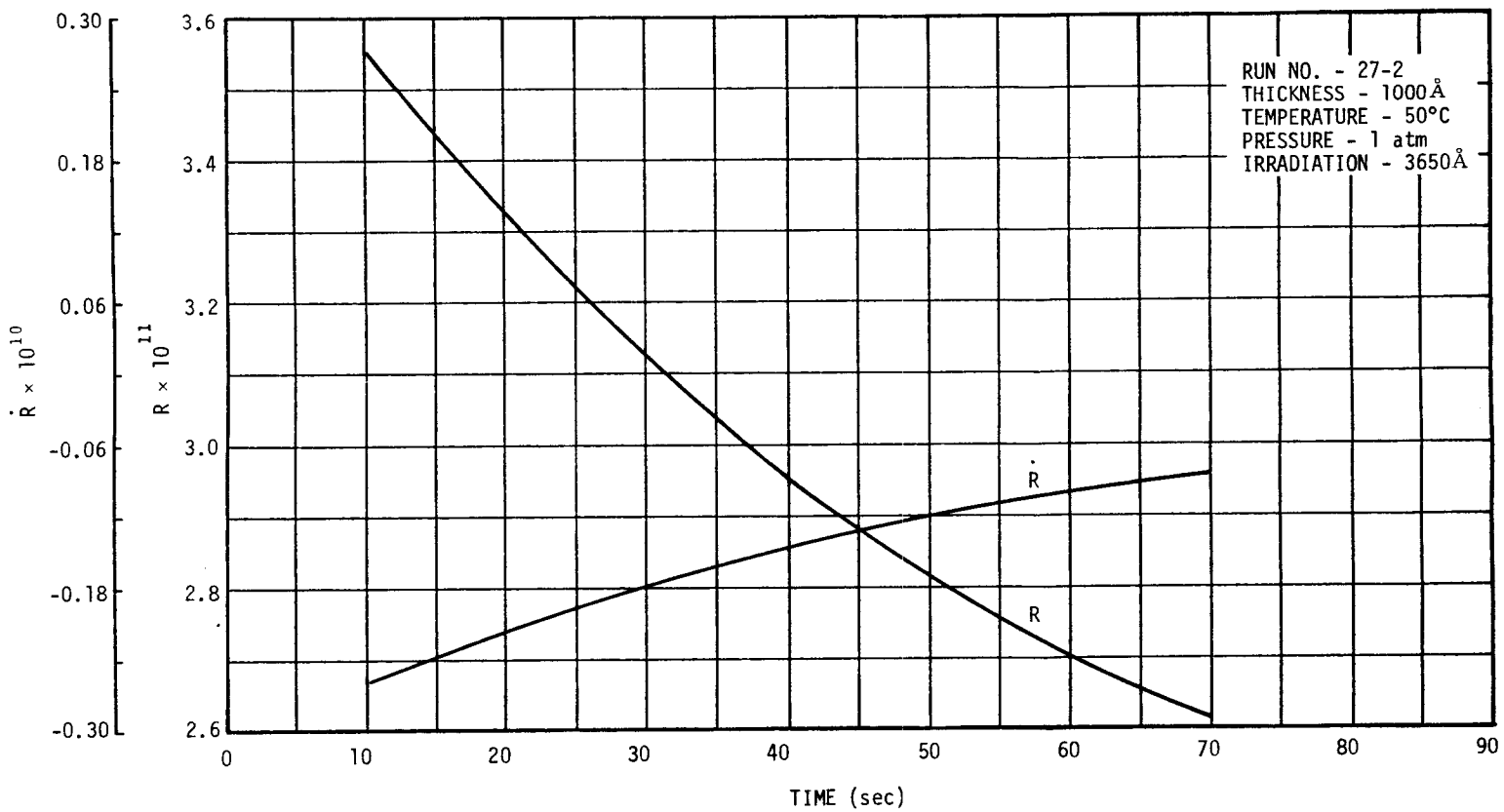
RUN NO. - 27-2
THICKNESS - 1000Å
TEMPERATURE - 50°C
PRESSURE - 1 atm
IRRADIATION - 3650Å
$\dot{R} \times 10^{10}$
$R \times 10^{11}$
0.30
0.18
0.06
-0.06
-0.18
-0.30
3.6
3.4
3.2
3.0
2.8
2.6
0
10
20
30
40
50
60
70
80
90
TIME (sec)
$\dot{R}$
R

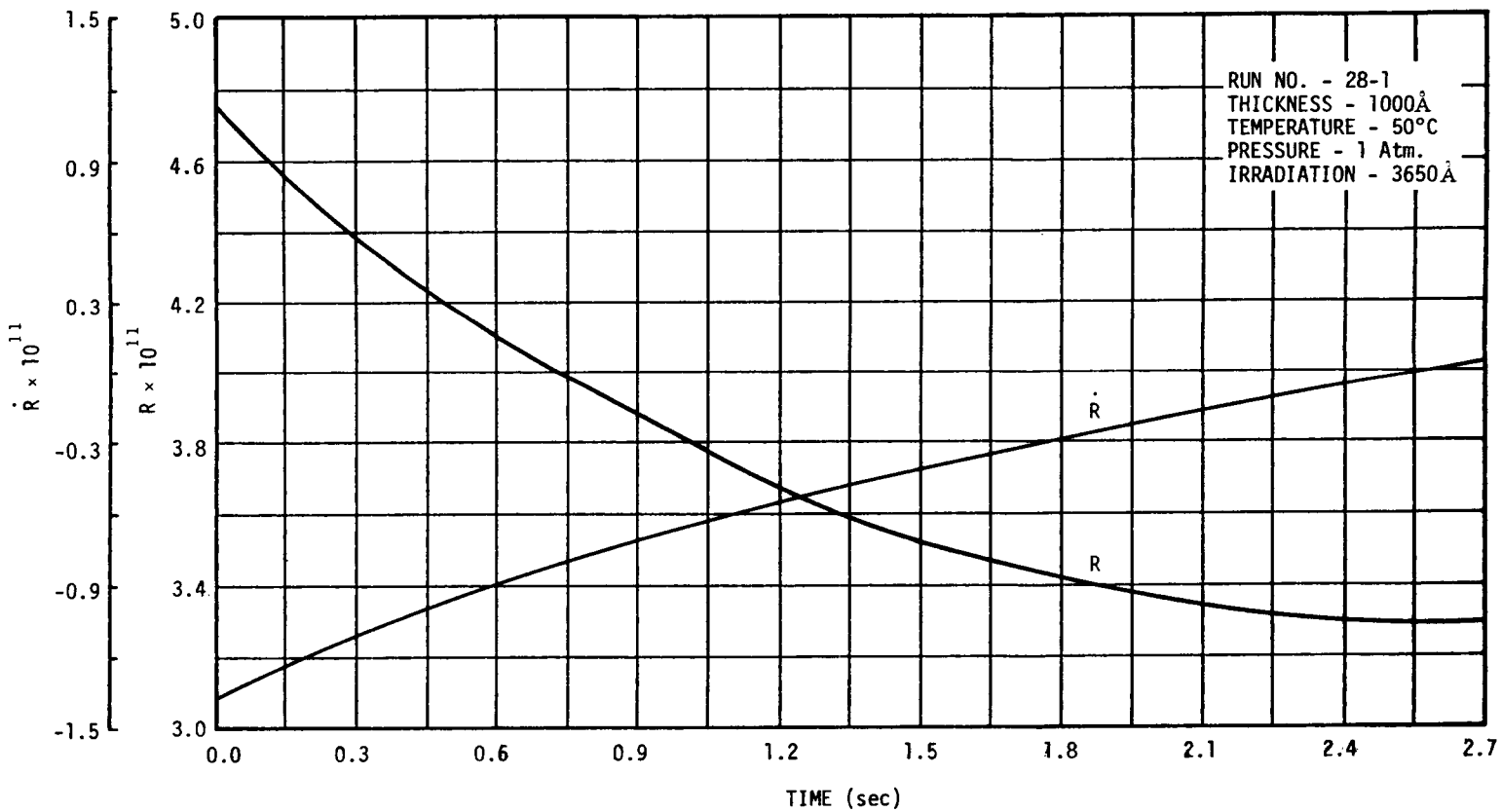
RUN NO. - 28-1
THICKNESS - 1000Å
TEMPERATURE - 50°C
PRESSURE - 1 Atm.
IRRADIATION - 3650Å
$\dot{R} \times 10^{11}$
$R \times 10^{11}$
1.5
0.9
0.3
-0.3
-0.9
-1.5
5.0
4.6
4.2
3.8
3.4
3.0
0.0
0.3
0.6
0.9
1.2
1.5
1.8
2.1
2.4
2.7
TIME (sec)
$\dot{R}$
R

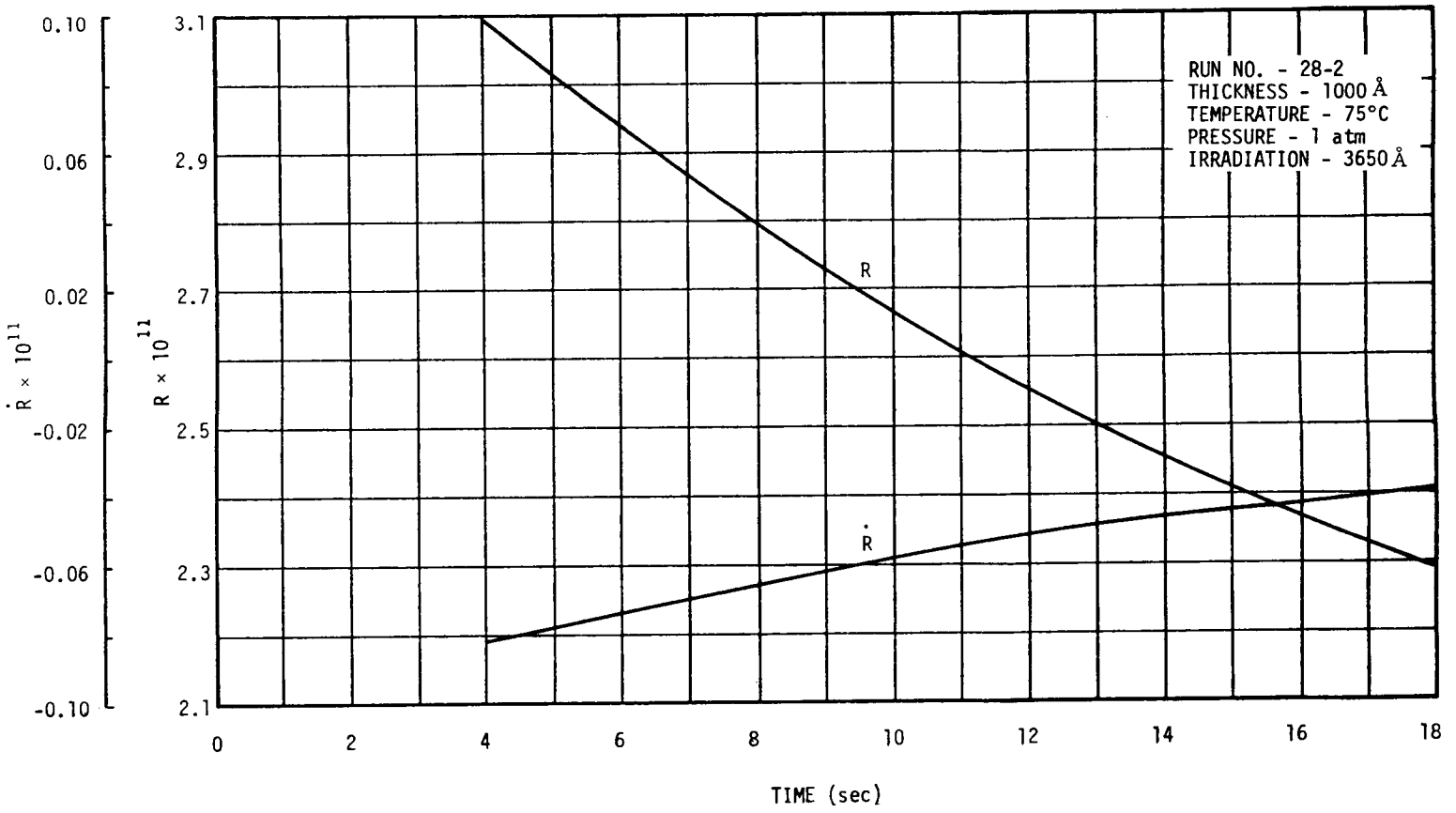
RUN NO. - 28-2
THICKNESS - 1000 Å
TEMPERATURE - 75°C
PRESSURE - 1 atm
IRRADIATION - 3650 Å
R
Ṙ
Ṙ × 10^11
R × 10^11
0.10
0.06
0.02
-0.02
-0.06
-0.10
3.1
2.9
2.7
2.5
2.3
2.1
0
2
4
6
8
10
12
14
16
18
TIME (sec)

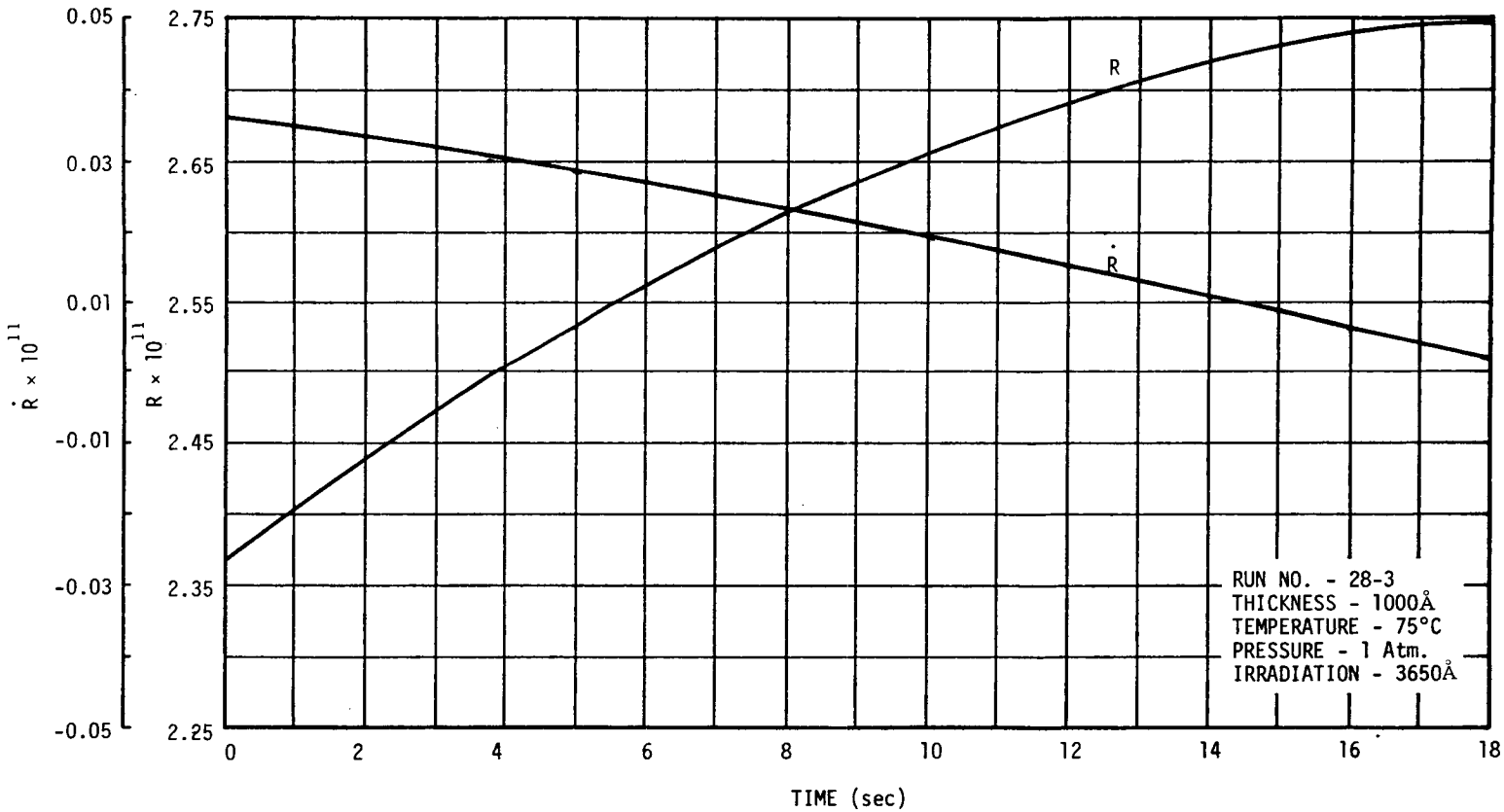
0.05
0.03
0.01
-0.01
-0.03
-0.05
$\dot{R} \times 10^{11}$
2.75
2.65
2.55
2.45
2.35
2.25
$R \times 10^{11}$
R
$\dot{R}$
0
2
4
6
8
10
12
14
16
18
TIME (sec)
RUN NO. - 28-3
THICKNESS - 1000Å
TEMPERATURE - 75°C
PRESSURE - 1 Atm.
IRRADIATION - 3650Å

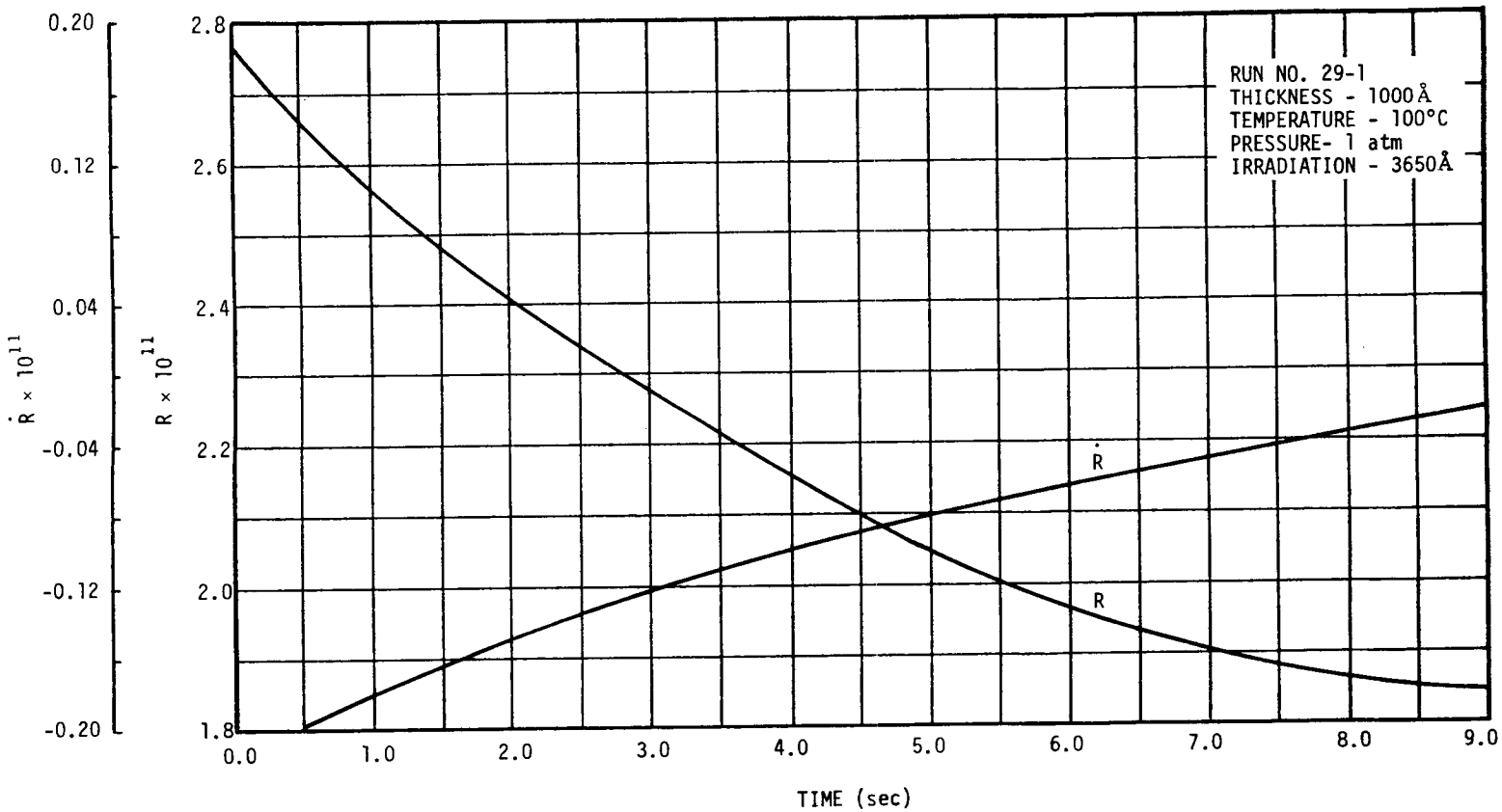
RUN NO. 29-1
THICKNESS - 1000Å
TEMPERATURE - 100°C
PRESSURE- 1 atm
IRRADIATION - 3650Å
$\dot{R} \times 10^{11}$
$R \times 10^{11}$
0.20
0.12
0.04
-0.04
-0.12
-0.20
2.8
2.6
2.4
2.2
2.0
1.8
0.0
1.0
2.0
3.0
4.0
5.0
6.0
7.0
8.0
9.0
TIME (sec)
$\dot{R}$
R

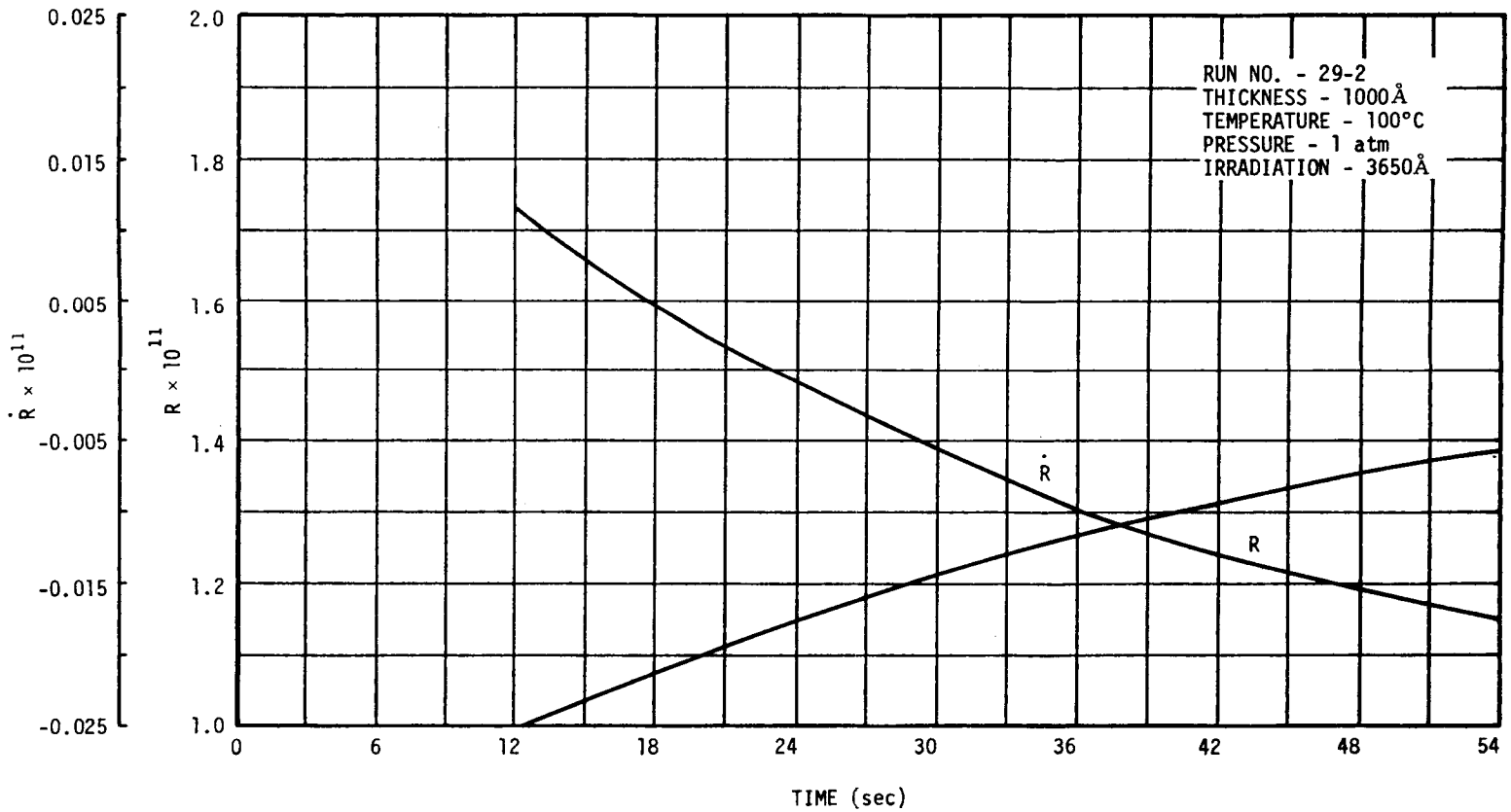
RUN NO. - 29-2
THICKNESS - 1000Å
TEMPERATURE - 100°C
PRESSURE - 1 atm
IRRADIATION - 3650Å
$\dot{R} \times 10^{11}$
$R \times 10^{11}$
0.025
0.015
0.005
-0.005
-0.015
-0.025
2.0
1.8
1.6
1.4
1.2
1.0
0
6
12
18
24
30
36
42
48
54
$\dot{R}$
R
TIME (sec)

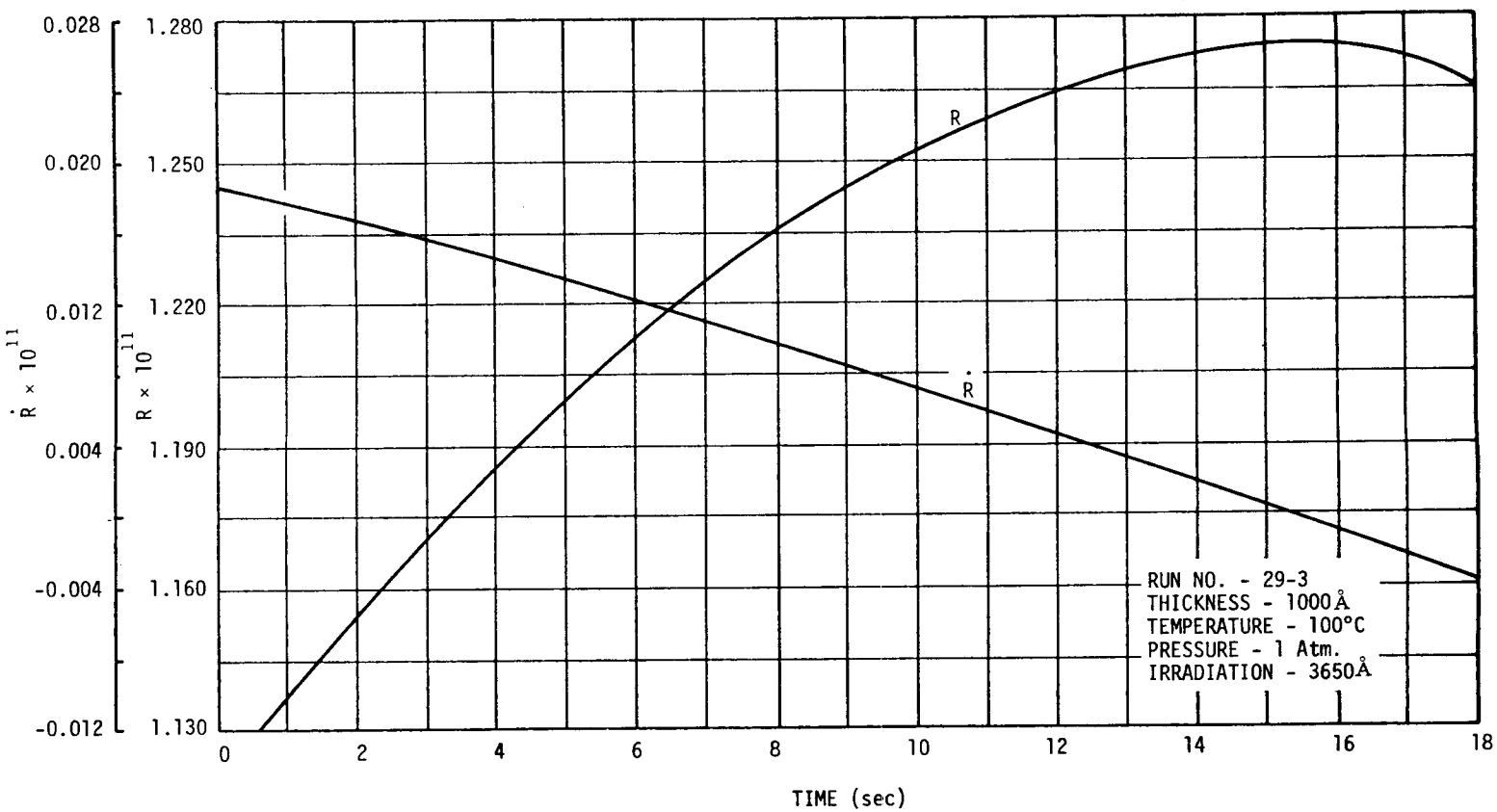
0.028
0.020
0.012
0.004
-0.004
-0.012
$\dot{R} \times 10^{11}$
1.280
1.250
1.220
1.190
1.160
1.130
$R \times 10^{11}$
R
$\dot{R}$
RUN NO. - 29-3
THICKNESS - 1000Å
TEMPERATURE - 100°C
PRESSURE - 1 Atm.
IRRADIATION - 3650Å
0
2
4
6
8
10
12
14
16
18
TIME (sec)

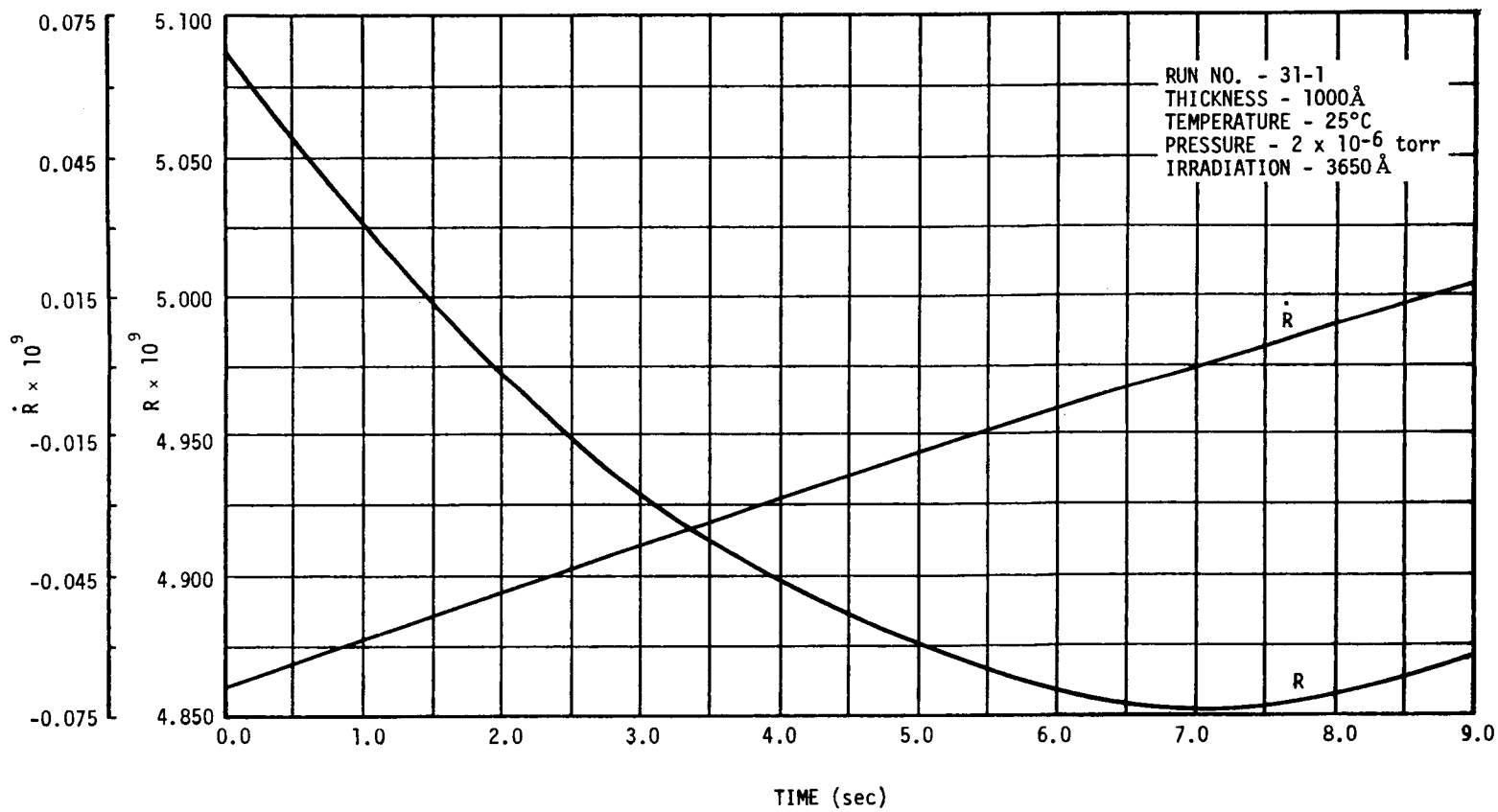
RUN NO. - 31-1
THICKNESS - 1000Å
TEMPERATURE - 25°C
PRESSURE - 2 x 10-6 torr
IRRADIATION - 3650 Å
Ṙ
R
Ṙ × 10^9
R × 10^9
0.075
0.045
0.015
-0.015
-0.045
-0.075
5.100
5.050
5.000
4.950
4.900
4.850
0.0
1.0
2.0
3.0
4.0
5.0
6.0
7.0
8.0
9.0
TIME (sec)

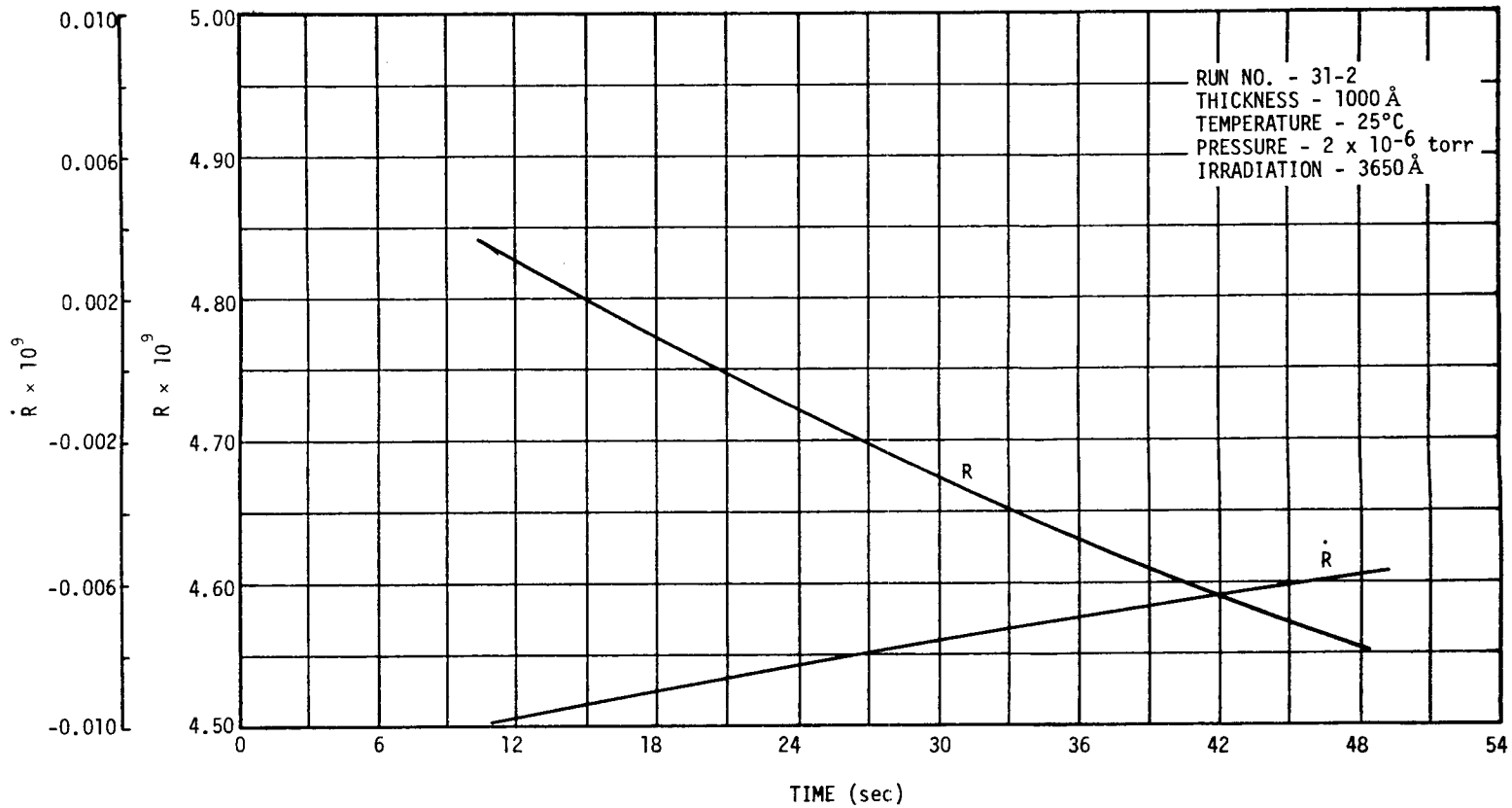
RUN NO. - 31-2
THICKNESS - 1000 Å
TEMPERATURE - 25°C
PRESSURE - 2 x 10-6 torr
IRRADIATION - 3650 Å
R
Ṙ
Ṙ × 10^9
R × 10^9
0.010
0.006
0.002
-0.002
-0.006
-0.010
5.00
4.90
4.80
4.70
4.60
4.50
0
6
12
18
24
30
36
42
48
54
TIME (sec)

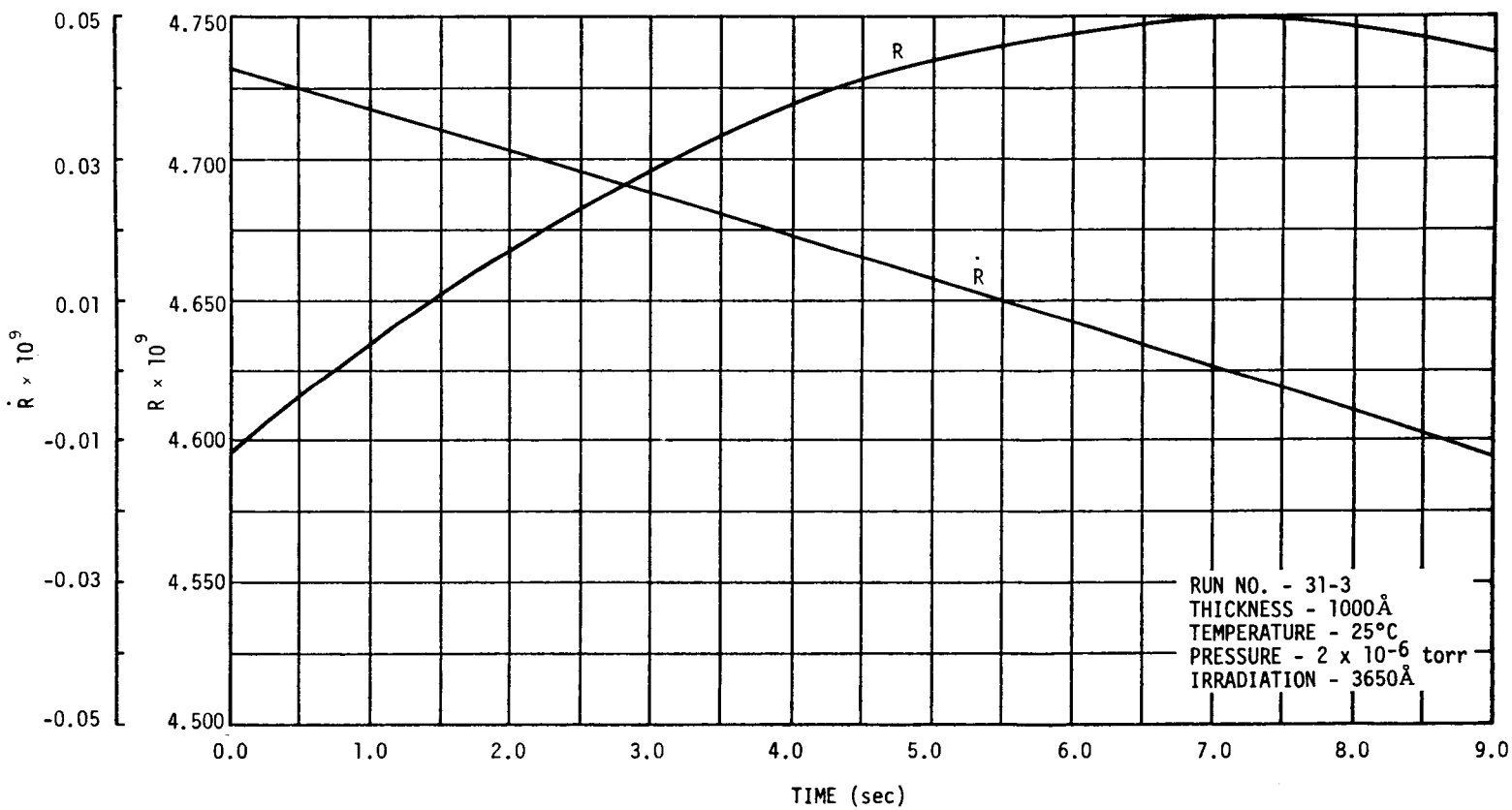
0.05
0.03
0.01
-0.01
-0.03
-0.05
$\dot{R} \times 10^9$
4.750
4.700
4.650
4.600
4.550
4.500
$R \times 10^9$
R
$\dot{R}$
RUN NO. - 31-3
THICKNESS - 1000Å
TEMPERATURE - 25°C
PRESSURE - 2 x 10^{-6} torr
IRRADIATION - 3650Å
0.0
1.0
2.0
3.0
4.0
5.0
6.0
7.0
8.0
9.0
TIME (sec)

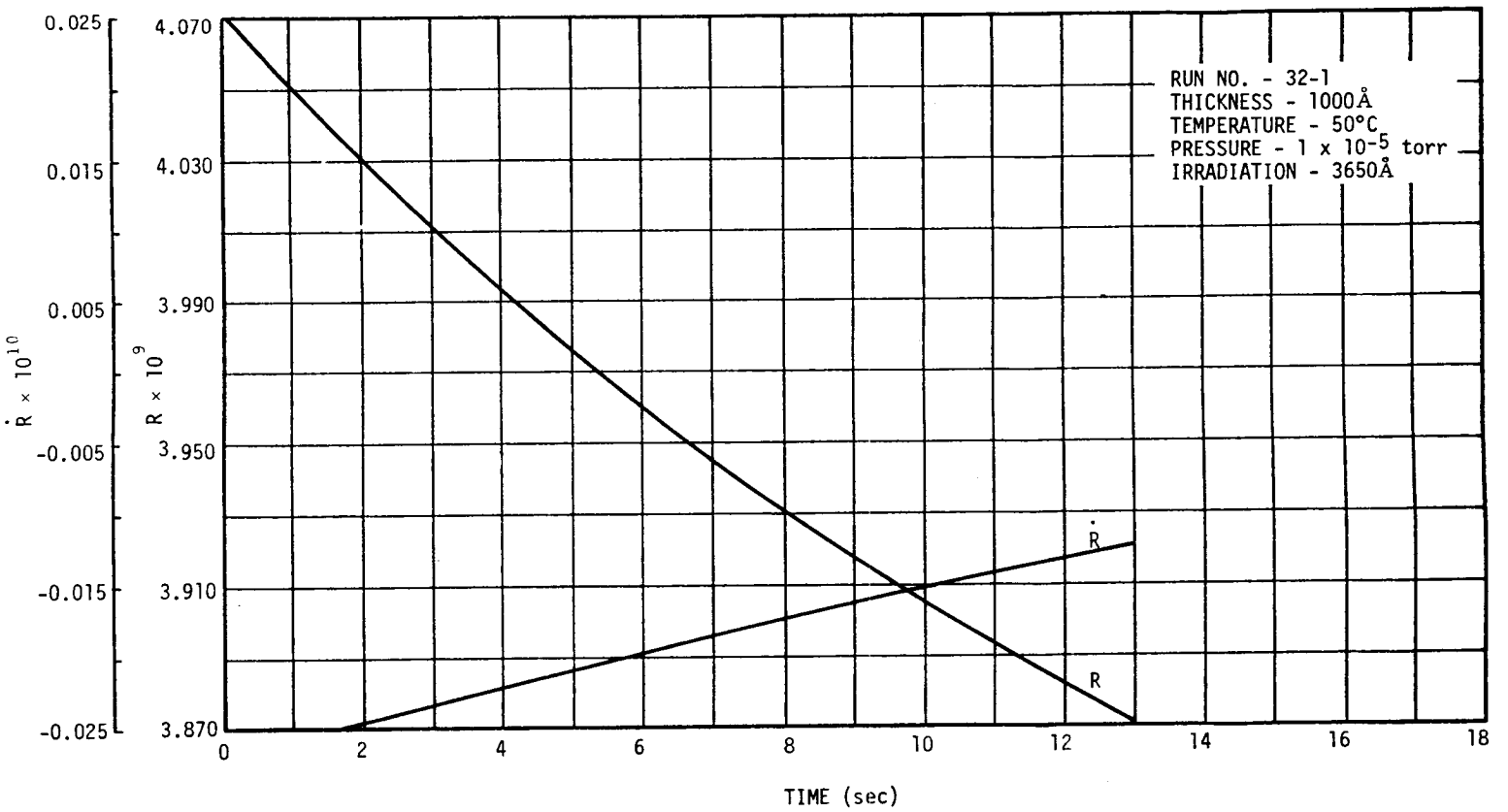
RUN NO. - 32-1
THICKNESS - 1000Å
TEMPERATURE - 50°C
PRESSURE - 1 x 10-5 torr
IRRADIATION - 3650Å
Ṙ × 10^10
R × 10^9
0.025
0.015
0.005
-0.005
-0.015
-0.025
4.070
4.030
3.990
3.950
3.910
3.870
0
2
4
6
8
10
12
14
16
18
TIME (sec)
Ṙ
R

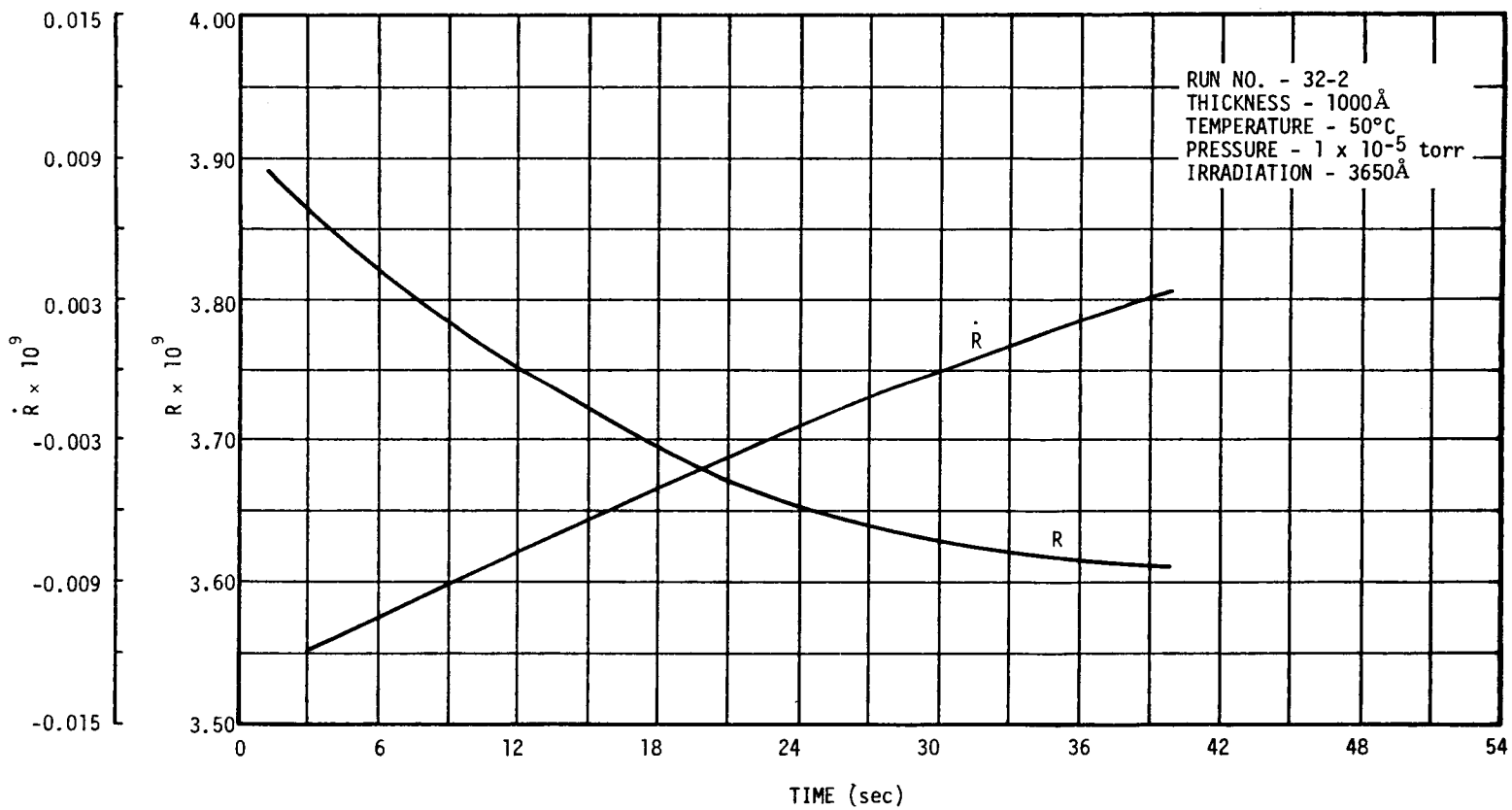
RUN NO. - 32-2
THICKNESS - 1000Å
TEMPERATURE - 50°C
PRESSURE - 1 x 10-5 torr
IRRADIATION - 3650Å
Ṙ
R
Ṙ × 10^9
R × 10^9
0.015
0.009
0.003
-0.003
-0.009
-0.015
4.00
3.90
3.80
3.70
3.60
3.50
0
6
12
18
24
30
36
42
48
54
TIME (sec)

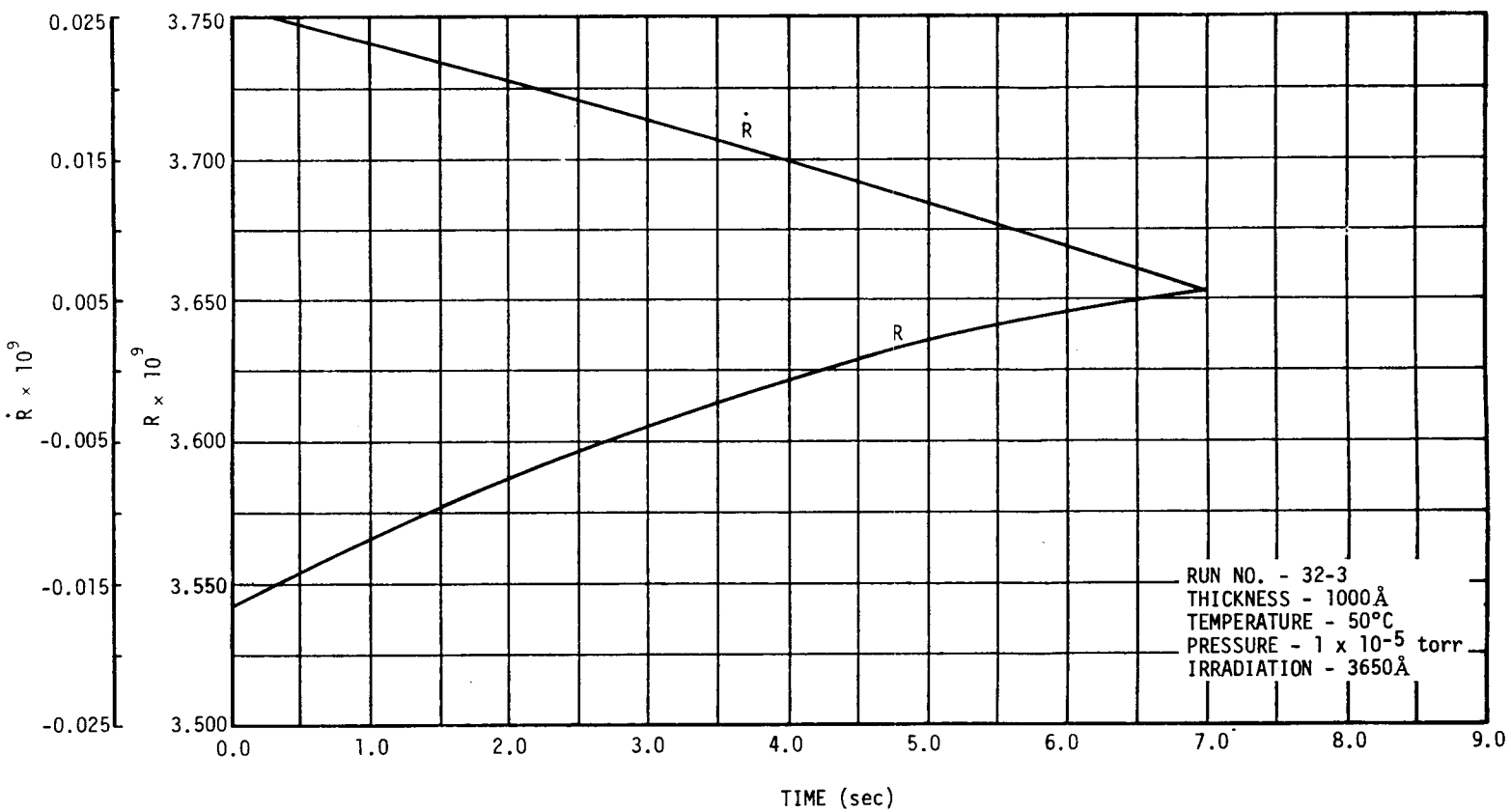
0.025
0.015
0.005
-0.005
-0.015
-0.025
$\dot{R} \times 10^9$
3.750
3.700
3.650
3.600
3.550
3.500
$R \times 10^9$
$\dot{R}$
R
0.0
1.0
2.0
3.0
4.0
5.0
6.0
7.0
8.0
9.0
TIME (sec)
RUN NO. - 32-3
THICKNESS - 1000Å
TEMPERATURE - 50°C
PRESSURE - 1 x 10^{-5} torr
IRRADIATION - 3650Å

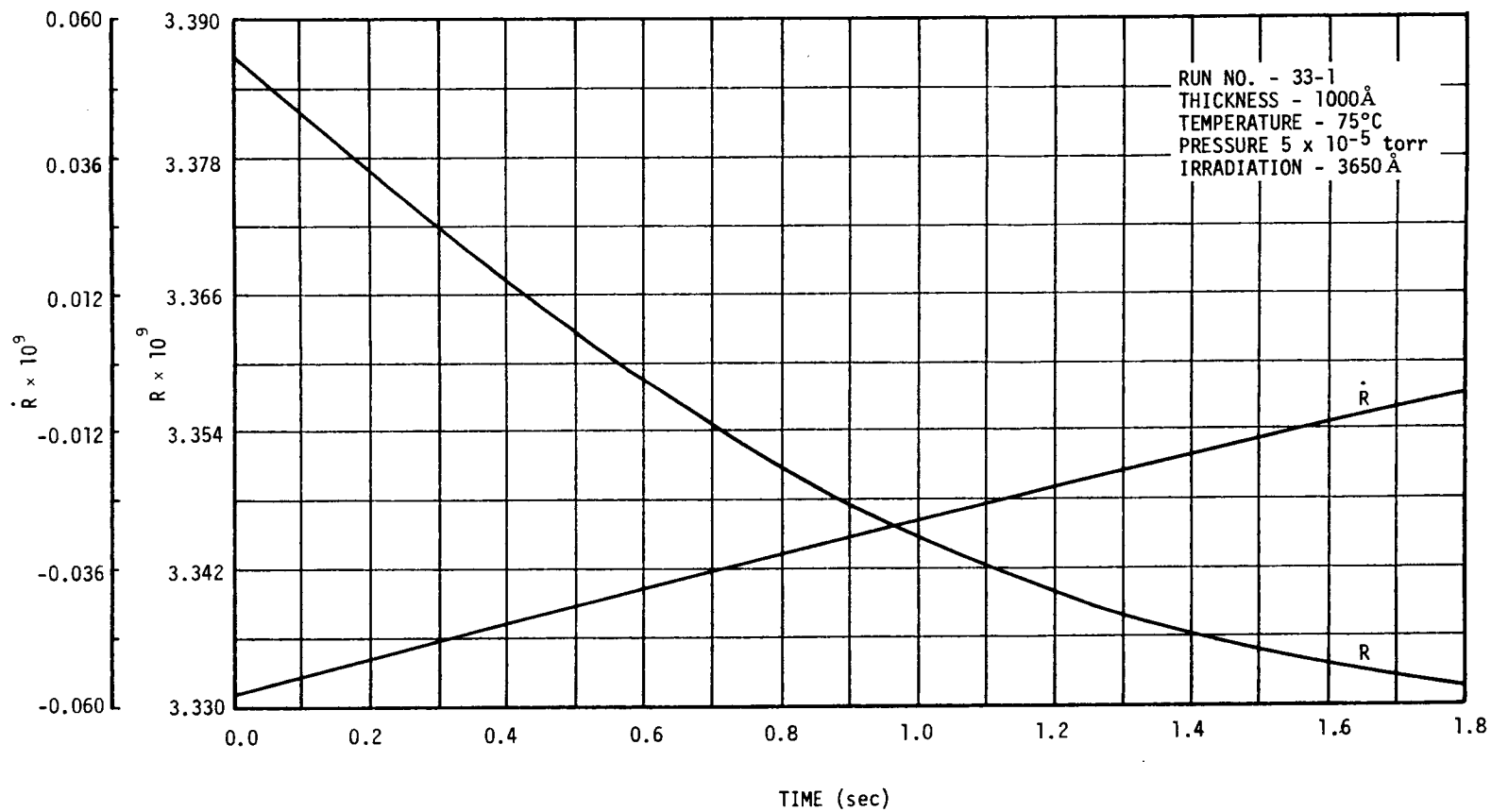
RUN NO. - 33-1
THICKNESS - 1000Å
TEMPERATURE - 75°C
PRESSURE 5 x 10-5 torr
IRRADIATION - 3650Å
Ṙ
R
Ṙ × 10^9
R × 10^9
0.060
0.036
0.012
-0.012
-0.036
-0.060
3.390
3.378
3.366
3.354
3.342
3.330
0.0
0.2
0.4
0.6
0.8
1.0
1.2
1.4
1.6
1.8
TIME (sec)

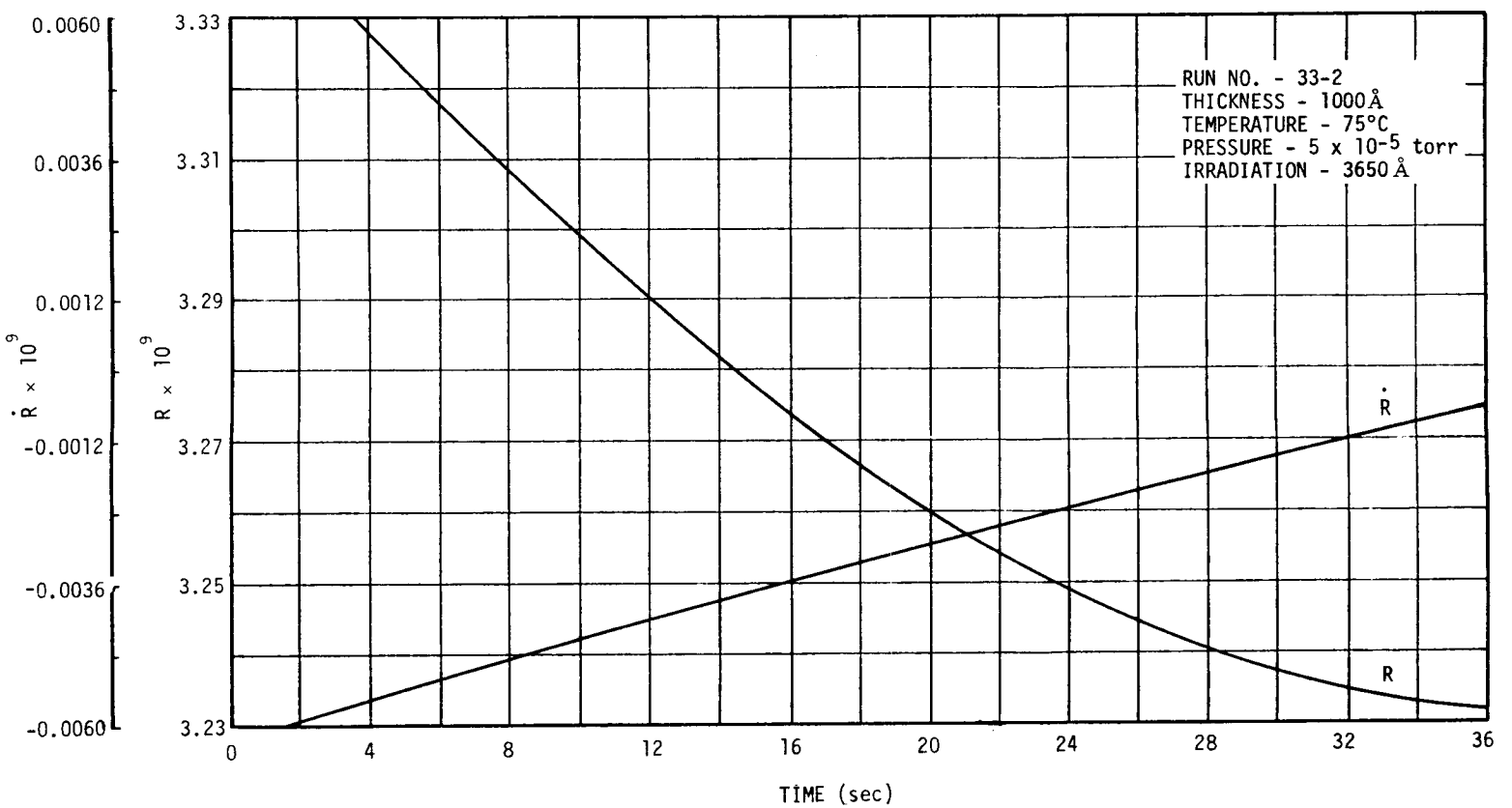
RUN NO. - 33-2
THICKNESS - 1000Å
TEMPERATURE - 75°C
PRESSURE - 5 x 10-5 torr
IRRADIATION - 3650Å
Ṙ
R
Ṙ × 10^9
R × 10^9
0.0060
0.0036
0.0012
-0.0012
-0.0036
-0.0060
3.33
3.31
3.29
3.27
3.25
3.23
0
4
8
12
16
20
24
28
32
36
TIME (sec)

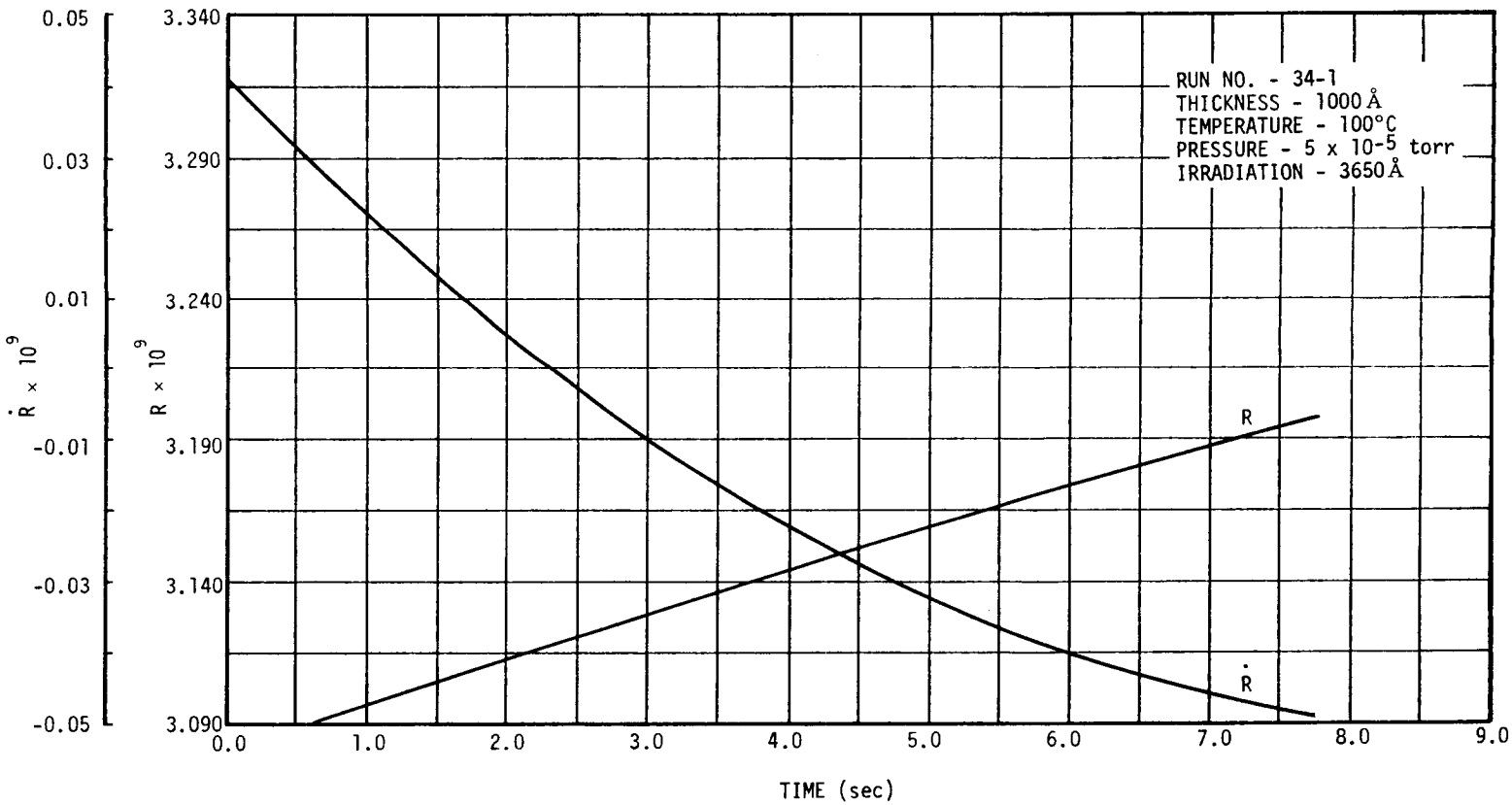
RUN NO. - 34-1
THICKNESS - 1000 Å
TEMPERATURE - 100°C
PRESSURE - 5 x 10-5 torr
IRRADIATION - 3650 Å
R
Ṙ
Ṙ × 10^9
R × 10^9
0.05
0.03
0.01
-0.01
-0.03
-0.05
3.340
3.290
3.240
3.190
3.140
3.090
0.0
1.0
2.0
3.0
4.0
5.0
6.0
7.0
8.0
9.0
TIME (sec)

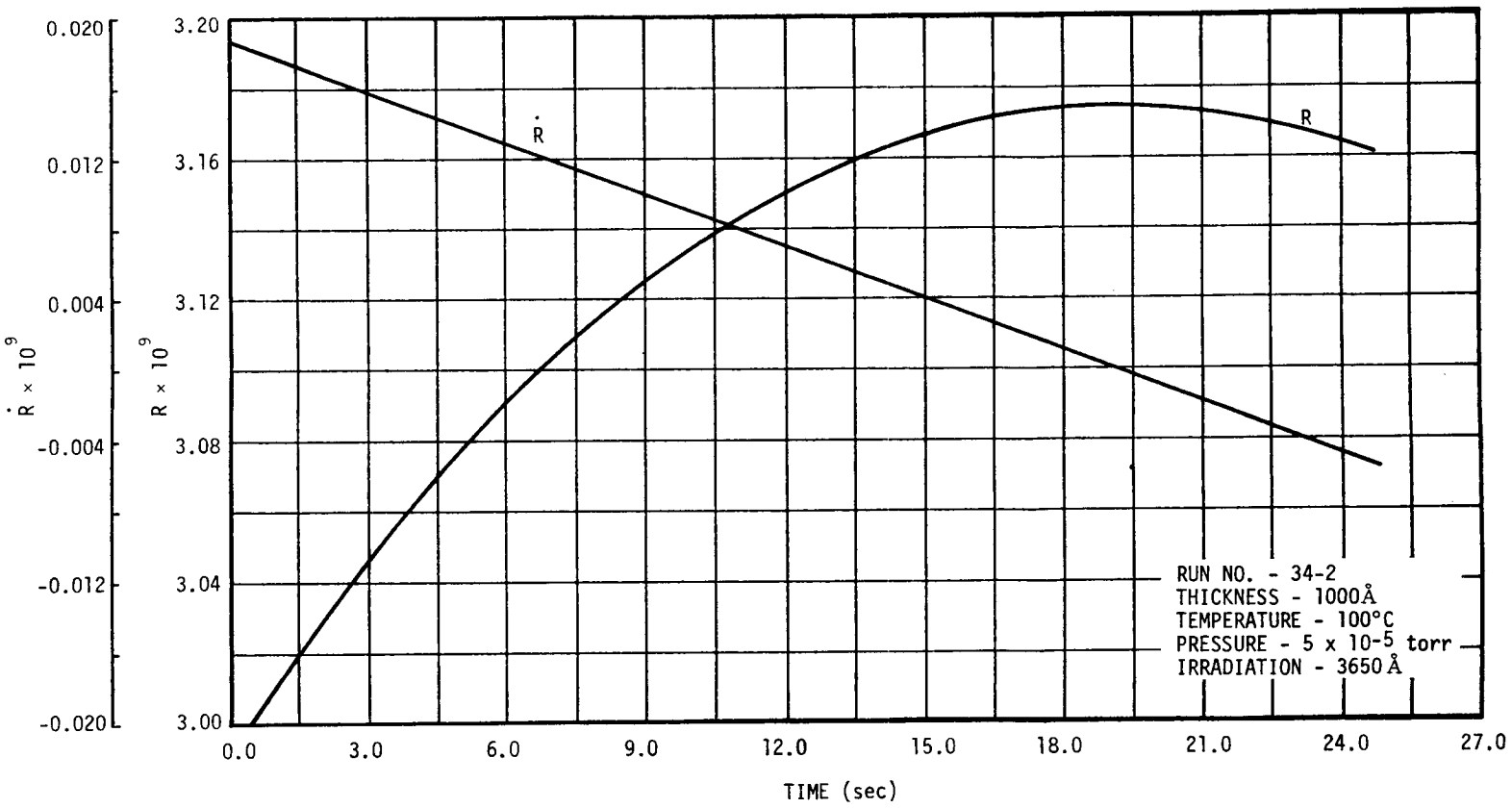
0.020
0.012
0.004
-0.004
-0.012
-0.020
$\dot{R} \times 10^9$
3.20
3.16
3.12
3.08
3.04
3.00
$R \times 10^9$
$\dot{R}$
R
RUN NO. - 34-2
THICKNESS - 1000Å
TEMPERATURE - 100°C
PRESSURE - 5 x 10-5 torr
IRRADIATION - 3650Å
0.0
3.0
6.0
9.0
12.0
15.0
18.0
21.0
24.0
27.0
TIME (sec)

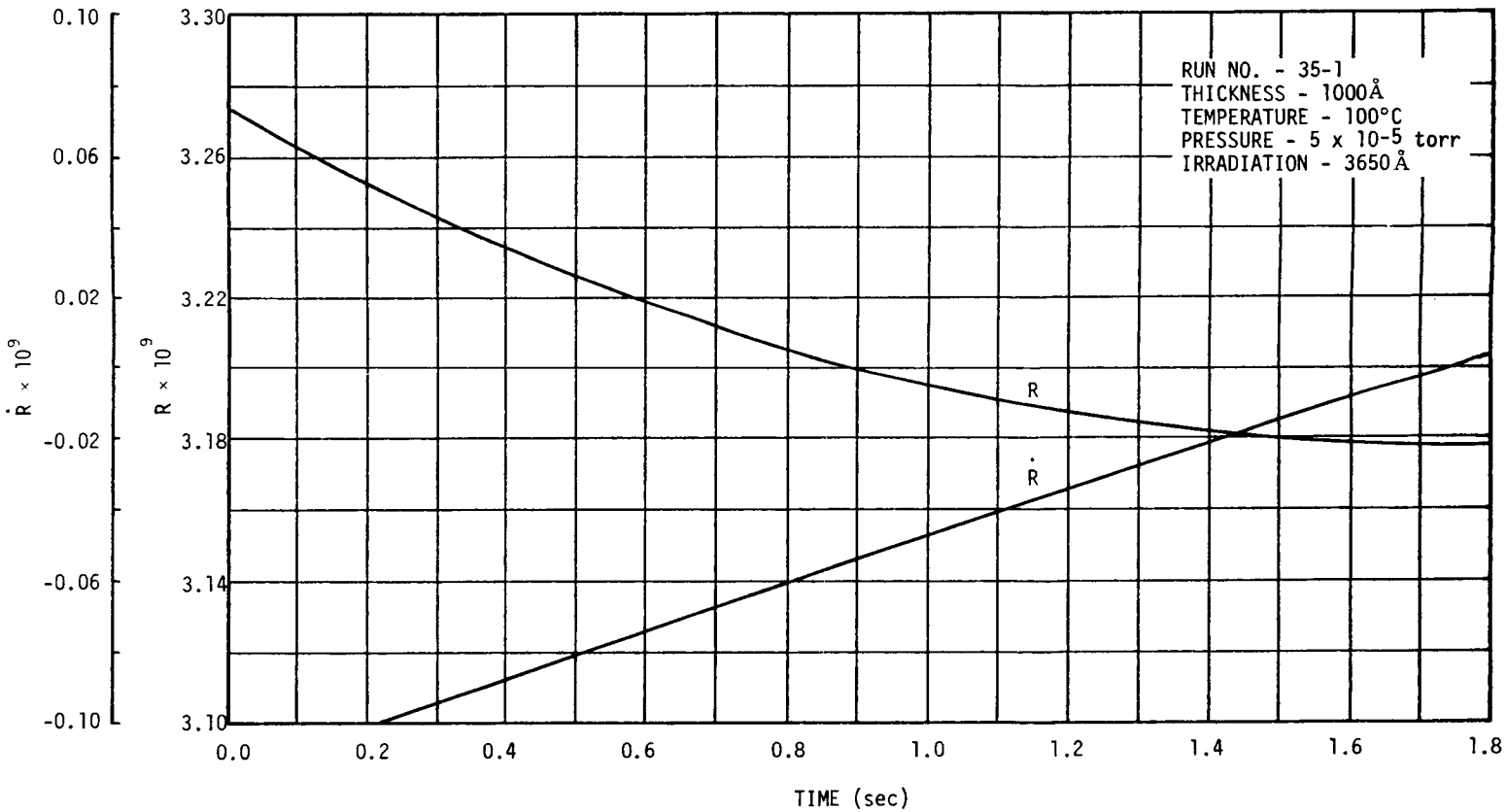
RUN NO. - 35-1
THICKNESS - 1000Å
TEMPERATURE - 100°C
PRESSURE - 5 x 10-5 torr
IRRADIATION - 3650Å
R
Ṙ
Ṙ × 10^9
R × 10^9
0.10
0.06
0.02
-0.02
-0.06
-0.10
3.30
3.26
3.22
3.18
3.14
3.10
0.0
0.2
0.4
0.6
0.8
1.0
1.2
1.4
1.6
1.8
TIME (sec)

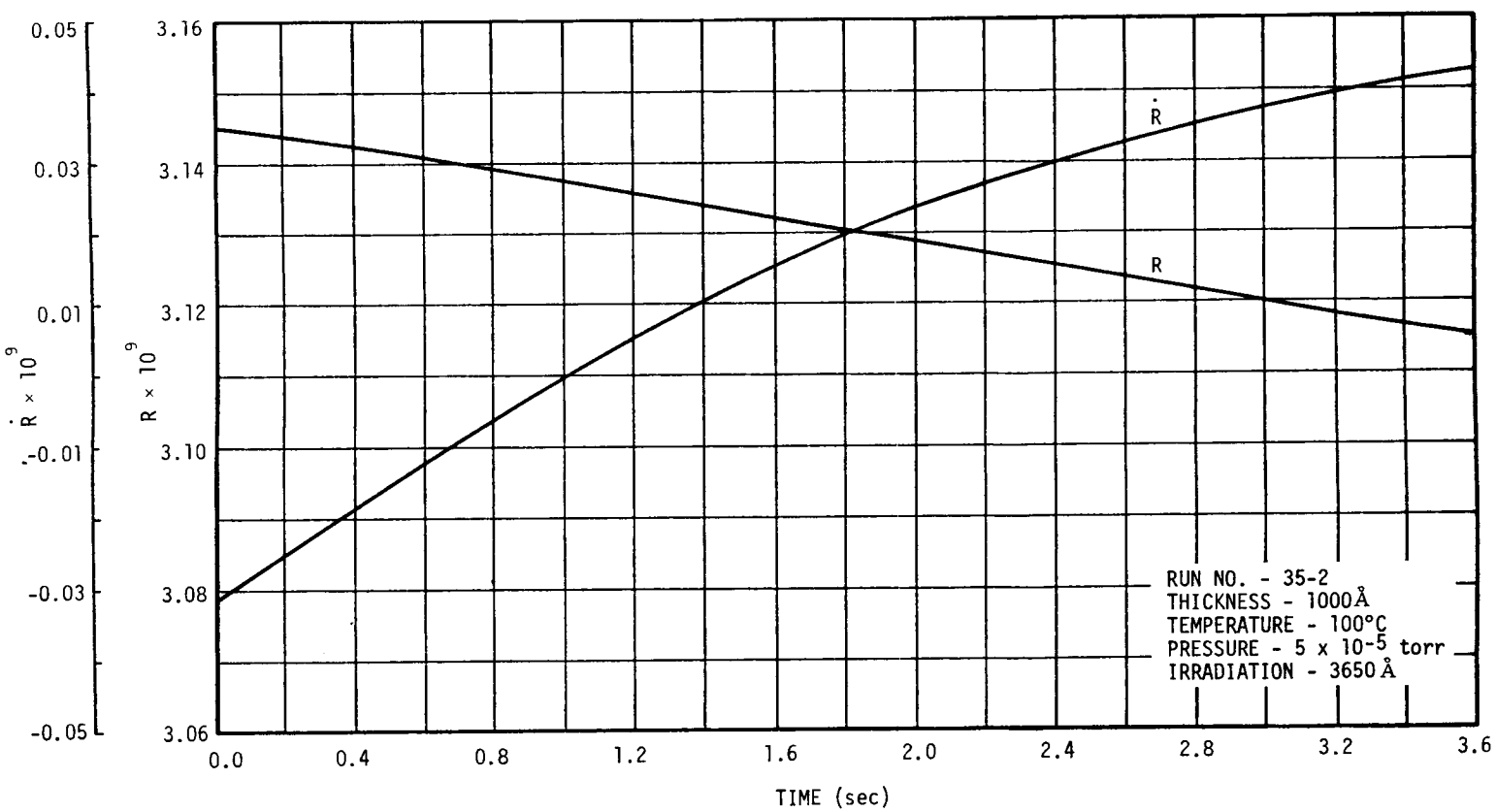
0.05
0.03
0.01
-0.01
-0.03
-0.05
$\dot{R} \times 10^9$
3.16
3.14
3.12
3.10
3.08
3.06
$R \times 10^9$
0.0
0.4
0.8
1.2
1.6
2.0
2.4
2.8
3.2
3.6
TIME (sec)
$\dot{R}$
R
RUN NO. - 35-2
THICKNESS - 1000Å
TEMPERATURE - 100°C
PRESSURE - 5 x 10^{-5} torr
IRRADIATION - 3650Å

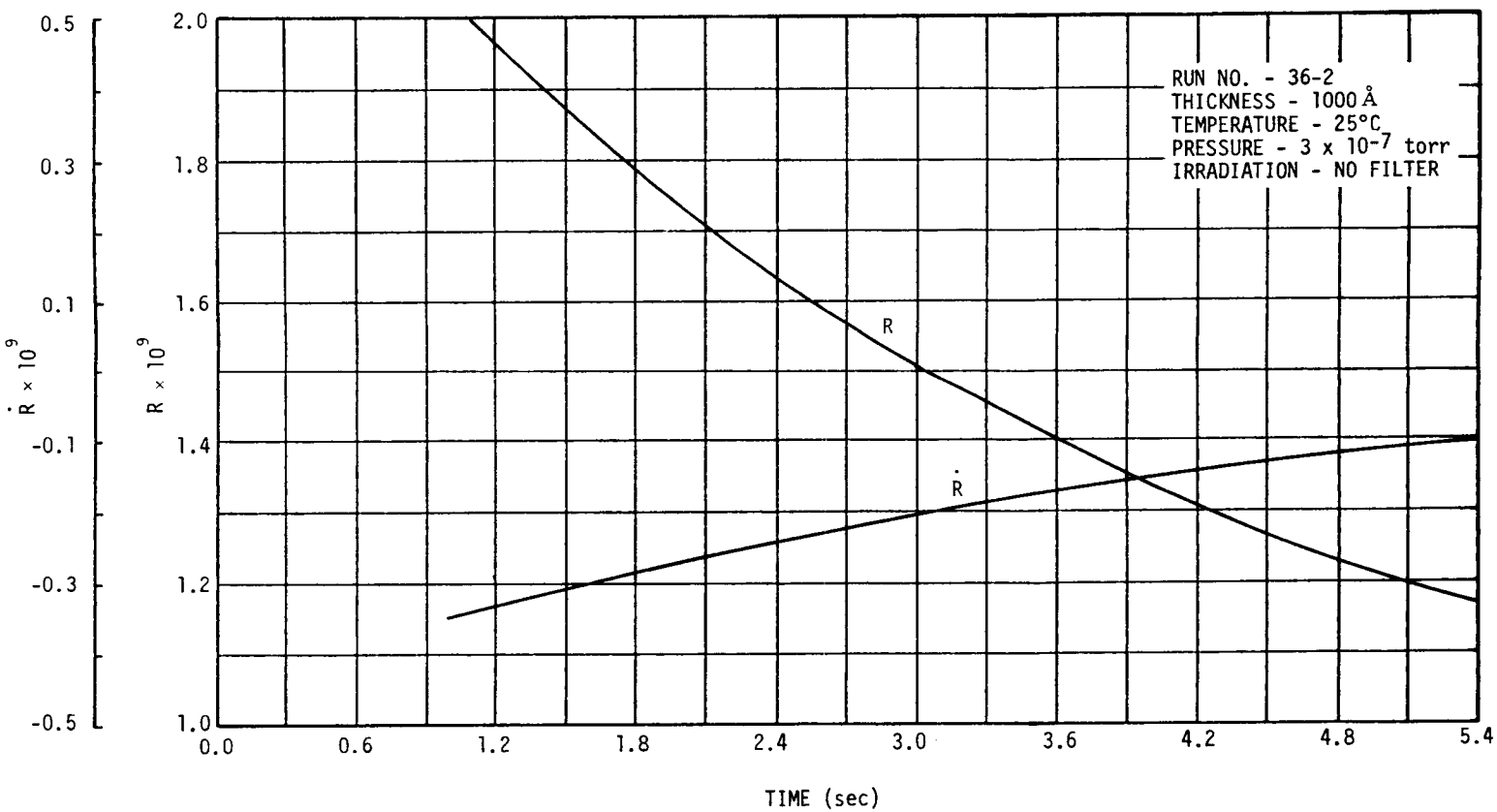
RUN NO. - 36-2
THICKNESS - 1000 Å
TEMPERATURE - 25°C
PRESSURE - 3 x 10-7 torr
IRRADIATION - NO FILTER
R
Ṙ
Ṙ × 10^9
R × 10^9
0.5
0.3
0.1
-0.1
-0.3
-0.5
2.0
1.8
1.6
1.4
1.2
1.0
0.0
0.6
1.2
1.8
2.4
3.0
3.6
4.2
4.8
5.4
TIME (sec)

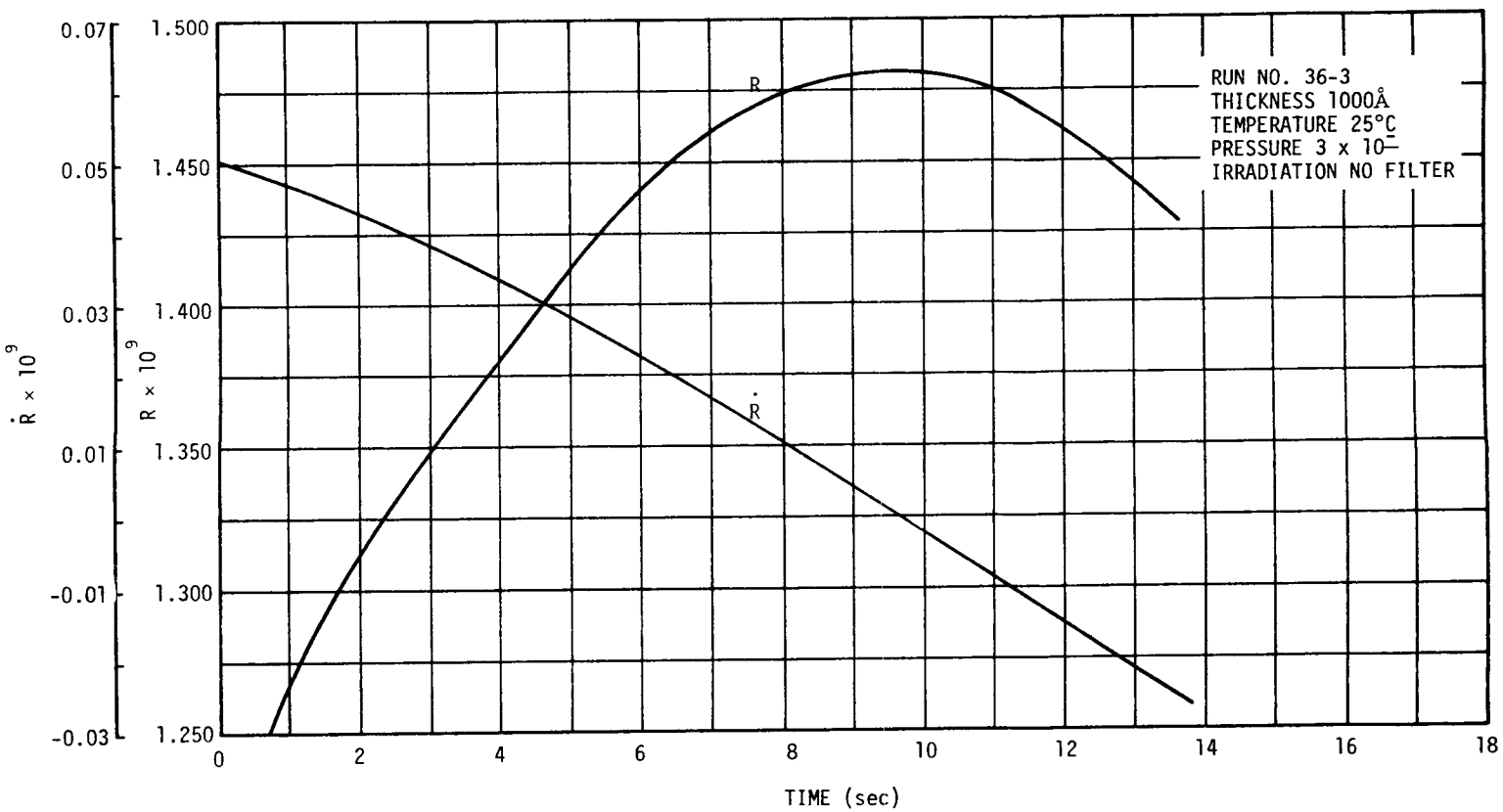
RUN NO. 36-3
THICKNESS 1000Å
TEMPERATURE 25°C
PRESSURE 3 x 10⁻
IRRADIATION NO FILTER
R
Ṙ
Ṙ × 10⁹
R × 10⁹
0.07
0.05
0.03
0.01
-0.01
-0.03
1.500
1.450
1.400
1.350
1.300
1.250
0
2
4
6
8
10
12
14
16
18
TIME (sec)

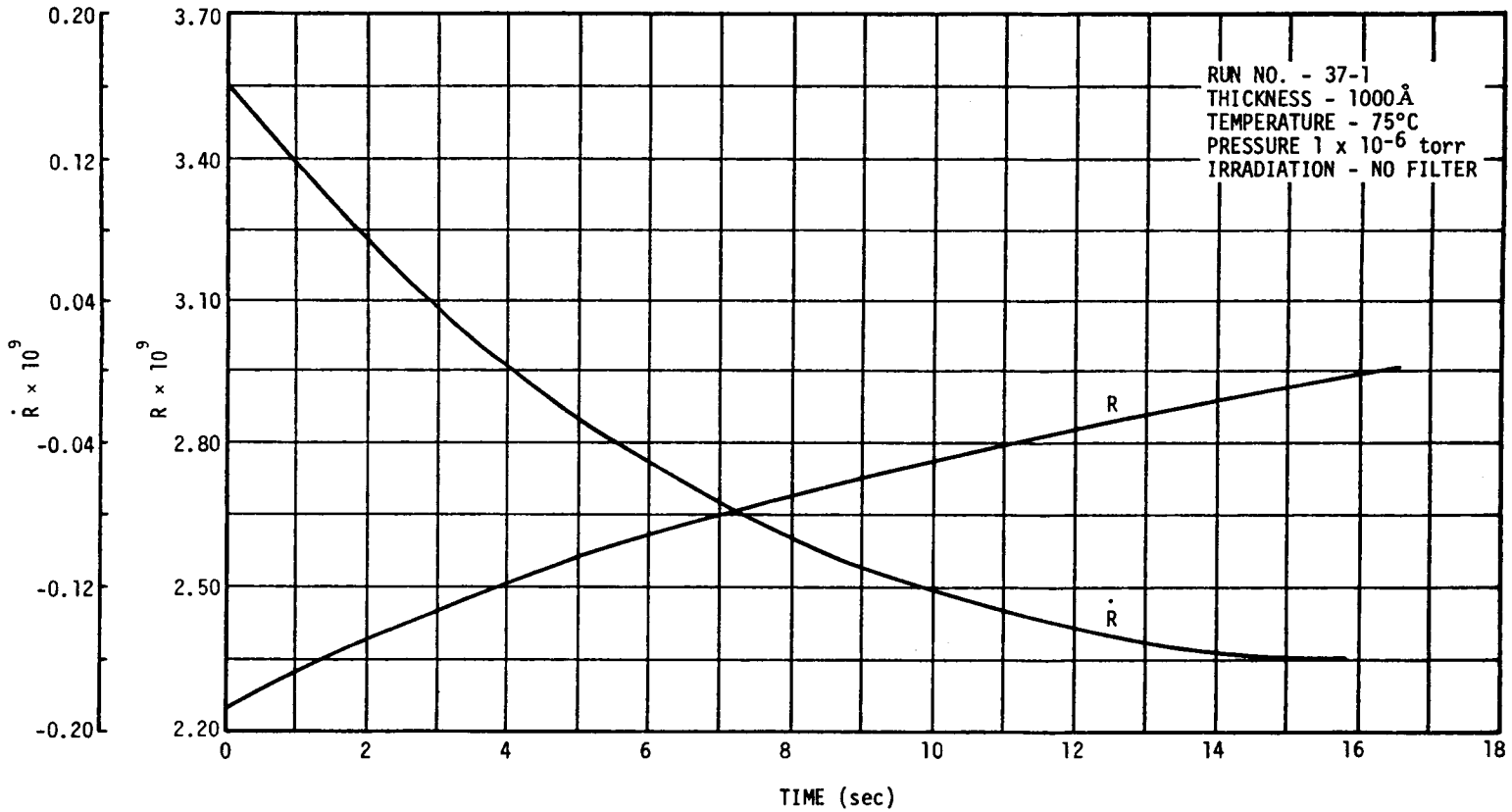
RUN NO. - 37-1
THICKNESS - 1000Å
TEMPERATURE - 75°C
PRESSURE 1 x 10-6 torr
IRRADIATION - NO FILTER
R
Ṙ
Ṙ × 10^9
R × 10^9
0.20
0.12
0.04
-0.04
-0.12
-0.20
3.70
3.40
3.10
2.80
2.50
2.20
0
2
4
6
8
10
12
14
16
18
TIME (sec)

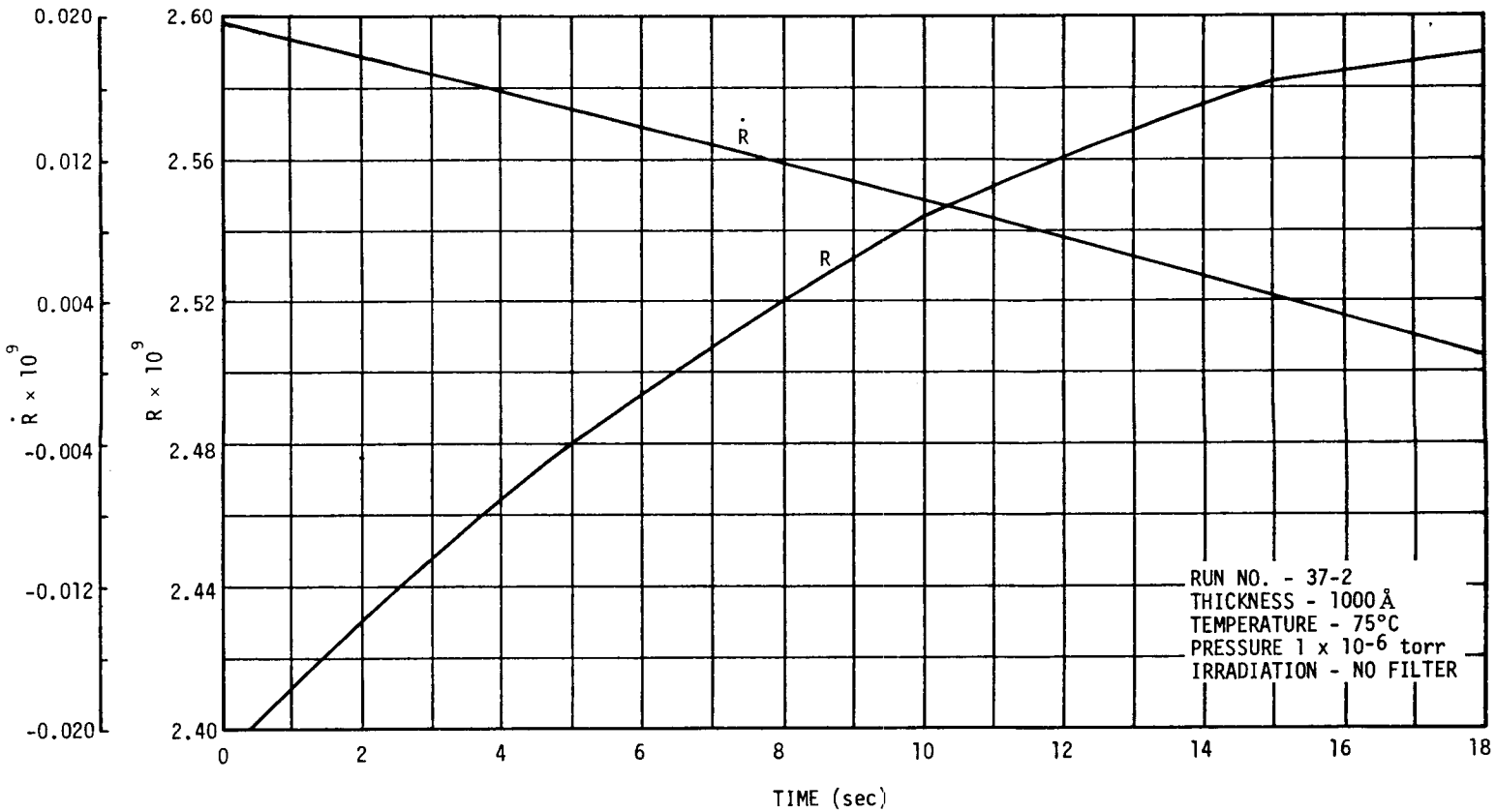
0.020
0.012
0.004
-0.004
-0.012
-0.020
$\dot{R} \times 10^9$
2.60
2.56
2.52
2.48
2.44
2.40
$R \times 10^9$
0
2
4
6
8
10
12
14
16
18
TIME (sec)
$\dot{R}$
R
RUN NO. - 37-2
THICKNESS - 1000 Å
TEMPERATURE - 75°C
PRESSURE 1 x 10^{-6} torr
IRRADIATION - NO FILTER

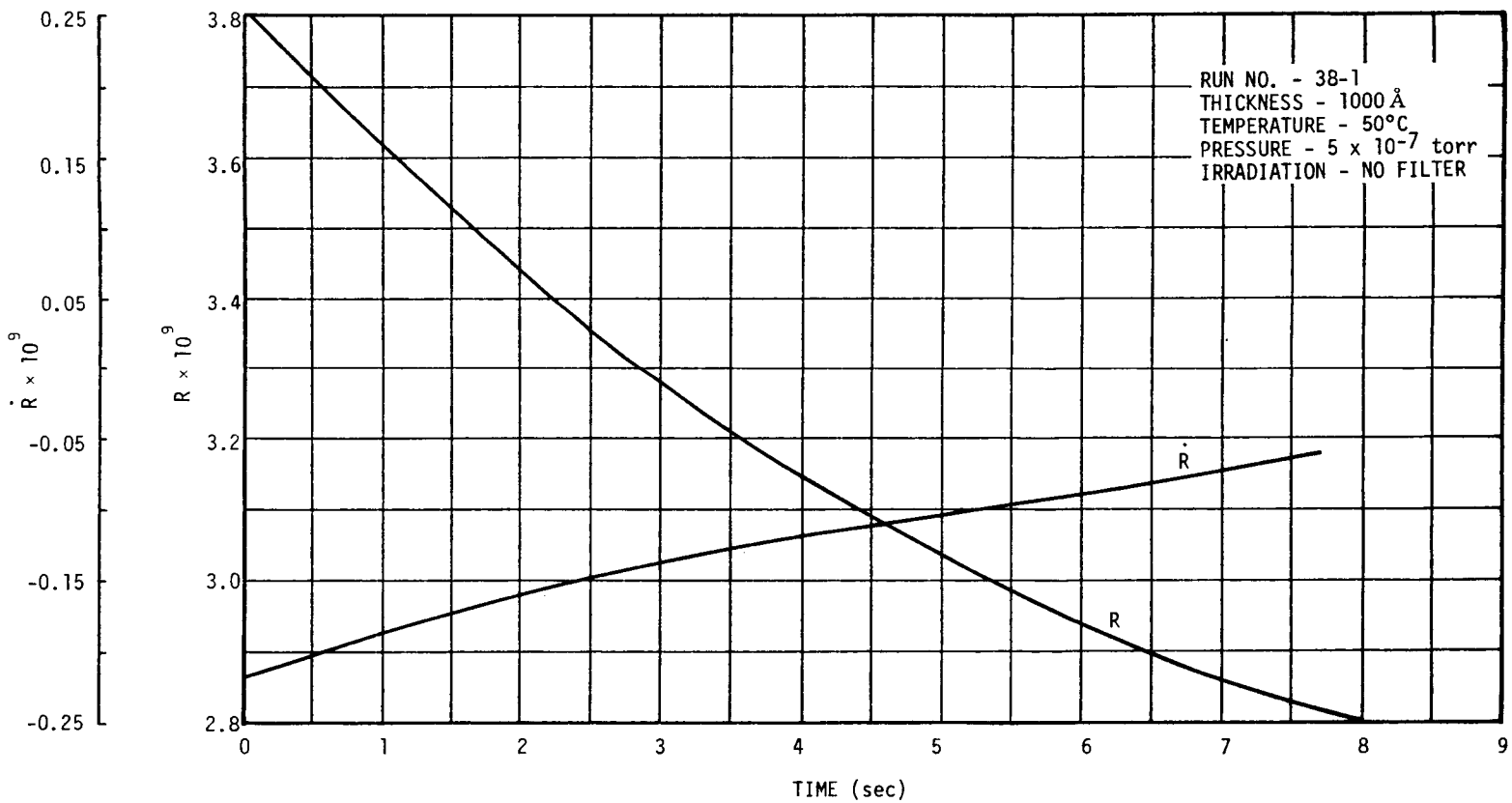
RUN NO. - 38-1
THICKNESS - 1000 Å
TEMPERATURE - 50°C
PRESSURE - 5 x 10^-7 torr
IRRADIATION - NO FILTER
Ṙ × 10^9
R × 10^9
0.25
0.15
0.05
-0.05
-0.15
-0.25
3.8
3.6
3.4
3.2
3.0
2.8
0
1
2
3
4
5
6
7
8
9
TIME (sec)
Ṙ
R

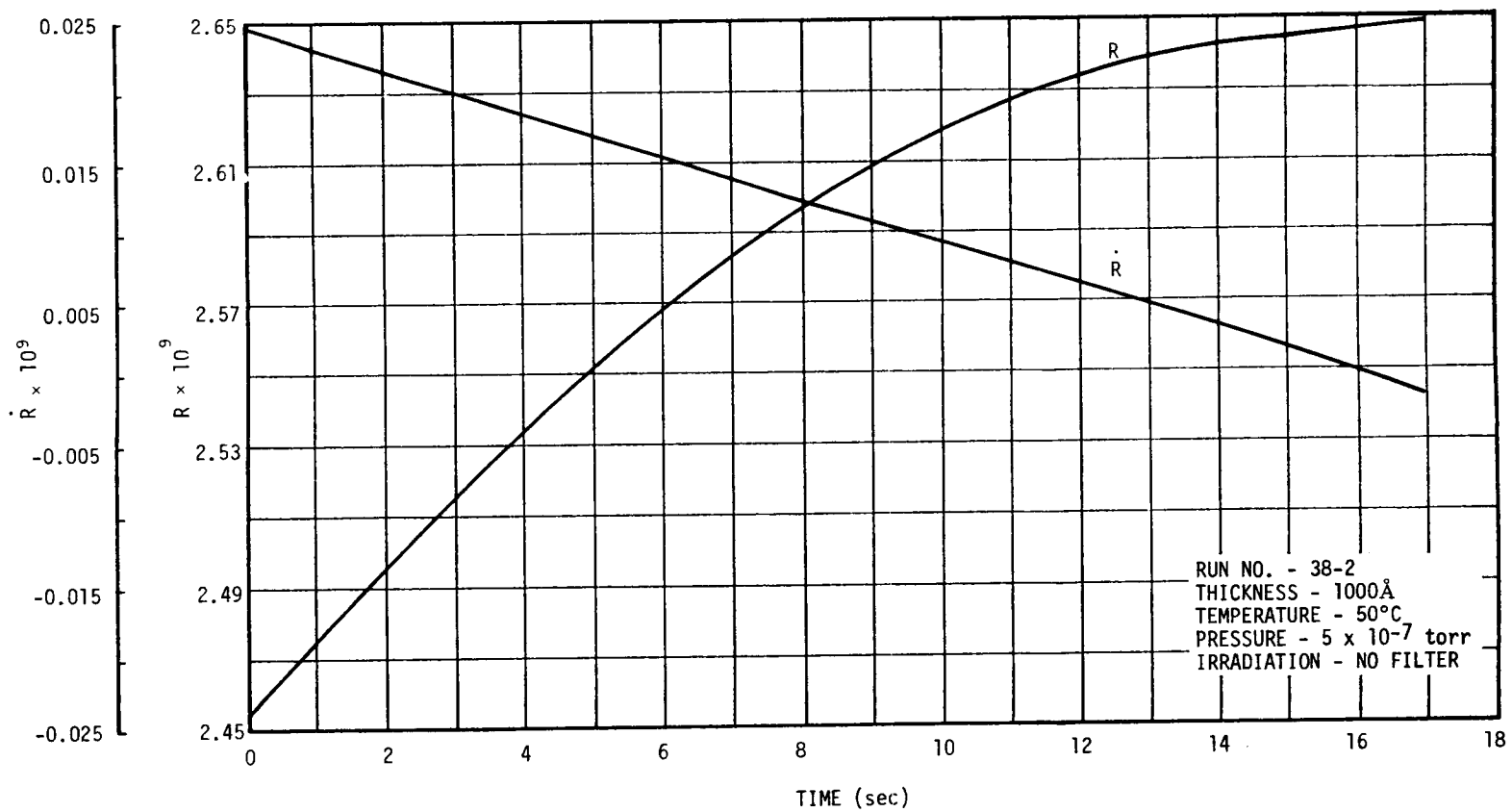
0.025
0.015
0.005
-0.005
-0.015
-0.025
$\dot{R} \times 10^9$
2.65
2.61
2.57
2.53
2.49
2.45
$R \times 10^9$
0
2
4
6
8
10
12
14
16
18
TIME (sec)
R
$\dot{R}$
RUN NO. - 38-2
THICKNESS - 1000Å
TEMPERATURE - 50°C
PRESSURE - 5 x 10^{-7} torr
IRRADIATION - NO FILTER

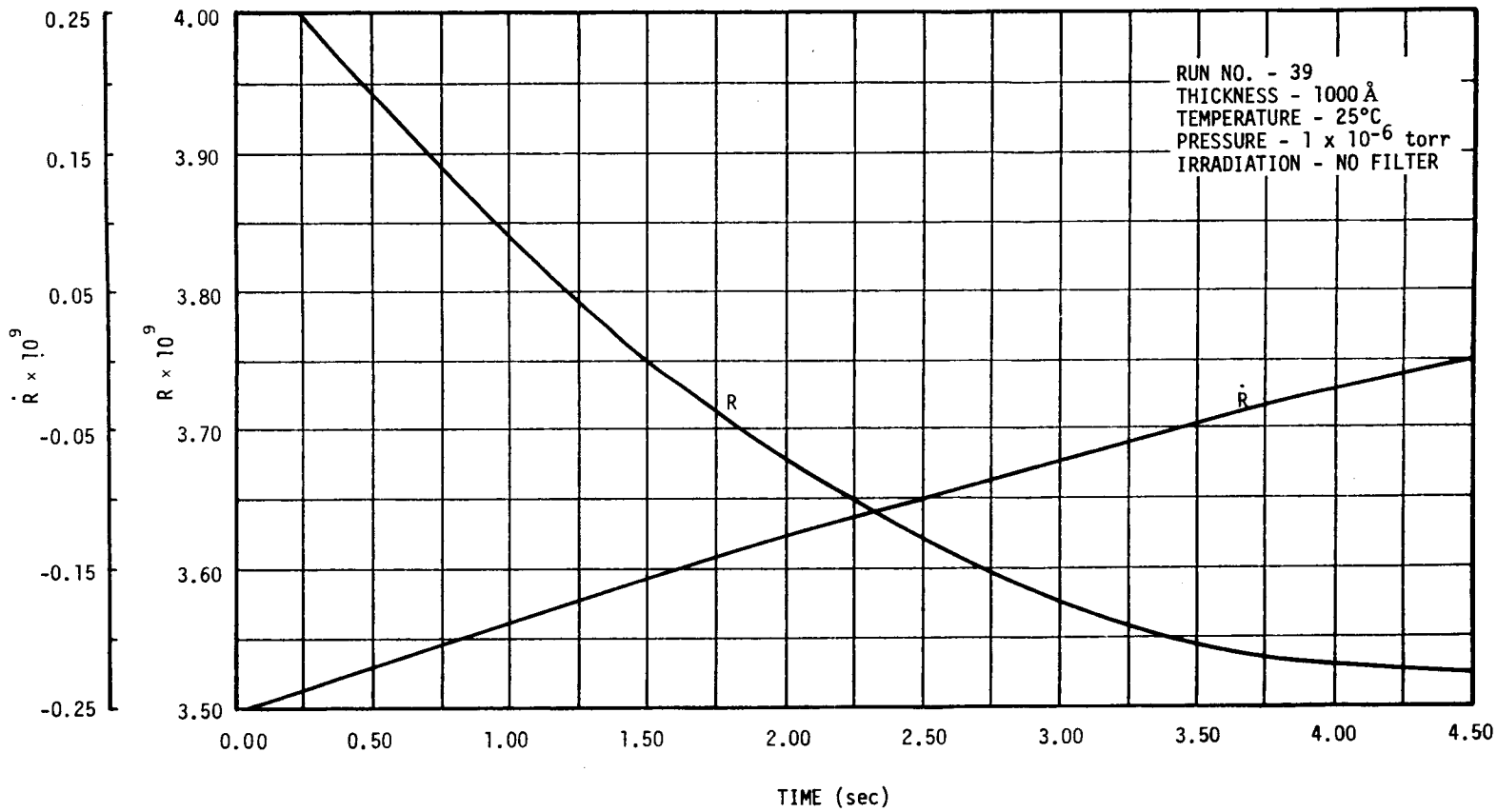
RUN NO. - 39
THICKNESS - 1000 Å
TEMPERATURE - 25°C
PRESSURE - 1 x 10^-6 torr
IRRADIATION - NO FILTER
R
Ṙ
Ṙ × 10^9
R × 10^9
0.25
0.15
0.05
-0.05
-0.15
-0.25
4.00
3.90
3.80
3.70
3.60
3.50
0.00
0.50
1.00
1.50
2.00
2.50
3.00
3.50
4.00
4.50
TIME (sec)

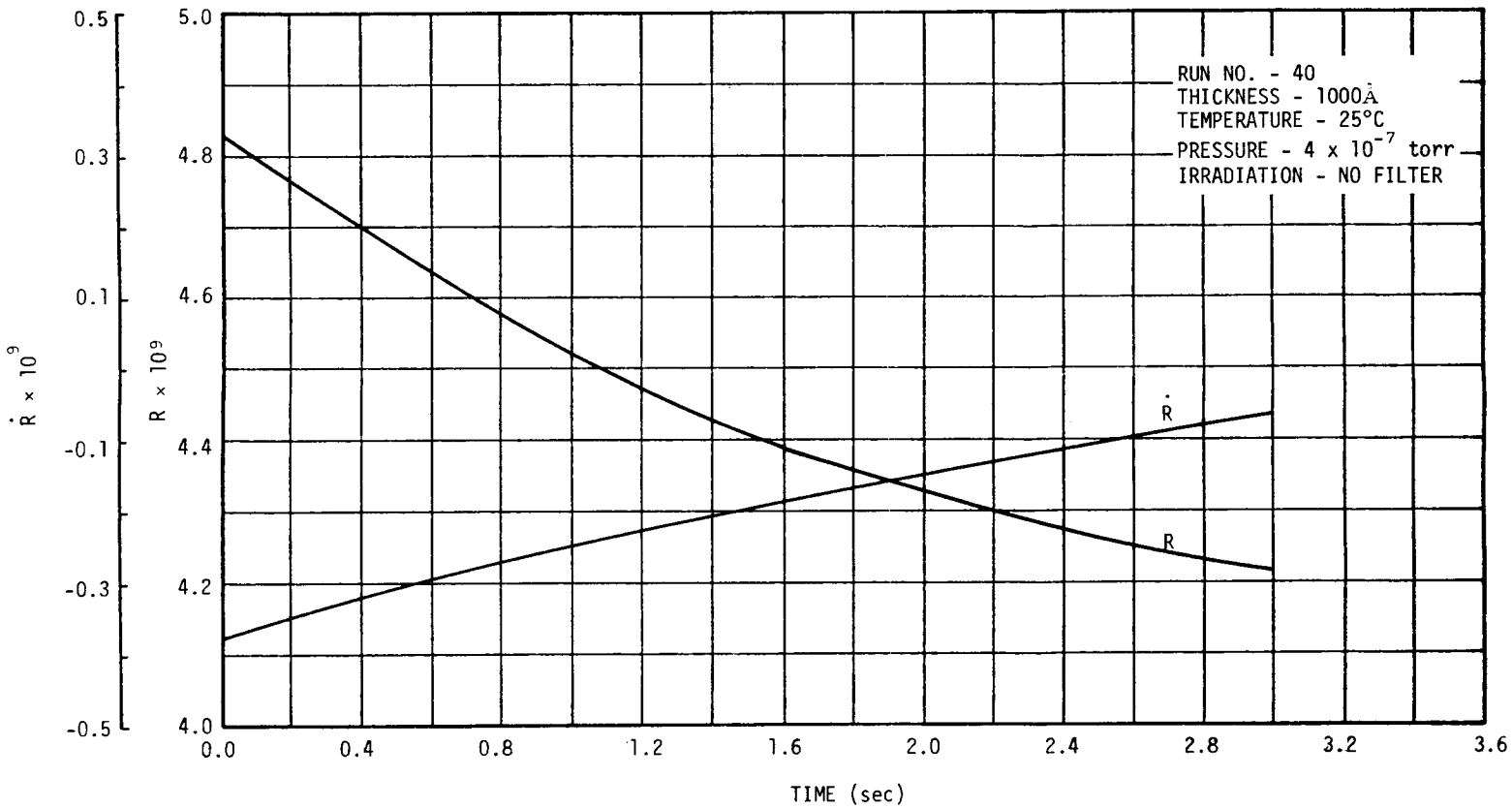
RUN NO. - 40
THICKNESS - 1000Å
TEMPERATURE - 25°C
PRESSURE - 4 x 10^-7 torr
IRRADIATION - NO FILTER
Ṙ
R
Ṙ × 10^9
R × 10^9
0.5
0.3
0.1
-0.1
-0.3
-0.5
5.0
4.8
4.6
4.4
4.2
4.0
0.0
0.4
0.8
1.2
1.6
2.0
2.4
2.8
3.2
3.6
TIME (sec)

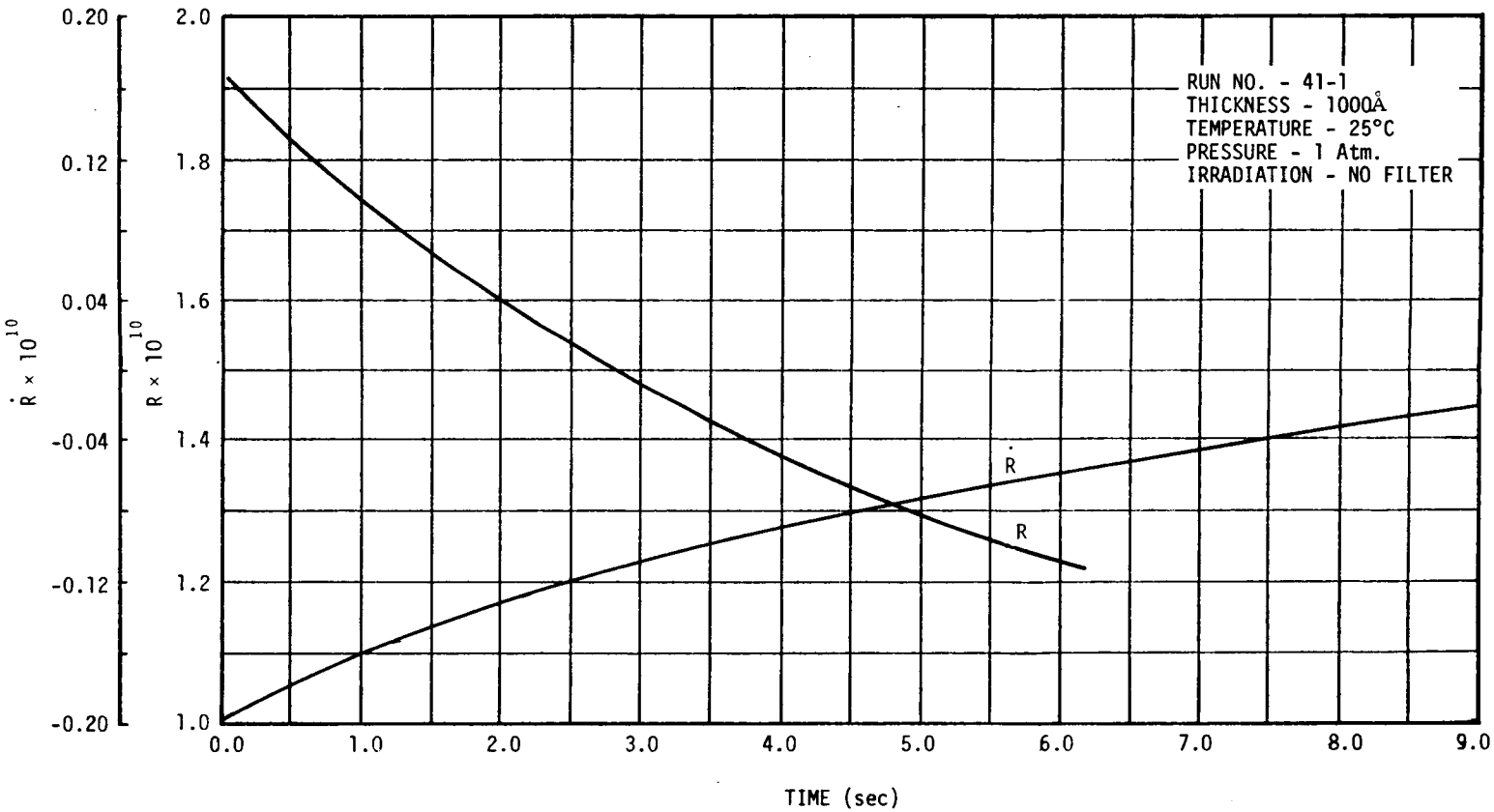
RUN NO. - 41-1
THICKNESS - 1000Å
TEMPERATURE - 25°C
PRESSURE - 1 Atm.
IRRADIATION - NO FILTER
Ṙ × 10^10
R × 10^10
0.20
0.12
0.04
-0.04
-0.12
-0.20
2.0
1.8
1.6
1.4
1.2
1.0
0.0
1.0
2.0
3.0
4.0
5.0
6.0
7.0
8.0
9.0
TIME (sec)
Ṙ
R

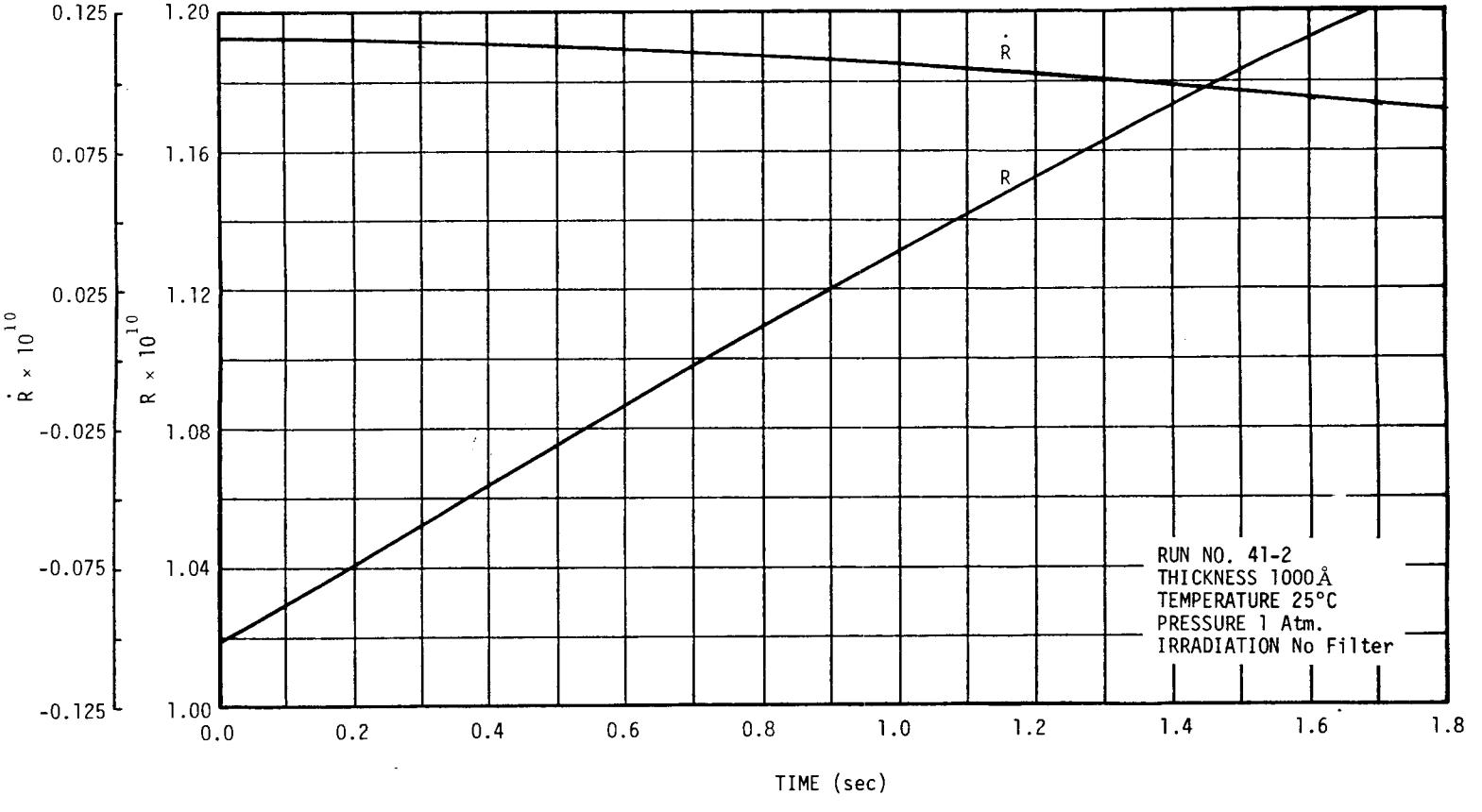
0.125
0.075
0.025
-0.025
-0.075
-0.125
$\dot{R} \times 10^{10}$
1.20
1.16
1.12
1.08
1.04
1.00
$R \times 10^{10}$
0.0
0.2
0.4
0.6
0.8
1.0
1.2
1.4
1.6
1.8
TIME (sec)
$\dot{R}$
R
RUN NO. 41-2
THICKNESS 1000Å
TEMPERATURE 25°C
PRESSURE 1 Atm.
IRRADIATION No Filter

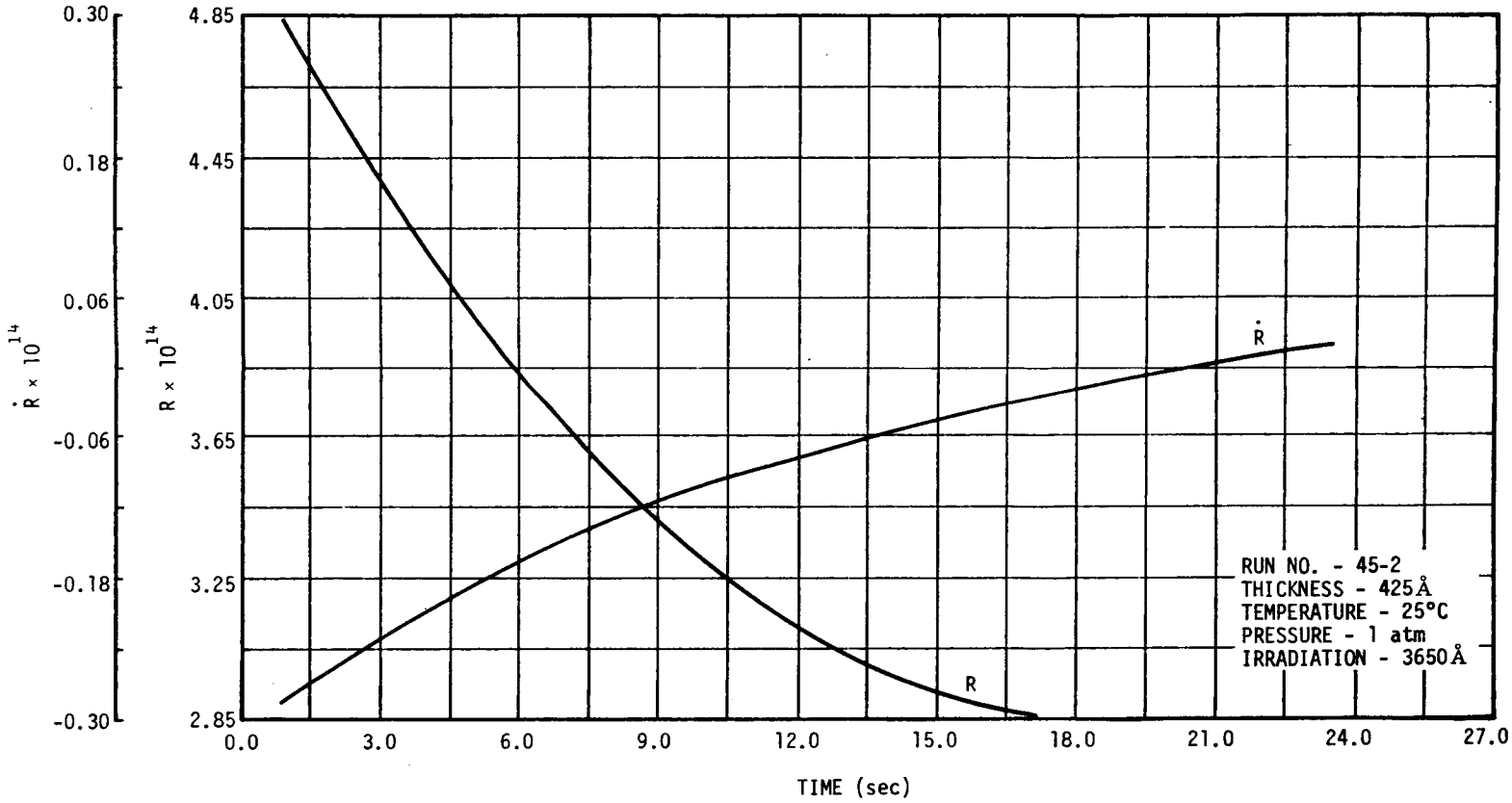
0.30
0.18
0.06
-0.06
-0.18
-0.30
$\dot{R} \times 10^{14}$
4.85
4.45
4.05
3.65
3.25
2.85
$R \times 10^{14}$
0.0
3.0
6.0
9.0
12.0
15.0
18.0
21.0
24.0
27.0
TIME (sec)
$\dot{R}$
R
RUN NO. - 45-2
THICKNESS - 425Å
TEMPERATURE - 25°C
PRESSURE - 1 atm
IRRADIATION - 3650Å

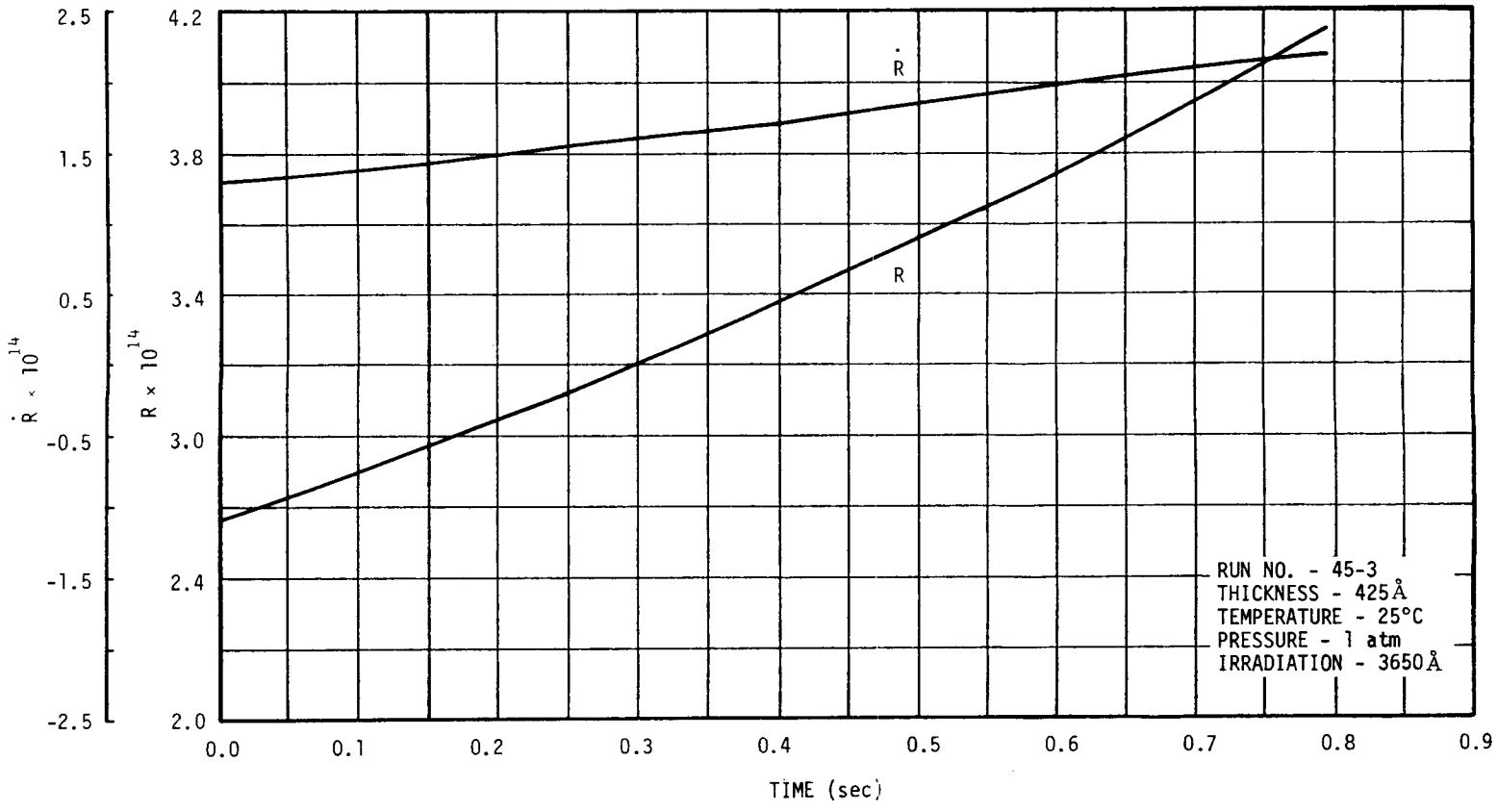
2.5
1.5
0.5
-0.5
-1.5
-2.5
$\dot{R} \times 10^{14}$
4.2
3.8
3.4
3.0
2.4
2.0
$R \times 10^{14}$
0.0
0.1
0.2
0.3
0.4
0.5
0.6
0.7
0.8
0.9
TIME (sec)
$\dot{R}$
R
RUN NO. - 45-3
THICKNESS - 425Å
TEMPERATURE - 25°C
PRESSURE - 1 atm
IRRADIATION - 3650Å

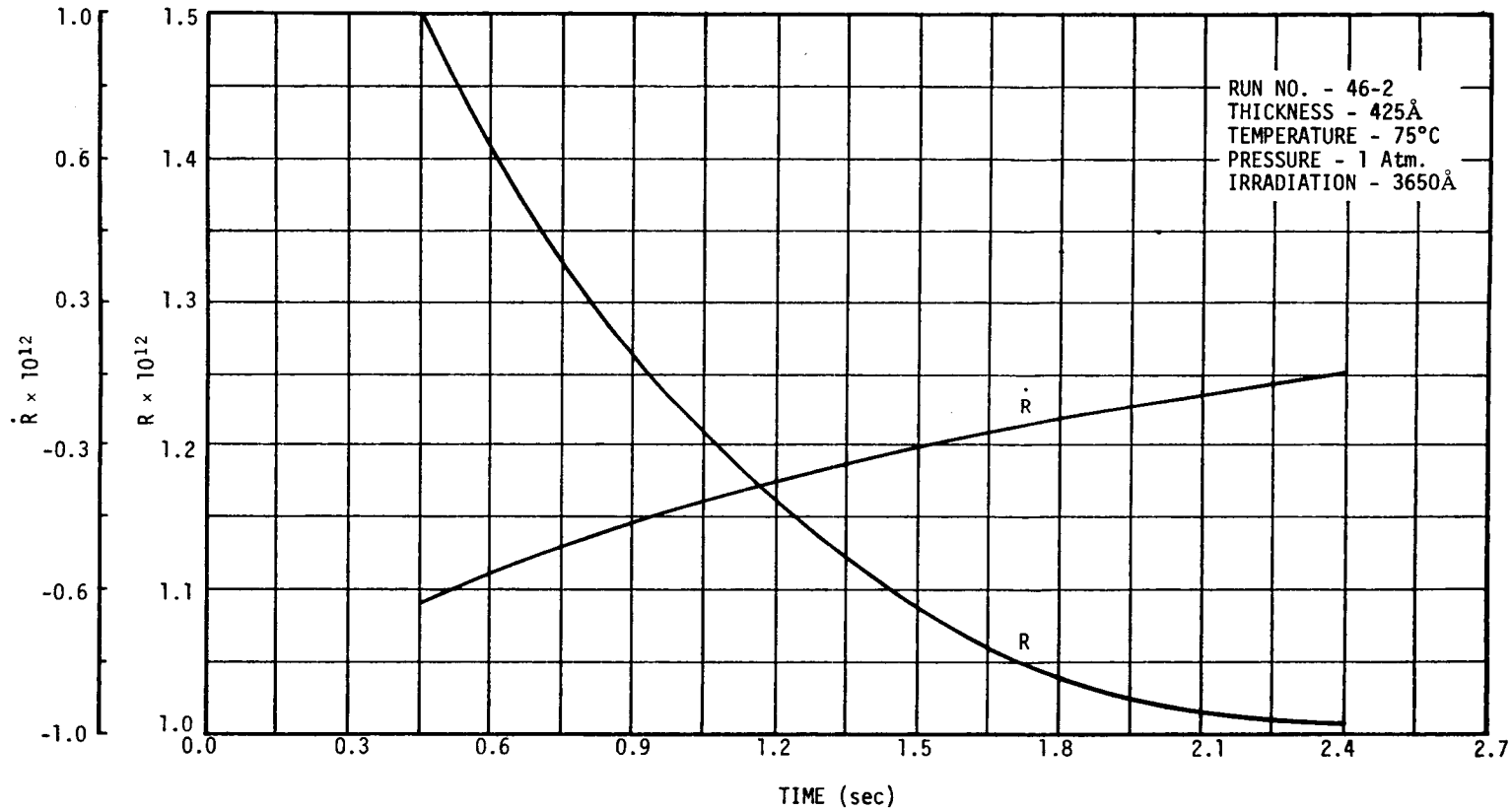
RUN NO. - 46-2
THICKNESS - 425Å
TEMPERATURE - 75°C
PRESSURE - 1 Atm.
IRRADIATION - 3650Å
Ṙ × 10^12
R × 10^12
1.0
0.6
0.3
-0.3
-0.6
-1.0
1.5
1.4
1.3
1.2
1.1
1.0
0.0
0.3
0.6
0.9
1.2
1.5
1.8
2.1
2.4
2.7
TIME (sec)
Ṙ
R

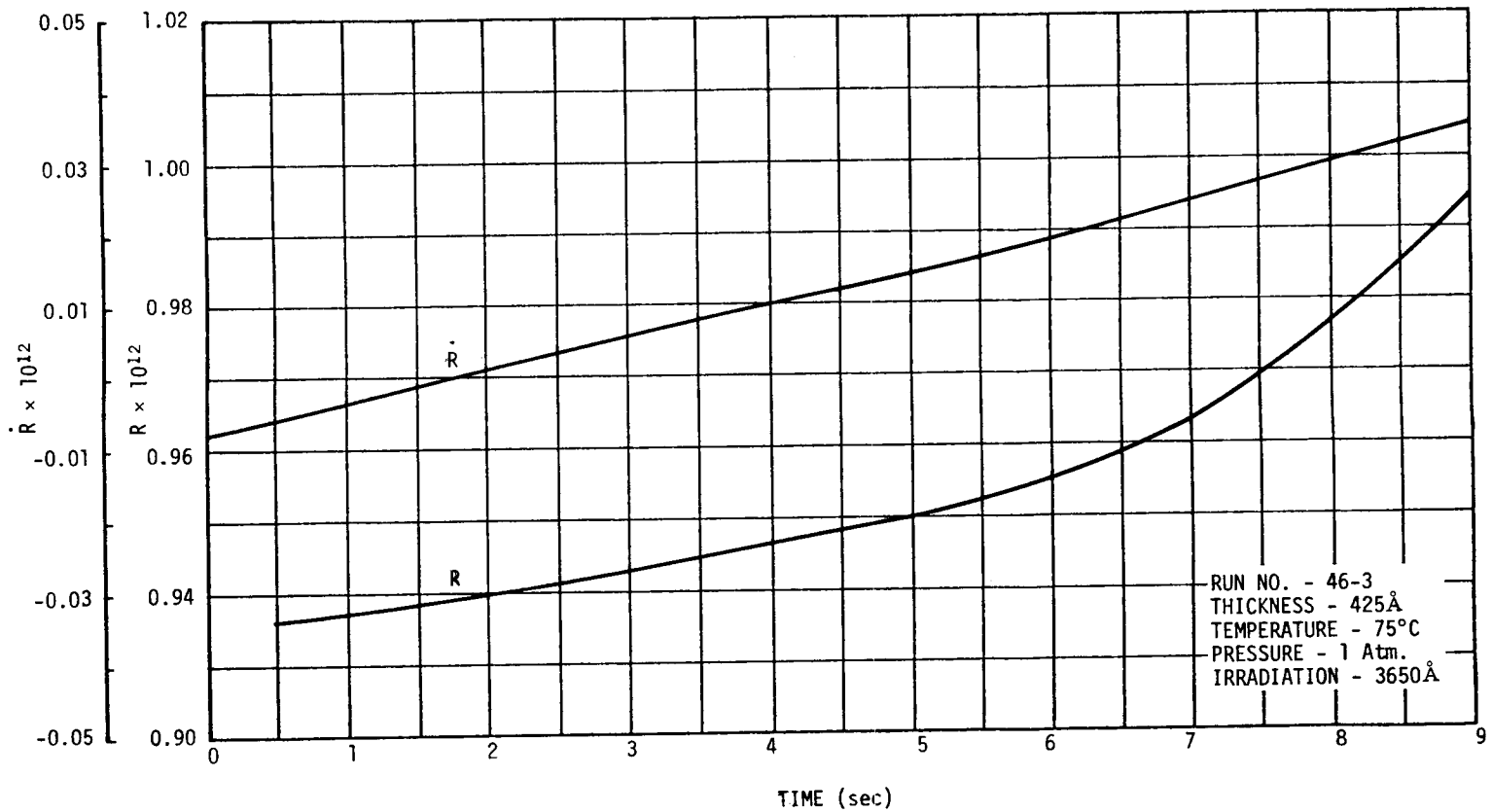
0.05
0.03
0.01
-0.01
-0.03
-0.05
$\dot{R} \times 10^{12}$
1.02
1.00
0.98
0.96
0.94
0.90
$R \times 10^{12}$
$\dot{R}$
R
0
1
2
3
4
5
6
7
8
9
TIME (sec)
RUN NO. - 46-3
THICKNESS - 425Å
TEMPERATURE - 75°C
PRESSURE - 1 Atm.
IRRADIATION - 3650Å

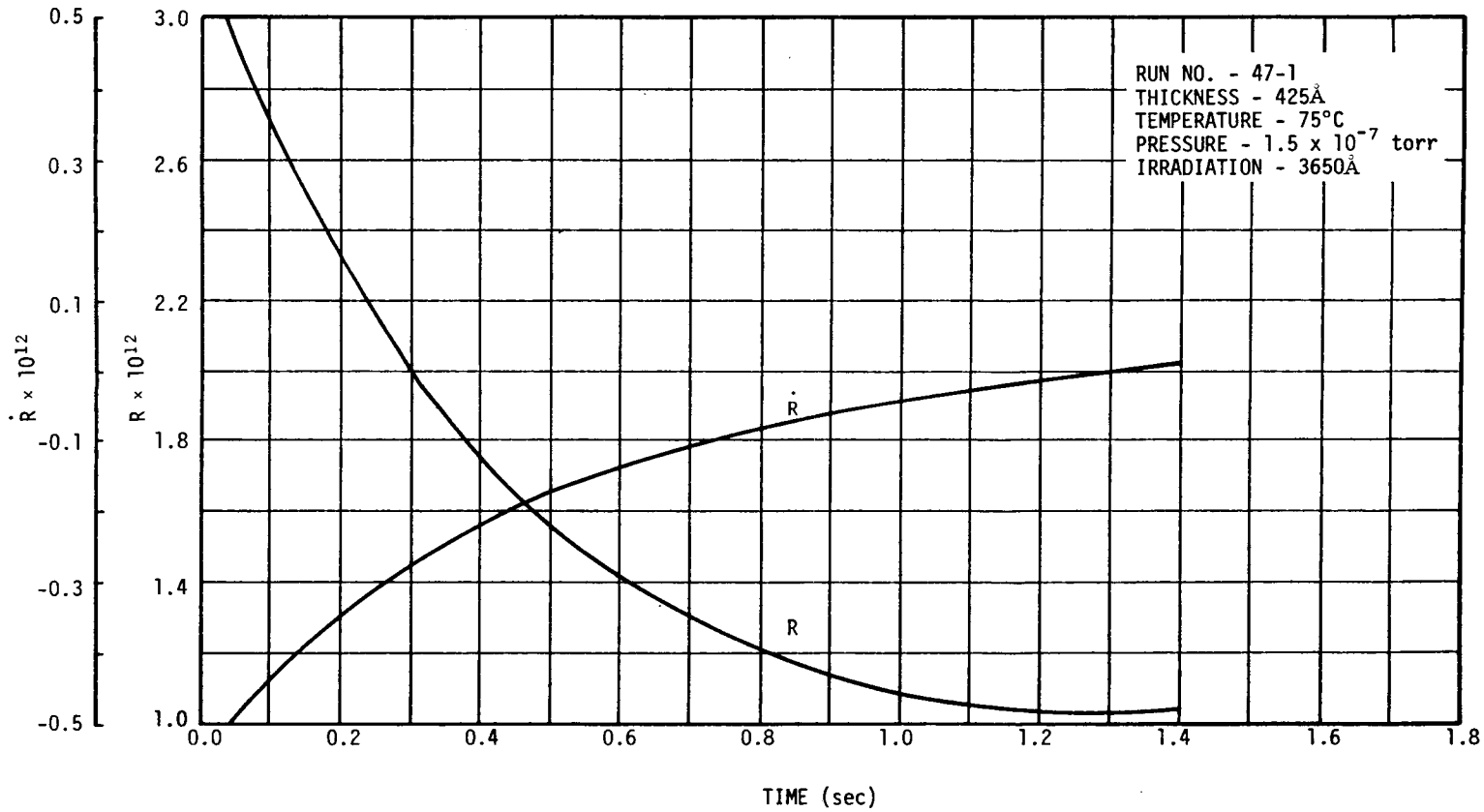
RUN NO. - 47-1
THICKNESS - 425Å
TEMPERATURE - 75°C
PRESSURE - 1.5 x 10^-7 torr
IRRADIATION - 3650Å
Ṙ × 10^12
R × 10^12
0.5
0.3
0.1
-0.1
-0.3
-0.5
3.0
2.6
2.2
1.8
1.4
1.0
0.0
0.2
0.4
0.6
0.8
1.0
1.2
1.4
1.6
1.8
Ṙ
R
TIME (sec)

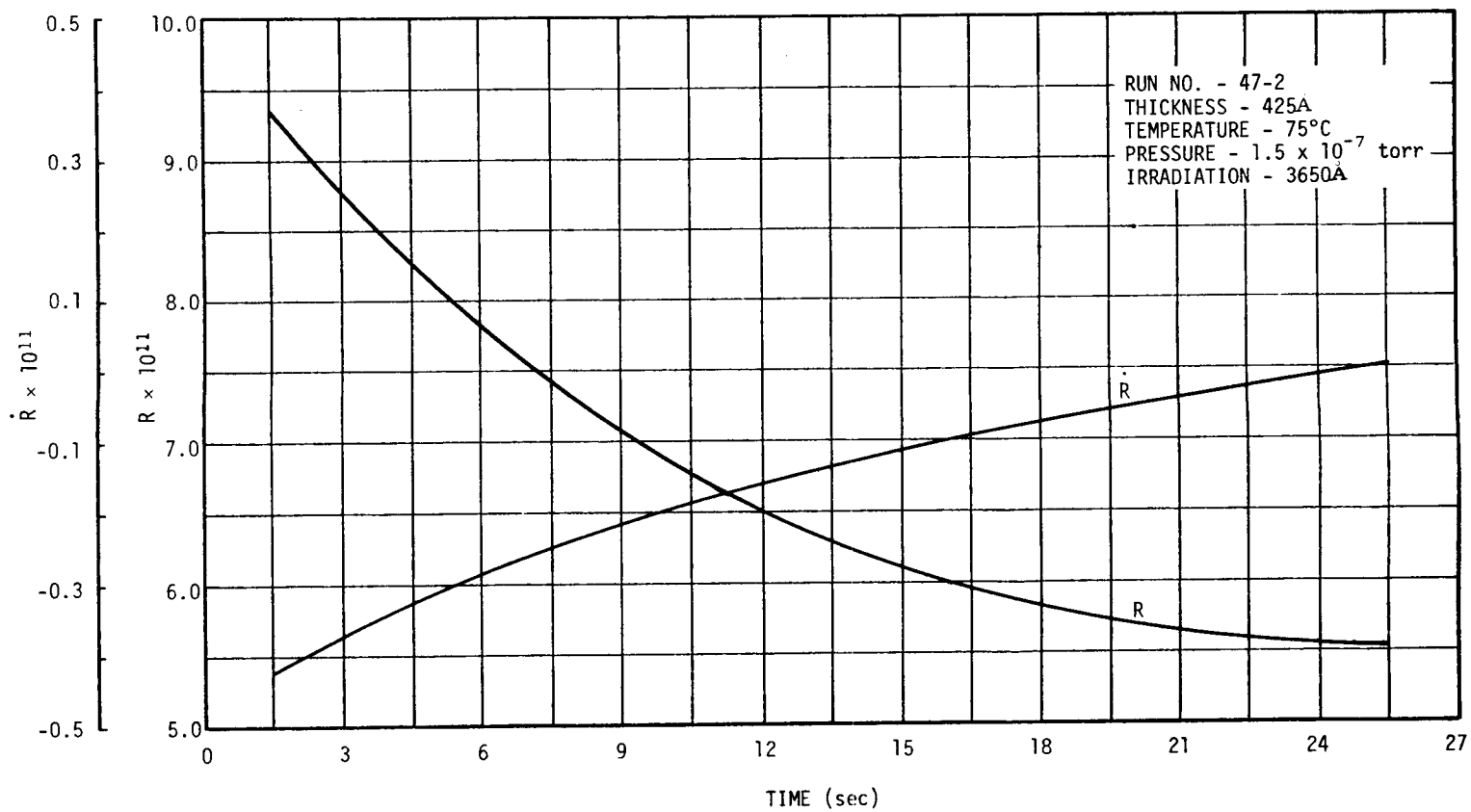
RUN NO. - 47-2
THICKNESS - 425Å
TEMPERATURE - 75°C
PRESSURE - 1.5 x 10^-7 torr
IRRADIATION - 3650Å
Ṙ
R
Ṙ × 10^11
R × 10^11
0.5
0.3
0.1
-0.1
-0.3
-0.5
10.0
9.0
8.0
7.0
6.0
5.0
0
3
6
9
12
15
18
21
24
27
TIME (sec)

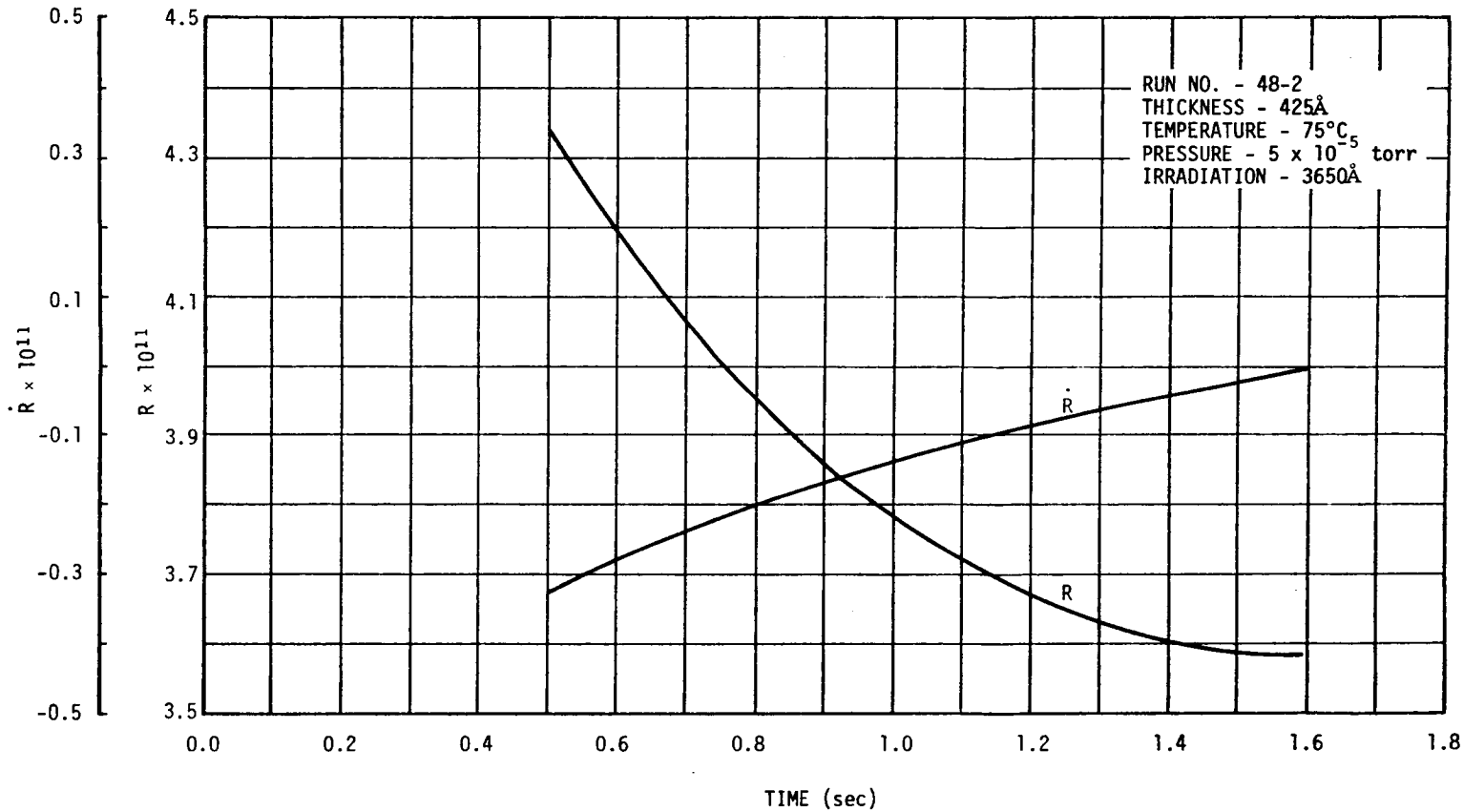
RUN NO. - 48-2
THICKNESS - 425Å
TEMPERATURE - 75°C
PRESSURE - 5 x 10^-5 torr
IRRADIATION - 3650Å
Ṙ × 10^11
R × 10^11
0.5
0.3
0.1
-0.1
-0.3
-0.5
4.5
4.3
4.1
3.9
3.7
3.5
0.0
0.2
0.4
0.6
0.8
1.0
1.2
1.4
1.6
1.8
TIME (sec)
Ṙ
R

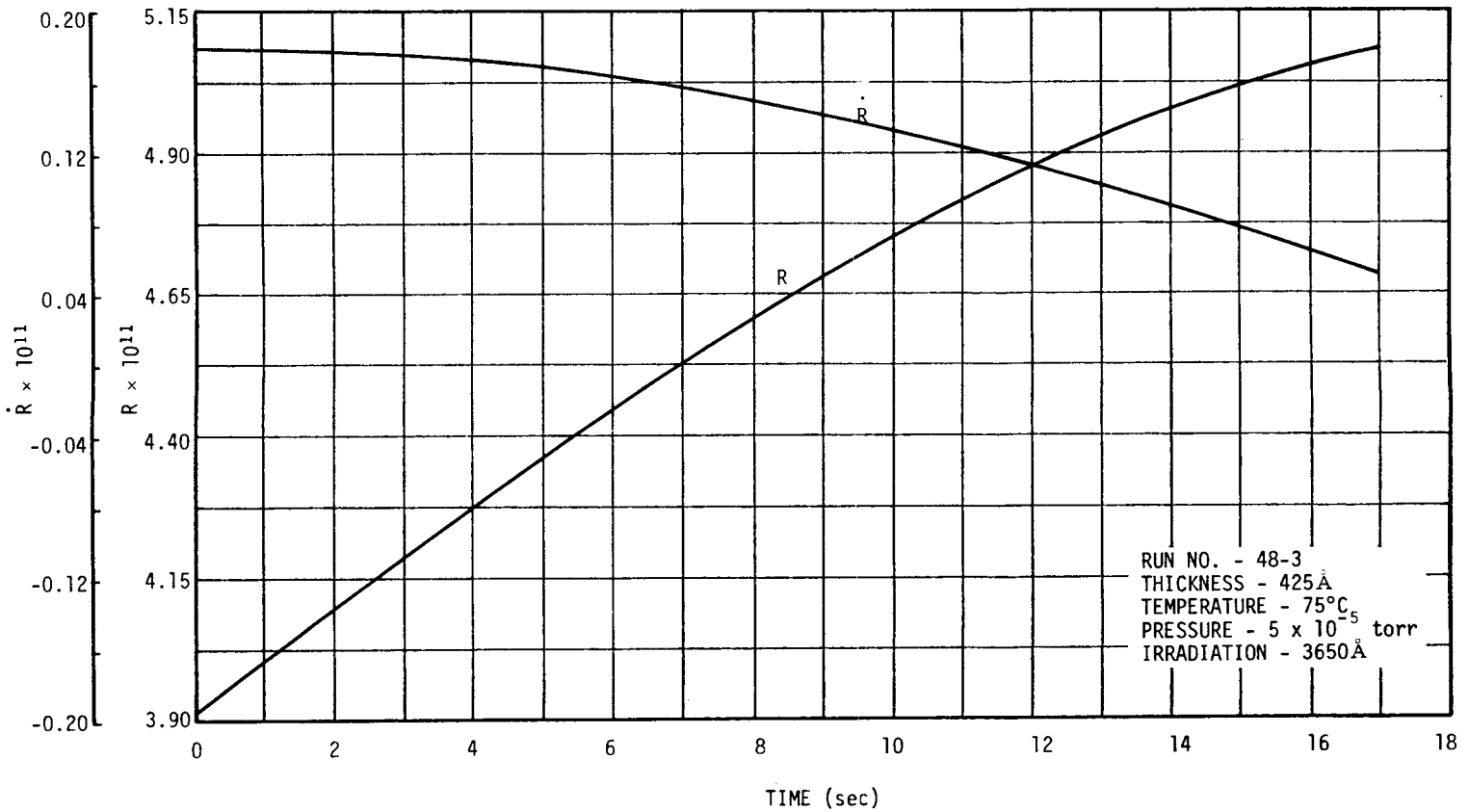
0.20
0.12
0.04
-0.04
-0.12
-0.20
$\dot{R} \times 10^{11}$
5.15
4.90
4.65
4.40
4.15
3.90
$R \times 10^{11}$
0
2
4
6
8
10
12
14
16
18
TIME (sec)
$\dot{R}$
R
RUN NO. - 48-3
THICKNESS - 425Å
TEMPERATURE - 75°C
PRESSURE - 5 x 10^{-5} torr
IRRADIATION - 3650Å

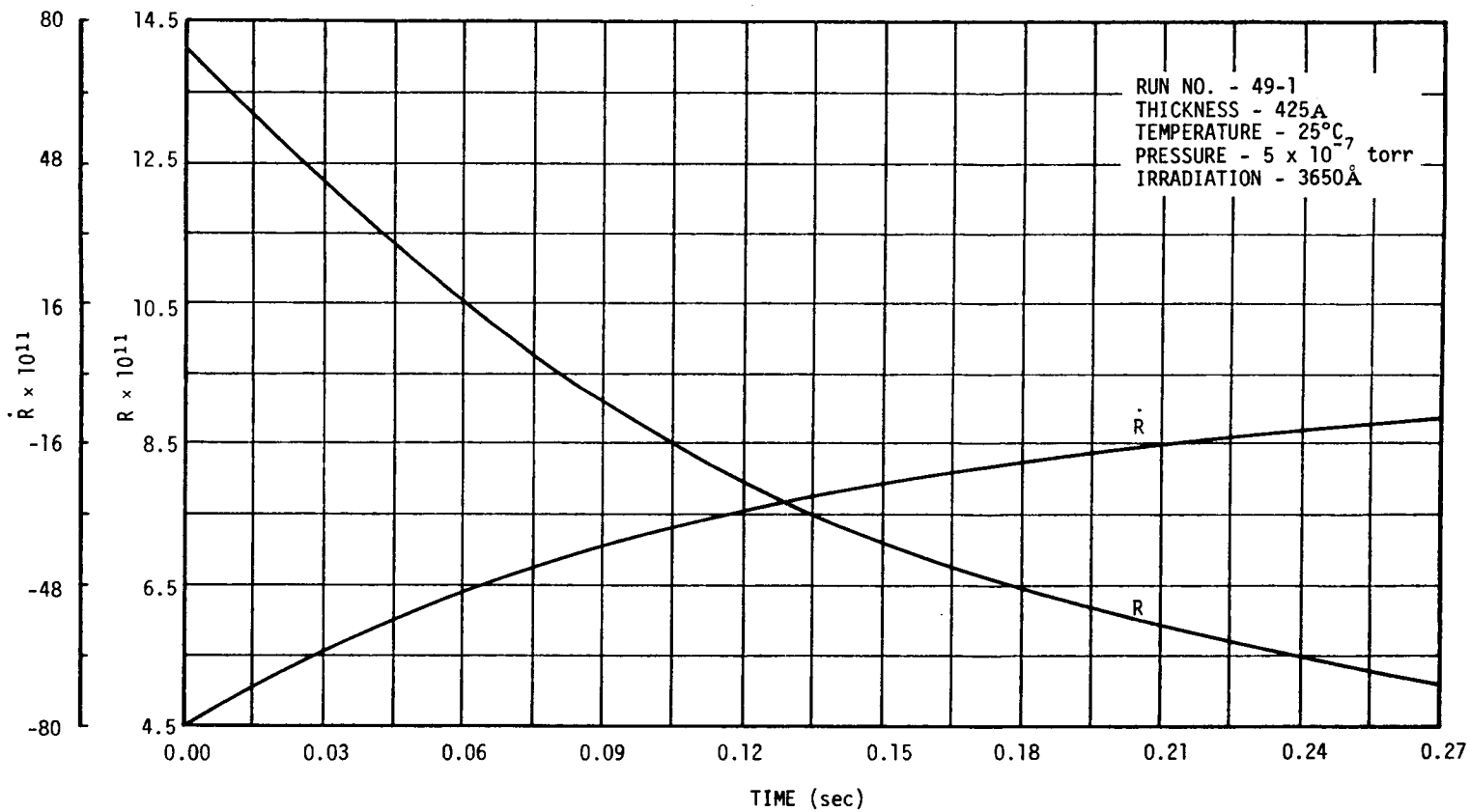
RUN NO. - 49-1
THICKNESS - 425Å
TEMPERATURE - 25°C
PRESSURE - 5 x 10^-7 torr
IRRADIATION - 3650Å
Ṙ
R
Ṙ × 10^11
R × 10^11
80
48
16
-16
-48
-80
14.5
12.5
10.5
8.5
6.5
4.5
0.00
0.03
0.06
0.09
0.12
0.15
0.18
0.21
0.24
0.27
TIME (sec)

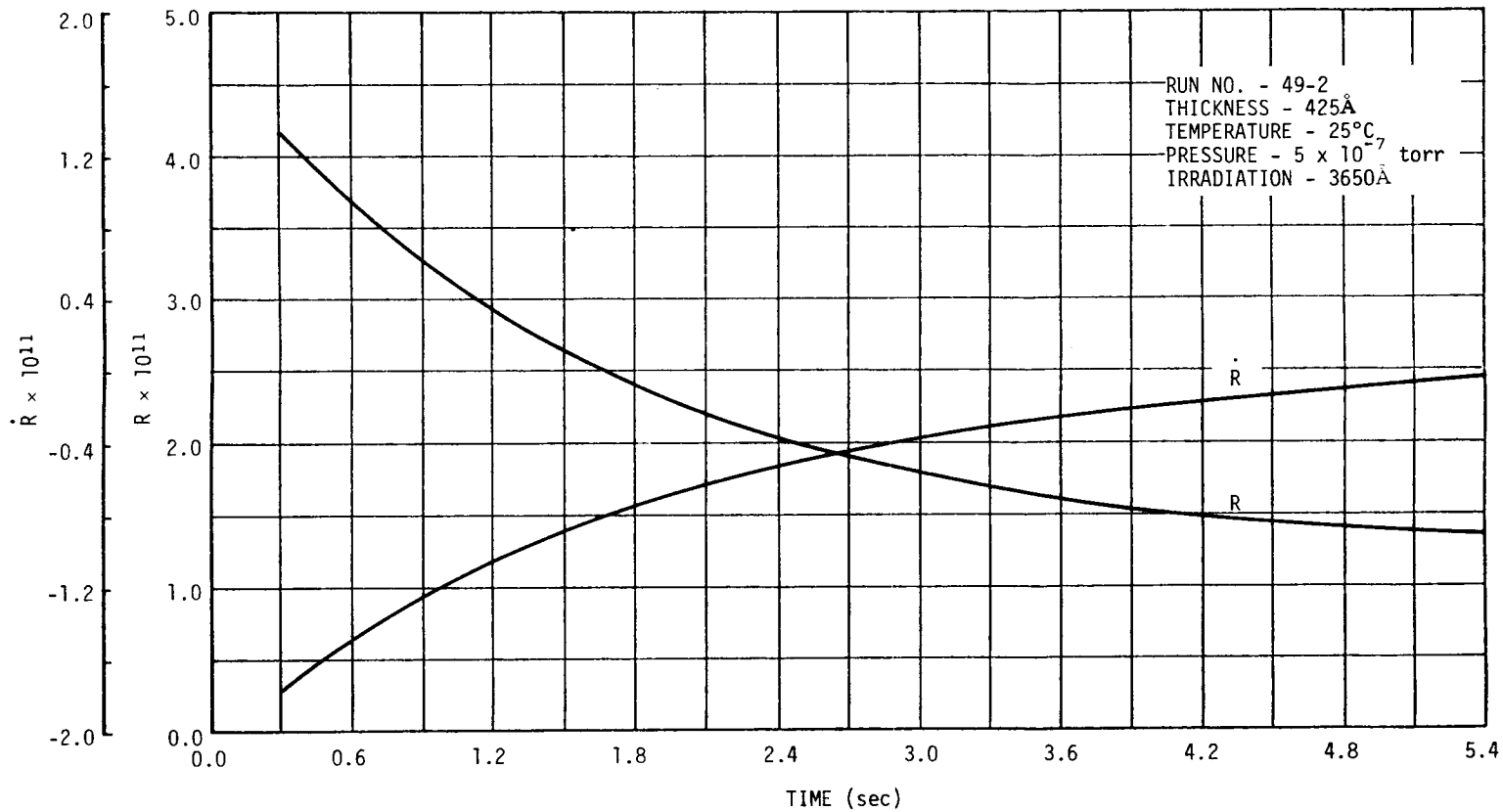
RUN NO. - 49-2
THICKNESS - 425Å
TEMPERATURE - 25°C
PRESSURE - 5 x 10^-7 torr
IRRADIATION - 3650Å
Ṙ
R
Ṙ × 10^11
R × 10^11
2.0
1.2
0.4
-0.4
-1.2
-2.0
5.0
4.0
3.0
2.0
1.0
0.0
0.0
0.6
1.2
1.8
2.4
3.0
3.6
4.2
4.8
5.4
TIME (sec)

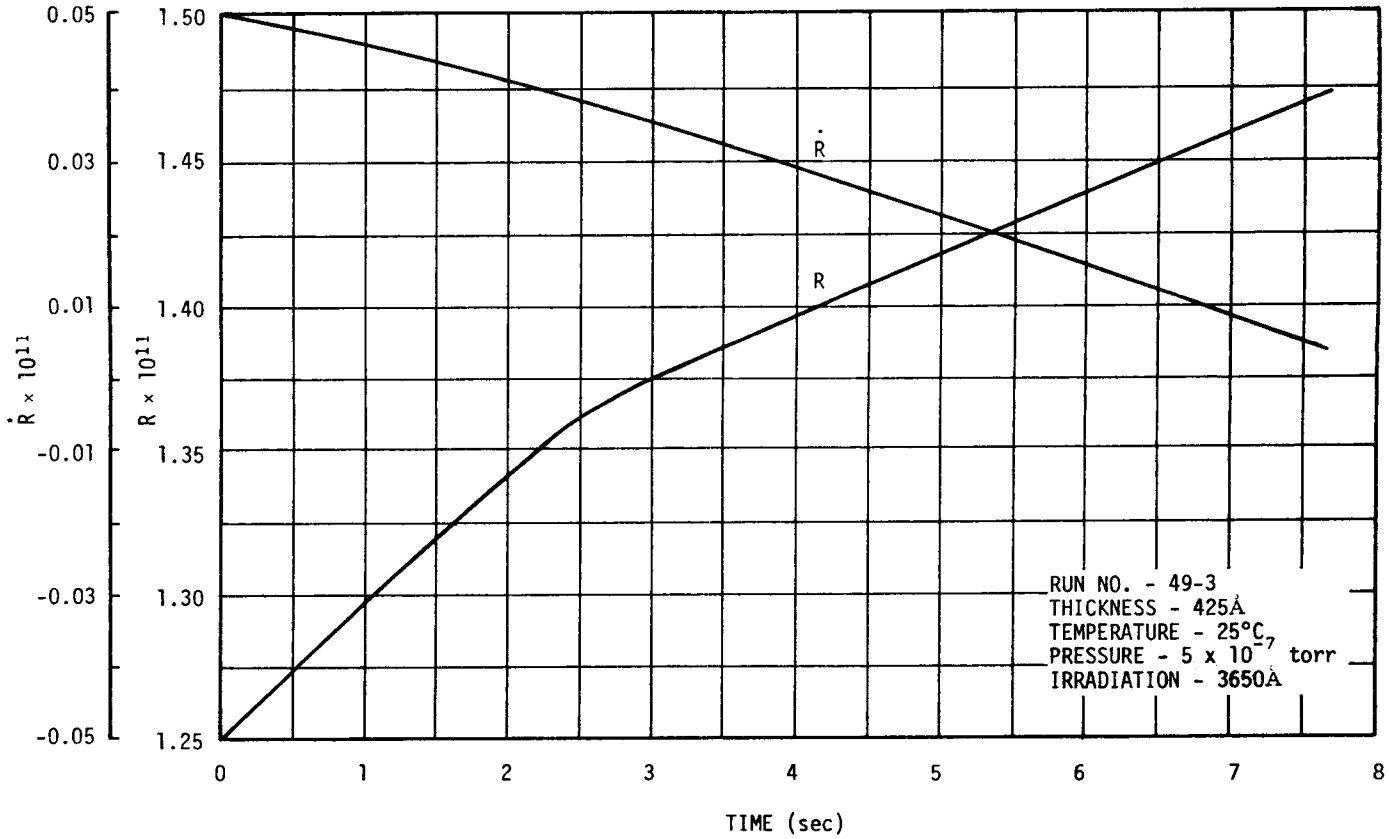
0.05
0.03
0.01
-0.01
-0.03
-0.05
$\dot{R} \times 10^{11}$
1.50
1.45
1.40
1.35
1.30
1.25
$R \times 10^{11}$
$\dot{R}$
R
RUN NO. - 49-3
THICKNESS - 425Å
TEMPERATURE - 25°C
PRESSURE - 5 x 10^{-7} torr
IRRADIATION - 3650Å
0
1
2
3
4
5
6
7
8
TIME (sec)

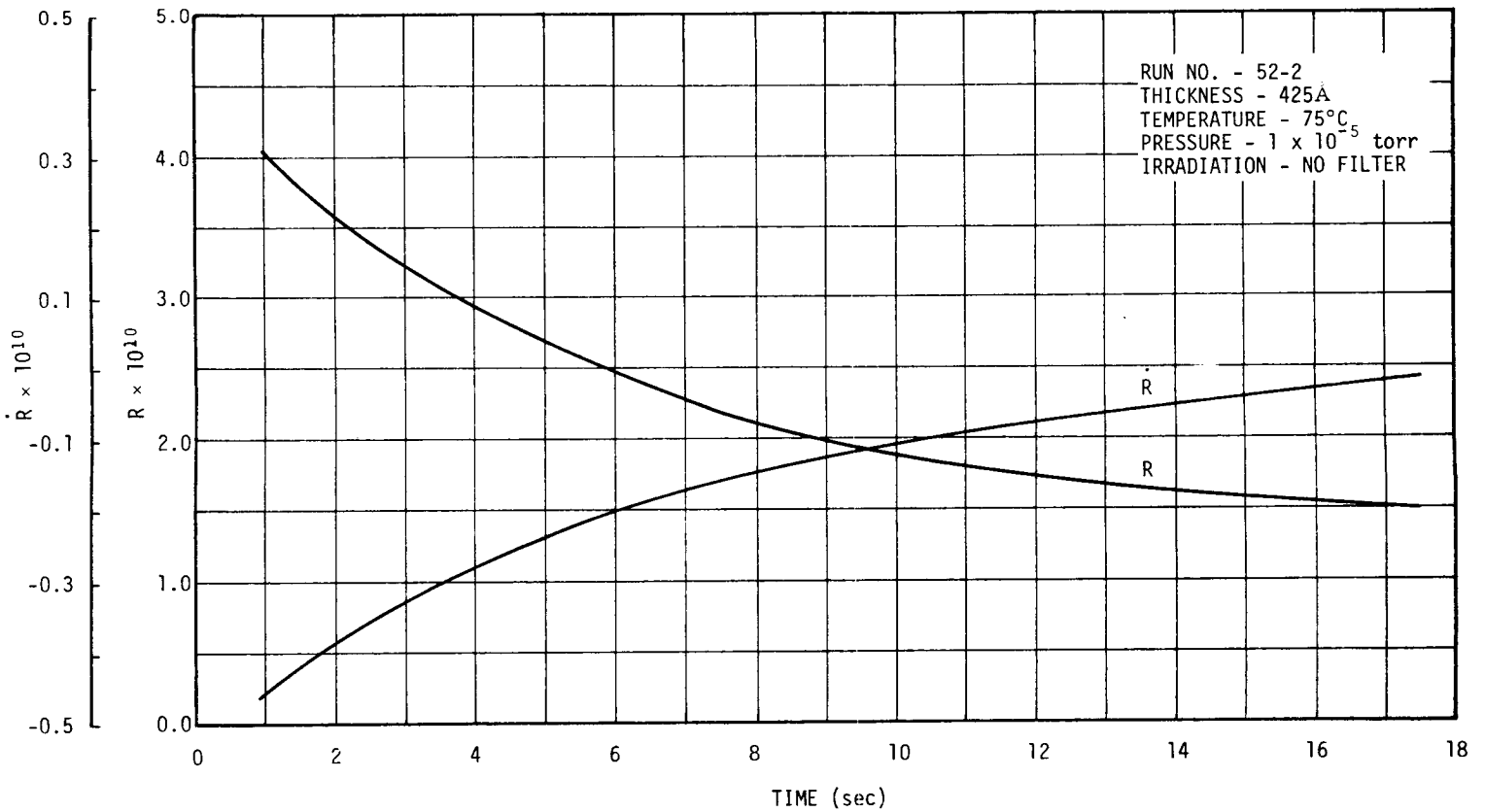
RUN NO. - 52-2
THICKNESS - 425Å
TEMPERATURE - 75°C
PRESSURE - 1 x 10^-5 torr
IRRADIATION - NO FILTER
Ṙ
R
Ṙ × 10^10
R × 10^10
0.5
0.3
0.1
-0.1
-0.3
-0.5
5.0
4.0
3.0
2.0
1.0
0.0
0
2
4
6
8
10
12
14
16
18
TIME (sec)

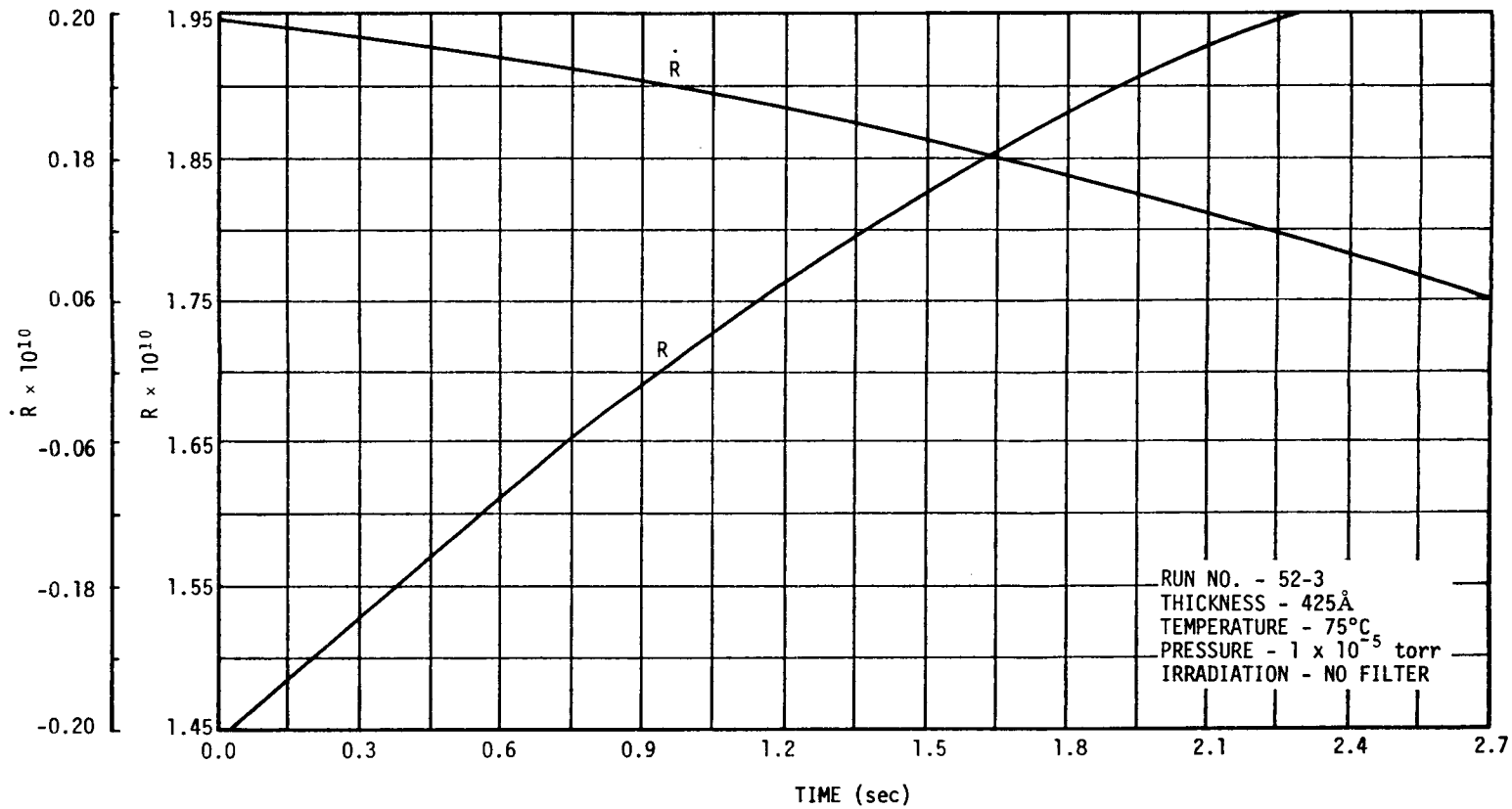
0.20
0.18
0.06
-0.06
-0.18
-0.20
$\dot{R} \times 10^{10}$
1.95
1.85
1.75
1.65
1.55
1.45
$R \times 10^{10}$
$\dot{R}$
R
0.0
0.3
0.6
0.9
1.2
1.5
1.8
2.1
2.4
2.7
TIME (sec)
RUN NO. - 52-3
THICKNESS - 425Å
TEMPERATURE - 75°C
PRESSURE - 1 x 10^{-5} torr
IRRADIATION - NO FILTER

DOCUMENT CONTROL DATA - R&D

(Security classification of title, body of abstract and indexing annotation must be entered when the overall report is classified)

1. ORIGINATING ACTIVITY *(Corporate author)* Research Laboratories Brown Engineering Company, Inc. Huntsville, Alabama	2a. REPORT SECURITY CLASSIFICATION Unclassified 2b. GROUP N/A

3. REPORT TITLE

"Hall and Photoresponse Measurements Associated with Ultraviolet and Near Ultraviolet Degradation of Thin Zinc Oxide Films"

4. DESCRIPTIVE NOTES *(Type of report and inclusive dates)*

Technical Note, May 1967

5. AUTHOR(S) *(Last name, first name, initial)*

McDaniel, M. L.; Mitchell, R. R.; Watson, H. J.

6. REPORT DATE May 1967	7a. TOTAL NO. OF PAGES 163	7b. NO. OF REFS 11
8a. CONTRACT OR GRANT NO. NAS8-20166 b. PROJECT NO. N/A c. d.	9a. ORIGINATOR'S REPORT NUMBER(S) TN R-229 9b. OTHER REPORT NO(S) *(Any other numbers that may be assigned this report)* None	

10. AVAILABILITY/LIMITATION NOTICES

None

11. SUPPLEMENTARY NOTES None	12. SPONSORING MILITARY ACTIVITY Research Projects Laboratory Marshall Space Flight Center NASA

13. ABSTRACT

The optical and electrical parameters of zinc oxide change (degrade) as a result of material exposure to certain spectral radiation; the causal spectral range is in the visible and ultraviolet. Charge carrier density and majority carrier mobility have been measured in thin, polycrystalline, zinc oxide film; these measurements were made for several levels of degradation.

Photoresponse, as a manifestation of degradation, is compared for ambient pressures of one atmosphere and approximately 10^{-10} atmospheres. This response study is made for two spectral levels, 3650 Å and 4350 Å radiation.

14. KEY WORDS

thin-film
mobility
zinc oxide
conductivity
ultraviolet
irradiation